Prolyl hydroxylase domain proteins in venous thrombus resolution

Grover, Steven Philip

Awarding institution:
King's College London

Prolyl hydroxylase domain proteins in venous thrombus resolution

Steven Philip Grover

Thesis submitted for the degree of
Doctor of Philosophy
2015

Academic Department of Surgery
Cardiovascular Division
School of Medicine
King's College London
1st Floor North Wing
St Thomas' Hospital
Lambeth Palace Road
SE1 7EH

Statement of originality

The work contained in this thesis is my own original work, except where acknowledged in the text.

Acknowledgements

I would like to express my deepest gratitude to my supervisor, Professor Alberto Smith, and co-supervisors, Mr Bijan Modarai and Dr Julia Humphries, without whose expert guidance and support it would not have been possible to complete this work.

My sincere thanks are due to Dr Massimiliano Mazzone for provision of knockout mice used in this study and for welcoming me into his laboratory. I would like to thank past and present members of the academic department of surgery for their camaraderie and advice in particular Mr Prakash Saha.

I would like to acknowledge the British Heart Foundation and King's College London for financial support. I am grateful for additional support received from the Cardiovascular Division and the Division of Imaging Sciences.

I am forever indebted to my parents, Clare and Philip, for their unwavering love, support and encouragement.

This work is dedicated to my father, Dr Philip Grover, a fellow scientist, whose own endeavours have served as a constant source of inspiration.

Abstract

The prolyl hydroxylase domain (PHD) proteins serve as critical regulators of the cellular response to tissue hypoxia, like that present in the early venous thrombus, through regulation of hypoxia-inducible factor 1α (HIF1α) stability. This study sought to determine: (i) the expression of PHD1, PHD2 and PHD3 at the gene and protein level during natural thrombus resolution; (ii) the effect of gene specific deletion of *Phd2* on thrombus resolution; (iii) the effect of pan-PHD inhibition on thrombus resolution; and (iv) the contribution of endogenous VEGFR signalling to thrombus resolution.

All three PHD isoforms were expressed in the naturally resolving thrombus at the gene and protein level. Gene expression of *Phd1* remained invariant while *Phd2* and *Phd3* expression demonstrated distinct temporal patterns. PHD isoforms were localised to the cellular component of the thrombus, with morphological analysis suggesting expression in both neutrophils and macrophages. Constitutive heterozygous *Phd2* gene deletion failed to increase HIF1α stabilisation as was not associated with increased thrombus resolution. Inducible homozygous *Phd2* gene deletion significantly enhanced HIF1α nuclear accumulation and transcriptional activity but thrombus resolution was unchanged. Pharmacological inhibition of PHD isoforms with novel small molecule inhibitor, AKB-4924 and JNJ-42041935, signficantly increased HIF1α nuclear accumulation and transcriptional activity. Treatment with these inhibitors significantly increased thrombus neovascularisation but thrombus resolution was unaffected. Blocking of endogenous VEGFR signalling using the pan-VEGFR inhibitor axitinib significantly impaired thrombus resolution. Axitinib treated thrombi remained larger and more occlusive for an extended period of time and this was associated with significant reductions in thrombus neovascularisation, macrophage recruitment and collagen deposition.

Inhibition of PHD activity promotes thrombus neovascularisation, but other mechanisms are likely to regulate the removal of thrombus. Studies of thrombus resolution in *Phd2* gene specific knockouts indicate that PHD2 activity does not play a major role in thrombus resolution. However, endogenous VEGFR signalling activity, downstream of HIF, is necessary for thrombus resolution.

Table of contents

Index of figures

Index of tables

Abbreviations

2-OG	2-oxoglutarate
2ME	2-methoxyestradiol
ANOVA	analysis of variance
bHLH	beta hela loop helix
BMDAC	bone marrow derived angiogenic cells
BSA	bovine serum albumin
CBP	CREB-binding protein
CCR	chemokine (c-c motif) receptor
cDNA	complementary DNA
CTAD	c-terminal activation domain
CXCR	CXC chemokine receptor
DFO	desferrioxamine
DMOG	dimethyloxaloylglycine
DNA	deoxyribonucleic acid
DVT	deep vein thrombosis
EIM	electrolytic injury model
ELISA	enzyme linked immunosorbent assay
eNOS	endothelial nitric oxide synthase
EPO	erythropoietin
FFPE	formalin fixed paraffin embedded
FIH	factor inhibiting HIF
GFP	green fluorescent protein
GMCSF	Granulocyte macrophage colony stimulating factor
H&E	haematoxylin and eosin
HFUS	high frequency ultrasound
HIF	hypoxia inducible factor
HRE	hypoxia responsive element
HRP	horseradish peroxidase
IFNy	interferron gamma
IKKB	inhibitor of nuclear factor kappa-B kinase subunit beta
IL	interleukin
iNOS	inducible nitric oxide synthase
IVC	inferior vena cava
LMWH	low molecular weight heparin
MCP1	monocyte chemoattractant protein
MCSF	macrophage colony stimulating factor
microCT	micro computed tomography

MMP	matrix metalloproteinase
MSB	martius scarlet blue
nAU	nano gold
NFAT	nuclear factor of activated T cells
NFDM	non-fat dried milk
NFkB	nuclear factor kappaB
NLS	nuclear localisation sequence
NO	nitric oxide
NTAD	n-terminal activation domain
ODDD	oxygen dependent degradation domain
PAS	per arnt sim
PBS	phosphate buffered saline
PCR	polymerase chain reaction
PE	pulmonary embolism
PET	positron emission tomography
PHD	prolyl hydroxylase domain
PlGF	placental growth factor
PTS	post thrombotic syndrome
PVDF	polyvinylidene difluoride
RIN	RNA integrity number
RNA	ribonucleic acid
ROI	region of interest
SA	streptavidin
SE	standard error
TAE	tris-acetate buffer
TBS	tris-buffered saline
tPA	tissue plasminogen activator
uPA	urokinase plasminogen activator
uPAR	uPA receptor
VEGF	vascular endothelial growth factor
VEGFR	VEGF receptor
VHL	von Hippel Lindau
VTE	venous thromboembolism
VWF	von Willebrand factor

Chapter 1 General Introduction

1.1 Deep Vein Thrombosis

Deep vein thrombosis (DVT) is a common condition with an annual incidence of approximately 1 in a 1000 in the general population[1, 2]. In the United Kingdom DVT is responsible for more deaths per annum than breast cancer, road traffic accidents, hospital inquired infections and HIV combined[3]. Common sequalae of DVT include pulmonary embolism (PE) and chronic venous insufficiency or post thrombotic syndrome (PTS), which are significant sources of mortality and morbidity respectively.

PE occurs when thrombus material from an incident DVT breaks off from the original nidus and travels to the pulmonary arterial tree where it can become lodged, occluding the pulmonary artery or distal branches (Fig 1.1). PE results in hypo-perfusion of the lung and right ventricular pressure overload. The incidence of PE in the general population is estimated to be between 2-4/10,000/yr[4]. The prognosis of patients diagnosed with acute PE is poor with a 1-year mortality rate of ~25%[4, 5].

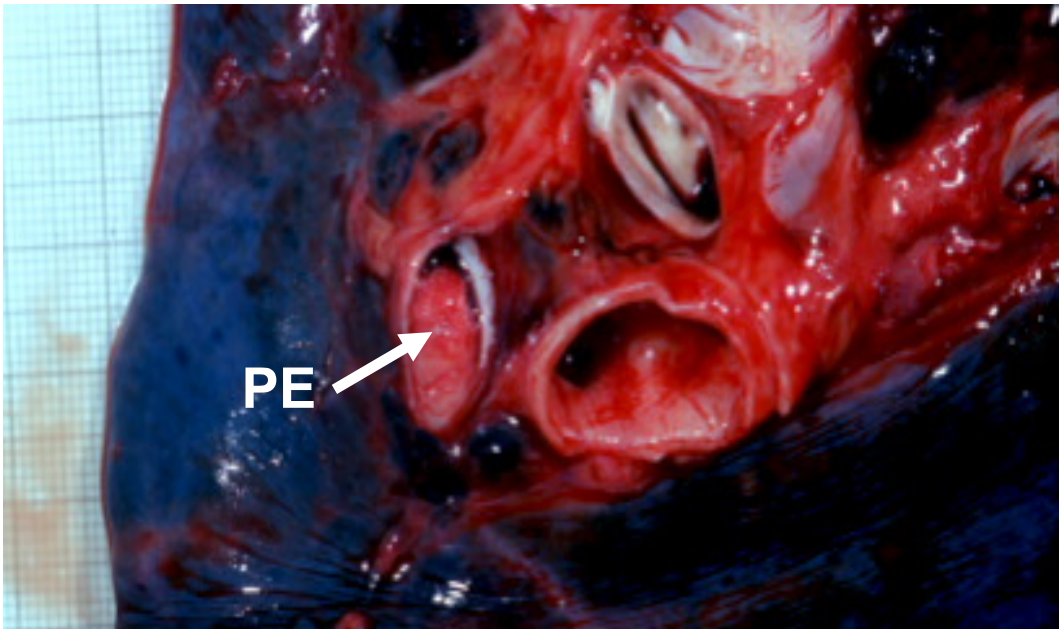

Figure 1.1 Pulmonary embolism

A pulmonary embolus present in the lung identified post-mortem.

Venous thrombi resolve naturally by a process of organisation that ultimately leads to vein recanalisation[6]. Incomplete thrombus resolution can contribute to venous insufficiency through a combination of residual vein obstruction and valvular incompetence, causative factors in the development of PTS. PTS is common in patients after an episode of DVT, occurring in 20-45% of patients[7, 8]. PTS is characterised by chronic leg pain, oedema and skin changes result in chronic leg ulceration in over 30% of patients (Fig 1.2)[9]. Management of this debilitating syndrome costs the NHS in excess of £500 million per annum[10].

Figure 1.2 Chronic leg ulceration in a patient suffering form PTS

1.2 Current treatment

Anticoagulation, using low molecular weight heparin followed by warfarin, is the standard treatment for patients with DVT. These drugs whilst efficacious in the prevention of secondary thrombotic events do not accelerate natural resolution of the initial thrombus. The advent of pharmacological thrombolysis and neo-adjuvant mechanical thrombectomy has facilitated the removal of acute thrombi, however, few patients currently receive this treatment strategy.

1.2.1 Anticoagulants

Warfarin is an indirect vitamin K antagonist that inhibits vitamin K epoxide reductase required for the reduction of vitamin K[11]. Activation of both the intrinsic and extrinsic coagulation cascades requires vitamin K mediated carboxylation of coagulation factors II, VII, IX and X (Fig 1.3). Contrastingly vitamin K dependent carboxylation is required for activation of the endogenous anticoagulants protein C and protein. Loss of carboxylation as a result of warfarin treatment results in a net inactivation of the coagulation cascade.

Unfractioned heparin is a potent anticoagulant with the capacity to bind and activate antithrombin III, a natural anticoagulant that inactivates factors IIa, Xa and IXa. Unfractioned heparin is of limited clinical utility as it must be administered intravenously, has a narrow therapeutic range and is associated with a significant risk of haemorrhage. Low molecular weight heparin (LMWH), ranging from 5 to 30kDa in molecular weight, was initially developed as a prophylactic agent for the prevention of DVT. LMWH are now routinely used in patients with DVT to prevent clot propagation and to treat underlying hypercoagulation. LMWH, when compared with unfractioned heparin, offers improved pharmacokinetic stability, can be administered by subcutaneous injection, has a lower risk of hemorrhage and has a high efficacy.

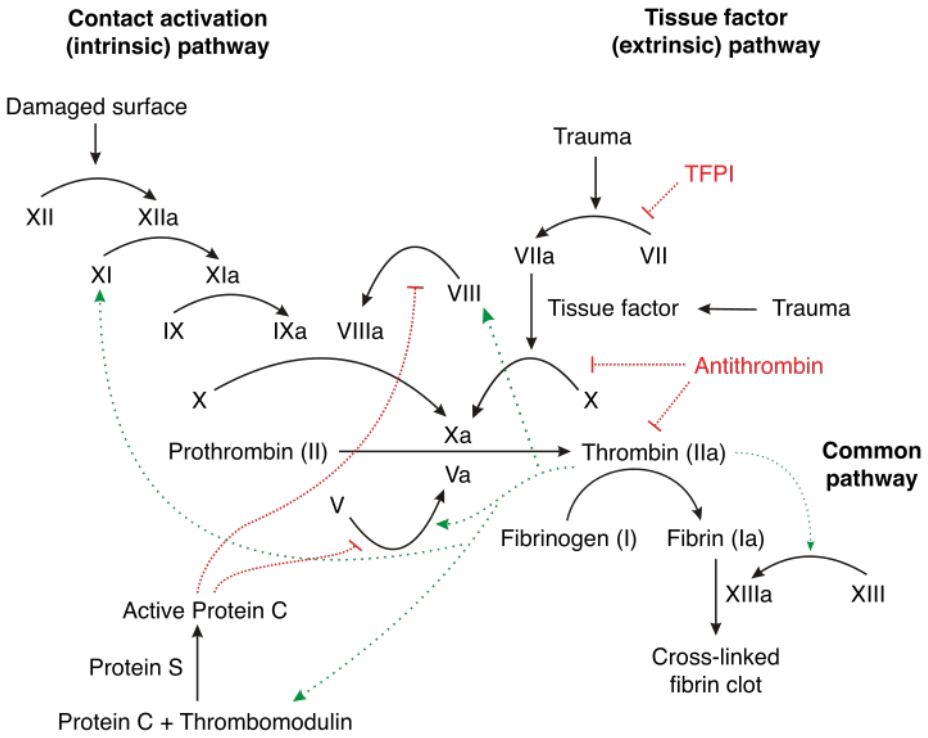

Figure 1.3 Schematic representation of the coagulation cascade

The classical coagulation cascade involves the step-wise activation of a series of pro-enzyme in both the contact activation (extrinsic) and tissue factor (intrinsic) pathways resulting in thrombin activation and generation of cross-linked fibrin (common pathway). A number of agonists (green arrow) and antagonists (red arrow) have been identified that further regulate flux through the cascade.

1.2.2 Thrombolysis

Catheter directed thrombolysis is a powerful approach for the treatment of acute venous thrombi. Intravascular administration of agents such as urokinase plasminogen activator (uPA), tissue-type plasminogen activator (tPA) and streptokinase facilitate dissolution of the clot by cleaving plasminogen to form plasmin, the major fibrinolytic enzyme. Thrombolysis is most effective in patients with acute illeofemoral DVT (<14days since the onset of symptoms). Contraindications for thrombolysis include patients with a recent history of trauma, stoke, major surgery or active internal haemorrhage. Neo-adjuvant mechanical thrombectomy may also be used in conjunction with catheter directed thrombolysis to physically disrupt organised components of the thrombus.

1.3 Thrombus formation

Venous thrombi are laminar structures, composed of layers of granular leukocytes (neutrophils) and platelets (Lines of Zahn) encompassed by an erythrocyte mass trapped in a fibrin mesh (Fig 1.4)[12]. Three main factors, referred collectively as Virchow's triad, contribute towards thrombogenesis: endothelial disturbance, reduced blood flow and blood hypercoagulability (Fig 1.5)[13]. It is thought that the presence of at least two of these factors is sufficient to promote venous thrombosis.

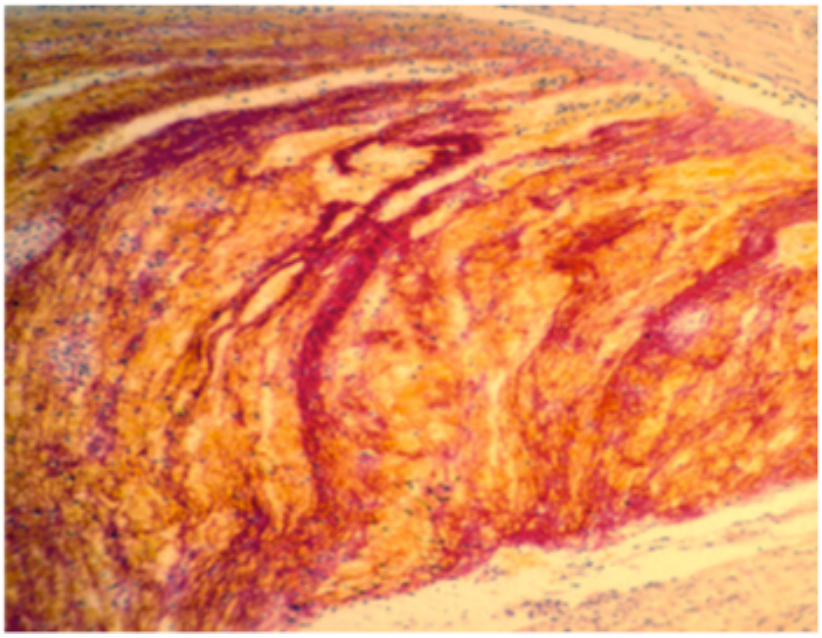

Figure 1.4 Laminar structure of a human thrombus

Martius scarlet blue stained section of a human venous thrombus with typical laminar striations of fibrin (red) in an erythrocyte rich mass (yellow).

1.3.1 Reduced blood flow

Thrombi often form in deep veins of the lower limbs where gravitational stasis is greatest[14]. Reduced blood flow is also observed in patients suffering from paralysis or prolonged periods of bed rest[15]. The loss of pulsatile venous flow may impinge on normal valve function and result in stasis of blood within the valve cusp[16]. Loss of oxygen exchange within the valve cusp leads to the formation of a hypoxic environment and may be sufficient to induce local endothelial dysfunction[17].

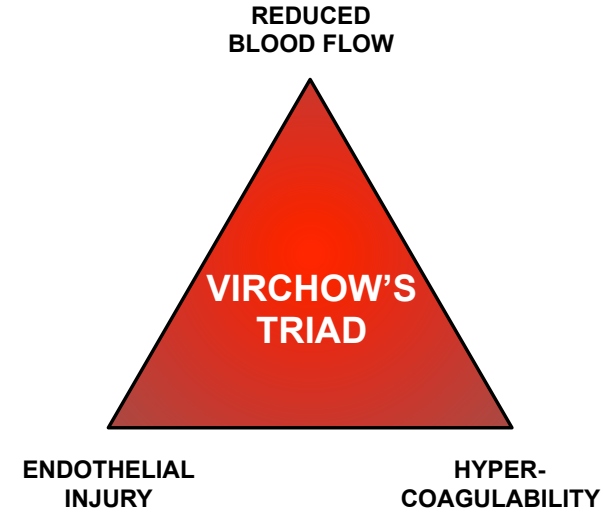

Figure 1.5 Virchow triad

A triad of factors, first described by Rudolph Virchow in 1856 (reduced blood flow, endothelial injury and hypercoagulability) are thought to contribute to the generation of thrombosis in the veins.

1.3.2 Endothelial injury

Under physiological conditions the vascular endothelium suppresses coagulation and inflammation by: generating prostacyclins and nitric oxide that inhibit platelet aggregation[18]; expressing heparin sulphate and thrombomodulin on their surface that facilitate the inactivation of thrombin[19]. Endothelial disturbance, whether activation, dysfunction or damage, decreases the production of these endogenous anti-coagulants resulting in a local pro-thrombotic state. Endothelial disturbance may occur as a result of physical trauma or systemic inflammation.

1.3.3 Hypercoagulability

A number of inheritable thrombophilias, including factor V Leiden, prothrombin gene mutation, protein C and S deficiency, predispose patients to DVT[20-22]. The frequency of factor V Leiden in the population is approximately 5%, however this phenotype is found in 20% patients with DVT[23]. There are a number of acquired risk factors such as malignancy, the use of oral contraceptives, myelopoliferative disorders and diabetes mellitus that also result in a hypercoagulable state[24].

1.4 Cellular and molecular regulators of venous thrombus resolution

Venous thrombi resolve through natural processes that involve accumulation of inflammatory cells and other, less defined, nucleated cells; neovascularisation and tissue organisation that eventually lead to vein recanalisation and restoration of blood flow (Fig 1.6) [6, 25]. Venous thrombi in man resolve to varying degrees, with a significant proportion of patients exhibiting impaired or incomplete thrombus resolution[26, 27].

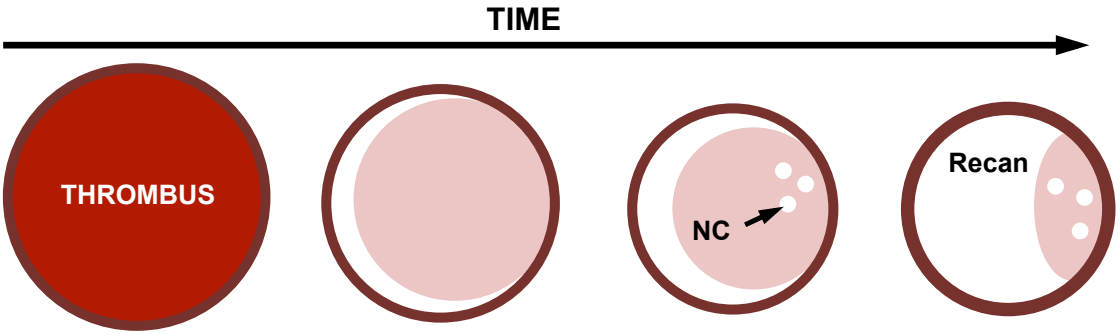

Figure 1.6 Thrombus resolution

The acute erythrocyte rich venous thrombus is largely occlusive and undergoes extensive remodelling resulting in gradual recanalisation (Recan) of the vessel lumen as a result of tissue organisation and neovascular channel (NC) formation that restores blood flow through the thrombosed vessel.

1.4.1 Extracellular matrix

During venous thrombus resolution the extracellular matrix (ECM) undergoes extensive remodelling (Fig 1.7). Fibrin, deposited during formation, is the major ECM component found in acute venous thrombi and forms a mesh that traps successive layers of erythrocytes and leukocytes[28]. Endogenous degradation of fibrin is mediated by a series of enzymes that constitute the fibrinolytic system. Plasmin, generated by the proteolytic activation of plasminogen, is the main active fibrinolytic enzyme[29]. Two proteases, tissue plasminogen activator (tPA) and urokinase plasminogen activator (uPA), are responsible for the generation of plasmin[30, 31]. The activity of tPA and uPA is controlled by negative regulators the plasminogen activator inhibitors (PAIs).

Studies of thrombus resolution in animals deficient for uPA observed an almost complete absence of thrombus resolution demonstrating the importance of endogenous fibrinolytic activity[32]. Interestingly, tPA activity was not required as knockouts of this protease did not demonstrate impaired thrombus resolution and suggests the two enzymes have distinct biological activity[32]. Accelerated resolution of thrombi transfected with adenoviral uPA further reinforces the importance of this process[32]. The plasminogen activator inhibitors (PAIs) 1 and 2 serve to limit the endogenous activity of tPA and uPA. Deletion of either PAI gene significantly enhances venous thrombus resolution[33].

As the thrombus resolves collagen is deposited in significant quantities. Collagen is likely remodeled in the resolving venous thrombus by a family of serine proteases with diverse proteolytic activities, the matrix metalloproteinases (MMPs)[34]. Protein expression and activity of MMP2 and MMP9 has been detected in the resolving venous thrombus[35, 36]. MMP activity plays an important role in the resolution of venous thrombi. Deletion of MMP2 significantly impairs venous thrombus resolution, whereas increased MMP9 activity enhances this process[37]. This is further supported by the reduced thrombus resolution observed MMP2/MMP9 double knockouts and MMP9 knockouts treated with an MMP2 inhibitor[38]. Other ECM components may also be present in the resolving venous thrombus, however, a complete analysis of the ECM has yet to be undertaken.

1.4.2 Neutrophils

Neutrophils, the most abundant leukocyte in the circulation, are present in large numbers in the acute thrombus[25]. Depletion of neutrophils significantly impairs the resolution of venous thrombi *in vivo* highlighting the important contribution of this cell type[39]. Activated neutrophils are an important source of the fibrinolytic enzyme uPA and its receptor (uPAR)[40]. *In vitro* experiments suggest that neutrophil mediated thrombolysis occurs in an uPA/uPAR dependent manner[40, 41]. This finding is supported *in vivo* as deletion of uPA in the bone marrow, where neutrophils derive, impairs venous thrombus resolution[32].

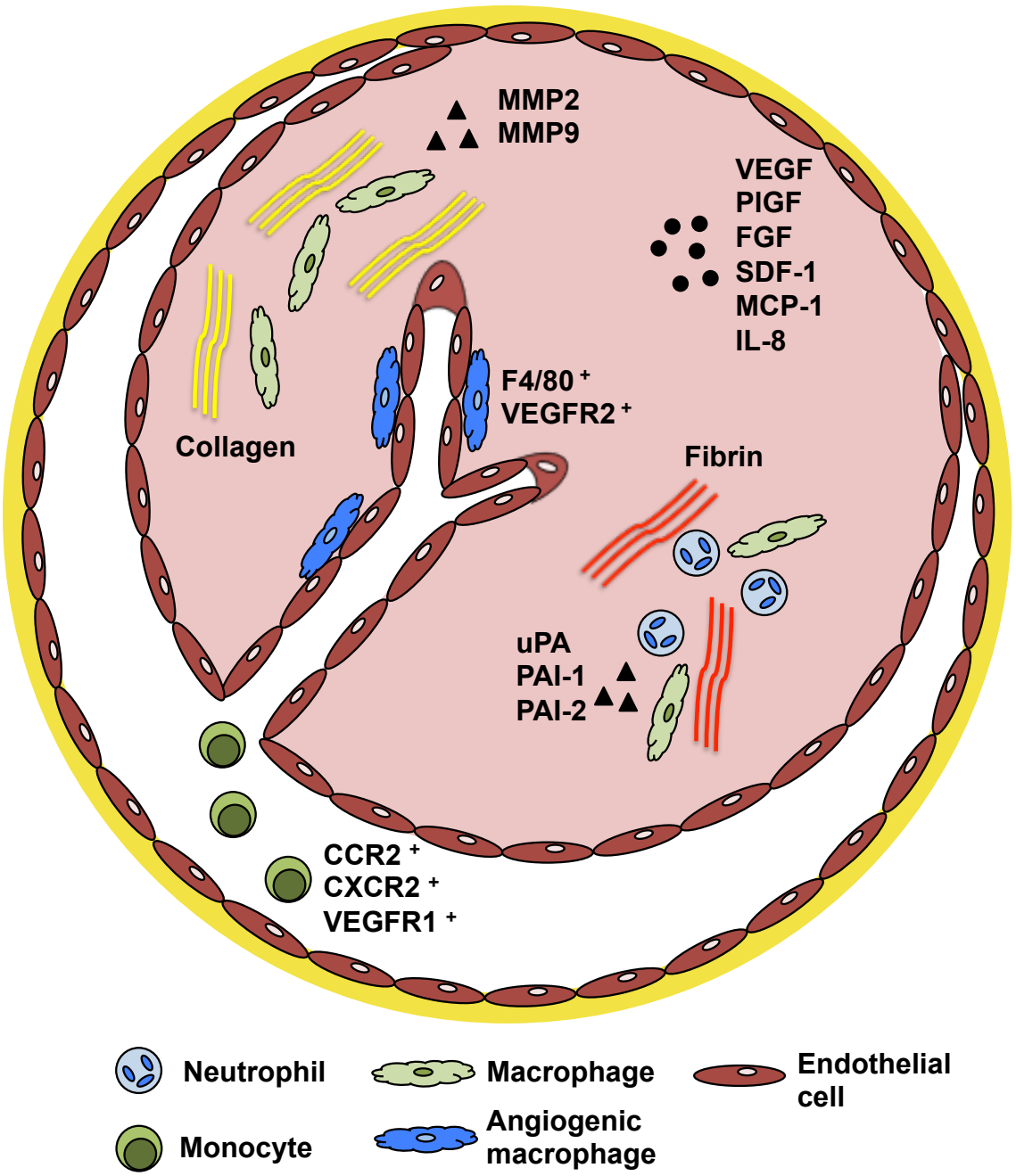

Figure 1.7 Molecular and cellular regulators of venous thrombus resolution

Resolution of venous thrombi is a highly dynamic process thought to involve a number of processes including extensive neutrophil / macrophage dependent remodelling of extracellular matrix components such as fibrin or collagen and development of neovascular channels that together aid in recanalisation of the thrombosed vessel and restoration of blood flow.

1.4.3 Monocyte/ macrophages

The monocyte/macrophage is found in increasing numbers in the resolving venous thrombus[25]. Blocking the recruitment of monocyte/macrophages into the thrombus through knockout of surface receptors, CXCR2 or CCR2, impairs thrombus resolution[42, 43]. Conversely, administration of CXCR2 and CCR2 ligands, IL8 or MCP1, enhance venous thrombus resolution[44]. CCR2 expression is required for monocyte chemotaxis and mobilisation from the bone marrow[45, 46], while the IL8 and MCP1 mediate monocyte adhesion to the vascular endothelium and thereby facilitate migration from the intravascular space to tissues[47]. These findings suggest that monocyte mobilisation, chemotaxis and adhesion are important processes for the recruitment of these cells to the thrombus.

Other chemokines also play an important role in monocyte/ macrophage mediated resolution of venous thrombi (Fig 1.7). Vascular endothelial growth factor A (VEGFA) is abundantly expressed in the naturally resolving venous thrombus [48]. Gene mediated over expression and direct injection of VEGFA results in increased macrophage recruitment and accelerated thrombus resolution[49-51].

1.4.4 Endothelial cells

The formation of neovascular channels is a hallmark of the organising venous thrombus in both experimental models and man (Fig 1.7)[52]. Thrombus neovascular channels are lined by cells that stain positively for endothelial markers such as CD31 and vWF[52]. VEGF signalling is also important for the development of neovascular channels[53]. VEGFA overexpression in the thrombus was found to significantly increase neovascular channel formation[49-51]. This likely occurs in a VEGF receptor 2 (VEGFR2) dependent manner as thrombus neovascularisation is impaired in endothelial cell specific *Vegfr2* knockouts[54]. Channel formation may be supported by a subset of pro-angiogenic monocytes expressing Tie2[55]. Tie2 expressing monocytes, co-expressing the macrophage marker CD68 and the endothelial cells marker VEGFR2, are recruited from the bone marrow into the thrombus and accumulate in neovascular channel rich regions of the thrombus[56]. However, the contribution of neovascular channels towards thrombus resolution is a

source of contention. While increased neovascularisation is consistently observed in treatments that accelerate thrombus resolution[49-51, 57] interventions in which only neovascularisation was increased, such as treatment with basic fibroblast growth factor, failed to accelerate thrombus resolution[58]. It remains to be seen whether thrombus neovascularisation is required for resolution.

1.5 Tissue hypoxia

In disease states hypoxia can be characterised as an insufficiency in the supply of molecular oxygen to tissues. Tissue hypoxia is a hallmark of a number of human pathophysiologies including tumourigenesis[59], myocardial infarction[60] and thrombosis[57]. The presence of hypoxia may stem from either the blockage of blood vessels that perfuse pre-existing tissues, as in myocardial infarction, or alternatively from the presence of metabolically active avascular tissues, such as is the case in cancer and thrombosis.

With respect to venous thrombosis hypoxia, present in the cusp of venous valves, is thought to play an important role during formation [61] but is also likely to be involved in subsequent resolution. Measurement of oxygen tension in murine venous thrombi has shown that newly formed thrombus is acutely hypoxic compared to that of venous blood[57]. Oxygen tension in the thrombus rises with time, which may be a function of increasing organisation and recanalisation.

Tissue hypoxia triggers a number of alterations in cellular activity in an attempt to adapt to conditions of low oxygen availability. Among the best-studied adaptation is the shift in metabolism towards non-oxidative anaerobic glycolysis[62]. Changes in cellular metabolism in co-ordination with other anti-apoptotic adaptations serve to enhance survival of cells under hypoxic conditions[63]. Of particular relevance to thrombus resolution hypoxia is also closely associated with the formation of angiogenic channels and the recruitment of macrophages[64, 65]. Interrogation of this cellular adaptation at the molecular level has identified a family of transcription factors, the hypoxia inducible factors (HIFs), as critical regulators of this response[66].

1.6 Hypoxia inducible factor

HIF protein subunits form a family of basic helix-loop-helix Per Arnt Sim domain containing transcription factors. The functional unit of HIF is a heterodimer consisting of a constitutively expressed subunit (HIFβ) and an oxygen sensitive subunit (HIFα). Three separate loci have been identified (*Hif1, 2, 3*) for each subunit. All HIFα paralogues possess a centrally located oxygen dependent degradation domain (ODDD)[67]. The ODDD contains two proline residues, Pro402 and Pro564 in HIF1α, that are subject to hydroxylation by a family of prolyl hydroxylase domain (PHD) enzymes and factor inhibiting HIF (FIH) in an oxygen-dependant manner[68].

1.6.1 HIF1α

HIF1α is a 120kDa protein encoded by the *Hif1a* gene present on chromosome 14 in man. HIF1α protein demonstrates a high level of evolutionary conservation sharing ~90% amino acid homology between mouse and man. HIF1α represents the prototypical alpha subunit the domain structure of which was characterized in the mid 90s (Fig 1.8)[69, 70]. The HIF1α N terminal region contains bHLH and PAS domains accompanied by a nuclear translocation sequence (NLS). The HIF1α C terminal region contains the ODDD domain, including an N terminal transactivation domain (NTAD), a C terminal transactivation domain (CTAD) and an additional NLS.

Hif1a gene and HIF1α protein expression has been detected in a range of human tissues including the brain, liver, heart, spleen, kidney and liver[71]. A number of transcriptional regulators that mediate *hif1a* gene expression have been identified and include nuclear factor kappa-light-chain-enhancer of activated B cells (NFκB), and members of the nuclear factor of activated T-cells (NFAT) family of transcription factors[72]. Active HIF1α, localised to the nucleus and complexed with HIF1β, upregulates a broad range of genes based on the presence of a functional HRE (Table 1.1).

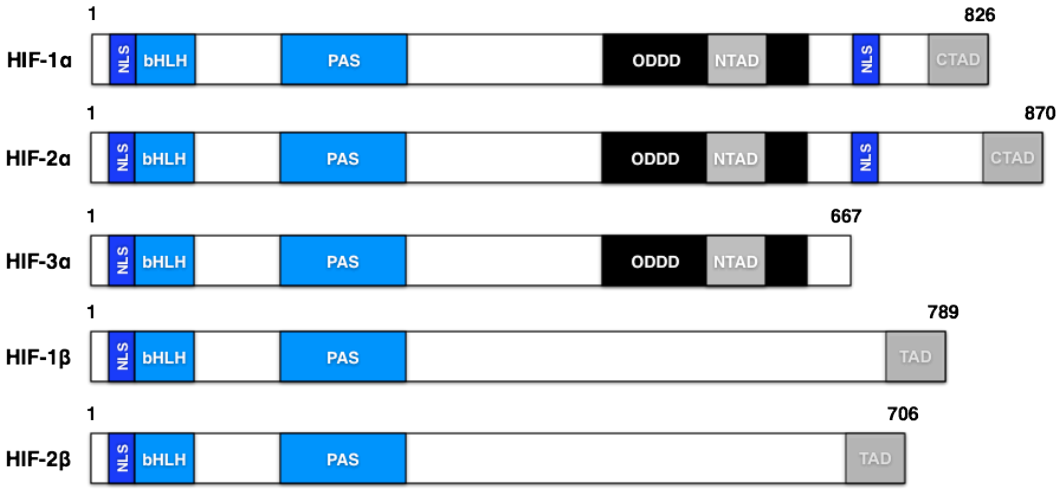

Figure 1.8 HIF subunit domain architecture

All HIF subunits have been found to contain highly conserved nuclear localisation sequences (NLS), βhelix-loop-helix (bHLH), per arnt sim (PAS) domains and C terminal trans-activation domains (CTAD). HIF-α subunits also possess an oxygen dependent degradation domains (ODDD) containing an N terminal trans-activation domain (NTAD). Both HIF1α and HIF2α contain an additional NLS and trans-activation domain towards the C terminus.

HIF1α is required for development, as mice deficient for HIF1α (HIF1α$^{-/-}$) demonstrate impaired cardiac and vascular development and die mid-gestation at E10.5[73]. Cell specific HIF1α$^{-/-}$ mice have been used to investigate a number of cellular processes. Myeloid specific HIF1α$^{-/-}$ mice demonstrate impaired recruitment of these cells to sites of inflammation suggesting that HIF1α expression is required for mounting the monocyte and neutrophil response to inflammation *in vivo*[74, 75]. HIF1α is also essential for the development and maintenance of populations of haematopoietic stem cell, precursors for the myeloid lineage[76, 77]. Deletion of *Hif1a* in Tie2 expressing cells, which includes endothelial and haematopoietic cells, results in reduced mobilisation of bone marrow derived cells and impaired wound revascularisation[78].

In the resolving venous thrombus increased stabilisation of HIF1α, achieved by treatment with the PHD inhibitor l-mimosine, was found to significantly increase thrombus resolution in a murine model[57]. L-mimosine treatment, as well as reducing thrombus volume, significantly increased vein lumen receanalisation,

macrophage content, neovascularisation and was associated with increased expression of the HIF1α target gene *Vegfa*[57]. However, direct injection of the adenoviral construct CA5 into the thrombus, resulting in an equivalent increase in HIF1α stabilisation, did not affect accelerate venous thrombus resolution[79].

Conversely, pharmacological destabilisation of HIF1α, using the anti-angiogenic agent 2-methoxyestradiol (2ME), has been used to demonstrate the importance of basal HIF1α transcriptional activity. 2ME is a naturally occurring estrogen metabolite first described as an inhibitor of microtubule formation[80]. The HIF1α destabilizing effects of 2ME observed *in vivo* are thought to be secondary to loss of microtubule formation[81]. Treatment with 2ME decreased thrombus resolution, vein lumen recanalisation, macrophage content and neovascularisation, and was associated with impaired nuclear accumulation of HIF1α and reduced VEGF protein expression[82].

Pharmacological manipulation of HIF1α demonstrates the importance of the hypoxic response in mediating thrombus resolution. However, the pharmacological agents used thus far have limited specificity and a number of HIF1α independent effects may have been involved. Alternate more targeted strategies may provide further evidence for the direct role of HIF1α in thrombus resolution and enable elucidation of upstream and downstream signalling mechanisms.

Table 1.1 Selected HIF1α target genes

Gene	Protein name	Ref
CHEMOKINES AND CHEMOKINE RECEPTORS		
CXCR4	chemokine (C-X-C motif) receptor 4	83
ENG	endoglin	84
PDGFB	platelet-derived growth factor beta polypeptide	85
TGFA	transforming growth factor, alpha	86
VEGFA	vascular endothelial growth factor A	87
VEGFR1	vascular endothelial growth factor receptor 1	88
EXTRACELLULAR MATRIX		
P4HA1	procollagen-4-prolyl hydroxylase	89
LOX	lysyl oxidase	90
MMP14	matrix metallopeptidase 14	91
MMP2	matrix metallopeptidase 2	91
PLAUR	plasminogen activator, urokinase receptor	92
PAI1	plasminogen activator inhibitor 1	92
METABOLISM		
ALDOA	aldolase A, fructose-bisphosphate	93
ENO1	enolase 1, (alpha)	93
GAPDH	glyceraldehyde-3-phosphate dehydrogenase	94
GLUT1	glucose transporter 1	89
LDHA	lactate dehydrogenase A	93
PFKL	phosphofructokinase, liver	95
PGK1	phosphoglycerate kinase 1	95
PKM2	pyruvate kinase, muscle	95
PFKFB3	6-phosphofructo-2-kinase/fructose-2,6-biphosphatase 3	96
HYPOXIA		
PHD2	prolyl hydroxylase domain containing protein 2	97
PHD3	prolyl hydroxylase domain containing protein 3	98
CITED2	cbp/p300-interacting transactivator	99
VASOACTIVE		
EDN1	endothelin 1	100
NOS2A	nitric oxide synthase 2 (inducible)	101
NOS3	nitric oxide synthase 3 (endothelial)	102
HMOX1	heme oxygenase 1	103
ERYTHROPOIESIS		
EPO	erythropoeitin	104

1.6.2 HIF2α

HIF2α is a 95kDa protein encoded by the *Epas1* gene present on chromosome 2 in man. HIF2α demonstrates a high level of evolutionary conservation sharing ~90% amino acid homology between mice and man. Despite the highly similar domain structure observed between HIF1α and HIF2α these proteins share only 50% amino acid homology. Mice deficient for HIF2α also die at mid-gestation (E9.5-15) as a result of impaired vascular development[105-107]. These studies suggest that while HIF2α knockout mice reach a latter stage of embryogenesis than HIF1α$^{-/-}$, HIF2α is still essential during development.

HIF2α has also been found to regulate a number of post-developmental processes. HIF2α, and to a lesser extent HIF1α regulate erythropoeitin (EPO) production, with deletion of *Hif2a* in hepatocytes resulting in reduced EPO production in response to an anemic insult[108]. As with HIF1α, HIF2α is an important regulator of angiogenesis as endothelial deletion of *Hif2a* results in reduced vascularisation of ischaemic limbs and tumours[109]. However, a number of HIF2α specific processes such as iron absorption have also been described. Expression of the divalent metal transporter 1 (DMT1), required for iron influx is regulated by HIF2α but not HIF1α[110]. Furthermore, HIF2α$^{-/-}$ results in impaired neutrophil apoptosis that is not observed in HIF1α$^{-/-}$ neutrophils[111]. Comparison of gene arrays in HIF1α and HIF2α overexpression systems reveals distinct transcriptional targets that would support a divergent role for HIFα subunits[112, 113].

1.6.3 HIF3α

HIF3α is a 72kDa protein encoded by the *Hif3a* gene present on chromosome 19 in man. Two variants of HIF3α have been described that are generated by the alternate splicing of *Hif3a* mRNA, neonatal and embryonic PAS (NEPAS) and inhibitory PAS (IPAS)[114, 115]. All three variants are considered transcriptional repressors. HIF3α and NEPAS form heterodimers with HIF1β and bind to HREs but the lack of a CTAD significantly reduces the transcriptional activity of these factors compared to HIF1α and HIF2α[116]. IPAS forms heterodimers with other HIFα subunits and lacks both a CTAD and NTAD preventing binding to HREs and rendering this variant transcriptionally

inactive[117]. The ability of IPAS to bind both HIF1α and HIF2α enables this variant to act as a transcriptional repressor of these subunits.

Homozygous *Hif3a* gene knockouts are viable, unlike those for HIF1α or HIF2α, demonstrating only mild cardiac and pulmonary defects[118]. In agreement with the role of HIF3α as a transcriptional repressor gene deletion results in increased expression of HIF1α and HIF2α transcriptional targets[118]. Conditional deletion of *Hif3a* in the epithelium has demonstrated the requirement of HIF3α for normal lung development and revealed novel HRE-independent transcriptional responses[119].

1.6.4 Regulation of HIF

Given the vital role of HIF signalling in marshalling the cellular response to tissue hypoxia activity of this transcription factor is tightly regulated. Under normoxic conditions HIFα is subject to hydroxylation by PHD enzymes (Fig 1.9). Hydroxylated HIFα forms a complex with von Hippel Lindau (VHL)[120] and elongin C[121]. The HIF-VHL-Elongin C complex may be stabilised by spermidine/spermine N^1-acetyltransferase 2 (SSAT2)[122]. Recruitment of the E3 ubiquitin ligase complex[123] and subsequent polyubiquitination of HIFα targets the protein for degradation by the proteasome[124].

Under hypoxic conditions oxygen becomes a limiting factor for the activity of PHD enzymes and unhydroxylated HIFα translocates to the nucleus[125], where HIFα subunits form heterodimers with HIFβ paralogues[126]. Both HIF1α and HIF2α heterodimerisation with HIF1β has been observed experimentally[127]. Formation of HIFα and HIFβ heterodimers, by interaction of the beta helix loop helix (bHLH) and Per Arnt Sim (PAS) domains, is essential for HIF transcriptional activity[128], through binding of specific DNA sequence known as hypoxic response elements (HREs). The HRE contains two distinctive structures; a HIF binding site with the consensus sequence (A/G)CGTG[129] and a HIF ancillary sequence[130] thought to recruit alternate transcription factors.

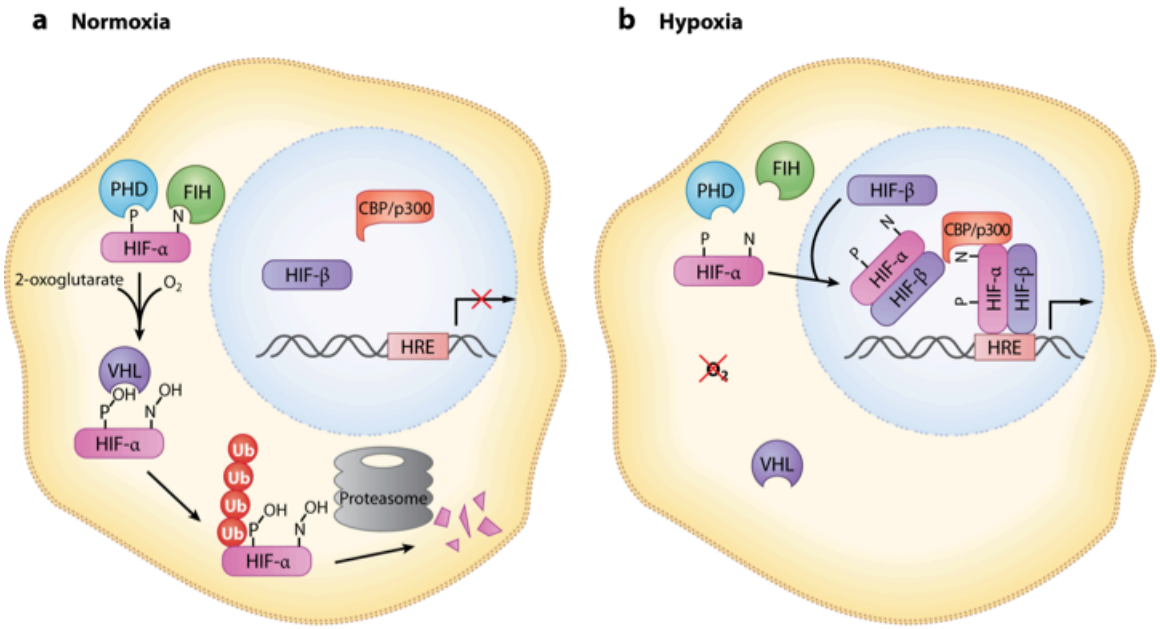

Figure 1.9 Regulation of HIF1α transcriptional activity

(a) Under normoxic conditions HIFα subunits are hydroxylated by PHD and FIH in an oxygen and 2-oxoglutarate dependent manner. Recruitment of VHL to hydroxylated HIFα results in ubiquitination and subsequent proteasomal degradation. (b) During periods of hypoxia in which oxygen is limited HIFα remains unhydroxylated and translocates to the nuclear. Nuclear HIFα forms heterodimers with HIFβ and recruits the co-activators CBP/p300 necessary for initiation of transcription. Adapted from[131].

1.7 Prolyl hydroxylase domain proteins

The prolyl hydroxylase domain proteins (PHDs), also known as HIF prolyl hydroxylases, form part of a wider family of 2-oxoglutarate (2-OG) dependent dioxygenases[107, 132, 133]. PHD enzymes require the co-substrates oxygen and 2-OG in order to hydroxylate target proteins. In addition the enzyme requires both iron and ascorbate as co-factors[120, 134]. The dependence of PHD enzymes on molecular oxygen provides a novel mechanism for cellular oxygen sensing. In humans and mice three PHD isozymes have been identified (PHD-1-3)[135].

The domain architecture of the PHD isozymes has yet to be fully characterised. The highly conserved C-terminus has a double stranded beta helix (DSBH) motif, which is likely to confer enzymatic activity[136]. The function of the divergent N-terminus has yet to be elucidated, but may contribute to isoform conformation, localisation or target selectivity[135]. The crystal structure of PHD2 complexed with the HIFα ODDD has afforded considerable insight into the hydroxylation mechanism[137]. It has been hypothesised that binding of 2-OG and molecular oxygen to conjugated Fe^{2+}, resulting in the formation of Fe^{3+} or Fe^{4+}, primes the active site for target hydroxylation[137]. Additionally, hydroxylation of proline within the HIFα ODDD may alter residue conformation so as to allow binding of VHL and recruitment of the ubiquitin ligase complex[68].

Measurements of PHD enzyme kinetics are consistent with a role for these enzymes in oxygen sensing. All three isozymes have a high Km for oxygen in the range of 230-250μM[138]. PHD enzyme Km values exceed intracellular oxygen concentrations ensuring that activity is oxygen sensitive. PHD enzymes hydroxylate proline residues 402 and 564 of HIF1α (Fig 1.10)[120, 139]. The C-terminal residue, Pro564, was found to be hydroxylated efficiently by all isozymes whereas the N-terminal residue, Pro402, was less readily hydroxylated by PHD1 and PHD2 and not was not detected with PHD3[138]. More recently, an additional member of the PHD family has been identified, PHD-transmembrane (PHD-TM), which also hydroxylates prolines present inHIF1α with a preference for the C terminal residue[140]. Under normoxic conditions both proline residues are likely to be hydroxylated. A comparison of residue hydroxylation has proposed that loss of hydroxylation is dependent on the

severity of hypoxia[141]. Under decreasing levels of hypoxia hydroxylation of Pro402 was found to be lost first, followed by Pro564[141].

Analysis of PHD isozyme expression at the gene level reveals that all three isoforms are fairly ubiquitously expressed with high levels of *Phd1* in the testis, with *Phd2* and *Phd3* greatest in heart and skeletal muscle[142]. At the protein level PHD1 has been detected in the testis, skeletal muscle and spleen, while PHD2 and PHD3 expression was observed in the liver, spleen, kidney, skeletal muscle and heart[143-145]. Subcellular localisation of PHD isoforms has been examined in cells transfected with PHD-GFP constructs[146, 147]. PHD1 protein was localised exclusively in the nucleus whereas PHD2 and PHD3 protein expression was located in both the nucleus and cytoplasm. Cells expressing a PHD2 mutant unable to translocate to the nucleus, demonstrate impaired HIF1 α degradation under normoxic conditions which suggests that translocation affects the activity of this isoform[148].

The factors that contribute to basal levels of PHD isozyme expression are not fully understood. Estrogen signalling and the HIF target gene *Epo* have been found to stimulate expression of *Phd2*[149, 150]. Transcription of PHD isoforms may also be regulated by HIF as both *Phd2* and *Phd3* contain HREs within their respective promoters[97, 98]. This HIF regulated PHD expression may form part of a negative feedback loop, whereby increased expression of PHD isozymes under hypoxic conditions primes cells for reoxygenation, allowing rapid degradation of newly synthesised HIFα. As the posttranslational level PHD1 and PHD3 protein may be subject to proteasomal degradation under hypoxic conditions as both are targets for polyubiquitination by the ubiquitin ligase Siah2[151].

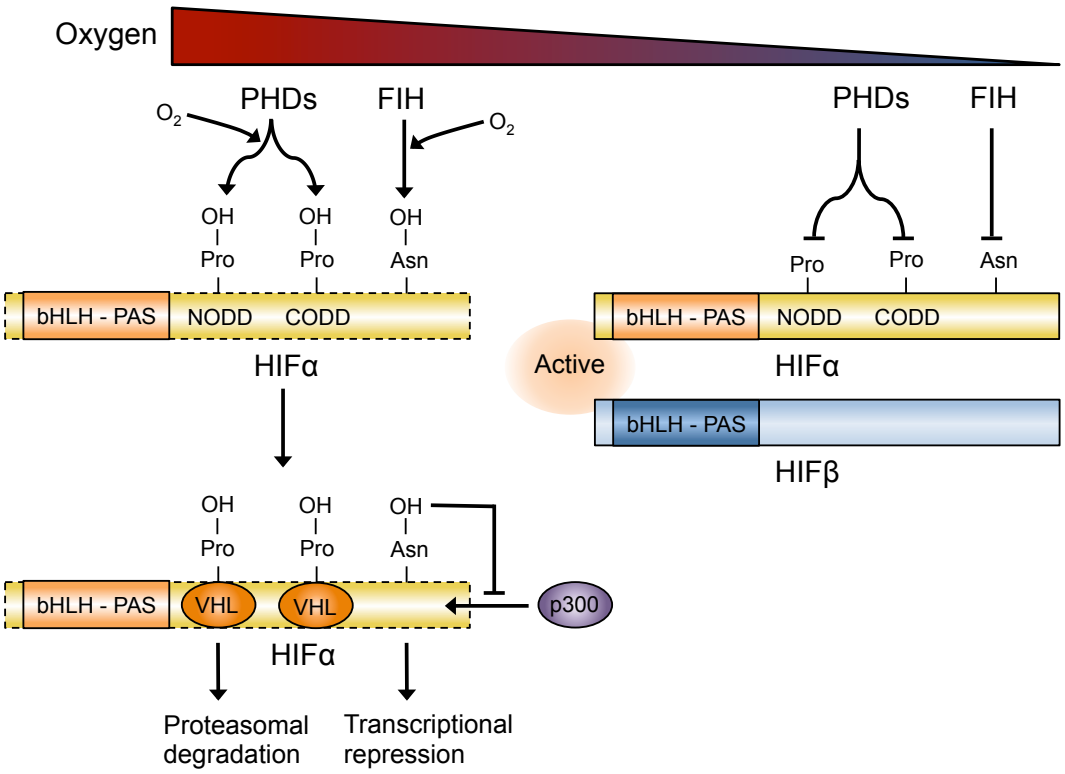

Figure 1.10 PHD mediated hydroxylation of HIFα

Under normoxic conditions PHD enzymes hydroxylate target proline residues present in HIFα (HIF1α Pro402 and Pro564) targeting these subunits for proteasomal degradation. HIFα subunits are also subject to hydroxylation by FIH at a specific asparagine residue (HIF1α Asn803) that prevents recruitment of the transcriptional coactivator CBP/p300. Under hypoxic conditions PHD and FIH enzymes are inactive leaving HIFα subunits free to translocate to the nucleus. Adapted from[152].

Regulation of HIFα isoform degradation is considered a major role of PHD isozymes. Additional targets of PHDs have been identified by the presence of conserved prolyl hydroxylation consensus sites. Inhibitor of nuclear factor kappa-B kinase subunit beta (IKKB) contains a putative prolyl hydroxylation consensus sequence proximal to a phosphorylation site[153]. IKKB is a potent activator of NF-κB and could therefore mediate the transcription of numerous inflammatory genes, including chemotactic cytokines and growth factors that might influence thrombus resolution[154]. Hydroxylation at this site has yet to be confirmed, although *Phd1* gene silencing results in an acute increase in IKKB activity[153].

1.7.1 PHD1

PHD1 is a 44kDa protein encoded by the *Egln2* gene (referred to as *Phd1*) present on chromosome 19 in man. Constitutive homozygous *Phd1* gene knockouts appear to develop normally[155]. However, PHD1 has been found to mediate a number of cellular processes *in vitro* and *in vivo*. PHD1 is an important regulator of cell cycle progression through hydroxylation of a novel target Cep192, a protein involved in centriole formation during metaphase[156]. PHD1 also acts as a key mediator of cellular metabolism, *Phd1* gene deletion results in increased cellular glycolysis and tolerance to tissue hypoxia in a HIF2α dependent manner[144]. Interestingly, knockdown of PHD1 protein expression serves to limit oxidative stress-induced neuronal cell death[157]. Taken together these findings suggest that the loss of PHD1 may help limits oxidative damage through a shift towards anaerobic respiration.

1.7.2 PHD2

PHD2 is a 46kDa protein encoded by the *Egln1* gene (referred to as *Phd2*) present on chromosome 1 in man. Post-transcriptional modification of *Phd2* mRNA results in the generation of a number of splice variants with loss of exon 3 resulting in loss of catalytic activity[138]. Unlike PHD1, constitutive homozygous *Phd2* gene knockouts demonstrate embryonic lethality dying at E12.5 as a result of severe heart and placental defects[155]. Lethality of mice deficient for PHD2 reaffirms the importance of this isoform in the regulation of HIFα subunit stability. However, abnormalities in myocardial development appear to take place in a HIF1α independent manner suggesting other regulatory activities for this isoform[155].

PHD2 is an important mediator of tissue oxygenation through regulation of angiogenesis. Knockdown of PHD2 protein expression alters a number of angiogenic processes including vessel formation and normalisation[158, 159]. *In vitro* studies suggest that increased angiogenesis after PHD2 knockdown is mediated by both HIF1α and NFkB[158, 159]. Heterozygous *Phd2* gene knockouts did not demonstrated increase vessel formation, instead improving vessel structure through HIF1α dependent upregulation of sVEGFR1 and VE cadherin[160].

PHD2 has also been found to protect the brain during periods of cerebral ischaemia. In a murine model of mid cerebral artery occlusion (MCAO), constitutive heterozygous *Phd2* gene deletion, but not homozygous deletion of *Phd1* and *Phd3*, significantly reduced infarct size and was associated with increased capillary density[161]. A study of cerebral ischaemia in neuron-specific homozygous *Phd2* knockouts suggests that neuronal loss of PHD2 was strongly cerebroprotective independent of capillary density[162]. In conditions of hyperoxia, as opposed to hypoxia, inducible homozygous deletion of *Phd2* was found to protect retinal microvasculature[163].

PHD2 also affects macrophage heterogeneity. *Phd2* gene deletion in a murine model of critical limb ischemia results in increased numbers of alternatively activated (M2) macrophages, with pro-angiogenic potential, that accumulate in the ischaemic tissue[164]. Ang1 has been proposed as an endogenous inhibitor of *Phd2* gene expression resulting in skewing of macrophages towards an M2 phenotype[165]. Interestingly, no difference in macrophage skewing occurs in PHD2 deficient tumours, indicating that cell phenotype may be influenced by differences in the hypoxic micro-environment[166].

Abnormalities in PHD2 are strongly associated with familial erythrocytosis in which patients present with elevated erythrocyte counts and an increased haematocrit[131]. A number of loss in function mutations in *Phd2* have been identified that induce erythrocytosis through elevated production of the HIFα target gene EPO[105, 167, 168]. In murine *Phd2* gene knockouts complementary increases in EPO expression and haematocrit have been observed[143, 169, 170].

1.7.3 PHD3

PHD3 is a 27kDa protein encoded by the *Elgn3* gene (referred to as *Phd3*) present on chromosome 14 in man. Two splice variants of *Phd3* have been identified with excision of exon 1 resulting in loss of catalytic activity[138, 171]. Deletion of *Phd3* is tolerated in mice with no apparent embryonic abnormalities observed[155].

PHD3 expressed in macrophages has been found to contribute to phenotypic skewing of this cell type. Loss of PHD3 in peritoneal macrophages results in increased expression of proinflammatory markers, consistent with classical (M1) activation[172]. PHD3 deficient macrophages demonstrate enhanced migration and phagocytosis, mediated by both HIF1α and NFkB[172]. However, there is conflicting evidence as skewing of monocytes towards an M1 phenotype results in high levels of PHD3 protein expression, whereas PHD3 expression is almost completely absent in alternatively activated (M2) macrophages[173]. Macrophages deficient in PHD3 also demonstrate enhanced cell survival *in vitro* independent of HIF1α stabilisation[174].

PHD3 is also expressed in neutrophils and potently upregulated in response to hypoxia[175]. PHD3 deficient neutrophils demonstrated reduced survival in a model of inflammation, however migration and phagocytosis were preserved[175]. The anti-apoptotic activity of PHD3 is surprising given that HIF1α and HIF2α both promote neutrophil survival during inflammation[111, 176]. An additional role for PHD3 has recently been identified in regulating lipid and glucose handling. *Phd3* gene deletion in the liver was found to confer improved insulin sensitivity and glucose homeostasis providing protection against diet induced diabetes[177].

1.7.4 Factor Inhibiting HIF

Factor inhibiting HIF (FIH) is a highly related 2-OG dependent dioxygenase targeting HIFα subunits for hydroxylation at specific asparagine residues[178, 179]. FIH is a 40kDa protein encoded by the *Hif1an* gene present on chromosome 10. Unlike PHD proteins, FIH mediated hydroxylation of HIF1α results in transcriptional inactivation as opposed to proteasomal degradation[180, 181]. FIH is expressed in a broad range of tissues and deletion during embryogenesis results in an elevated metabolism and resistance to diet induced weight gain[182].

As well as hydroxylating HIFα subunits FIH also targets a number of ankyrin repeat domain-containing proteins. As with PHD isoforms FIH activity has been found to modulate NFkB signalling through oxygen dependent hydroxylation of IKKB although the functional consequence of this modification remains unclear[183]. Additionally, FIH has been found to hydroxylate members of the Notch family of receptors[184, 185]. Hydroxylation by FIH at two sites in the Notch

intracellular domain significantly repressed activity of the receptor providing evidence of oxygen-dependent regulation in Notch signalling[185]. A further target of FIH, ankyrin repeat and SOCS box protein 4, undergoes poly-ubiquitination and proteolysis upon hydroxylation suggesting that FIH also has the capacity to target proteins for proteasomal degradation[186]. The extent of FIH mediated hydroxylation of target proteins other than HIF and the contribution of this to the observed FIH knockout phenotype has still to be determined.

1.8 HIF1α gene therapy

Developments in adenoviral mediated gene delivery have enabled the generation and delivery of degradation resistant HIF1α constructs *in vivo*. The CA5 construct is protected from hydroxylation and subsequent proteasomal degradation by deletion of residues 392-520 and two mis-sense mutations (Pro567Thr and Pro658Gln)[187]. Production of degradation resistant HIF1α by the CA5 construct enables transcription of HIF1α target genes in normoxic or marginally hypoxic tissues. The therapeutic effects of CA5 have been explored in a variety of disease models using multiple gene delivery mechanisms. In a rabbit model of hind limb ischaemia, adenoviral expression of CA5 (AdCA5) was found to improve angiogenesis and restore blood flow to the ischaemic limb inducing expression of pro-angiogenic factors including VEGF, PlGF and MCP-1[188]. On further investigation AdCA5 transfection was found to mobilise angiogenic cells of leukocyte origin into the circulation in a HIF1α dependent manner[189]. Transfection of AdCA5 into the ischaemic limb of mice improved limb perfusion accompanied by a marked increase in vessel density consistent with the pro-angiogenic activity of HIF1α[190] and was superior to transfection of adenoviral VEGF in restoration of limb perfusion[191].

An initial small-scale trial of AdCA5 injection into the limbs of patients with severe critical limb ischaemia has reported beneficial outcomes. In 14 out of 32 patients rest pain resolved and 5 out of 18 patients had complete ulcer healing after treatment with AdCA5[192]. Empty vector controls were not used in this study, which was a significant limitation. While these studies demonstrate the therapeutic potential of increased HIF1α stabilization transfection of murine

venous thrombi with AdCA5 failed to improve resolution[79]. The therapeutic potential of a HIF2α constitutively active variant has yet to be investigated.

1.9 Pharmacological PHD inhibition

Inhibition of PHD enzymes using a range of pharmacological agents has proved effective in protecting tissues in a range of ischaemic disorders. PHD inhibitors, in general, fall into one of four main classes; (i) iron chelators, (ii) 2-OG mimetics or (iii) active site blockers. Some inhibitors may satisfy the requirements of multiple classes (Table 1.2). These inhibitors demonstrate varying degrees of enzyme specificity and efficacy and affect a range of biological processes, some of which may be highly pertinent to thrombus resolution.

1.9.1 Angiogenesis

HIF1α transcriptional targets include a number of pro-angiogenic factors including VEGFA, VEGFR1, eNOS and iNOS. The ability of PHD inhibition to stimulate therapeutic angiogenesis has been is of considerable interest. A number of PHD inhibitors, including deferoxamine (DFO), TM6008 and TM6089, have been found to increase endothelial cell tubule formation *in vitro* [193-195]. *In vivo* hydralazine, TM6008 and TM6089 treatments enhanced formation of neovascular channels in a sponge model of angiogenesis[194, 196]. In addition the PHD inhibitor hydralazine was also found to increase circulating levels of VEGF measured in the plasma[196]. Dimethyloxalylglycine (DMOG) treatment in a murine model of critical limb ischaemia significantly increased capillary fibre ratio, a measure of angiogenesis, and expression of VEGFA and VEGFR1[197].

Recruitment of bone marrow-derived angiogenic cells (BMDAC) to the ischaemic limb is thought to be an important component of angiogenesis[198]. Injection of DMOG treated BMDACs into the ischaemic limb has proven insufficient to promote angiogenesis[199]; whereas injection of DMOG treated BMDAC in conjunction with adenoviral overexpression of constitutively active HIF1α in the ischaemic limb increases functional recovery and limb salvage

when compared to HIF1α transfection alone[199]. Increased β2 integrin expression was observed after treatment of BMDAC with DMOG in vitro[199], which suggests BMDACs may have a role in angiogenesis through increased endothelial cell adhesion.

1.9.2 Ischaemia protection

The ability of PHD inhibitors to precondition tissues in advance of an ischaemic insult has also been investigated. Pharmacological preconditioning with the PHD inhibitor DMOG in a rabbit model of myocardial infarction significantly reduced infarct size[200]. Both *in vivo* and *in vitro* studies found DMOG pretreatment results in increased HIF1α stabilisation, induction of IL-10 protein expresssion and reduced production of IL-8, suggesting that HIF1α may be an important modulator of the inflammatory response within the ischaemic myocardium[200, 201].

Similar protective effects of increased HIF1α stabilisation were observed in a murine model of myocardial infarction after treatment with DMOG alone or in conjunction with *Phd2* gene knockdown[202]. Gene silencing identified PHD2 as the main isoform involved in HIF1α stabilisation within the ischaemic myocardium[202]. Preconditioning via either approach was ablated when combined with gene silencing of HIF1α suggesting that the protective effects of DMOG are dependent on HIF1α stabilisation. DFO also significantly reduced infarct size in a murine model of myocardial infarction[203]. Increased oxygen radical accumulation was observed in the myocardium pre-treated with DFO indicating that PHD inhibition may promote oxidative stress. Recently a novel PHD inhibitor, GSK360A, that acts as a competitive inhibitor of 2-OG at the PHD active site was found to be cardioprotective in rat models of both myocardial infarction and ischemia reperfusion injury[204, 205].

Pre-treatment with the PHD inhibitor, FG-4487 in a murine model of renal ischaemia reperfusion injury was found to preserve kidney function[206], suggesting that PHD inhibition protects against reperfusion injury. The inhibitors l-mimosine and DMOG have also been used in the same model and provide similar levels of protection[207]. Further examination of the protective mechanism provided by DMOG pretreatment identified iNOS as a key mediator with

pharmacological blockade of iNOS ameliorating the observed renal protection[208].

A wide range of PHD inhibitors have also been found to confer protection against cerebral ischaemia. DMOG, DFO, Compound A and Ethyl 3,4-dimethylbenzoate (3,4-DHB) have all been found to limit infarct size in rat models of cerebral ischaemia, accompanied by consistently increased HIF1α stabilization and induction of target genes including *Vegf*, *Enos* and *Epo*[209-212].

Table 1.2 Small molecule PHD inhibitors

Inhibitor	Mechanism	Specificity (IC50)	Application	Refs
Dimethyloxalylglycine	2-OG Mimetic	PHD, FIH, CPH	Ischaemic disorders	197, 202, 213-215
Deferoxamine	Fe^{2+} Chelator	Fe2+ dependent enzymes	Ischaemic disorders	203, 210, 216-219
Ethyl 3,4-dimethylbenzoate	Active Site, Fe^{2+} Chelator	PHD2 (330 μM), PHDs, FIH	Ischaemic disorders	210, 213, 216, 220
FG-0041	Active Site, Fe^{2+} Chelator	PHDs, FIH*, CPH (2 μM)	Myocardial Ischaemia	221
FG-2216	Not described	PHD, CPH	Anemia	222, 223
FG-2229	Active Site, Fe^{2+} Chelator	PHDs, FIH*, CPH (1 μM)	Ischaemic disorders	224
FG-4383	2-OG Mimetic	PHD2 (2.6μM) FIH*	Anemia	225
FG-4497	Active Site	PHDs, FIH*	Kidney Failure	226
GSK360A	2-OG Mimetic	PHDs (10-120nM)	Myocardial Ischaemia	204, 205
TM-6008	Active Site, Fe^{2+} Chelator	PHD2 (0.57 μM), PHDs*, FIH*	Ischaemic disorders	194
TM-6089	Active Site	PHDs (not determined), FIH*	Ischaemic disorders	194
JNJ-42041935	2-OG Mimetic	PHDs, PHD2 (100-117nM)	Anemia	227, 228
Compound A	Active Site	PHD2 (3.8 μM), PHDs*, FIH	Cerebral Ischaemia	210, 229
l-Mimosine	Fe^{2+} Chelator	PHD, CPH and others (455 μM)	Kidney Failure, DVT	57, 210, 230
AKB-4924	Fe^{2+} Chelator	PHDs, PHD2 (14 μM)	Inflammation	231-234

*Inferred activity, adapted from[152]

1.9.3 Inflammation

There is an increasing body of evidence to suggest that PHD inhibition may be effective in limiting the cellular response to inflammation. In murine models of drug induced colitis treatment with DMOG, FG4497 and AKB-4924 markedly reduced inflammatory damage to the bowel[215, 233-236]. The reduced severity of colitis after PHD inhibitor treatment is probably a result of increased epithelial cell survival and reduced production of pro-inflammatory cytokines including IL6 and IL8[233, 236].

1.9.4 Erythrocytosis

Numerous PHD inhibitors including; DMOG, FG-2216, FG-4497, GSK360A and JNJ42041935, have been found to potently increase measurements of haematocrit[202, 204, 227, 237, 238]. Corresponding with PHD knockout studies this is accompanied by sustained induction of EPO expression[105, 167, 168]. Increased haemoglobin concentrations and erythrocyte counts further supports the erythrocytosis-inducing properties of these agents. Sustained treatment with DFO in patients with erythropoiesis significantly improved haematocrit levels highlighting this approach as a potential therapy for anemia[239, 240].

1.10 Rationale

The early venous thrombus has been identified as an acute source of tissue hypoxia, correlating with stabilisation of the pro-angiogenic transcription factor HIF1α[57]. Increasing nuclear accumulation of HIF1α in the thrombus by treatment with the broad activity PHD inhibitor l-mimosine accelerated resolution and was accompanied by increased neovascular channel formation and macrophage recruitment[57]. The generation of PHD specific gene knockouts has enabled the contribution of individual isoforms to be assessed in vivo. PHD2 has been identified as a critical regulator of HIF1α stability[241] with gene deletion resulting in increased angiogenesis and recruitment of myeloid cells[158]. A number of new PHD inhibitors have been developed that offer improved target specificity.

1.11 Hypothesis and aims

It was hypothesised that PHD enzyme expression in the resolving thrombus limits HIF1α stability and that inactivation of PHD enzyme activity would accelerate venous thrombus resolution in a HIF1α dependent manner.

This study sought to determine:

(i) the expression of PHD1, PHD2 and PHD3 at the gene and protein level during natural thrombus resolution

(ii) the effect of gene specific deletion of *Phd2* on thrombus resolution

(iii) the effect of pharmacological pan-PHD inhibition on thrombus resolution

(iv) the requirement of endogenous VEGFR signalling for thrombus resolution.

Chapter 2 Characterisation of venous thrombus resolution in a murine model

2.1 Introduction

A number of murine model have been developed to study venous thrombus resolution *in vivo*[242]. The development of these models have been necessitated by ethical barriers to studying thrombus resolution in man and the failure of *in vitro* models to sufficiently recapitulate the complexity of this disease. Murine models of venous thrombosis are primarily induced by the manipulation of a Virchow's triad.

Ferric chloride induced endothelial dysfunction has proven an effective method in the induction of venous thrombi in both the femoral veins and IVC[243-245]. Application of ferric chloride was initially thought to cause localised endothelial denudation[246], however, in a recent study endothelial integrity was preserved in the presence of thrombus[247]. An electrolytic IVC model (EIM) that passes direct current across the vessel wall also results in efficient thrombus formation[248, 249]. The EIM model stimulates thrombogenesis by inducing endothelial dysfunction and localised endothelial denudation. Consistent thrombus weights have been reported, however, this model is hindered by the relatively small thrombi produced and a lack of detailed characterisation.

Ligation of the inferior vena cava (IVC) is another commonly used model of venous thrombosis[42, 250, 251]. Formation using this model, while highly efficient, takes place in the absence of flow that is likely to affect structure and cellular composition. Alternatively, a number of studies have used stenosis of the IVC, which permits residual blood flow through the vessel, to induce thrombosis[250, 252-254].However, the major limitation of this surgical technique is the highly variable formation efficiencies reported (45-100%)[255].

The St Thomas' model of IVC thrombosis is highly efficient resulting in thrombus formation in over 90% of surgeries. This model satisfies two tenants of Virchow's triad, namely reduced blood flow and endothelial dysfunction, which may account for the high efficiency of thrombus induction. Thrombi formed are lamina in structure, with layers of erythrocytes and leukocytes (lines of Zahn), which closely resembles thrombi found in man[256].

This chapter was intended to provide further data on the dynamics of thrombus resolution in the St Thomas' model and inform the selection of time-points for interventional studies. Additionally, it provided the opportunity to quantify changes in the composition of the thrombus.

2.2 Aim

To characterise changes in thrombus size, vein recanalisation, and thrombus organisation (fibrin, collagen and red cell content) during venous thrombus resolution in the St Thomas' model of IVC stenosis.

2.3 Methods

2.3.1 The St Thomas' model of venous thrombosis

All animal work was carried out in accordance with the Animal (Scientific Procedures) Act 1986. BALB/c mice 8-10 weeks in age were anaesthetised with isoflourane (5%, 1.0 l/min O_2) in an induction chamber (VetTech, UK). The abdomen was shaved, disinfected (0.05% w/v chlorhexidine gluconate, Medlock Medical, UK) and draped (Kruuse, Denmark) in preparation for surgery. A midline laparotomy was made, extending anteriorly until the xiphoid process. The intestines were externalised and wrapped in wetted gauze. Blunt dissection with cotton swabs was used to reveal the retroperitoneal structures. Under microscopic visualisation (S6D, Leica, Germany) the inferior vena cava (IVC) was mobilised and separated from the aorta by blunt dissection. A length of 4-0 silk suture material (Ethicon, UK) was passed behind the IVC inferior to the left renal vein (Fig 2.1A). A length of 5-0 prolene suture material (Ethicon, UK) was placed on the IVC longitudinally prior to constriction of the IVC by tying of the silk suture (Fig 2.1B). The prolene was removed to generate the required level of stenosis (~90%). A neurovascular surgical clip (Fine Scientific Tools, Germany) was applied to the IVC inferior at two locations distal to the site of stenosis for 20secs. The bowels were internalised and perioperative buprenorphine (Vetergesic, Alstoe, UK) administered to the wound edge and peritoneal cavity. Layered closure of the laparotomy with 4-0 polydiaxanone suture material (Ethicon, UK) was achieved using continuous sutures for the peritoneal and skin layer. Postoperatively animals were housed in a warmed recovery chamber (25°C) overnight.

2.3.2 Tissue processing

Thrombi were excised *in situ* with the surrounding inferior vena cava and fixed in 10% formyl saline overnight (VWR, UK) for histological analyses. Samples were processed (TP1020 tissue processor, Leica, Germany) and embedded in paraffin wax (TES99 tissue embedder, Medite, Germany). Transverse sections (5μm) were cut at 500μm intervals throughout the entire length of the thrombus for subsequent histological staining and analysis.

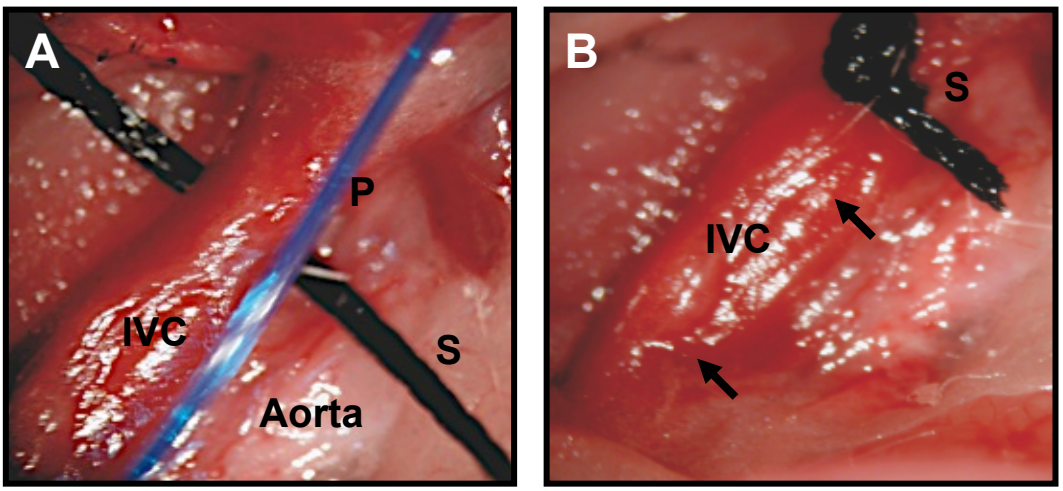

Figure 2.1 Surgical induction of venous thrombosis

(A) Dissection between the IVC and aorta distal to the right renal vein allows passage of the silk suture (S) between the vessels. The silk suture is tied onto a piece of prolene suture (P) placed alongside the IVC which once removed generates a stenosis. (B) Endothelial dysfunction is induced by application of a neurovascular clip to regions of IVC distal to the site of stenosis (indicated by black arrows).

2.3.3 Martius scarlet blue (MSB) staining

I would like to acknowledge Mr Prakash Saha for assistance with MSB staining.

The composition of the thrombus was assessed by MSB. Sections were warmed for 30mins at 60^{o}C and were then dewaxed by 2x 5min xylene washes. Sections were rehydrated through graduated alcohol washes (100%, 75% and 50%) and rinsed in tap water for 5mins. Sections were pretreated with Bouin's solution (5% v/v acetic acid, 9% w/v formaldehyde, 0.9% v/v picric acid, Sigma, UK) at 60°C for 1hr. All staining was conducted at room temperature unless otherwise stated. Nuclei were counterstained with Mayer's haematoxylin (Clintech, UK) for 5mins and washed in distilled water for 5mins. Sections were stained in martius yellow (2% w/v phosphotungstic acid, 0.5% w/v Martius yellow in 95% v/v ethanol, Sigma, UK) for 2mins and washed in distilled water. Sections were stained with brilliant crystal scarlet (1% w/v crystal ponceau 6R in 2% v/v acetic acid, Sigma, UK) for 10mins and washed in distilled water. Staining was differentiated in a solution of 1% w/v phosphotungstic acid (Sigma, UK) for 10mins and washed in distilled water. Sections were then stained in analine blue (2% w/v in 1% v/v acetic acid, Sigma, UK) for 10mins and washed

in distilled water. Sections were rapidly dehydrated through graded alcohols (50%, 75% and 100%) to avoid loss in stain intensity. Slides were cleared in xylene and mounted with coverslips in DPX medium.

2.3.4 Haematoxylin and eosin staining

Sections were dewaxed and rehydrated as described in section 2.2.3. Sections were then stained in Mayers haematoxylin (Clin-Tech, UK) for 5mins followed by 5mins washing in running tap water. Staining was differentiated in 1% v/v acetic acid (Sigma, UK) in 100% alcohol (Sigma, UK) for 3secs, followed by a further 5min wash in running tap water. Sections were stained in eosin (Clin-Tech, UK) for 2mins and washed in running tap water for 30secs. Sections were dehydrated, cleared and mounted as described in Chapter 2.2.3.

2.3.5 Image analysis

Images were captured at either 50x or 200x magnification with a Leica light microscope (DMRB, Leica, Germany) using a microscope mounted digital camera (Micropublisher 3.3, QImaging, Canada) on a motorised stage (ProScan, Datacell, UK). Histogram-based thresholding with Image Pro Plus software (Media Cybernetics, UK) was used to select areas of staining[257]. Measurements of thrombus cross-sectional area were obtained using Image Pro Premier software (Media Cybernetics, UK) from which thrombus volume were reconstructed.

2.3.6 Statistical analysis

Normality of data was assessed by Kolmogorov-Smirnoff tests to inform selection of appropriate parametric and non-parametric tests. Differences in measurements of thrombus volume and vein lumen were assessed by one-way analysis of variance (1-way ANOVA) and post-hoc Bonferroni. Differences in measurements of thrombus cross-sectional area and composition were assessed by Kruskal-Wallis. In all cases $P<0.05$ was considered statistically significant. Statistical analyses were conducted using Prism Software (v5, Graphpad, USA). Parametric data represented as mean ± SE and non-parametric data presented by individual data points with median.

2.4 Results

To evaluate the dynamics of thrombus resolution histological measurements of thrombus volume and vein lumen recanalisation were made at days 1, 7, 14 and 21 post-induction. Thrombus volume decreased significantly over time ($P<0.0001$, 1-way ANOVA, Fig 2.2A) with thrombus volume significantly less at days 14 and 21 than at days 1 and 7 ($P<0.05$, post-hoc Bonferonni). Vein lumen recanalisation increased significantly over time ($P<0.0001$, 1-way ANOVA, Fig 2.2B) with vein lumen recanalization significantly greater at days 14 and 21 than at days 1 and 7 ($P<0.05$, post-hoc Bonferonni).

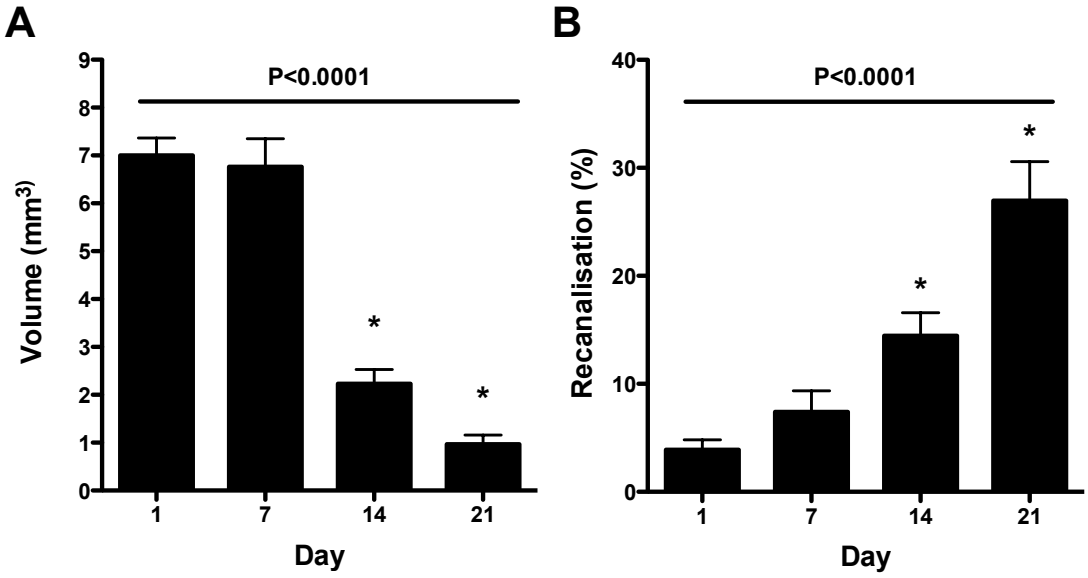

Figure 2.2 Changes in thrombus volume and vein lumen recanalisation
Histological measurements of (A) thrombus volume and (B) vein lumen recanalisation at days 1, 7, 14 and 21 post-induction (n=5 /group /time-point). Thrombus volume decreased and vein lumen increased significantly over time ($P<0.0001$, 1-way ANOVA). Data represented as mean ± SE. *$P<0.05$ day1 vs day14, day1 vs day21, day7 vs day14, day7 vs day 21.

A marked degree of heterogeneity in thrombus cross-sectional area was apparent when analysing sections taken throughout the length of the thrombus. To appreciate the scale of this heterogeneity measurement of thrombus cross-sectional areas were made at days 1, 7, 14 and 21 post-induction. Median thrombus cross-sectional area was found to decrease significantly with time (P<0.0001, Kruskal-Wallis, Fig 2.3-2.4). MSB staining revealed the changing composition of the resolving venous thrombus with significant changes in the erythrocyte, fibrin and collagen content during resolution (P<0.0001, Kruskal-Wallis, Fig 2.5-2.6).

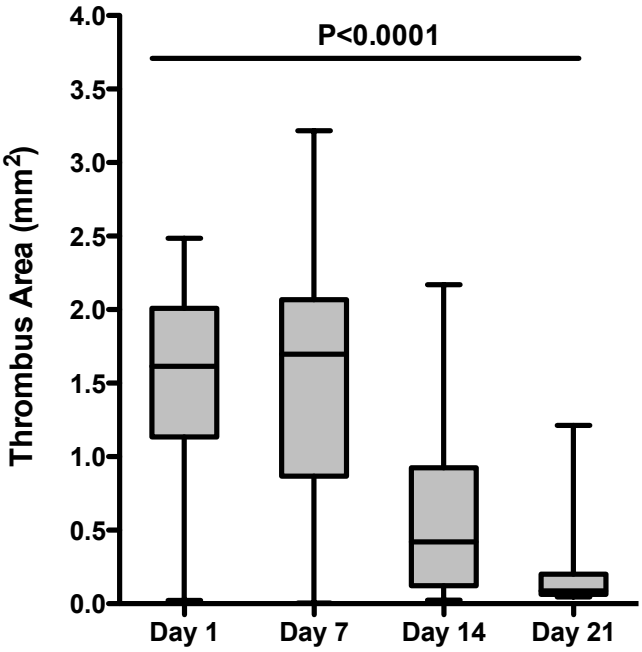

Figure 2.3 Heterogeneity in thrombus cross-sectional area

Thrombus cross-sectional area (n=32-37 /time-point) at days 1, 7, 14 and 21 post-induction was found to decrease significantly over time (P<0.0001, Kruskal-Wallis), data represented by box-and-whisker plots (median, interquartile range, range).

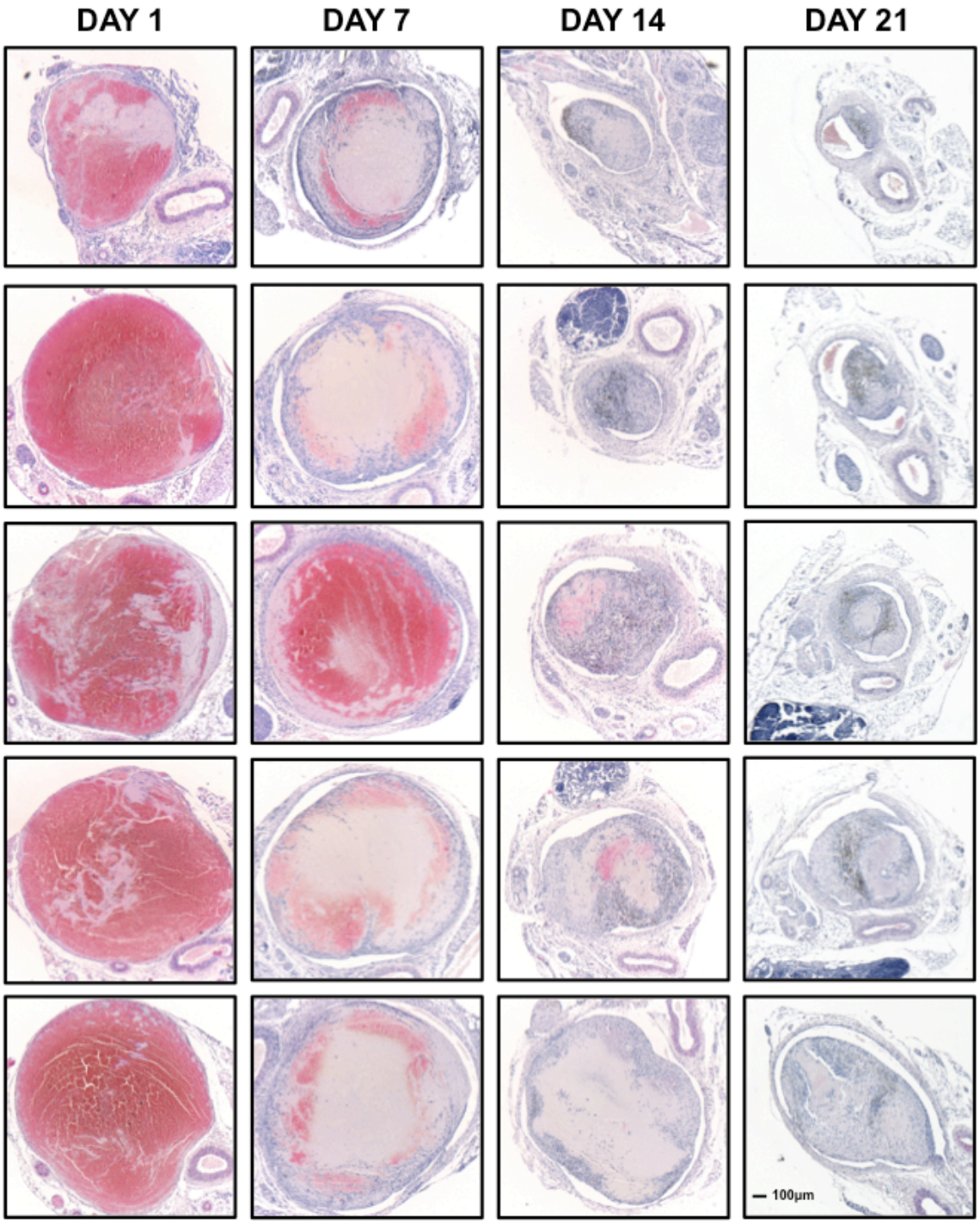

Figure 2.4 Representative H&E stained thrombus micrographs

Representative H&E stained micrographs of thrombus at days 1, 7, 14 and 21 post-induction demonstrating the degree of thrombus heterogeneity. Heterogeneity was particularly evident in thrombus at 14 and 21 days post-induction.

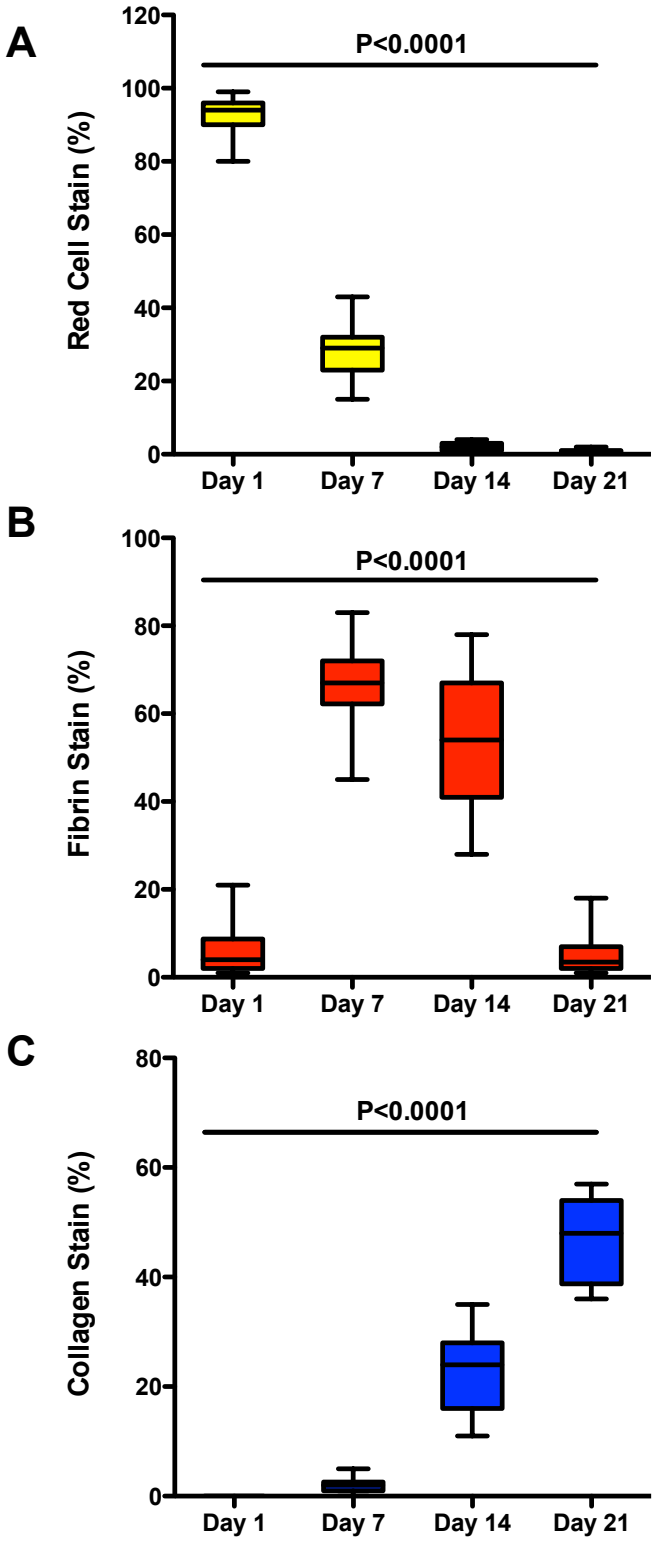

Figure 2.5 Thrombus red cell, fibrin and collagen content

Thrombus sections (n=12-42 per time-point) at days 1, 7, 14 and 21 post-induction stained with MSB were segmented and their respective (A) red cell, (B) fibrin and (C) collagen content calculated as a percentage of thrombus area. The content of the thrombus was found to change significantly over time (P<0.0001, Kruskal-Wallis), data represented by box-and-whisker plots (median, interquartile range, range). Adapted from [257].

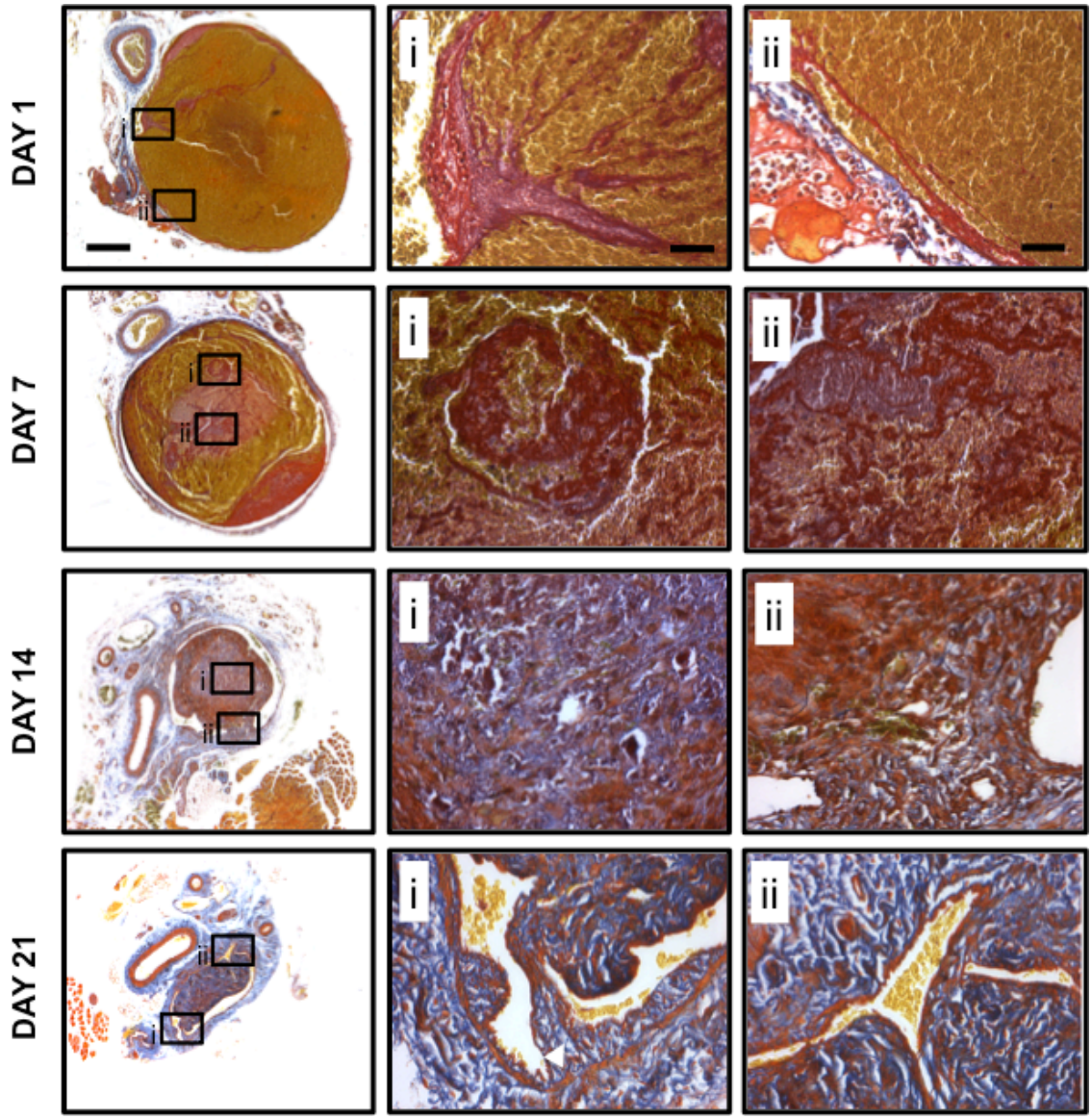

Figure 2.6 Representative MSB stained thrombus micrographs

Representative MSB stained thrombus micrographs at days 1, 7, 14 and 21 post-induction (yellow = erythrocytes, red = fibrin, blue = collagen). Micrographs taken at an original magnification of 50x and 200x with error bars of 200μm and 25μm respectively. Adapted from [257].

2.5 Discussion

Measurements of thrombus volume are consistent with those of previous studies, with thrombus resolution taking in excess of 21 days[32, 257]. The rate of thrombus resolution was most pronounced between days 7 and 14 post-induction (~70%), identifying this as an important time-point for future studies. A notable absence in thrombus resolution was evident between days 1 and 7 post-induction. This could be explained by an initial lag phase in the thrombus resolution. Alternatively, thrombus propagation, reported in both mice and man, may occur post-formation with thrombus volume peaking between these two time-points[254]. However, given observed reductions in erythrocyte content, that would likely form the majority of the propagating thrombus, this is unlikely. A consistent increase in vein lumen recanalisation was also measured. Recanalisation of the lumen, occurring as a result of contraction of the thrombus from the vein wall and possibly some contribution from the coalescence of neovascular channels that appear during organisation of the thrombus, is important for restoration of blood flow through the thrombosed vessel[51, 258].

A number of previous studies of venous thrombus resolution have relied on single representative measures of thrombus cross-sectional area[32, 51]. In this study, it was clear, from the measurement of thrombus cross-sectional area at various points throughout the length of the thrombus, that there is a marked degree of heterogeneity in thrombus area throughout its length. This highlights the difficulty in obtaining reproducible estimates of thrombus resolution by from single measurements of cross-sectional area. Estimate of thrombus volume by measuring cross-sectional area at defined lengths throughout the whole thrombus, provides a more reproducible and accurate measure of thrombus burden[54, 57].

In addition to changes in size the venous thrombus also undergoes extensive remodeling of the extracellular matrix. Quantification of erythrocyte, fibrin and collagen content of the thrombus was achieved by segmentation of MSB stained sections. The acute thrombus was comprised mainly of erythrocytes that were rapidly cleared from the thrombus and were largely absent by day 14. The percentage area of the thrombus stained positively for fibrin peaked

between days 7 and 14 post-induction suggesting fibrin may be deposited or matures after initial thrombus formation. Finally, deposition of collagen within the thrombus increased with time rising from undetectable levels in the day 1 thrombus to cover roughly 50% of the mean thrombus area by day 21. The increasing levels of collagen observed within the resolving thrombus suggest that this process may serve as a useful marker of thrombus organisation.

Chapter 3 PHD gene and protein expression during thrombus resolution

3.1 Introduction

High levels of HIF1α nuclear accumulation and transcriptional activity have been measured in the acute venous thrombus. The scale of HIF1α stabilisation observed has been attributed to poor oxygenation of the early thrombus that results in a marked degree of tissue hypoxia[57]. Reduced thrombus oxygenation is likely to limit the oxygen dependent hydroxylation of HIF1α by PHD enzymes that is required for degradation. As the thrombus resolves and tissue oxygenation improves decreasing levels of HIF1α nuclear accumulation are observed. Improved oxygenation is likely to restore PHD enzyme activity and allow resumption of HIF1α proteasomal degradation.

Three prototypical members of the PHD family of enzymes have been identified encoded by three separate genes; *Egln1*, *Egln2* and *Egln3* (according to accepted convention these genes will be referred to as *Phd2*, *Phd1* and *Phd3* respectively). The expression of *Phd1*, *Phd2* and *Phd3* appears to be fairly ubiquitous[142]. However, expression of their respective protein products; PHD1, PHD2 and PHD3 demonstrates a degree of tissue specificity[143]. At the cellular level PHD protein expression has been observed in a number of cell types present in the resolving venous thrombus in particular, neutrophils and macrophages[173, 176].While HIF1α protein expression has been measured in the resolving venous thrombus, by both enzyme linked-immunosorbent assay (ELISA) and immunohistochemistry, the temporal and spatial expression patterns of PHD isoforms during thrombus resolution have not been determined.

3.2 Aim

To quantify PHD isoform expression in the resolving venous thrombus.

3.3 Methods

3.3.1 Thrombus induction

Thrombus induction was performed as described in Chapter 2.2.1. Thrombi were harvested at days 1, 3, 7 and 11 post-induction (n=5 mice/time point) for analysis by qPCR. Thrombi were harvested at days 1, 3, 7 and 14 post-induction for immunohistochemical (IHC) analysis (n=5 mice/time point). Murine kidney was also collected for use as positive control tissue. For IHC, tissue was processed as described in Chapter 2.3.2. Thrombi separated found surrounding vein wall were harvested at days 1, 3, 7 and 14 post-induction for biochemical analysis by western blotting. Murine kidney, heart, liver, spleen and lung were collected for optimisation of western blotting. For biochemical analysis tissues were snap frozen in liquid nitrogen.

3.3.2 RNA extraction

Thrombi were separated from the IVC and immersed in RNase Zap (Ambion, UK) prior to snap freezing in liquid nitrogen and storage at -80°C. Frozen samples were homogenised in 800µl of Trizol (Invitrogen, UK) using an RNase free microcentrifuge tube homogenisation kit (Anachem, UK) and incubated at room temperature for 10mins. Chloroform (160µl) was added and the sample shaken vigorously for 20secs to achieve phase separation. Samples were incubated on ice for 10mins followed by centrifugation at 10,000g for 15mins at 4°C. The upper aqueous phase was collected into an RNAse free microcentrifuge tube and diluted with one volume of 70% ethanol.

RNA extraction was performed using the RNeasy mini kit (Qiagen, UK) according to the manufacturers instructions. Samples were added to an RNeasy mini-column and centrifuged at 10,000g for 15secs. The eluate was re-applied and the mini-column centrifuged at 10,000g for 15secs. The mini-column was washed with 350µl of RW1 buffer and centrifuged at 10,000g for 15secs. An DNA cleavage step was performed by incubation with 10µl of DNAase (Qiagen, UK) for 15mins at room temperature. The mini-column was washed with 350µl of kit RW1 buffer and centrifuged at 10,000g for 15secs, transferred to a fresh

2ml collection. The column was washed twice with 500µl of kit RPE buffer with a 15sec, 10,000g centrifugation step in between. Eluates were discarded and the silica membrane in the column dried by centrifugation at 10,000g for 1min. RNase free water (33µl, Qiagen, UK) was applied to the mini-column and incubated for 10mins at room temperature. RNA was eluted from the mini-column into an RNase free microcentrifuge tube, by centrifugation at 10,000g for 1min. On extraction RNA was immediately stored at -80°C.

3.3.3 RNA quantification and integrity

The concentration of RNA in the processed samples was measured spectrophotometrically using a NanoDrop 1000 (Thermo Fisher Scientific, USA). The absorbance spectrum of RNA has a single peak with a maximum of 260nm. This spectrum also provides a measure of RNA purity with an absorbance ratio (260nm/280nm) of less 1.8 indicating such as of contaminants including DNA and phenol. RNA integrity was also assessed using a microfluidics chip (RNA 6000 Nano assay, Agilent, Germany) run on a 2100 Bioanalyser (Agilent, Germany) according to the manufacturers instructions, representative RIN analyses provided in Appendix A1. RNA samples with an RNA integrity number (RIN) of greater than 7 were considered suitable for subsequent qPCR analysis.

3.3.4 RNA ethanol precipitation

RNA samples with low purity as determined by analysis of absorbance spectra underwent ethanol precipitation. RNA sample volumes were normalised to 100µl by the addition of RNase free water and placed on ice, 10µl of 3M sodium acetate (pH 5.2) added and the sample mixed by vortexing. This was followed by addition of 220µl of ice-cold 100% ethanol (Sigma, UK) with thorough mixing and incubation at -80°C for 2hrs. RNA was pelleted by centrifugation at 14,000g for 10mins at 4°C. The supernatant was decanted and 500µl of ice cold 70% ethanol wash added to the pellet. Samples were centrifuged at 14,000g for 5mins at 4°C. The supernatant was decanted and the RNA pellet air-dried prior to dissolution in the required volume of RNase free water (Qiagen, UK).

3.3.5 Thrombus micro-array

The expression of PHD and HIFα subunits was analysed in a pre-existing murine micro-array dataset conducted by Dr Julia Humphries. In this dataset thrombus gene expression was analysed at days 1, 3, 7 and 11 post-induction (n=3 per group) on a murine gene 1.0 sense target (ST) arrays (Affymetrix, USA) used according to the manufacturers instructions. A complete methodology for the generation of microarray data can be found in Appendix A2. Subsequent expression data was normalised by the robust multi-array analysis (RMA) algorithm using Expression Console Software (Affymetrix, USA).

3.3.6 cDNA synthesis

Reverse transcription of RNA was performed using a high capacity RNA-to-cDNA kit (Applied Biosystems, USA) according to the manufacturers instructions. The reaction mixture comprised of 4µl of master mix and up to 16µl of RNA template with the addition of nuclease free water to give a total reaction volume of 20µl containing 400ng of RNA. Non-reverse transcribed controls were generated by substitution with a master mix lacking reverse transcriptase. The reaction was conducted using a PTC 200 thermocycler (MJ Research, UK) under the following conditions; 5mins at 25°C, 30mins at 42°C and 5mins at 85°C. The cDNA was stored at -80°C.

3.3.7 qPCR confirmation

(i) Primer pair design Design of primer pairs was conducted using ProbeFinder software (Roche, USA) derived from the primer3 algorithm[259] using Ensembl ID inputs (Table 3.1). The use of probe based amplification detection required selection of primer pairs that encompassed a universal probe library (UPL, Roche, USA) binding sequence. Where possible intron spanning primers were selected. Site specificity was confirmed by crosschecking with a murine genome library (blastn, NCBI). Standard de-salted primers were purchased (Integrated DNA technologies, UK) and resuspended in nuclease free water (Amplicon, UK) to a stock concentration of 200µM. Aliquots of a working stock of 20µM were prepared by further dilution with nuclease free water. Appropriate reaction specific UPL fluorescent DNA probes were selected using the ProbeFinder software (Roche, USA).

Table 3.1 PCR primer sequences

Primer	Sequence	Probe
Hif1a Left	tcccctctcctgtaagcaag	#53
Hif1a Right	tcgacgttcagaactcatcct	
Hif2a Left	ggagctcaaaaggtgtcagg	#3
Hif2a Right	caggtaaggctcgaacgatg	
Hif3a Left	ctgcccagaaaaacaagacc	#94
Hif3a Right	ctccaagtccagagtgtcagg	
Phd1 Left	ggaacccacatgaggtgaa	#71
Phd1 Right	aacacctttctgtcccgatg	
Phd2 Left	cgtctctcagtgattccaacc	#108
Phd2 Right	actgttaggtcggtcgaagc	
Phd3 Left	tgtctggtacttcgatgctga	#29
Phd3 Right	agcaagagcagattcagtttttc	
Vegfa Left	gtacctccaccatgccaagt	#64
Vegfa Right	tgggacttctgctctccttc	
Gapdh Left	gggttcctataaatacggactgc	#52
Gapdh Right	ccattttgtctacgggacga	
Actb Left	ctaaggccaaccgtgaaaag	#64
Actb Right	accagaggcatacagggaca	
Gak Left	cggacaccaaccactttctt	#47
Gak Right	aacccagtctctggttctttttc	
Hif1a (2) Left	ttacgtgtgagaaaacttctggat	#98
Hif1a (2) Right	gccatctagggctttcagataa	

(*ii) Validation of primer pairs by end-point PCR analysis*

Pooled thrombus cDNA was subject to end-point PCR using the HotStar DNA polymerase master mix (Qiagen, UK) according to the manufacturer's instructions. A reaction mix for each gene of interest was prepared by addition of 10µl master mix, 2µl of coral load, 0.5µl of the forward and reverse primers (20uM), 1ul of template cDNA and 6ul of DNAse free water. Amplification was performed in a thermocycler (MJ Mini Thermocycler, Biorad, UK) under the following conditions; an initial 5mins at 95°C, 40 cycles of 1min at 94°C, 1 minute at 60°C, 30secs at 72°C with a final 10mins at 72°C. For subsequent qPCR cDNA was diluted 10 fold in nuclease free water. The PCR product was stored at -80°C.

PCR products were separated by agarose gel electrophoresis. A 5% agarose gel was prepared by dissolving 5g of agarose (Sigma, UK) in 100ml of TAE buffer (Ambion, UK) by heating in a microwave. The gel was allowed to cool

and 10µl of SYBRsafe (Invitrogen, UK) intercalating agent was added prior to casting. The agarose gel was poured into a casting tray (Flowgen, UK) with both ends sealed and a comb inserted. After solidifying the comb was removed and the tray positioned in the electrophoresis tank (Flowgen, UK). The agarose gel was immersed in 1xTAE buffer. Samples were loaded into the wells accompanied by an ultra low range DNA ladder (Fermentas, UK). Samples were electrophoresed at 20V for 20mins followed by 60mins at 100V. Bands were visualised using the ChemiDoc MP gel documentation system (Biorad, UK). Band size was estimated using ImageLab software (Biorad, UK).

(iii) Primer efficiency

Primer efficiency was calculated by generating a 5-point dilution series of pooled cDNA samples. Plots of Ct versus log [cDNA] were generated in SDS2.4 (Applied Biosystems, USA) and gradient values obtained. Efficiencies were calculated using the equation E=10 (-1/slope)-1 and values are provided in Appendix A3.

(iv) qPCR

The qPCR reaction mix for each gene of interest was prepared as follows.

	Volume	Final Concentration
TaqMan Universal PCR master mix	25µl	1x
Forward Primer (20µM)	0.5µl	200nM
Reverse Primer (20µM)	0.5µl	200nM
UPL Probe	0.5µl	100nM
Nuclease free water	3.5µl	
cDNA	20µl	

Robotic dispensing (Biomek/FX, Beckman Coulter, UK) was used to aliquot 20µl of cDNA template followed by 30µl of gene specific master mix into a 96-well plate. Reaction volumes of 10µl were dispensed in quadruplicate into a 384-well plate. The plate was sealed, vortexed and centrifuged prior to loading. The plate was run on a Real-Time PCR thermal cycler (ABI 7900HT, Roche Applied Biosystems, USA) under the following conditions; an initial 2mins at 50°C was followed by 10mins at 95°C before 40 cycles of 15secs at 95°C and 1min at 60°C. Representative standard curve and uknown amplification curves are provided in Appendix A4.

(v) Quantification of gene expression

A standard curve approach was used to quantify gene expression. Serial dilutions of pooled cDNA were subject to qPCR alongside unknowns used to generate a standard curve for each gene of interest. Standard curves were generated by plotting CT values against log [cDNA] using SDS software (Roche Applied Biosystems, USA). Interpolation of the standard curve enabled quantification of genes of interest. Normalisation of data was achieved using the housekeeping genes *Actb* and *Gak*.

3.3.8 Western blotting

Snap frozen kidney and thrombus tissue samples were processed using either radioimmunoprecipitation buffer (RIPA, Pierce Thermo Scientific, USA; 5mM Tris-HCl, 30mM NaCl, 0.2% NP-40, 0.2% sodium deoxycholate, 0.02% SDS) or a nuclear-cytoplasmic extraction kit (NE-PER, Thermo Pierce, UK) for subsequent biochemical analysis. For total protein extraction tissue was cut into 5mm pieces washed with PBS, homogenised in RIPA buffer (10µl per 1mg) supplemented with protease inhibitors (Halt protease inhibitor, Pierce Thermo Scientific, USA) and incubated on ice for 10mins. The lysate was clarified by centrifugation at 16,000xg for 10mins, the supernatant was then transferred to microcentrifuge tubes for storage at -80^{o}C. For the nuclear-cytoplasmic extraction tissue was cut into 5mm pieces washed with PBS and homogenised in 400µl of CER I buffer (based on 40mg of tissue) supplemented with protease inhibitors, vortexed thoroughly and incubated on ice for 10mins. Ice-cold CER II buffer was added (22µl), the sample vortexed and incubated on ice for 1min. The sample was vortexed and then centrifuged at 16,000xg for 5mins. The supernatant containing cytoplasmic proteins was removed and stored at -80^{o}C. The pellet was resuspended in 200µl of ice-cold NER, vortexed for 10secs every 10mins for a total of 40mins. The sample was again centrifuged at 16,000xg for 5mins, the supernatant containing the nuclear fraction was transferred to a microcentrifuge tube and stored at -80^{o}C.

Total soluble protein of tissue nuclear and cellular extracts was quantified using a bicinchoninic acid assay kit (Thermo Pierce, UK). Serial dilutions of bovine serum albumin (BSA) were prepared from a 2mg/ml stock to generate a standard curve (1.0, 0.5, 0.25, 0.125, 0.063, 0.031, 0.00mg/ml). BSA standard

or unknowns (10µl) were added to a 96-well plate in triplicate. After addition of 200µl of assay reagent to each well the plate was sealed and incubated at 37°C for 30mins. Absorbance was measured at 562nm using a spectrophotometer (SpectraMax 340, Molecular Devices, USA). The BSA standard curve was plotted using a 4-perameter fit, from which concentrations of unknown were interpolated.

Sample concentration was normalised by addition of RIPA, CERI or NER buffer. Protein samples were prepared for electrophoresis by addition of 5x Laemmli buffer; 60mM Tris-HCl pH 6.8, 2% (w/v) SDS, 10%(v/v) glycerol, 5% (v/v) β-mercaptoethanol, 0.01% (w/v) bromophenol blue and heat denatured at 95°C for 5mins. Samples were loaded into precast 4-20% gradient polyacrylamide gels (Bio-Rad, UK) alongside pre-stained molecular weight standards (SeeBlue Plus2, Invitrogen, UK) at 120V for approximately 45 minutes in running buffer; 25mM Tris, 192mM Glycine, 0.1% (w/v) SDS pH 8.3. Proteins were transferred to PVDF membranes electrophoretically at 2.5A (~25V) for 7 minutes using a Trans Blot Turbo system (Bio-Rad, UK) and Trans Blot Turbo PVDF packs (Bio-Rad, UK) containing proprietary transfer buffer.

Membranes were washed in tris buffered saline (TBS, 25mM Tris, 0.15M NaCl, pH7.2) supplemented with 0.1% Tween 20 (TBST, Sigma, UK). Membranes were blocked in 5% non-fat dried milk (NFDM, Marvel, UK) dissolved in TBST for 1hr at room temperature. Primary antibodies were prepared at the required concentration (Table 3.2) by dilution in 5% BSA and incubated with membranes overnight at 4°C. Membranes were washed in TBST (3x 5mins) prior to incubation with streptavidin HRP conjugated secondary antibody diluted in 5% NFDM (Table 3.2) for 1hr at room temperature. Membranes were again washed in TBST (3x 5mins) prior to detection of specific antibody antigen complexes by addition of a chemi-luminescent substrate (Western C, Bio-Rad, UK) visualised using a gel documentation system (Chemi Doc MP, Bio-Rad, UK). The molecular weights of specific antigen antibody complexes were estimated from the relative position of the prestained molecular weight marker using ImageLab software (BioRad, UK).

Table 3.2 Antibodies used for western blotting

Antigen	Final Ab concentration (µg/ml)	Dilution	Antibody (Cat no)	Manufacturer
PHD1	1.0	1/2500	ab108980	Abcam, UK
PHD2	0.5	1/5000	ab109088	Abcam, UK
PHD3	0.9	1/2500	ab30782	Abcam, UK
α-Tubulin	1.0	1/1000	NB600-506	Novus Bio, UK
Histone H3	1.0	1/1000	9715	Cell Signaling, USA
Anti-Rabbit	Unknown	1/100,000	A0545	Sigma, UK
Anti-Rat	Unknown	1/10,000	A5795	Sigma, UK

3.3.9 IHC localisation of PHD protein

To localise PHD protein expression in the resolving venous thrombus an IHC technique was used. In order to optimise PHD antigen retrieval staining was assessed after treatment in both citrate and tris based buffers at a number of temperatures in kidney tissue acting as a positive control (Fig 3.1). Antibody staining was optimised under a number of primary antibody concentrations and incubation times (Fig 3.1). In tissues where poor staining was evident signal amplification was tested using either HRP polymer or biotinyl tyramide (Fig 3.1).

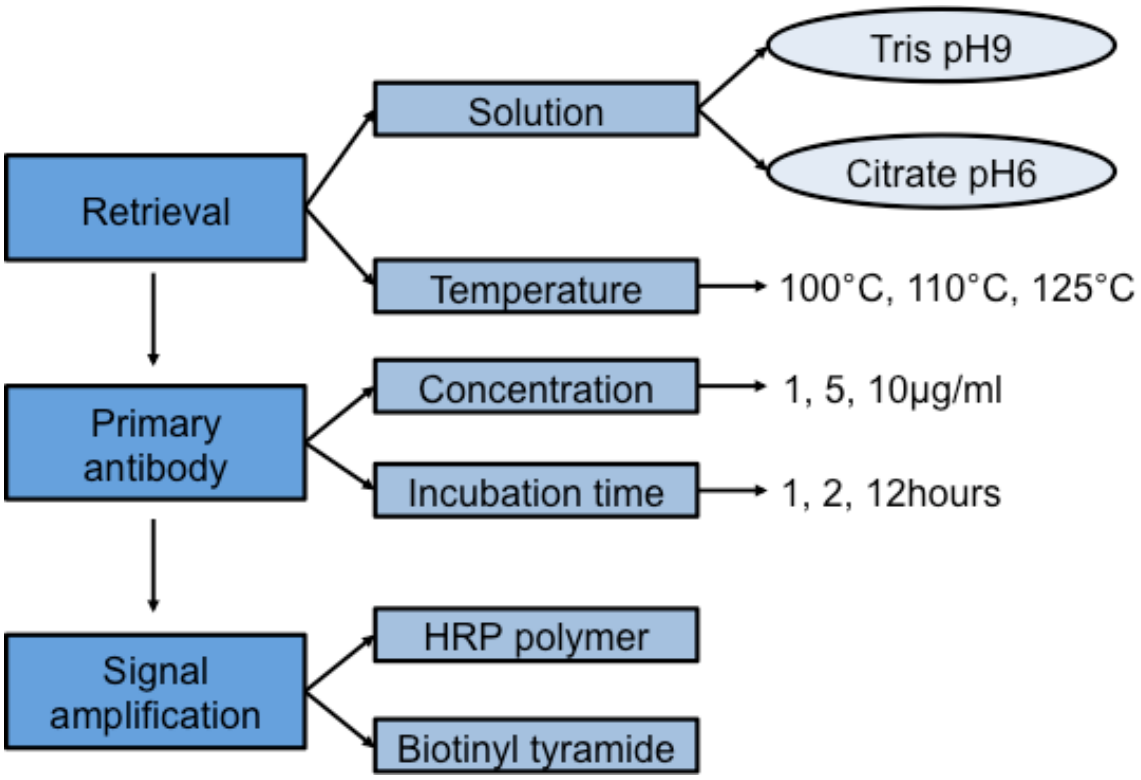

Figure 3.1 Optimisation of PHD immunohistochemistry

To optimise the staining of PHD proteins by immunohistochemistry a number of antigen retrieval, primary antibody and signal amplification conditions were assessed.

Paraffin wax sections were warmed for 30mins at 60°C to soften the wax. Sections were deparaffinised in two 5min xylene washes. Endogenous peroxidase activity was quenched by incubation of sections in 1%(v/v) hydrogen peroxide in 100% ethanol for 30mins. Sections were rehydrated through gradated alcohol washes and rinsed in tap water for 5mins. Heat mediated antigen retrieval was carried out using an antigen access unit (Menarini Diagnostics, UK) at 125°C for 1min with citrate (pH6) or Tris-HCL (pH9) buffered retrieval solutions (Menarini Diagnostics, UK). Sections were washed in two changes of phosphate buffered saline (PBS, Sigma, UK), ringed using a wax pen (Dako), blocked for 10mins using a serum free protein block (Dako) and incubated with primary antibodies raised against PHD1 (5µg/ml, Abcam, UK), PHD2 (5µg/ml, Abcam, UK) and PHD3 (5µg/ml, Abcam, UK) diluted in

PBS for 1hr at room temperature in a humid chamber. Sequential sections were incubated with rabbit IgG as a control. Slides were washed three times in PBS for 10mins, incubated with biotinylated goat anti rabbit antibody for 45mins at room temperature and washed in 3x10min PBS washes. Sections were incubated with extravidin peroxidase (Sigma, UK) for 1hr at room temperature. Specific antigen antibody complexes were visualised colourimetrically using a chromogenic substrate (Vector SG, Vector laboratories, UK). Sections were washed in 3x10min PBS washes and counterstained in nuclear fast red (Vector laboratories, UK) for 7mins. Sections were rinsed in running tap water for 30secs prior to dehydration through graded alcohol solutions. Sections were cleared in 2x5min xylene washes, mounted with cover slips in DPX medium and allowed to dry overnight.

3.3.10 Polymer based amplification

An HRP polymer amplification kit (Menarini Diagnostics, UK) was used according to the manufacturers instructions. Sections were dewaxed, rehydrated and quenched for endogenous peroxidase activity as previously described (4.2.2). Sections were washed in 2 changes of PBS. Sections were ringed using a wax pen, blocked for 10mins with serum free protein block (Dako) and incubated with primary antibodies raised against PHD1 (5µg/ml, Abcam, UK), PHD2 (5µg/ml, Abcam, UK) and PHD3 (5µg/ml, Abcam, UK) diluted in PBS for 1hr at room temperature in a humid chamber. Slides were washed in 3x10min PBS washes and incubated with HRP polymer for 30mins at room temperature. Slides were washed in 3x10mins PBS washes and specific antigen antibody complexes were visualised colourimetrically using a chromogenic substrate (Vector SG, Vector laboratories, UK). Sections were washed in 3x10min PBS washes and counterstained in nuclear fast red (Vector laboratories, UK) for 7mins. Sections were rinsed in running tap water for 30secs prior to dehydration through graded alcohol solutions. Sections were cleared in 2x5min xylene washes, mounted with cover slips in DPX medium and allowed to dry overnight.

3.3.11 Biotinyl tyramide amplification

A biotinyl tyramide kit (Perkin Elmer, UK) was used according to the manufacturers instructions. Sections were dewaxed, rehydrated and quenched for endogenous peroxidase activity as previously described (4.2.2). Sections

were washed in 2 changes of 0.1M Tris-HCl, 0.15M NaCl and 0.05% (v/v) tween20 (TBS). Sections were ringed using a wax pen (Dako, UK) and incubated with the supplied blocking reagent for 30mins at room temperature. Sections were incubated with primary antibodies raised against PHD1 (5µg/ml, Abcam, UK), PHD2 (5µg/ml, Abcam, UK) and PHD3 (5µg/ml, Abcam, UK) diluted in blocking reagent for 1hr at room temperature in a humid chamber. Sequential sections were incubated with control rabbit IgG. Slides were washed three times in TBS for 10mins. Sections were incubated with biotinylated goat anti-rabbit antibody (4µg/ml, Sigma, UK) diluted in blocking reagent for 45mins at room temperature. Slides were washed three times in TBS for 10mins. Sections were incubated with supplied SA-HRP (1:100) diluted in blocking reagent for 30mins. Slides were subjected to 3x10min TBS washes. Sections were incubated with biotinyl tyramide (1:50) diluted in amplification diluent for 10mins. Slides were washed three times in TBS for 10mins. Sections were incubated with supplied SA-HRP (1:100) diluted in blocking reagent for 30mins. Slides were washed four times in TBS for 10mins. Specific antigen antibody complexes were visualised colourmetrically using a chromogenic substrate (Vector SG, Vector labs, UK). Sections were washed in 3xPBS for 10mins. Sections were counterstained in nuclear fast red (Vector labs, UK) for 7mins. Sections were washed in tap water for 30secs prior to dehydration through gradiated alcohol, followed by clearing in 2x5mins xylene washes. Slides were mounted with cover slips in DPX medium (Sigma, UK) and allowed to dry overnight.

3.3.12 Statistical analysis

Normality of data was assessed using Kolmogorov-Smirnoff tests to inform selection of appropriate parametric and non-parametric tests. Differences in measurements of gene expression were assessed by 1-way ANOVA and post-hoc Bonferroni. In all cases $P<0.05$ was considered statistically significant. Statistical analyses were conducted using Prism Software (v5, Graphpad, USA). Data represented as mean ± SE.

3.4 Results

3.4.1 Thrombus micro-array analysis

Phd1-3 gene expression was detected in a murine micro-array at days 1, 3, 7 and 11 after thrombus induction. No significant change in *Phd1* gene expression was observed (P>0.05, 1-way ANOVA, Fig3.2A). *Phd2* gene expression changed significantly over time (P<0.01, 1-way ANOVA, Fig3.2B) with expression significantly reduced at days 3 and 7 compared to day 1 (P<0.05, post-hoc Bonferonni). Similarly *Phd3* gene expression changed significantly over time (P<0.05, 1-way ANOVA, Fig3.2C) with expression significantly lower at day 7 compared to day 1 (P<0.05, post -hoc Bonferroni).

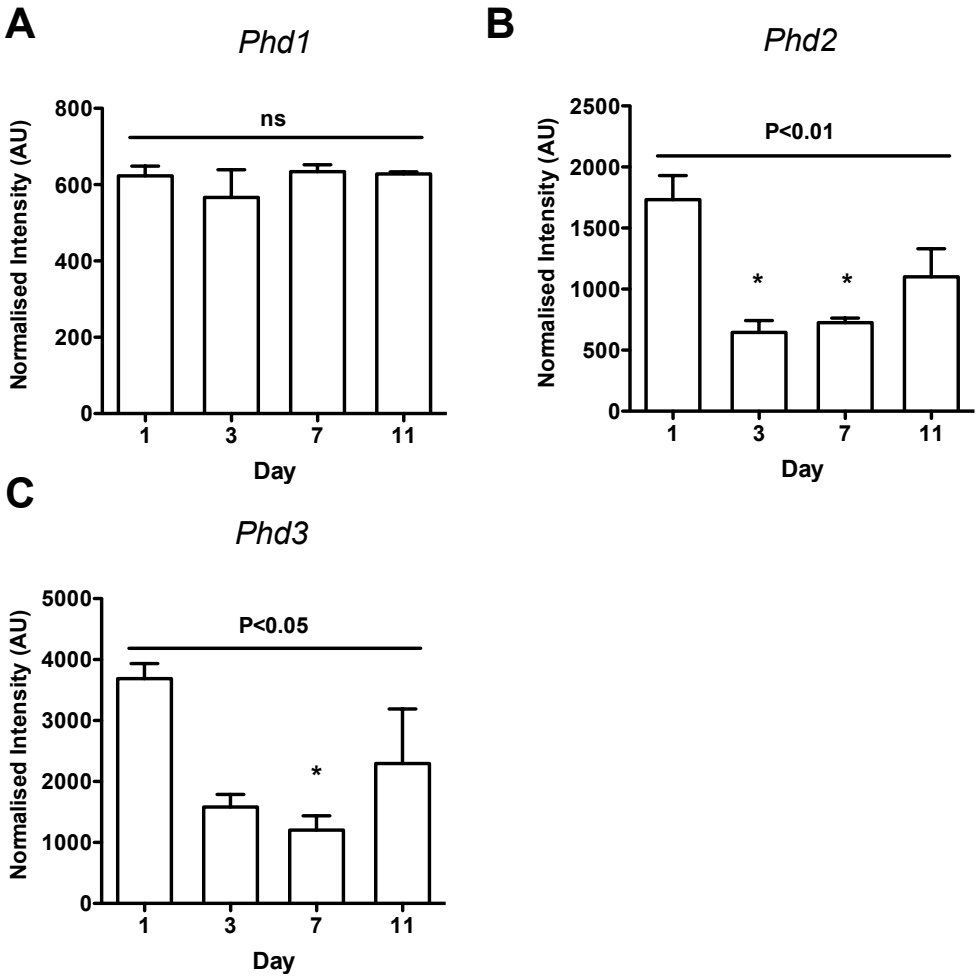

Figure 3.2 Thrombus *Phd1, 2* and *3* microarray gene expression

Microarray data of (A) *Phd1* (B) *Phd2* and (C) *Phd3* gene expression, expressed as normalised fluorescence intensity, was analysed (1-way ANOVA) Data represented as mean ± SE (n=3 per group). *Phd2* *P<0.05 day1 vs day3, day1 vs day7. *Phd3* *P<0.05 day1 vs day 7.

Hif1-3α gene expression was detected in a murine micro-array at days 1, 3, 7, 11 after thrombus induction. *Hif1α* gene expression changed significantly over the time-course of the experiment (P<0.001, 1-way ANOVA, Fig 3.3A) with gene expression significantly reduced at days 7 and 11 as compared to days 1 and 3. Gene expression of *Hif2α* also varied significantly over the time-course of the experiment (P<0.001, 1-way ANOVA, Fig 3.3B) gene expression was significantly higher at days 7 and 11 compared to day 1 (post-hoc Bonferroni). *Hif3α* gene expression was subject to significant changes with time (P<0.05, 1-way ANOVA, Fig 3.3C) with gene expression significantly lower at day 7 and 11 compared to day 1 (P<0.05, post-hoc Bonferroni).

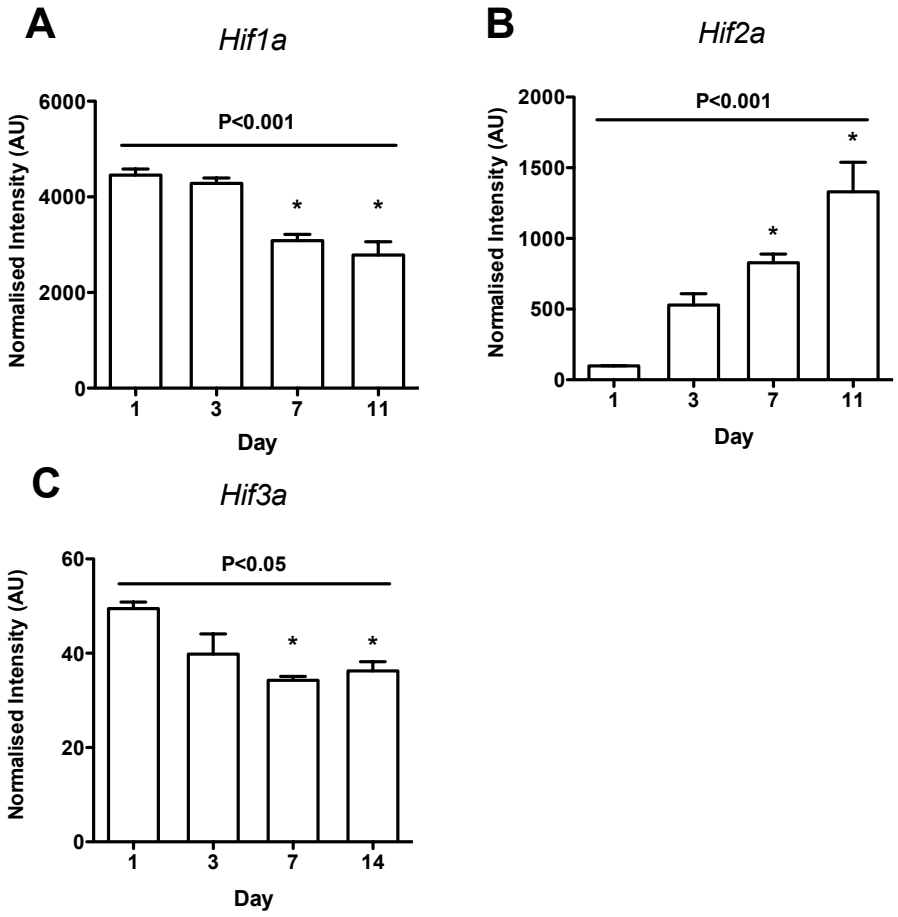

Figure 3.3 Thrombus *Hif1a, 2a* and *3a* microarray gene expression

Microarray data of (A) *Hif1a* (B) *Hif2a* and (C) *Hif3a* gene expression, expressed as normalised fluorescence intensity, was analysed (1-way ANOVA). Data represented as mean ± SE (n=3 per group). *Hif1a* *P<0.05 day1 vs day7, day3 vs day7, day1 vs day11, day3 vs day11. *Hif2a* *P<0.05 day1 vs day 7, day3 vs day7, day3 vs day11. *Hif3a* *P<0.05 day1 vs day7, day1 vs day11.

3.4.2 Primer validation

Primer pair design was validated by endpoint PCR of pooled thrombus cDNA. Single amplicons were generated for *Phd1, Phd2, Phd3, Hif1α, Hif2α, Hif3α, Vegfa, Actb, Gapdh and Gak*. Observed amplicon sizes closely matched (within 10%) the predicted values (Fig 3.4, Table 3.4).

3.4.3 Thrombus quantitative PCR

Expression of *Phd1, 2* and *3* genes was detected in murine thrombus at days 1, 3, 7 and 11 post-induction by qPCR. *Phd1* gene expression was not significantly altered over-time ($P>0.05$, 1-way ANOVA, Fig 3.5A). *Phd2* gene was significantly different over the time-course of the experiment ($P<0.05$, 1-way ANOVA, Fig 3.5B). Significant changes in *Phd3* gene expression were evident ($P<0.05$, 1-way ANOVA, Fig 3.5C) however, post-hoc tests failed to identify the source of this difference.

Hif1a and *Hif3a* gene expression was not detected by qPCR. *Hif2a* gene expression changed significantly over the time-course of the experiment ($P<0.05$, 1-way ANOVA, Fig 3.6). However, post-hoc tests failed to identify the source of this difference.

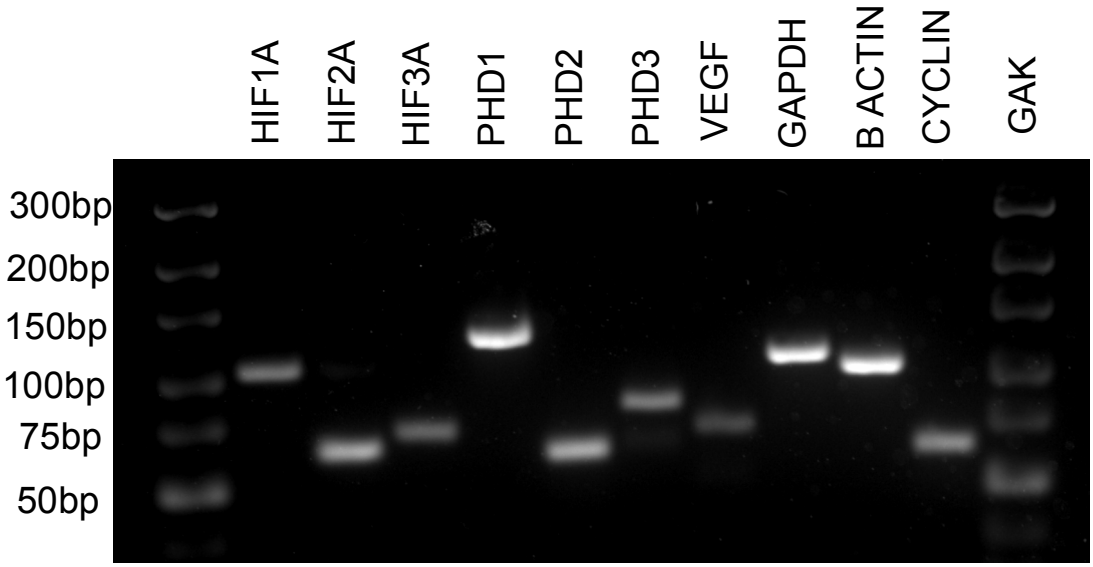

Figure 3.4 Primer validation

Agarose gel electrophoresis of end-point PCR product was used to validate genes of interest. Single discrete bands were observed for all target genes.

Table 3.3 End-point PCR amplicon sizes

Primer Pair	Expected (bp)	Observed (bp)
Hif1a	104	109
Hif2a	63	66
Hif3a	71	75
Phd1	125	130
Phd2	62	65
Phd3	85	88
Vegfa	63	77
Gapdh	112	116
Actb	104	108
Gak	64	66

In silico amplicon sizes correlate well with experimental observations.

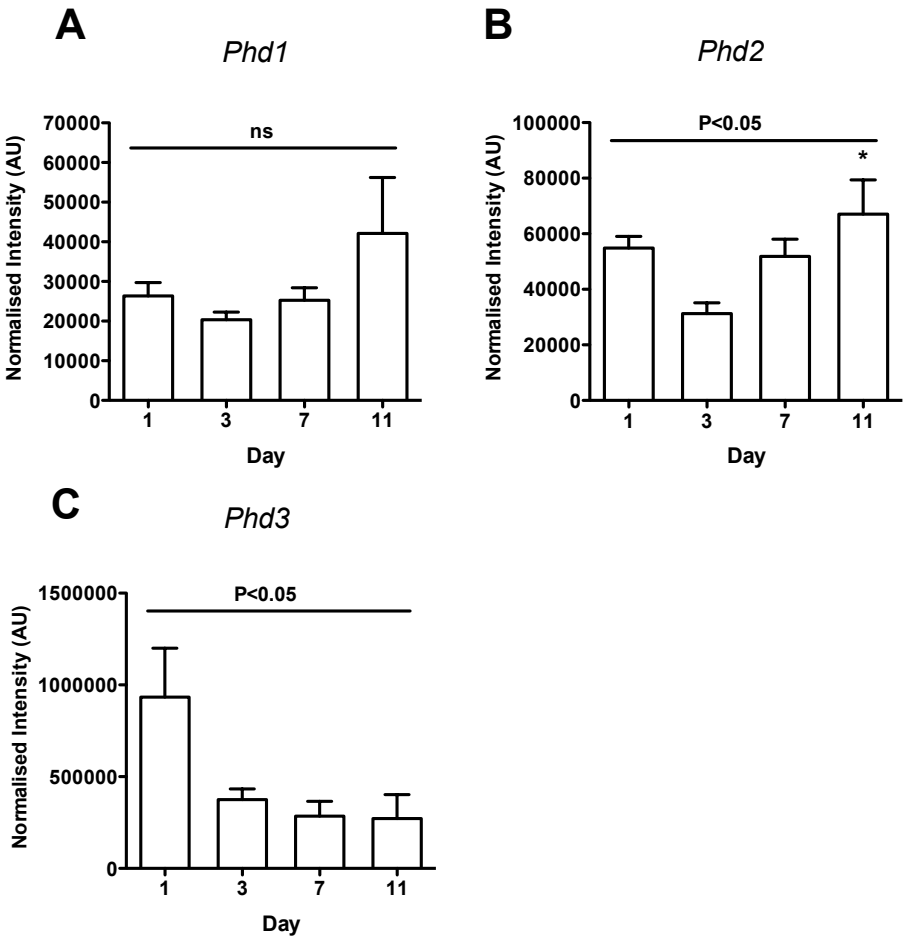

Figure 3.5 Thrombus *Phd1, 2* and *3* qPCR gene expression

Gene expression of (A) *Phd1*, (B) *Phd2*, and (C) *Phd3* was quantified by qPCR (1-way ANOVA, n=5 per group) and expressed as normalised fluorescence intensity, data represented as mean ± SE. *Phd2* *P<0.05 day3 vs day 11.

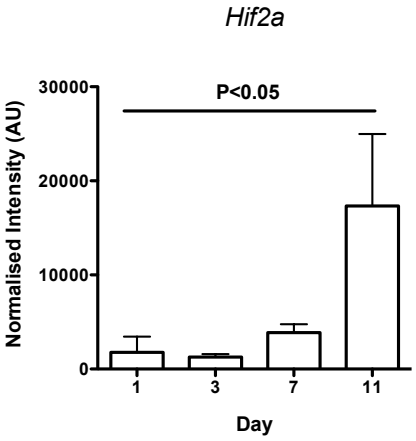

Figure 3.6 Thrombus *Hif2a* qPCR gene expression

Gene expression of *Hif2a* was quantified by qPCR (1-way ANOVA, n=5 per group) and expressed as mean normalized fluorescence intensity, data represented as mean ± SE.

3.4.4 Immunoblotting

An immunoblotting approach was used to visualise PHD1, 2 and 3 protein expression within thrombus. Immunoblotting was first optimised in total lysates of control tissues: heart, lung, kidney, liver and spleen (Fig 3.7). It was not possible to visualize PHD1 protein expression in any of the positive control tissues by immunoblotting. Immunoblots for PHD2 visualised a discrete band at 53kDa present in kidney and liver tissue lysates . PHD3 immunoblots identified a major band in kidney lysates with estimated molecular weight of 36kDa, a feint band with a lower molecular weight was also detected in heart tissue lysate. Expression of αTubulin, with an estimated molecular weight of 55kDa was expressed in all of the tissue lysates, although to varying degrees.

To investigate the expression of PHD isoforms in the thrombus total tissue lysates from samples harvested at days 1, 3, 7 and 14 post-induction were analysed alongside kidney tissue lysates serving as a positive control (Fig 3.8). As before PHD2 and PHD3 expression was present in kidney lysates. Expression of PHD1, PHD2 and PHD3 was not detectable in thrombus tissue lysates at any of the time-points studied. Expression of the loading control αTubulin in thrombus lysates, while markedly less than in kidney lysates, was detected at all time-points and remained relatively invariant.

The subcellular localisation of PHD isoforms was investigated in nuclear and cytoplasmic extracts of kidney tissue samples (Fig 3.9). PHD1 immunoblotting provided a discrete band of 51kDa present exclusively in the nuclear extracts. PHD2 and PHD3 protein expression was present mainly in cytoplasmic extracts with small amounts detectable in nuclear extracts. The cytoplasmic marker αTubulin was enriched in the cytoplasmic fraction with detectable levels also present in the nuclear compartment. Conversely the nuclear marker Histone H3 was enriched in the nuclear fraction with some protein also present in the cytoplasmic fraction. Representative whole-membrane images are provided in Appendix A5. Fresh and snap-frozen tissue samples were also assayed to determine whether the extraction protocol used remained robust in frozen tissue samples (Appendix A6). Nuclear and cytoplasmic components were well segregated in both fresh and frozen samples.

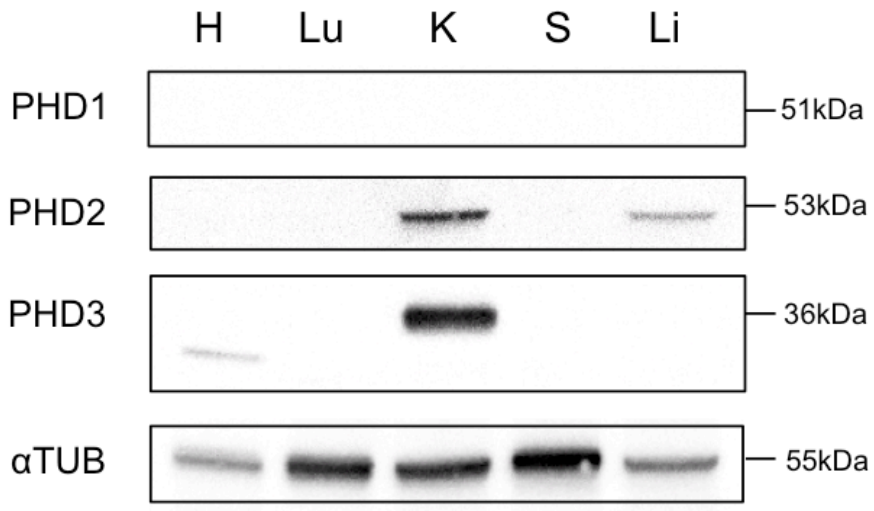

Figure 3.7 PHD1-3 protein expression in murine tissues

Representative immunoblots of PHD1-3 expression in murine heart (H), lung (Lu), kidney (K), spleen (S) and liver (Li) total tissue lysates. PHD1 protein was not detectable by immunoblotting in any of the tissue samples investigated. Immunoblotting revealed a discrete band for PHD2 at 53kDa in kidney and liver lysates. PHD3 protein expression was detected in kidney tissue lysate with a band at 36kDa, a lower molecular weight band was also detected in heart lysate. Expression of the loading control αTubulin was present in all samples with a discrete band at 55kDa.

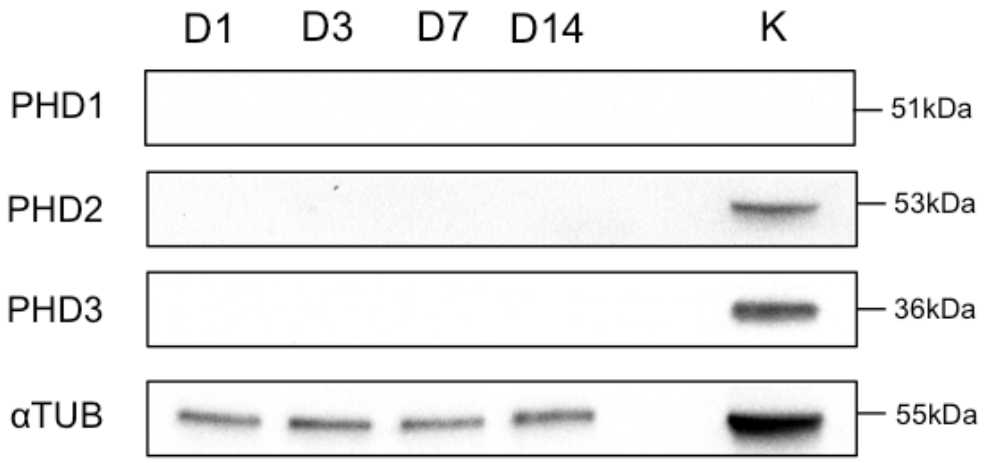

Figure 3.8 PHD1-3 protein expression in the resolving venous thrombus

Expression of PHD1-3 was not detectable in thrombus total tissue lysates at days 1, 3, 7 and 14 post-induction by immunoblotting. Expression of αTubulin was detectable in all thrombus tissue lysates and remained relatively invariant.

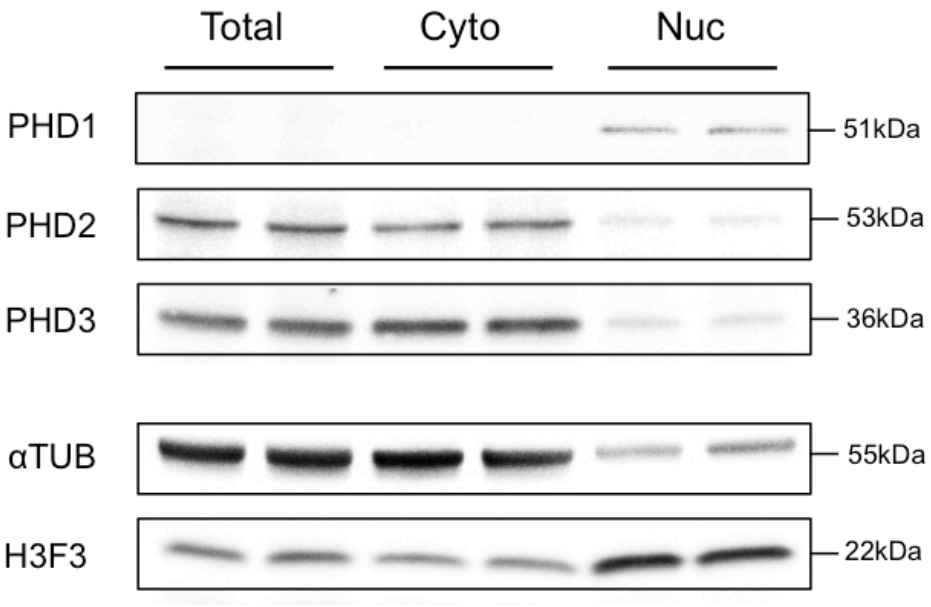

Figure 3.9 PHD 1-3 protein compartmentalisation in kidney tissue

The PHD protein content of kidney total, cytoplasmic and nuclear preparations was determined by immunoblotting. PHD1 protein was expressed specifically in nuclear extracts, with a discrete band at 51kDa, while remaining undetectable in total extracts. PHD2 and PHD3 proteins were present in cytoplasmic extracts and, to a lesser extent, nuclear extracts. The quality of protein separation was assessed by segregation of α-tubulin and histone h3 to the cytoplasmic and nuclear compartments respectively. A degree of cross contamination of nuclear components into the cytoplasmic compartment, and vice versa, was noted.

3.4.5 IHC

Localisation of PHD1-3 protein by immunohistochemistry was optimised using in formalin fixed paraffin embedded (FFPE) murine kidney sections. Using standard extravidin peroxidase signal amplification failed to localize PHD protein expression to the kidney. Additional amplification using an HRP polymer successfully localised protein expression of PHD1-3 in the kidney medulla (Fig 3.10). Localisation of PHD1-3 protein expression in FFPE of thrombus required additional signal amplification using a biotinyl tyramide based system. PHD1-3 protein expression was observed in the thrombus at days 1, 3 7 and 14 post-induction. PHD1 expression (Fig 3.11) at days 1 and 3 was associated with a polymorphonuclear cell infiltrate, although not all the cells were found to express this enzyme. PHD1 protein expression was markedly reduced at day 7 with positive staining localised to the thrombus periphery. At day 14 PHD1 protein was localised throughout the thrombus.

Similarly, positive staining for PHD2 was observed at all time-points (Fig 3.12). PHD2 protein expression at days 1 and 3 was again associated with polymorphononuclear cells. At day 7 a large number of cells continued to express PHD2 both within the thrombus core and periphery. At day 14 PHD2 protein was present in highly cellular regions of the organising thrombus, however, cellular staining for PHD2 appeared heterogeneous. Larger representative images for PHD2 localisation in the resolving thrombus are included in Appendix A7.

PHD3 protein expression was observed at all time-points of thrombus resolution investigated. PHD3 protein at days 1 and 3 was present in cells distributed throughout the thrombus (Fig 3.13). At day 7 PHD3 protein expression was largely restricted to the thrombus periphery. PHD3 protein expression at day 14 was associated with mononuclear cells the morphology of which was consistent with that of macrophages. PHD3 protein expression was again restricted to cell dense regions of the thrombus observed with a degree of heterogeneous staining.

PHD1-3 protein was quantified by calculating the percentage area stained positively for each of the isoforms throughout the length of the thrombus (Fig 3.14). The percentage of the thrombus stained positively for PHD1, PHD2 and PHD3 changed significantly with time ($P<0.0001$, 1-way ANOVA). Expression of all three PHD isoforms was significantly higher at day 14 vs days 1,3 and 7 ($P<0.05$, post-hoc Bonferroni).

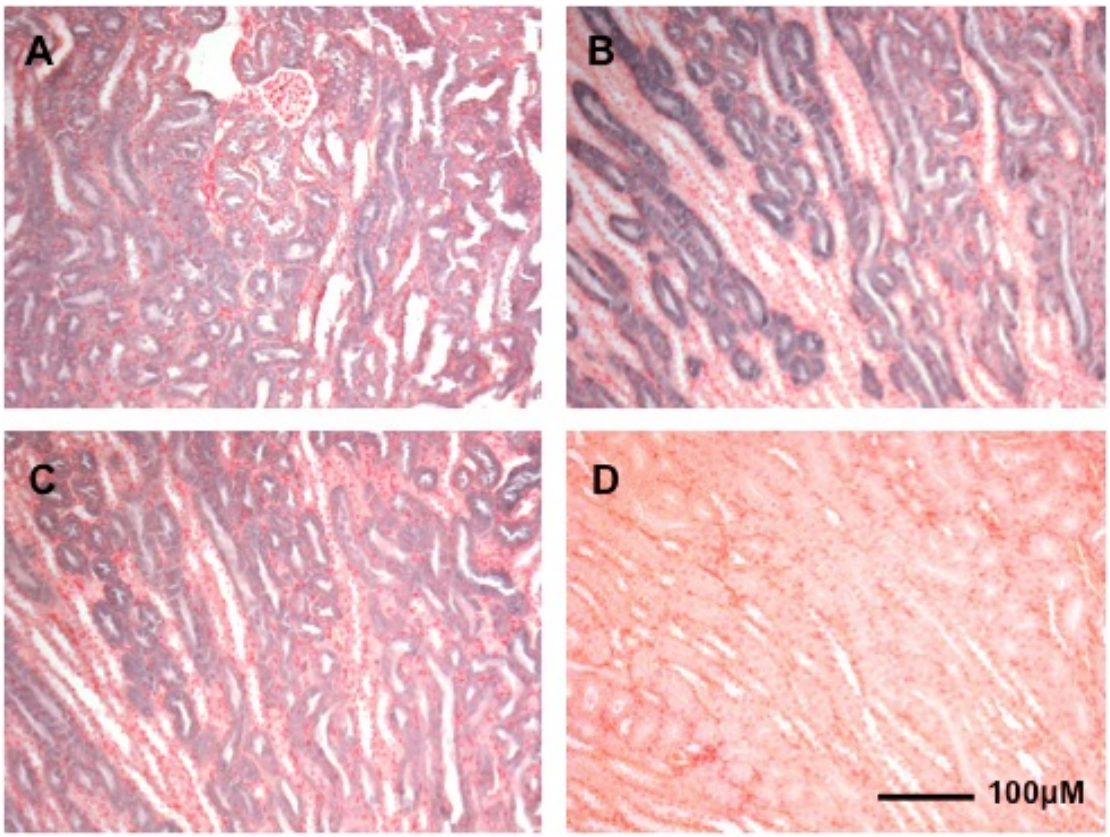

Figure 3.10 PHD1-3 kidney immunohistochemistry

FFPE kidney sections were used as positive controls for the optimisation of PHD1-3 immunohistochemistry. Positive staining for (A) PHD1, (B) PHD2 and (C) PHD3 was observed in the medulla. (D) Staining was absent in appropriate IgG controls.

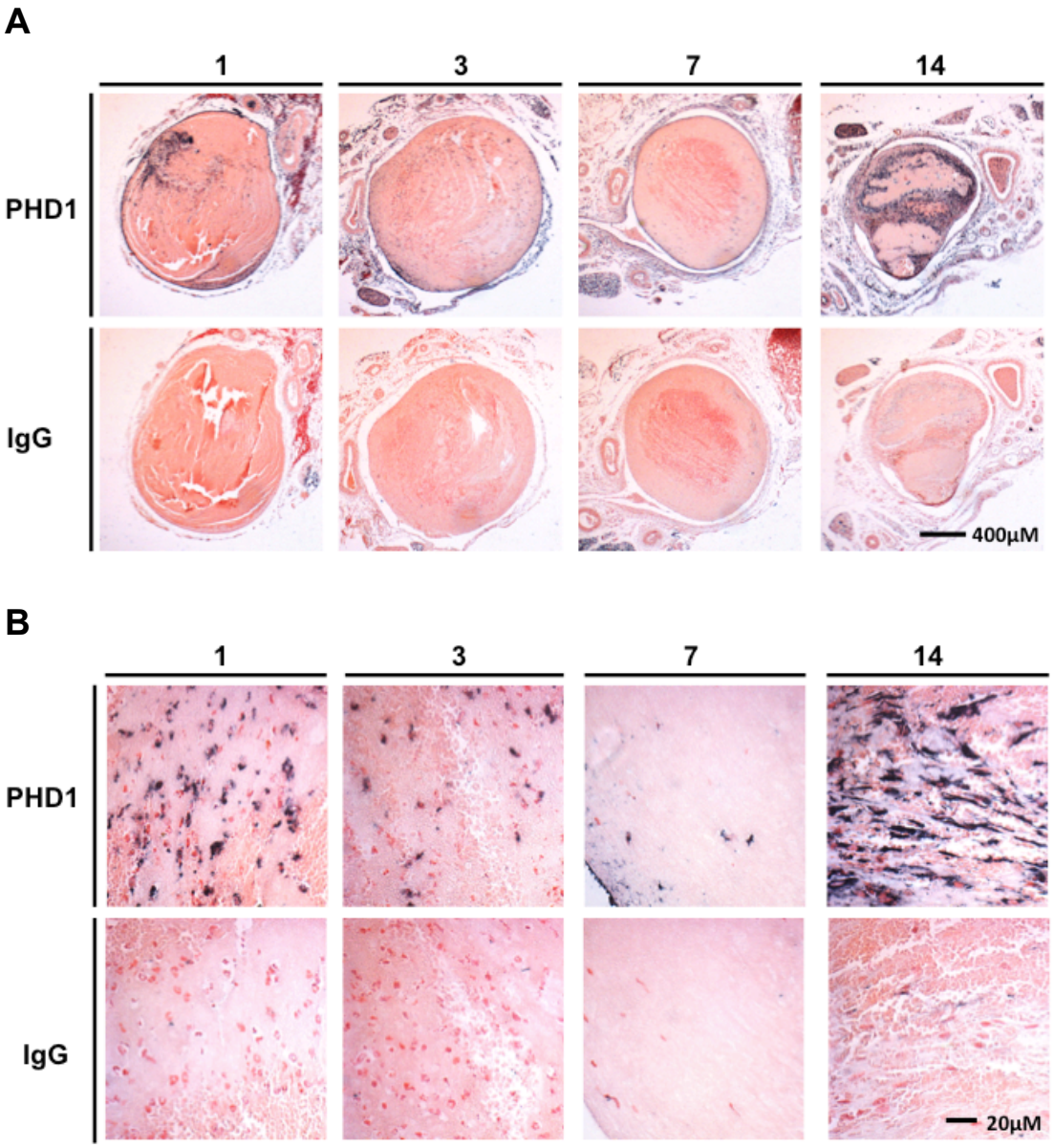

Figure 3.11 PHD1 immunohistochemistry in the resolving thrombus

Nucleated cells in the resolving thrombus stained positively for PHD1. Sequential sections were incubated with appropriate IgG as control. Images acquired at an original magnification of 250x (A) and 400x (B)

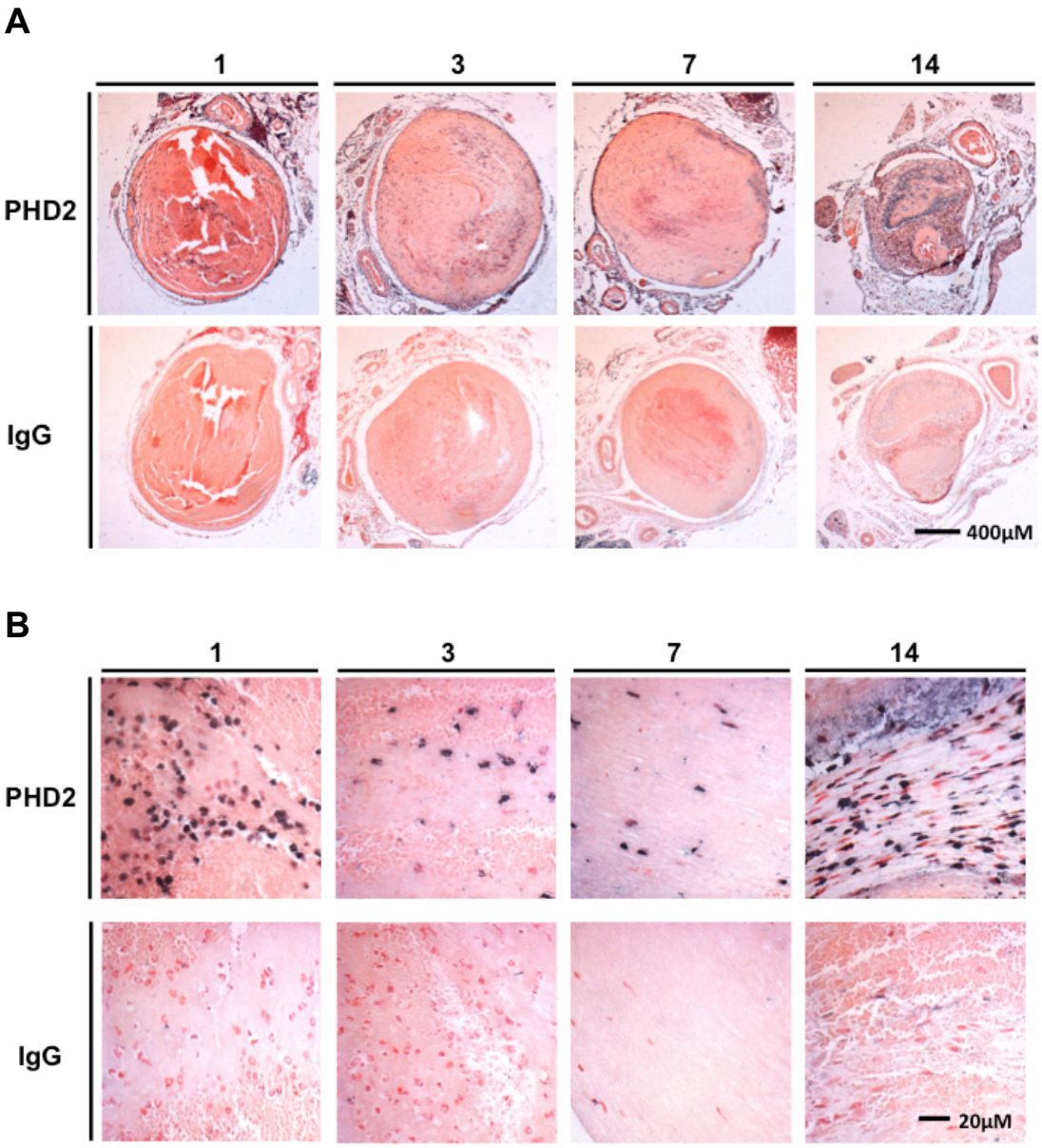

Figure 3.12 PHD2 immunohistochemistry in the resolving thrombus

Nucleated cells in the resolving thrombus stained positively for PHD2. Sequential sections were incubated with appropriate IgG as control. Images acquired at an original magnification of 250x (A) and 400x (B).

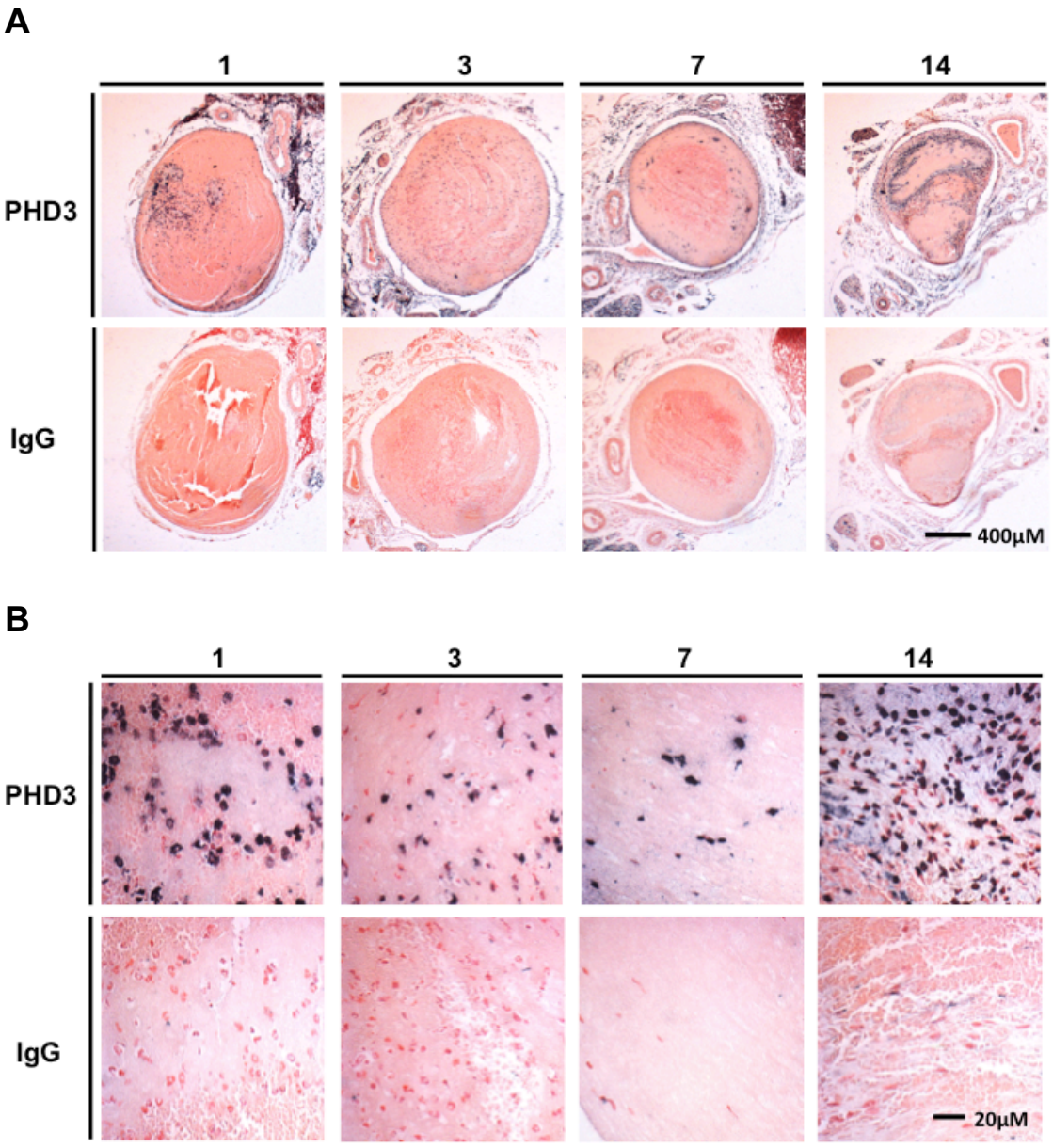

Figure 3.13 PHD3 immunohistochemistry in the resolving thrombus

Nucleated cells in the resolving thrombus stained positively for PHD3. Sequential sections were incubated with appropriate IgG as control. Images acquired at an original magnification of 250x (A) and 400x (B).

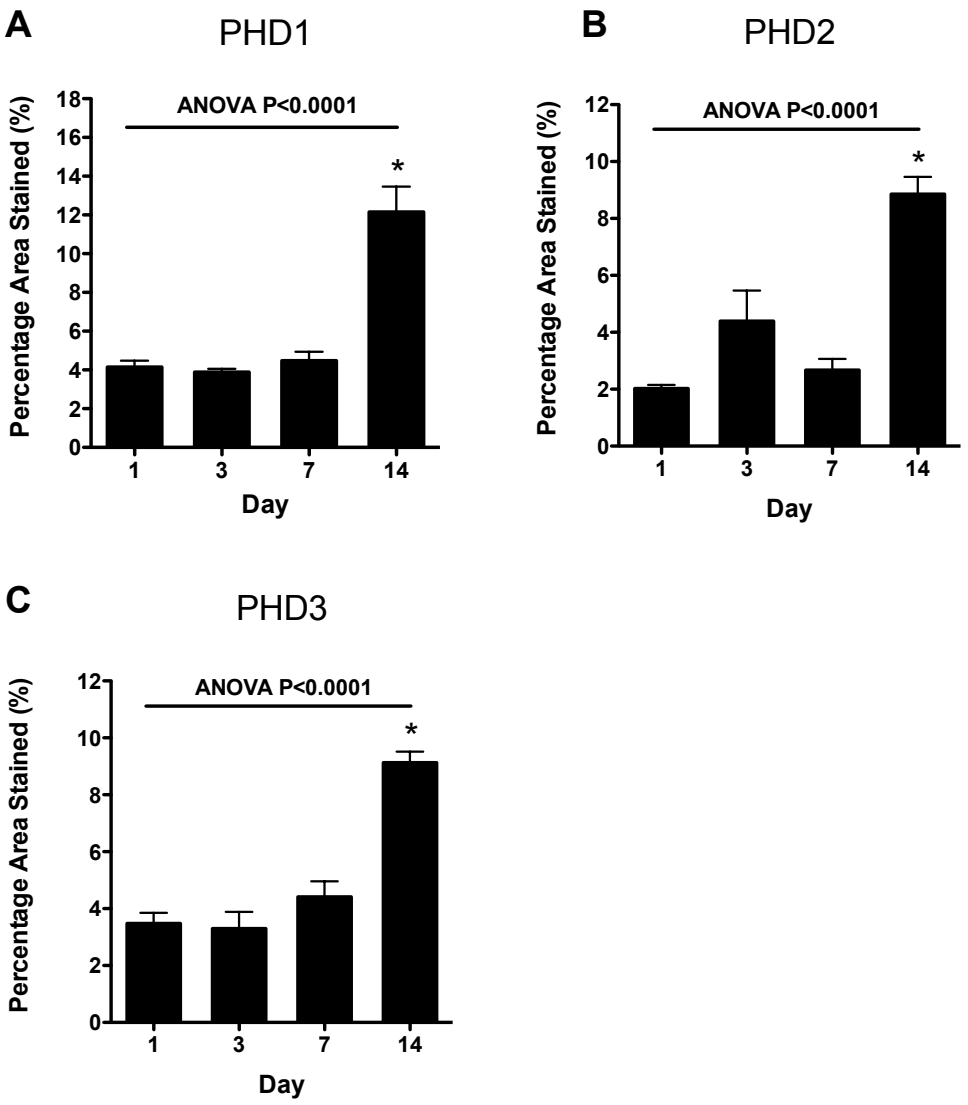

Figure 3.14 Quantification of PHD1-3 immunohistochemistry

Percentage area of thrombus stained positively for PHD1-3 (A-C) protein at days 1, 3, 7 and 14 post-induction (1-way ANOVA, n=5 per group). *P<0.05 day14 vs day, day14 vs day3 and day14 vs day7. Data represented as mean ± SE.

3.5 Discussion

Nuclear accumulation of HIF1α occurs early after thrombus formation (within 24hours)[57]. PHD isozymes play a critical role in the regulation of HIF1α stability with hydroxylation targeting this protein for polyibiquitination and proteasomal degradation. To further understand the molecular processes that regulate HIF1α accumulation in the thrombus it was considered important to characterise the expression of individual PHD isoforms.

PHD isoform expression was measured at the gene level by microarray and qPCR. *Phd1* gene expression remained relatively constant during thrombus resolution as measured by the micro-array and subsequently confirmed by qPCR. *Phd2* gene expression was significantly altered with time, as measured by both microarray and qPCR. Whilst time-point significant differences varied a similar reductions in *Phd2* expression at mid time-points were evident. Similarly, with *Phd3* significant temporal changes were observed by both techniques. A consistent trend towards decreased *Phd3* expression at later time-points was apparent.

Expression of *Phd2* and *Phd3* genes at early time-points after thrombus induction may be attributed to the high proportion of neutrophils found in the acute thrombus[25]. Human peripheral neutrophils express both *Phd2* and *Phd3* and, importantly, the expression of these genes is rapidly upregulated by either hypoxia or an inflammatory insult[176]. Both *Phd2* and *Phd3* genes contain HREs in their respective promoters[97, 98]. The upregulation of *Phd2* and *Phd3* under hypoxic conditions maybe a result of increased HIF1α transcriptional activity present in the acute venous thrombus[57, 260]. An HRE has yet to be identified in the promoter of *Phd1* and that may account, to some extent, for the observed invariance.

Attempts to quantify *Hif1a* and *Hif3a* by qPCR proved unsuccessful. The *Hif1a* primer pair was successfully validated by endpoint PCR using a pooled thrombus cDNA sample. However, no amplification was observed during the qPCR run. This suggests either that *Hif1a* gene is too weakly expressed for detection or that the fluorescent probe was not successfully incorporated. A

second primer pair with a different probe was also designed and successfully validated by endpoint PCR but again no amplification was observed. This would suggest that, surprisingly, despite high levels of nuclear HIF1α protein expression, *Hif1a* gene expression is not detectable by qPCR. *Hif3a* primer pair validation by endpoint PCR was also successful. However, during qPCR amplification of *Hif3a* was only observed after 38 cycles and did not allow for construction of a standard curve, precluding further analysis. *Hif2a* gene expression was readily detectable by both micro-array and qPCR and was found to increase significantly as the thrombus resolved. The finding is consistent with immunohistochemical analysis of HIF2α protein expression in the thrombus where the proportion of the thrombus stained positively increased with time[261]. HIF2α protein is potently upregulated in hypoxic macrophages inducing expression of *Vegfa* and cell migration and this cell type could contribute to the levels observed in the thrombus[262].

When designing of the qPCR experiment the use of three reference genes was originally intended. *Actb* and *Gapdh* are both standard reference genes whereas *Gak* was selected due to invariance in the microarray dataset. After optimisation *Gapdh* was excluded for use as a reference gene due to concerns over hypoxia-inducibility. *Gapdh* contains a promoter resident HRE and there have been numerous reports of hypoxia-mediated induction in neutrophils, macrophages and endothelial cells[176, 263, 264].

While expression of *Phd1*, *Phd2* and *Phd3* mRNA was observed in the thrombus it was necessary to confirm expression at the protein level. Western blotting for PHD1-3 isoforms in thrombus tissue lysates was optimised. Initial success was achieved in the detection of PHD isoforms in positive control tissues. Molecular weight estimations correlate well with predicted values and with the exception of PHD3 antibodies provided single discrete bands. It is possible that the lower molecular weight band corresponds to alternate splice variants of PHD3 that have been described in the literature[138, 171]. Alternatively as the antibody used to detect PHD3 protein was polyclonal this additional band may be a different protein with similar domain structure.

Attempts to detect PHD1-3 protein expression in the resolving venous thrombus by immunoblotting were unsuccessful. It is possible that PHD protein expression in the thrombus is relatively low. Immunohistochemical data supports this explanation as localisation required the maximum available level of signal amplification. Alternatively, there are a number of factors that may have led to the dilution of intracellular proteins in total tissue lysates. Carry over of blood when excising the thrombus may have diluted the samples with plasma proteins. The acute thrombus is also predominately composed of erythrocytes that may have further diluted out PHD protein expression in nucleated cells. The reduced intensity of αTubulin bands in thrombus lysates compared to those of kidney would support dilution of intracellular proteins.

Kidney FFPE sections were used to successfully optimise immunohistochemical localisation of PHD1-3 protein. The expression pattern of PHD1-3 correlated well with previous immunohistochemical studies in the rat and human kidney samples[265-267]. However, in contrast to the nuclear segregation observed by immunoblotting PHD1 localised to the cytoplasm and nucleus of the kidney medulla. Although PHD2 localisation did not require amplification, both PHD1 and PHD3 could only be localised clearly through the use of polymer-based amplification. Localisation of PHD1, 2 and 3 in the resolving thrombus represented a greater challenge because of the comparatively low levels of expression indicated by western blotting. A biotinyl tyramide amplification system, reported to provide approximately one thousand times greater sensitivity[268], was optimized and specific staining with low levels of background was achieved for all three isoforms.

For all three PHD isoforms protein expression was localized to the cellular component of the thrombus and was detectable at all time-points analysed. At early time-points PHD1-3 was expressed in cells morphologically consistent with neutrophils. This is consistent with previous reports in which expression of PHD1-3 was identified in circulating neutrophils by immunoblotting[175]. Only a proportion of cells present in the day 14 thrombus stained positively for PHD1, PHD2 or PHD3. It is possible that these cells are macrophages as this cell type is recruited in increasing numbers to the resolving venous thrombus. PHD3 protein is strongly expressed in classically activated (M1) macrophages but not

in alternatively activated (M2) cells that may explain the pattern of localisation[173]. It is unclear whether skewing of macrophages has a similar effect on the expression of PHD1 and PHD2, however deletion of *Phd2* has been found to skew macrophages towards an M2 phenotype[164].

Chapter 4 The effect of constitutive heterozygous *Phd2* gene deletion on thrombus resolution

4.1 Introduction

Constitutive *Phd* gene knockouts have been generated for each of the three PHD isoforms. Homozygous deletion of *Phd1* and *Phd3* is well tolerated, with no observed impairment in development[155]. However, homozygous deletion of *Phd2* results in severe placental and cardiac defects and embryonic death at mid to late gestation (E12.5-13.5)[155]. Ablation of PHD2, but not PHD1 or PHD3, expression is associated with a marked stabilisation of HIF1α and up-regulation of hypoxia responsive genes such as *Vegfa*; revealing the importance of this isoform in the regulation of HIF1α and associated transcriptional activity in the development of the embryo[155].

In contrast to homozygous *Phd2* gene deletion, mice heterozygous for *Phd2* develop with no apparent embryonic defects. PHD2 has an important role in regulating angiogenesis in vivo. Heterozygosity for *Phd2* results in reduced tumour metastasis, potentially mediated by endothelial normalisation and improved tumour oxygenation[269]. Heterozygous deficiency for *Phd2* also improves restoration of limb perfusion, through increased macrophage mediated collateralization, in a murine model of critical limb ischaemia and improved myocardial collateralisation after infarction[164]. Further studies have demonstrated that angiopoeitin 1, an important mediator of endothelial disruption during the initiating phase of angiogenesis, acts as an endogenous repressor of PHD2 required for skewing of macrophages towards a proangiogenic phenotype[165].

4.2 Aim

To investigate the effect of constitutive heterozygous *Phd2* gene deletion on thrombus resolution.

4.3 Methods

4.3.1 Breeding strategy

Male and female heterozygous *Phd2* knockout mice ($PHD2^{+/-}$) on a BALB/c background were crossed to obtain both heterozygous knockouts and wild-type littermate controls ($PHD2^{+/+}$).

4.3.2 *Phd2* genotyping

I would like to acknowledge Mr Jens Serneels and Mr Yannick Jonsson for genotyping of *Phd2* knockout mice. DNA was extracted from tail snips using the hot sodium hydroxide and Tris (HotSHOT) method. Tail snips placed into individual PCR tubes containing 75µl of 25mM NaOH, 0.2mM disodium EDTA (pH12) and heated in a thermocycler at 94°C for 30mins to digest tissue and extract DNA. The extraction solution was neutralised with 75µl of 40mM Tris-HCl (pH 5).

Tail snip DNA was genotyped by PCR using a three-primer approach in which wild-type and knockout samples generate amplification products of differing sizes when resolved in agarose gels. The following primers (Integrated DNA technologies, UK) were used for *Phd2* genotyping.

Table 4.1 Genotyping primers

Primer	Sequence
PHD2 common	5' aaattctaatcgtagctgatgtgagc 3'
PHD2 wildtype	5' acctatgatctcagcatttgggag 3'
PHD2 knockout	5' tcaggacagtgaagcctagaaactct 3'

OneTaq DNA polymerase master mix (New England Biosystems, USA) was used according to the manufacturers instructions. A reaction mix was prepared for each gene of interest containing 12.5µl of master mix, 1µl of each primer (10µM), 1µl of template DNA and 6.5µl of DNAse free water. Amplification was performed in a thermocycler (PTC-100, Biorad, UK) under the following conditions: an initial 2mins at 94°C, 40 cycles of 30secs at 94°C, 30secs at 59°C, 30secs at 72°C with a final 10mins at 72°C.

PCR products were resolved on a 1% agarose gel, prepared by dissolving 1g of agarose (Sigma, UK) in 100ml of TAE buffer (Ambion, UK) by heating in a microwave. The gel was allowed to cool and 10µl of SYBRsafe (Invitrogen, UK) intercalating agent added prior to casting. The agarose gel was poured into a casting tray (Flowgen, UK) with both ends sealed and a comb inserted. After solidifying the comb was removed and the tray positioned in the electrophoresis tank (Flowgen, UK). The agarose gel was immersed in 1xTAE buffer. Samples were loaded into the wells accompanied by GeneRuler low range DNA ladder (Fermentas, UK). Samples were electrophoresed at 20V for 20mins followed by 60mins at 100V. Bands were visualised using the ChemiDoc MP gel documentation system (Biorad, UK).

This three-primer approach results in the formation of two DNA products corresponding to the wildtype allele (340bp) and the knockout allele (380bp). In heterozygous knockouts bands for both products will be present whereas wildtype controls will present as a single band and allows for easy differentiation between genotypes.

4.3.3 Thrombus induction

Prior to thrombus induction mice were weighed and measurements of mass recorded for subsequent analysis. Thrombi were induced in the inferior vena cava of 6-12 week old $PHD2^{+/-}$ mice and wild-type littermate controls, as previously described in Chapter 2.3.1, in an operator-blinded manner. Thrombi were harvested at days 1, 14 and 21 post-induction for analysis by histology (Fig 4.1). Kidneys were also excised and snap frozen in liquid nitrogen for PHD western blot analysis.

4.3.4 Tissue processing

Thrombi were processed as described in Chapter 2.3.2. Snap frozen kidney samples were separated into cytosolic and nuclear fractions as described in Chapter 3.3.8.

4.3.5 H&E staining

Thrombus sections were stained with H&E as described in Chapter 2.3.4.

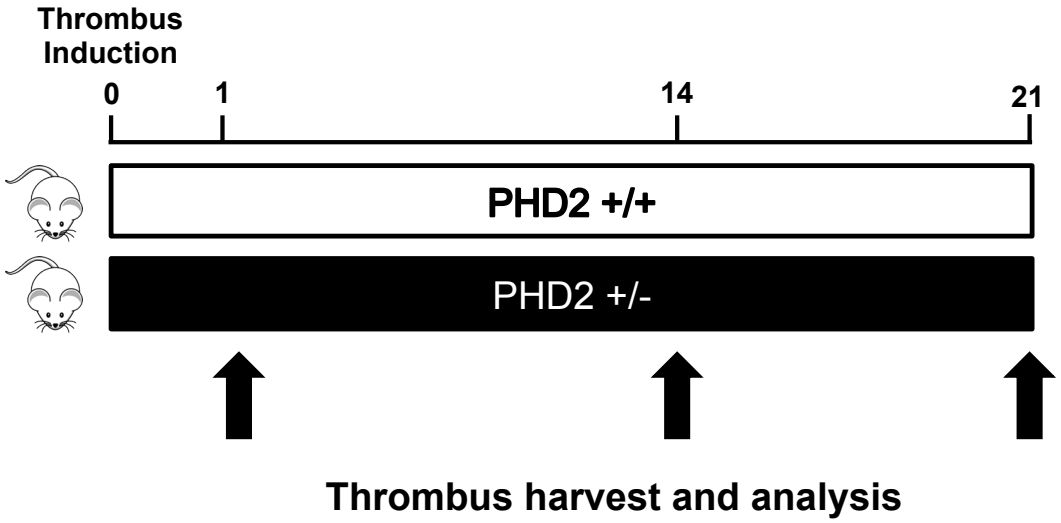

Figure 4.1 Study design

Thrombus was induced in 6-12wk old PHD2$^{+/-}$ and PHD2$^{+/+}$ mice on a Balb/c background. Thrombi were harvested at days 1, 14 and 21 post-induction for analysis by histology.

4.3.6 Immunohistochemical localisation of Mac-2

Sections were dewaxed, rehydrated through gradated alcohol washes and rinsed in tap water for 5mins. Endogenous peroxidase activity was quenched by incubating sections in 1%(v/v) hydrogen peroxide in PBS for 30mins. Heat-mediated antigen retrieval was carried out using an antigen access unit (Menarini Diagnostics, UK) at 110°C for 1min with citrate buffer (pH6, Menarini Diagnostics, UK). Sections were washed in two changes of PBS, ringed using a wax pen (Dako), blocked for 10mins using a serum free protein block (Dako) and incubated with primary antibody raised against Mac-2 (0.5µg/ml final concentration, clone M3/38, Biolegend, UK) diluted in PBS for 1hr and 2hrs respectively, at room temperature in a humidity chamber. Sequential sections were incubated with rat IgG at the appropriate primary antibody concentration to serve as negative controls. Slides were washed in PBS (3x10mins), incubated with biotinylated rabbit anti rat antibody (Dako, UK) for 45mins at room temperature and washed in PBS (3x10min). Sections were incubated with an extravidin peroxidase conjugate (Sigma, UK) for 1hr at room temperature. Specific antigen antibody complexes were visualised colourimetrically using a chromogenic substrate (Vector SG, Vector laboratories, UK). Sections were

washed in 3x10min PBS washes and counterstained in nuclear fast red (Vector laboratories, UK) for 7mins. Sections were rinsed in running tap water for 30secs prior to dehydration through graded alcohol solutions. Sections were cleared in 2x5min xylene washes, mounted with cover slips in DPX medium (Sigma, UK) and allowed to dry overnight.

4.3.7 Immunohistochemical localisation of CD31

Sections were dewaxed, rehydrated, quenched for endogenous peroxidase activity and antigen retrieved as previously described (4.3.4), followed by 3x2 min washes in PBS. Slides were carefully wiped dry around each section and the sections ringed using a wax pen. Care was taken not to allow sections to dry out before application of serum free protein block (Dako, 10mins at room temperature) to block non-specific antibody binding. Sections were incubated with primary antibodies raised against CD31 (0.2 µg/ml, Abcam, UK) for 2hrs at room temperature in a humid chamber. Sequential sections were incubated with rabbit IgG at the appropriate primary antibody concentration to serve as negative controls. Slides were washed in 3x10min PBS washes and incubated with HRP polymer for 30mins at room temperature. Slides were washed in 3x10mins PBS and specific antibody antigen complexes identified as described in Chapter 4.3.6. Sections were dehydrated through graded alcohol solutions, cleared in 2x5min xylene washes and mounted in DPX medium.

4.3.8 Localisation of collagen by picrosirius red staining

Sections were dewaxed and rehydrated, (4.3.4) and stained for collagen using a picrosirius red staining kit (Polysciences, UK). In brief, sections were incubated with a 0.2% (w/v) solution of phosphomolybdic acid for 2mins followed by a brief was in distilled water. Sections were then incubated in a 0.1% (w/v) solution of picrosirius red dissolved in a saturated solution of picric acid (3%, w/v), followed by a 2min incubation in 0.1N hydrochloric acid. Finally, sections were rapidly dehydrated through graded alcohols, cleared in 2x5min xylene washes and mounted in DPX.

4.3.9 Image analysis

Images were captured at either 50x or 200x magnification with a Leica light microscope (DMRB, Leica, Germany) using a microscope mounted digital camera (Micropublisher 3.3, QImaging, Canada) on a motorised stage

(ProScan, Datacell, UK). Thrombus was demarked using an region of interest (ROI) tool at each level using Image Pro Plus software (Media Cybernetics, UK) to provide cross sectional area, this was multiplied by the distance between levels and finally summated to provide quantitative data on thrombus volume (mm^3). Thrombus recanalisation was estimated by demarking the thrombus and the surrounding IVC using the ROI tool, recanalisation was expressed as a percentage of the total IVC lumen volume. Histogram-based thresh-holding with Image Pro Plus software (Media Cybernetics, UK) was used to select areas of Mac-2, Gr1 and picrosirius red staining. Thrombus neovascularisation was quantified by counting of CD31 positive channels. The percentage area of staining in all thrombus levels was assessed and the data represented as a mean percentage area or mean channel number.

4.3.10 Western blotting

Nuclear HIF1α and cytoplasmic PHD2 and PHD3 protein expression was determined by western blotting as described in Chapter 3.3.8. Nuclear HIF1α was detected using a rabbit anti-mouse antibody (NB100-479, Novus Biologicals, UK) at a concentration of 1μg/ml as previously reported[79]. Protein band intensity was quantified densitometrically using Image Lab software (Biorad, UK). Protein expression of cytoplasmic and nuclear extracts were normalised to αtubulin and Histone H3 respectively.

4.3.11 Statistical analysis

Kolmogorov-Smirnov tests were used to assess normality of data and parametric or non-parametric tests were used as appropriate. For data of mouse age, weight and parameters of thrombus resolution 2-way ANOVA was used. Chi-squared analysis was used to compare thrombus formation efficiency between knockouts and littermate controls. Densitometric values of PHD2, PHD3 and HIF1α protein expression on western blots were compared using Mann-Whitney U tests. In all cases $P<0.05$ was considered statistically significant. Statistical analyses were conducted using Prism Software (v5, Graphpad, USA). Parametric data represented as mean ± SE and non-parametric data represented as individual data points with median.

4.4 Results

4.4.1 Demographics of heterozygous *Phd2* knockout mice

Weight or age of heterozygous *Phd2* knockouts was not significantly different from their wild-type littermate controls at the time of thrombus induction (P>0.05, 2-way ANOVA, Table 4.2, Fig 4.2). Neither was there any significant difference between the proportions of each sex analysed at each time interval analysed. The efficiency of thrombus formation was not significantly different in *Phd2* knockout mice, 85% (21/25), when compared with wild-type littermate controls, 90% (16/18) as assessed by chi-square test (P>0.05).

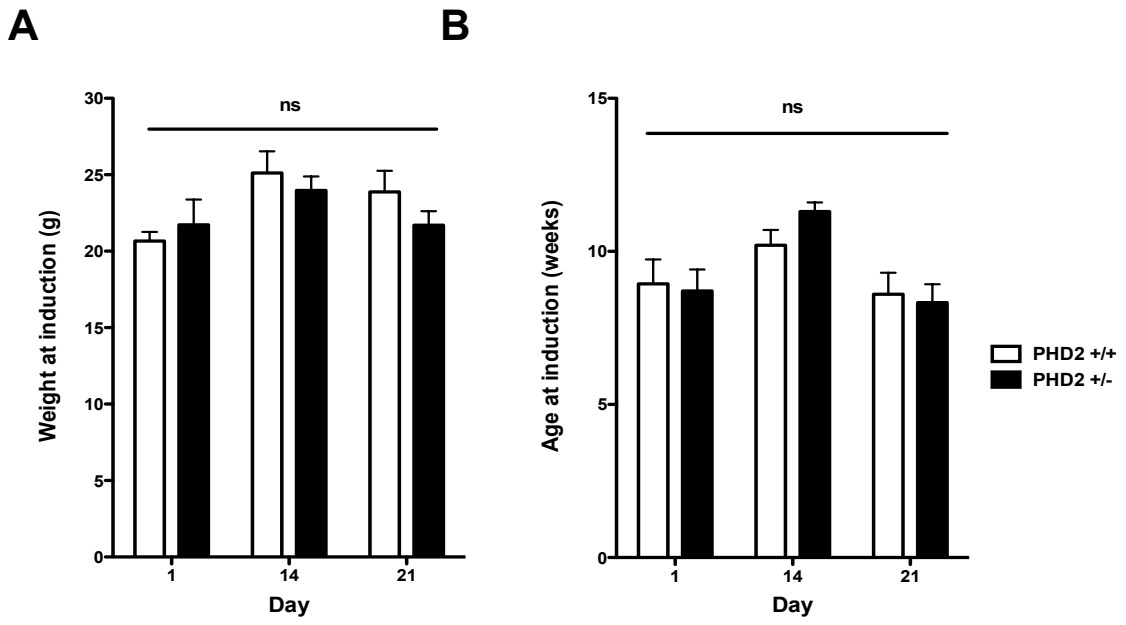

Figure 4.2 Demographics of heterozygous *Phd2* knockout and control mice

Measurements of mouse (A) weight (B) age and for $PHD2^{+/+}$ and $PHD2^{+/-}$ at the time of thrombus induction. No significant difference was observed in baseline characteristics (ns= P>0.05, 1-way ANOVA, n=5-9 per group). Data represented as mean ± SE.

4.4.2 Thrombus resolution in heterozygous *Phd2* knockout mice

Heterozygous deletion of *Phd2* did not have a significant effect on measures of thrombus resolution. There was also no significant difference in thrombus resolution (thrombus volume or vein recanalisation) or measures of thrombus organisation (recanalisation, collagen or macrophage content) between $PHD2^{+/-}$ mice and $PHD2^{+/+}$ littermate controls (1-way ANOVA, P>0.05, Table 4.3, Fig 4.3 A-C). Data of individual replicates is provided in Appendix B1.

Table 4.2 Demographics of heterozygous PHD2 knockout mice

Measure	Day	$PHD2^{+/+}$	$PHD2^{+/-}$
Weight (g)	1	20.7 ± 0.6	21.7 ± 1.7
	14	25.1 ± 1.4	24.0 ± 0.9
	21	23.9 ± 1.4	21.7 ± 0.9
Age (weeks)	1	8.94 ± 0.8	8.71 ± 0.7
	14	10.2 ± 0.5	11.3 ± 0.3
	21	8.60 ± 0.7	8.33 ± 0.6

Data represented as mean ± SE

Table 4.3 The effect of heterozygous PHD2 on thrombus resolution

Measure	Day	$PHD2^{+/+}$	$PHD2^{+/-}$
Volume (mm^3)	1	5.49 ± 0.7	5.92 ± 0.4
	14	2.13 ± 0.4	2.64 ± 0.3
	21	1.11 ± 0.2	0.58 ± 0.1
Recanalisation (%)	1	7.94 ± 1.1	5.97 ± 1.1
	14	24.0 ± 1.7	21.9 ± 1.2
	21	28.5 ± 3.2	37.2 ± 4.8
Neovascularisation (channels/level)	1	0.00 ± 0.0	0.00 ± 0.0
	14	13.5 ± 0.8	8.59 ± 0.6
	21	5.30 ± 0.9	7.27 ± 1.2
Macrophage content (%)	1	0.00 ± 0.0	0.00 ± 0.0
	14	7.89 ± 0.7	7.19 ± 0.7
	21	10.0 ± 0.6	9.14 ± 0.0
Collagen content (%)	1	0.55 ± 0.1	0.43 ± 0.1
	14	15.7 ± 0.8	14.4 ± 0.9
	21	33.5 ± 5.1	44.6 ± 4.3

Data represented as mean ± SE

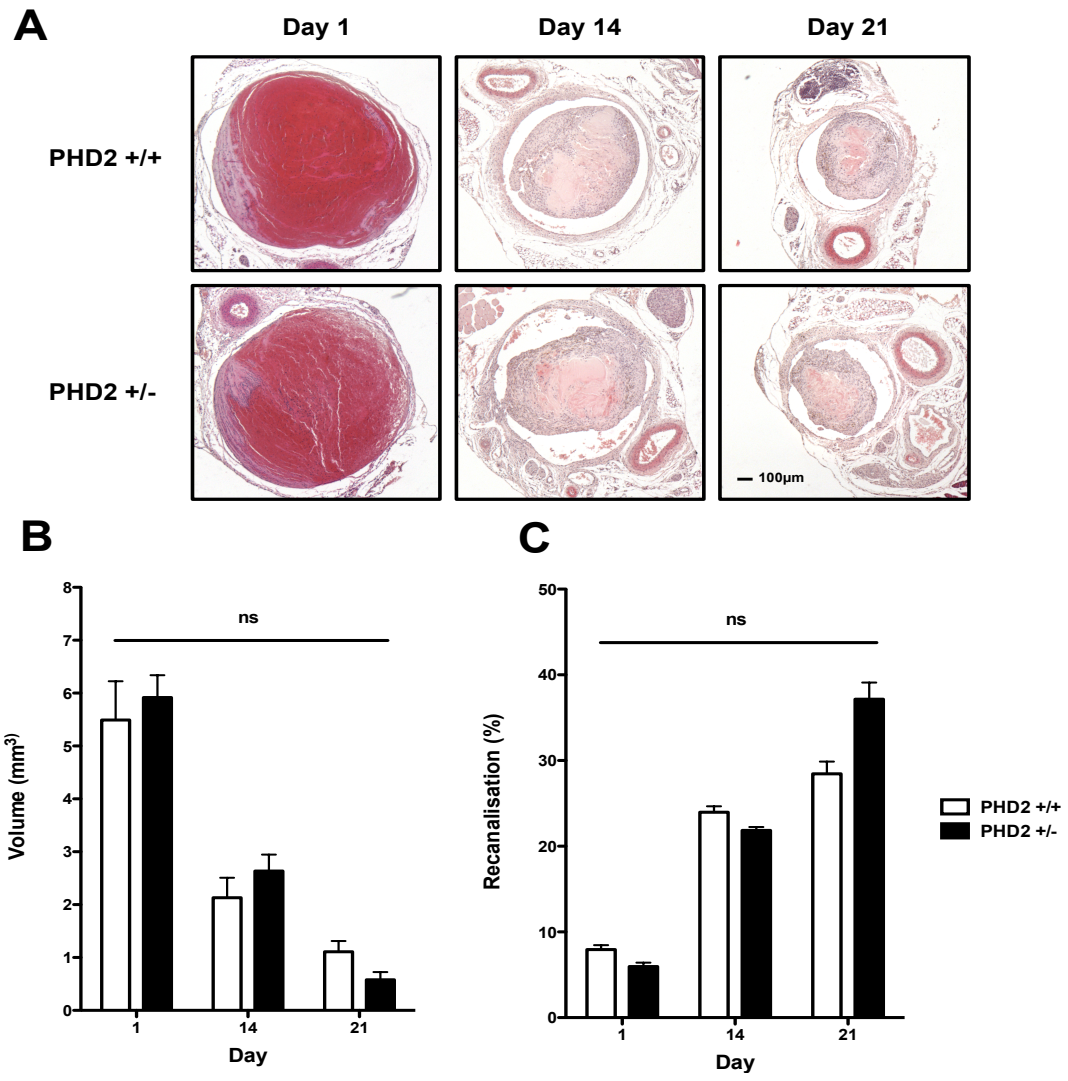

Figure 4.3 The effect of heterozygous *Phd2* gene deletion on thrombus resolution

(A) Representative haematoxylin and eosin stained micrographs of thrombi from PHD2$^{+/+}$ and PHD2$^{+/-}$ at days 1, 14 and 21 post-induction taken at an original magnification of x50. Histological measurements of (B) thrombus volume and (C) vein lumen percentage recanalisation demonstrating no significant difference between knockout and respective littermate controls (ns=P>0.05, 2-way ANOVA, n=5-9 per group). Data represented as means ± SE.

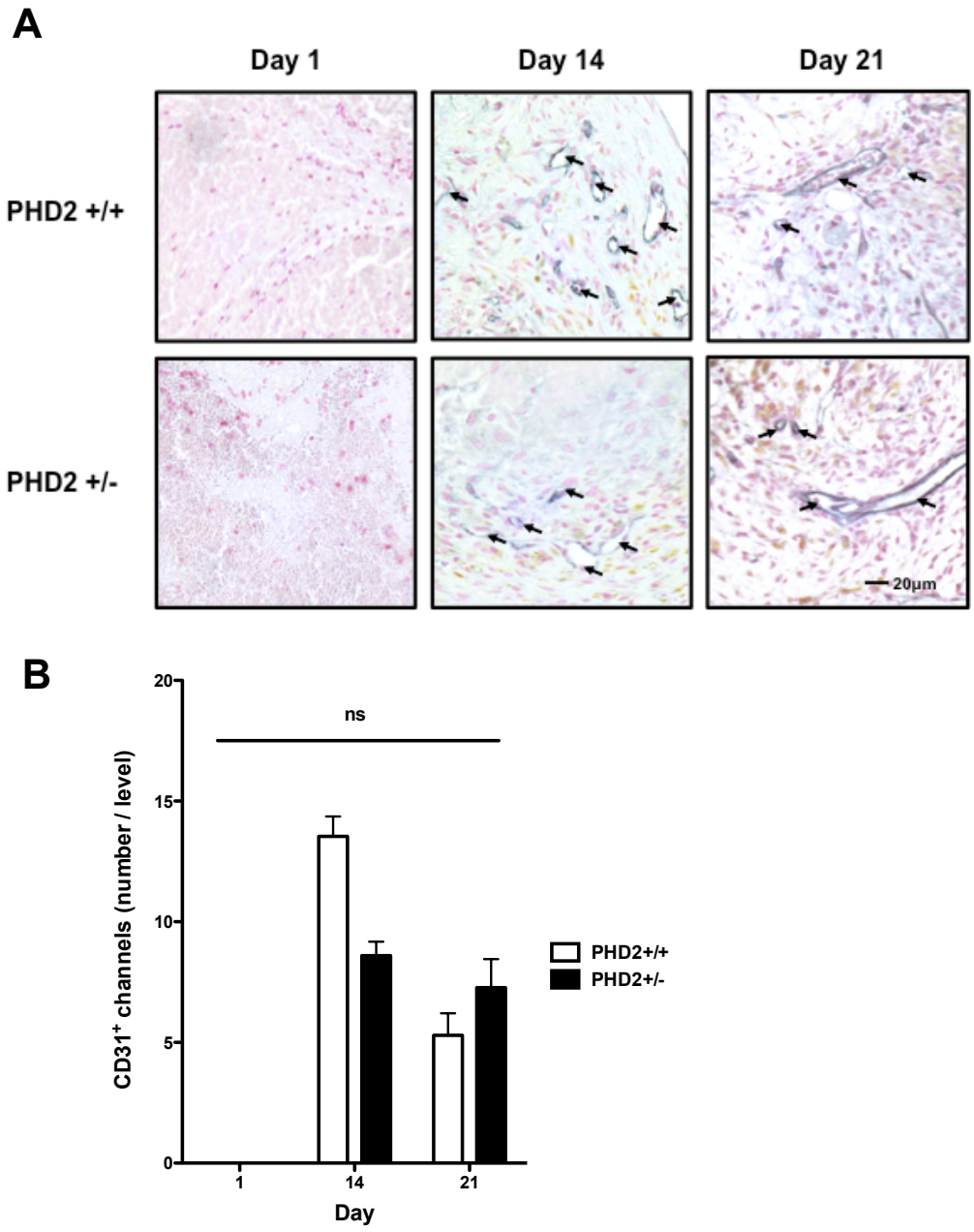

Figure 4.4 The effect of heterozygous *Phd2* gene deletion on thrombus neovascularisation

(A) Representative micrographs of CD31 positive neovascular channels in thrombi from PHD2$^{+/+}$ and PHD2$^{+/-}$ at days 1, 14 and 21 post-induction taken at an original magnification of x400. (B) Histological measurement of the percentage area of the thrombus stained postively for Mac-2 (ns= P>0.05, 2-way ANOVA, n=5-9 per group). Data represented as means ± SE.

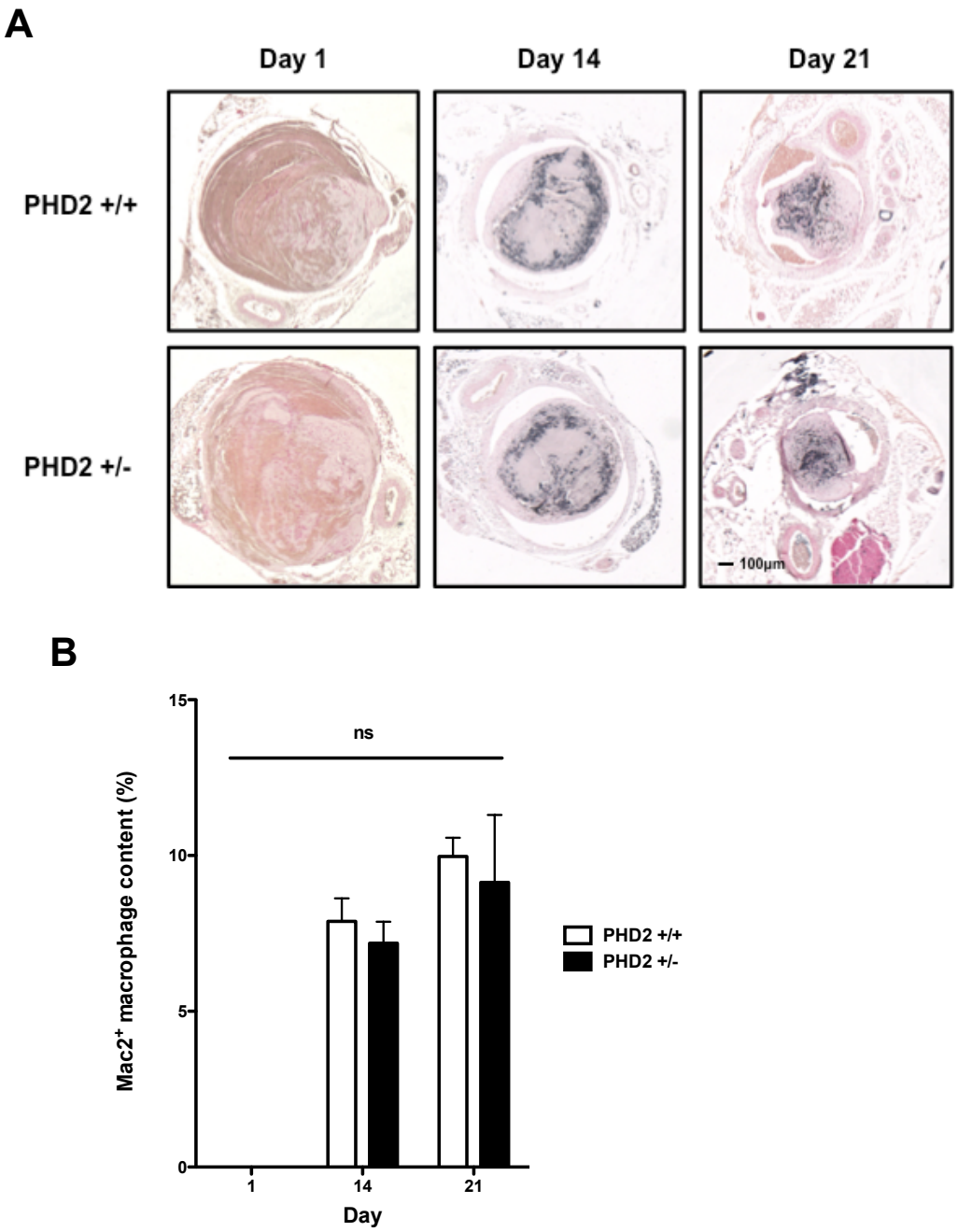

Figure 4.5 The effect of heterozygous *Phd2* gene deletion on thrombus macrophage content

(A) Representative Mac-2 stained micrographs of thrombi from $PHD2^{+/+}$ and $PHD2^{+/-}$ at days 1, 14 and 21 post-induction taken at an original magnification of x50. (B) Histological measurement of the percentage area of the thrombus stained postively for Mac-2 (ns= P>0.05, 2way ANOVA, n=5-9 per group). Data represented as means ± SE.

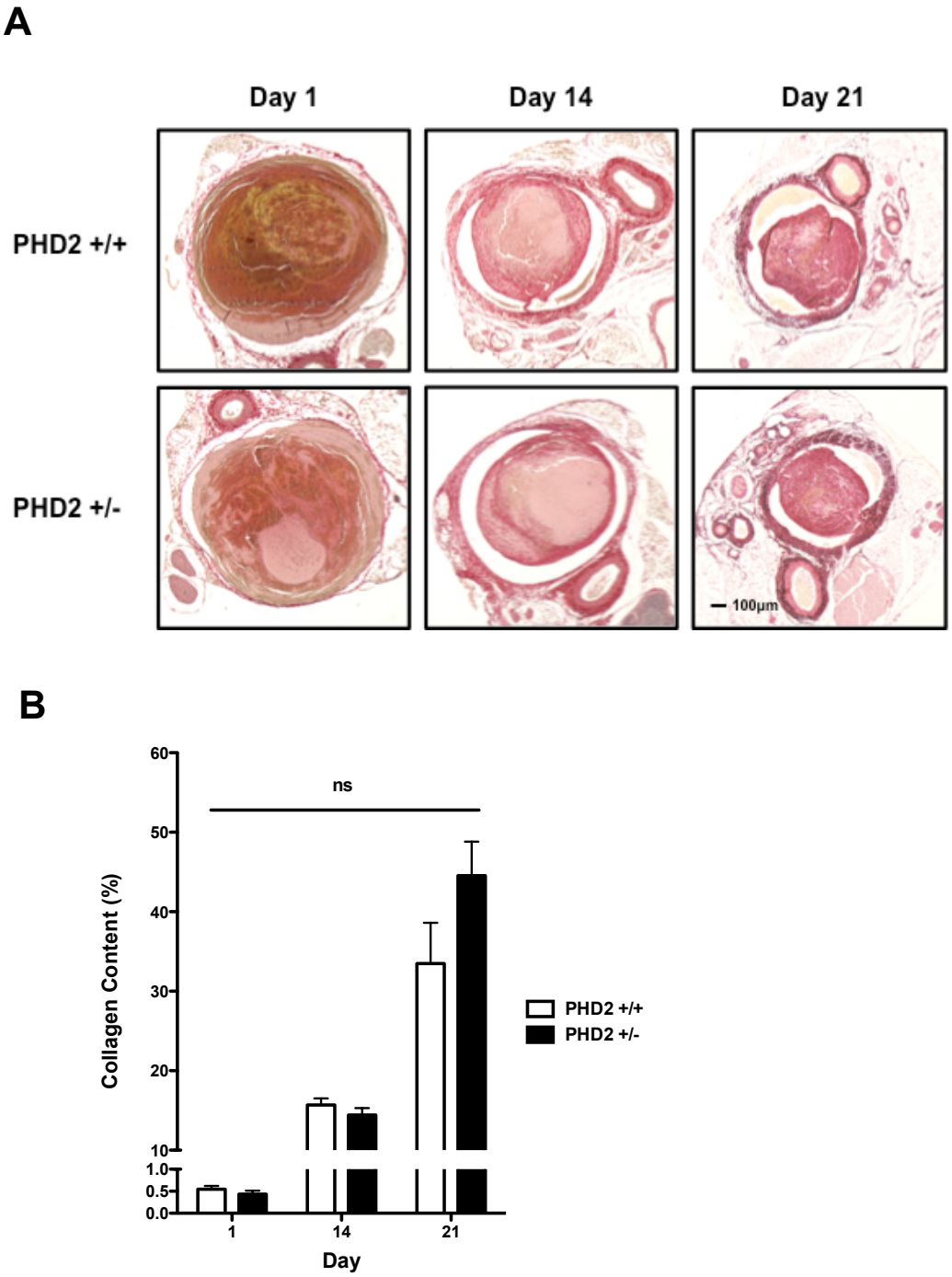

Figure 4.6 The effect of *Phd2* gene deletion on collagen deposition in the thrombus

(A) Representative picrosirius red staining of PHD2$^{+/+}$ and PHD2$^{+/-}$ thrombi at 1, 14 and 21days post-induction (mag x50). (B) Histological measurement of the percentage area of the thrombus stained postively for picrosirius red (ns= P>0.05, 2-way ANOVA, n=5-9 per group). Data represented as means ± SE.

4.4.3 Efficacy of *Phd2* gene deletion

Heterozygous *Phd2* gene deletion resulted in lower protein levels of PHD2 and PHD3 compared with wild-type littermate controls, but this did not reach statistical significance (P>0.05 Mann-Whitney U test, Fig 4.7). Nuclear HIF1α protein levels in these samples were similar in PHD2$^{+/-}$ and littermate controls (P>0.05, Fig 4.8).

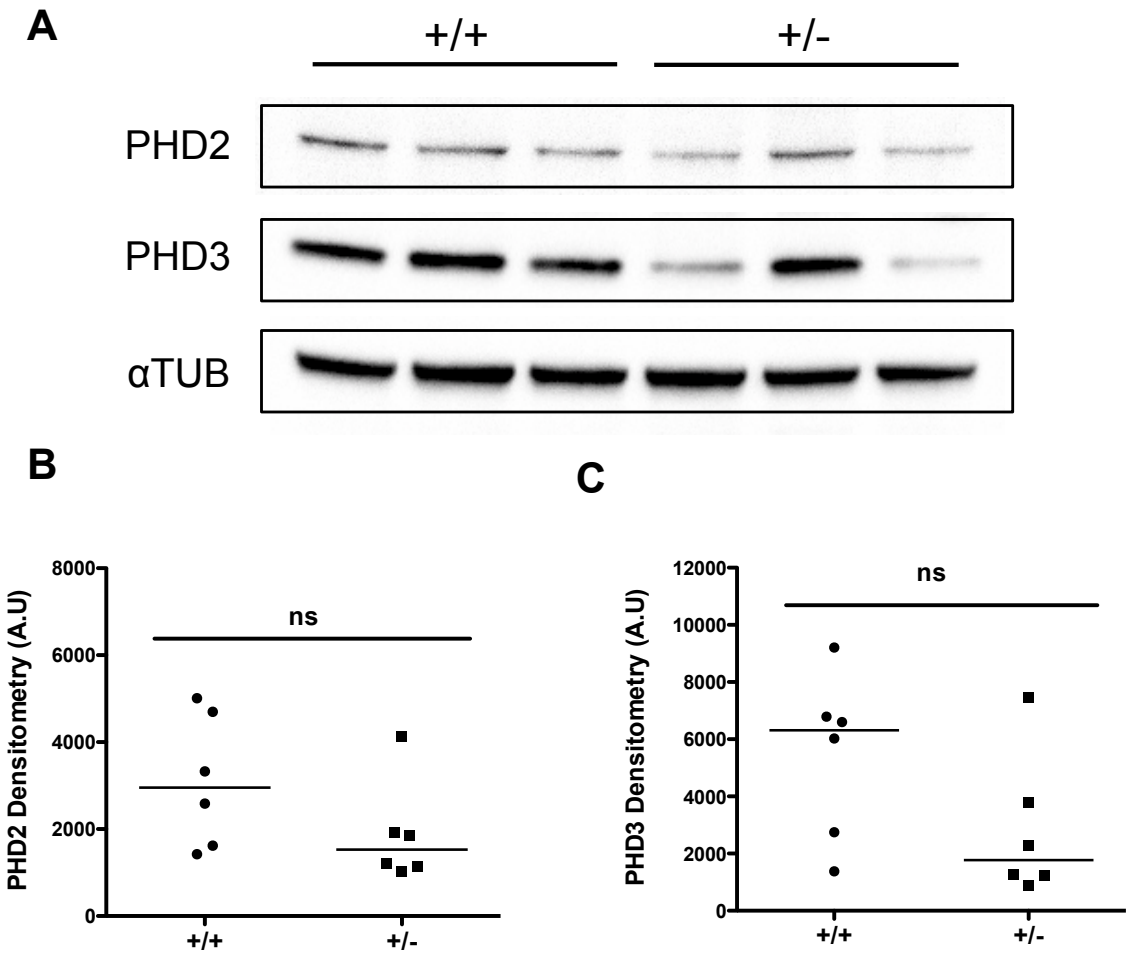

Figure 4.7 Immunoblot of cytoplasmic PHD2 and PHD3 in *Phd2* heterozygous knockout kidney

(A) Representative immunoblot of PHD2 and PHD3 protein expression in kidney cytoplasmic extracts from PHD2 heterozygous (+/-) knockouts and wild-type (+/+) littermate controls. Densitometric analysis of (B) PHD2 and (C) PHD3 protein expression normalised to αTubulin (ns= P>0.05, Mann-Whitney). Data represented as individual points and median.

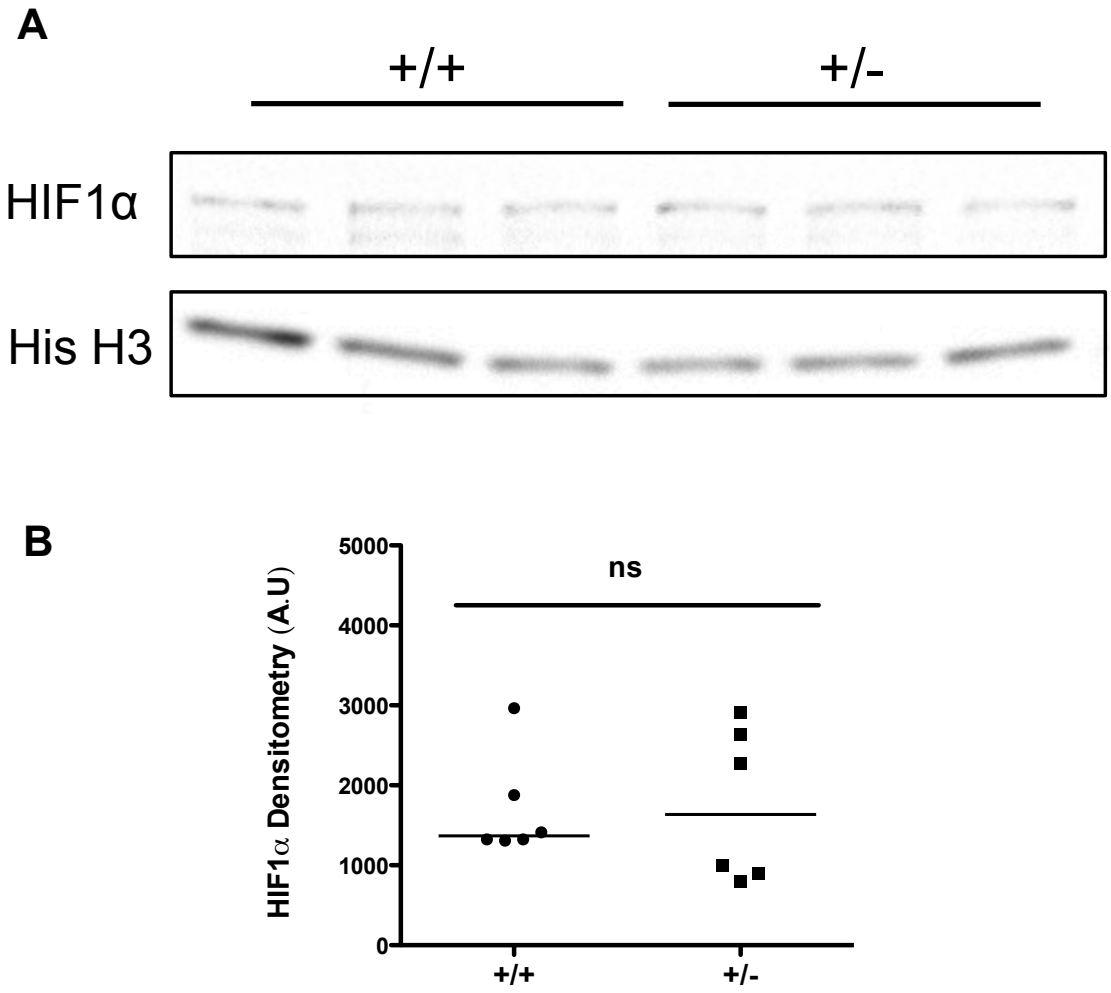

Figure 4.8 Immunoblot of nuclear HIF1α in *Phd2* heterozygous knockout kidney

(A) Representative immunblot of HIF1α protein expression in kidney nuclear extracts from PHD2 heterozygous knockouts and wild-type littermate controls. (B) Densitometric analysis of HIF1α protein expression normalised to Histone H3 (ns= P>0.05, Mann-Whitney). Data represented as individual points and median.

4.5 Discussion

Heterozygous deletion of the *Phd2* gene had no effect on any measure of thrombus resolution examined in this study that included; thrombus volume, vein recanalisation, thrombus neovascularisation, collagen and macrophage content. Measures of thrombus formation between wild-type and knockout were not signficantly different, suggesting that heterozygosity for *Phd2* does no affect thrombus formation. In agreement with this finding thrombus volumes 24hrs post induction were comparable between wild-type and *Phd2* heterozygous knockouts.

It was hypothesised that under situations of increased HIF1α stabilisation, such as that predicted after heterozygous *Phd2* gene deletion, increased neovascular channel formation and macrophage infiltration would be observed complementing previous observations in the thrombus after PHD inhibition[57]. The lack of significant difference in these markers of thrombus organisation is, however, consistent with previous findings in the same constitutive heterozygous knockout system where, during tumour development, vascularisation and leukocyte infiltration remained broadly unchanged[160]. Instead, heterozygous deletion of *Phd2* was associated with increased tumour vessel normalisation as demonstrated by improved vessel maturation and reduced vessel leakage[160]. Additionally recruitment of macrophages to sites of tissue hypoxia, such as the ischaemic hindlimb, does not appear to be altered by heterozygosity for *Phd2* instead resulting in skewing of this cell type towards an alternately activated phenotype[164]. These findings go some way to explaining the observed phenotypes with respect to venous thrombus resolution.

Kidney samples were analysed by western blotting in order to examine the effect of heterozygous *Phd2* gene deletion on PHD protein expression and HIF1α stabilisation as this technique was not sensitive enough to detect thrombus levels of PHDs. Despite marked reductions in the expression of PHD2 and PHD3 in the cytoplasmic fraction of $PHD2^{+/-}$ kidney extracts, this difference was not significant. The lack of significance with this degree of difference and a small sample number could have been the result of a Type-II error. This finding

is, however, similar to a study of tissue lysates from embryonic tissues, in which PHD2$^{+/-}$ mice were found to retain a large degree of PHD2 protein expression[155]. The reduction in PHD3 expression, if genuine would be surprising as the *Phd3* gene contains a promoter-resident HRE[98]. It would therefore be expected for *Phd3* gene expression to be upregulated in response to HIF1α stabilisation[270].

Heterozygous deletion of *Phd2* should have lead to increased nuclear accumulation of HIF1α. However, in the present study HIF1α stablisation was not increased in nuclear extracts from the kidneys of PHD2$^{+/-}$ mice. Whilst surprising this is in keeping with the previous data that showed efficient HIF1α degredation in PHD2$^{+/-}$ embryonic hearts[155]. Together, these data suggest that, at the tissue level, remaining expression of PHD2 in heterozygous knockouts is capable of hydroxylating the HIF1α and preventing stabilisation. Post-translational compensation in constitutive heterozygous gene deletents has been reported in the literature, occuring either as a result of reduced protein turnover or increased utilisation of the remaining mRNA[271]. It is possible that PHD1 and PHD3 expressed in the resolving venous thrombus may have compensated for the loss in PHD2 expression since both of these isozymes have been shown to hydroxylate HIF1α *in vitro*[272].

Quantification of protein expression by western blotting was associated with a large degree of variability. Kidney tissue samples were taken from the same region and were of equal mass for subsequent processing. Tissue samples were processed in batches containing equal numbers of knockout and control tissues to limit the potential of batch variability affecting protein extraction efficiency. One advantage of this immunoblotting approach, over alternative techniques such as ELISA, is that it allowed for normalisation of protein expression to house keeping genes, such as αTubulin and Histone H3.

The majority of studies investigating venous thrombus resolution selectively use 8-10 week old mice. This strategy is designed to avoid variability in thrombus induction that has, in part, been attributed to age**.** Age has been found to modulate thrombus formation with both propensity and speed of thrombosis increasing in models of accelerated aging[273, 274]. Mice over a broader age range

(7-12 weeks) were included in this study because of the limited supply of $PHD2^{+/-}$ mice. Relaxation of the study inclusion criteria could introduce additional biological variability into the experiment. In the present study mouse demographics were well controlled with no significant differences in either mouse age or mass at the time of thrombus induction. This suggests that changes in thrombus resolution are not likely to be obscured by differences in mouse demographics.

Chapter 5 The effect of inducible *Phd2* gene deletion on venous thrombus resolution

5.1 Introduction

No significant difference in thrombus resolution was observed after heterozygous gene deletion of *Phd2* (Chapter 4). Only a modest loss in cytoplasmic PHD2 protein expression was observed in *Phd2* heterozygous knockouts compared with wild type littermate controls and it is, therefore, possible that residual PHD2 protein expression may have been sufficient to limit the nuclear accumulation of HIF1α. It is not possible to study the effects of constitutive homozygous *Phd2* gene deletion as this genotype demonstrates embryonic lethality that precludes studies in adulthood[155]. An inducible cre recombinase loxP based *Phd2* knockout system has been developed allowing for deletion of PHD2 protein expression during adulthood[169].

The cre recombinase *LoxP* system, first identified as part of the replicative machinery of the P1 bactriophage, is a powerful tool for the manipulation of the murine genome[275]. The *LoxP* construct is a 34bp sequence containing an 8bp core flanked by two 13bp inverted repeats[276]. When *LoxP* constructs are inserted in the same orientation flanking a gene of interest this region can be excised upon expression of cre recombinase (Fig 5.1)[275]. Induction of cre recombinase expression can be controlled through use of tamoxifen inducible elements[277]. In addition gene deletion can be limited to selected tissues or cells by placing cre recombinase expression under the control of tissue specific promoter elements[277].

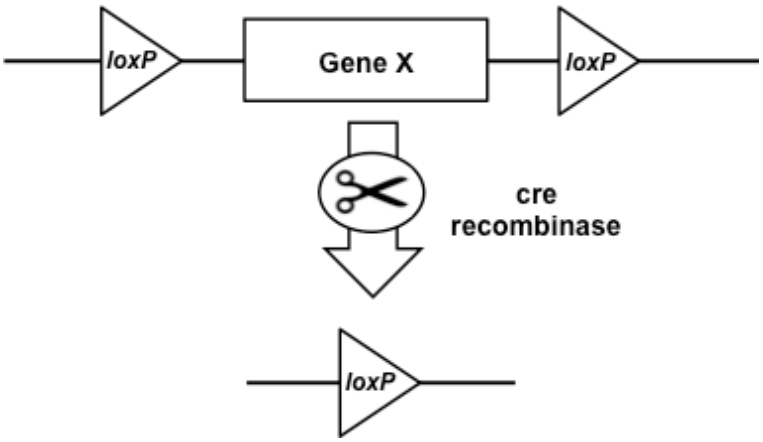

Figure 5.1 Schematic of *LoxP* cre mediated recombination
LoxP sites flanking a gene of interest allows for excision on expression of cre recombinase.

Initial observations of inducible all-cell homozygous *Phd2* knockout mice revealed significantly increased serum EPO, erythrocyte count and haematocrit[143, 169]. These hemodynamic changes, consistent with polycythemia, are associated with reduced survival thought to be a result of venous obstruction and cardiac hypertrophy[169]. Deletion of *Phd2* in CD68-expressing cells was also found to induce polycythemia with further evidence to suggest that this takes place in a HIF2α dependent manner[170].

Inducible gene deletion of *Phd2* has been studied in a number of pathologies relevant to venous thrombus resolution. In an orthotopic model of cancer global *Phd2* gene deletion increased markers of angiogenesis such as vessel coverage and perfusion, although not absolute vessel number[269]. These alterations in angiogenesis were not associated with changes in tumour volume in all-cell, endothelial, fibroblast or macrophage specific *Phd2* gene knockouts[269]. In a model of hypertension-induced cardiac remodelling macrophage specific *Phd2* gene deletion significantly reduced myocardial collagen gene expression and interstitial cardiomyocyte fibrosis[278].

5.2 Aim

To investigate the effect of all-cell inducible *Phd2* gene deletion on venous thrombus resolution

5.3 Methods

5.3.1 Breeding strategy

Breeding was carried out in the Mazzone laboratory (Katholieke Universiteit Leuven, Belgium). Breeding pairs with the following genotypes were crossed;

$PHD2^{fl/fl}$; $Rosa26creERT2^{+/-}$ x $PHD2^{fl/+}$; $Rosa26creERT2^{+/+}$

$PHD2^{fl/fl}$; $Rosa26creERT2^{+/+}$ x $PHD2^{fl/+}$; $Rosa26creERT2^{+/-}$

This enables generation of homozygous and heterozygous floxed PHD2 alleles in mice either with or without alleles for the conditional expression of cre recombinase. From these crossings the following genotypes were obtained with the following effective genotypes;

Table 5.1 Actual and effective genotypes of conditional PHD2 knockouts

Actual	Effective
$PHD2^{fl/fl}$; $Rosa26creERT2^{+/+}$	Wild-type
$PHD2^{fl/+}$; $Rosa26creERT2^{+/+}$	Wild-type
$PHD2^{fl/+}$; $Rosa26creERT2^{+/-}$	Heterozygous
$PHD2^{fl/fl}$; $Rosa26creERT2^{+/-}$	Homozygous

5.3.2 Genotyping

DNA was extracted as described in Chapter 4.3.2. Tail snip DNA was genotyped for both cre recombinase and *Phd2* floxed alleles. The following primers (Integrated DNA technologies, UK) were used.

Table 5.2 Genotyping primers

Primer	Sequence
CRE1	5’ cgccgtaaatcaatcgatgagttgcttc 3’
CRE2	5' gatgccggtgaacgtgcaaaacaggctc 3'
PHD2CKO1	5’ ccttccatgttggctcattccatt 3’
PHD2CKO1	5' tgctga-attgagttgcataccttg 3'

Separate reactions were prepared for genotyping of cre recombinase and *phd2* floxed alleles. OneTaq DNA polymerase master mix (New England Biosystems, USA) was used according to the manufacturers instructions. A reaction mix was prepared for each gene of interest containing 12.5µl of master mix, 1µl of each primer (10µM), 1µl of template DNA and 7.5µl of DNAse free water. Amplification was performed in a thermocycler (PTC-100, Biorad, UK) under the following conditions: an initial 2mins at 94°C, 40 cycles of 30secs at 94°C, 30secs at 62°C (*Cre*) or 53°C (*Phd2*), 30secs at 72°C with a final 10mins at 72°C. PCR products were resolved as described in Chapter 4.3.2.

5.3.3 Thrombus induction

Tamoxifen was administered at a dose of 1mg/mouse/day as previously reported[269] in mice 5 days before thrombus induction. This results in effective excision of *Phd2* alleles in floxed cre recombinase positive mice with cre recombinase negative mice serving as controls for both the presence of floxed alleles and tamoxifen treatment.

Mice received daily intraperitoneal injections of tamoxifen (1mg) for 5 days prior to induction of thrombosis. Thrombus was induced in 7-17 week old mice on a C57B/6 background with effective wild-type, heterozygous and homozygous genotypes. Mice received longitudinal 3D high frequency ultrasound scans of the infrarenal IVC at days 1, 7 and 14 post-induction (Fig 5).

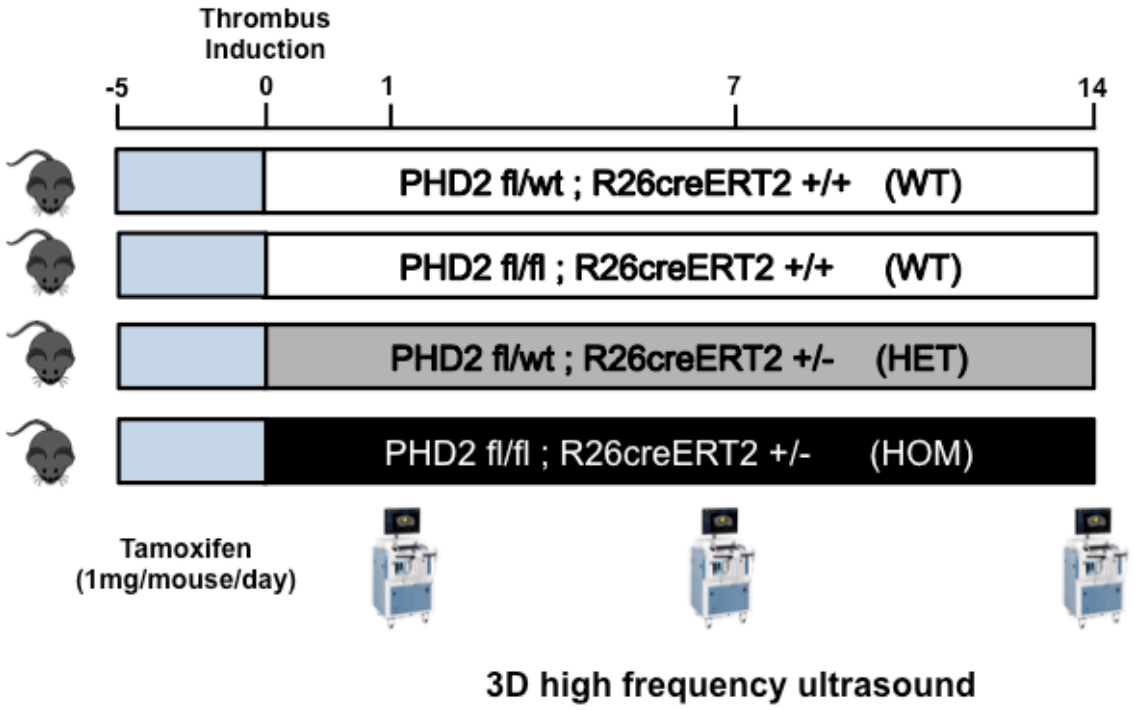

Figure 5.2 Study Design

Mice received daily 1mg injections of tamoxifen for five days preceeding thrombus induction. Thrombus was imaged at days 1, 7 and 14 post-induction by 3D-HFUS and by histology at day 14 post-induction.

5.3.4 3D High frequency ultrasound

Thrombus was visualised by 3D high frequency ultrasound (3D-HFUS) of the abdomen using a 40MHz ultrasound probe connected to a Vevo2100 imaging unit (Visual Sonics, Canada, Figure 5.3). Anaesthesia was induced by inhalation of isofluorane (5%, 1.0 l/min O_2) and maintained at 3.0-3.5% for the duration of the procedure. Hair was removed from the abdomen of the mouse by application of depilating cream. The mouse was secured to the imaging stage in the supine position and connected to the physiological monitoring unit to enable respiration gating during image acquisition. Ultrasound transmission gel was placed on the abdomen and the ultrasound probe secured to the stepper motor. The infra-renal IVC was located by traversal of the probe in the transverse orientation. A 12mm segment of the IVC, containing the thrombus, was imaged with data acquired at 108μm intervals at a maximum depth of 8mm. Image stacks were exported as DICOM files to allow for analysis using Osirix software (v5.5). Thrombus was manually segmented from surrounding

tissue using the closed polygon tool and the segments reconstructed as a 3D volume render from which measurements of thrombus volume were obtained, representative images of the segmentation process are provided in Appendix C1. I would like to acknowledge Stéphanie De Vleeschauwer and Melissa Swinnen (Katholieke Universiteit Leuven, Belgium) for assistance in developing this technique.

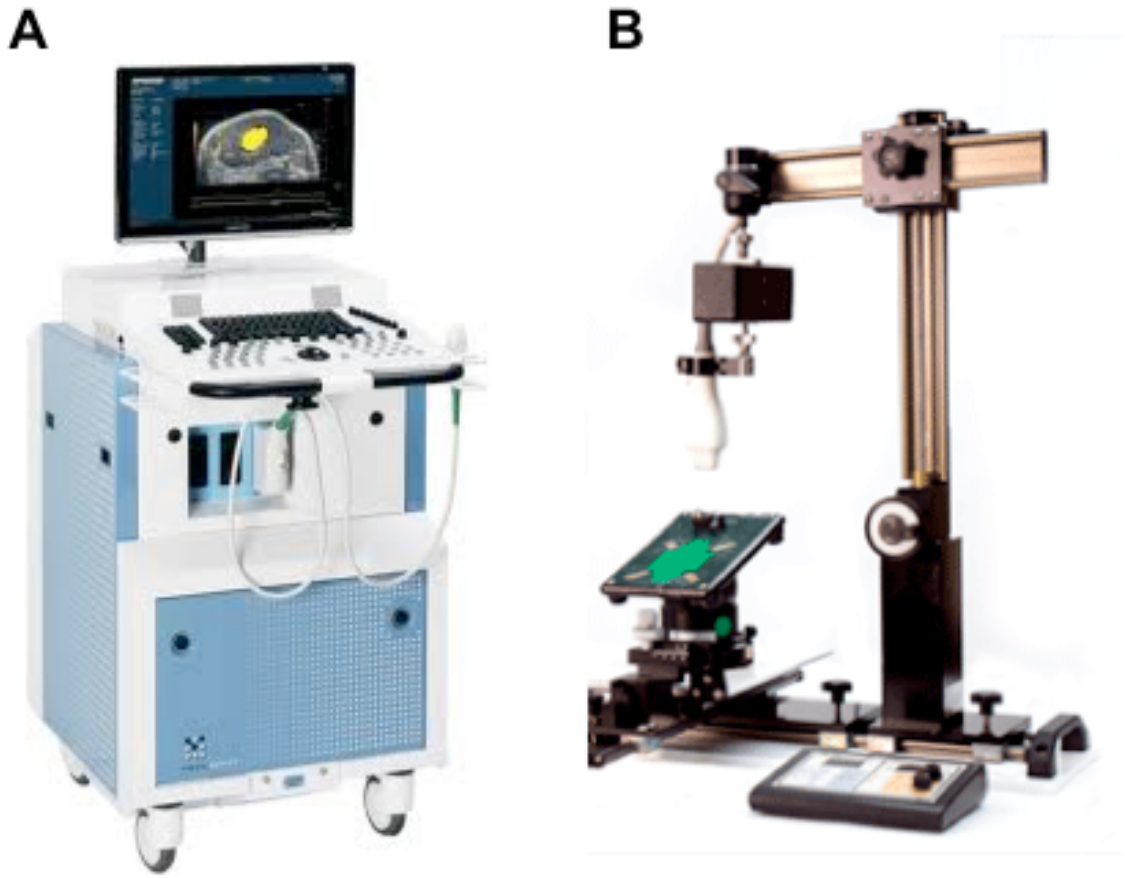

Figure 5.3 3D High frequency ultrasound

(A) The Vevo 2100 HFUS and (B) mounting of 3D stepper motor on integrated rail system with the probe.

5.3.5 Tissue processing

Tissues were harvested and processed as described in Chapter 4, Section 4.3.4.

5.3.6 Histology and immunohistochemistry

Thrombus sections were stained with H&E, CD31, Mac-2 and picrosirius red at described in Chapter 4, Sections 4.3.5-4.3.9.

5.3.7 Western blotting

Kidney samples were blotted for PHD2, PHD3, αTubulin, HIF1α and Histone H3 at detailed in Chapter 4, Section 4.3.10.

5.3.8 Haematocrit measurements

Blood was sampled by cardiac puncture, collected into graduated EDTA anti-coagulated tubes (Greiner Bio-One, UK) and centrifuged for 10mins at 10,0000xg. The total volume (TV) of blood collected and the mean corpuscular volume (MCV) were recorded and haematocrit reported as a percentage.

5.3.9 VEGF ELISA

The concentration of VEGF in murine plasma samples was quantified using a commercially available ELISA assay (Quantikine, R&D systems, USA) according to the manufacturers instructions. VEGF standard was serially diluted to provide a seven-point standard curve (500, 250,125, 52, 21, 16 and 8pg/ml) and calibrator diluent was used as a blank zero standard. Plasma samples were diluted 1 in 5 by addition of calibrator diluent. The microplate was prepared by addition of 50µl of assay diluent. Standards and samples were then added (50µl) in triplicate and incubated for 2hrs at room temperature. Samples were removed and wells washed 5 times by addition of 400µl of wash buffer using an automated washer (Multiwash III, TriContinent, USA). VEGF conjugate (100µl) was added to the wells and incubated for 2hrs at room temperature. Wash steps were repeated and 100µl of TMB peroxidase substrate solution added followed by a 30min incubation protected from light. Stop solution (100µl) was added and absorbance recorded at 450nm using a spectrophotometer (SpectraMax 340, Molecular Devices, USA). VEGF plasma concentrations were interpolated from the VEGF standard curve plotted using a 4-parameter fit.

5.3.10 Statistical analysis

Normality of data was assessed by Kolmogrov-Smirnov tests with parametric or non-parametric tests used as appropriate. Differences in thrombus volume and rate of resolution as determined by 3D-HFUS were interrogated by repeated-measure 2-way ANOVA with post-hoc Bonferroni. Mouse demographics and histological measurements of thrombus volume were assessed by 1-way ANOVA with post-hoc Bonferroni. Measurements of protein expression (PHD and HIF1 α) and blood haematocrit were interrogated by Kruskal-Wallis with Dunn's post-hoc tests. Measurements of plasma VEGF were analysed using a student's t-test. In all cases $P<0.05$ was considered statistically significant. Statistical analyses were conducted using Prism Software (v5, Graphpad, USA). Parametric data represented as mean ± SE and non-parametric data represented by individual data points with median.

5.4 Results

5.4.1 Visualisation and quantification of thrombus resolution by 3D HFUS

Thrombus was hyperechoic compared with blood (Fig 5.4). Segmentation of the thrombosed IVC at days 1, 7 and 14 post-induction enables reconstruction of 3D renders from which estimates of thrombus volume can be made (Fig 5.5). A 3D image stack of a representative day 1 thrombus visualised by 3D-HFUS is provided in Appendix C2.

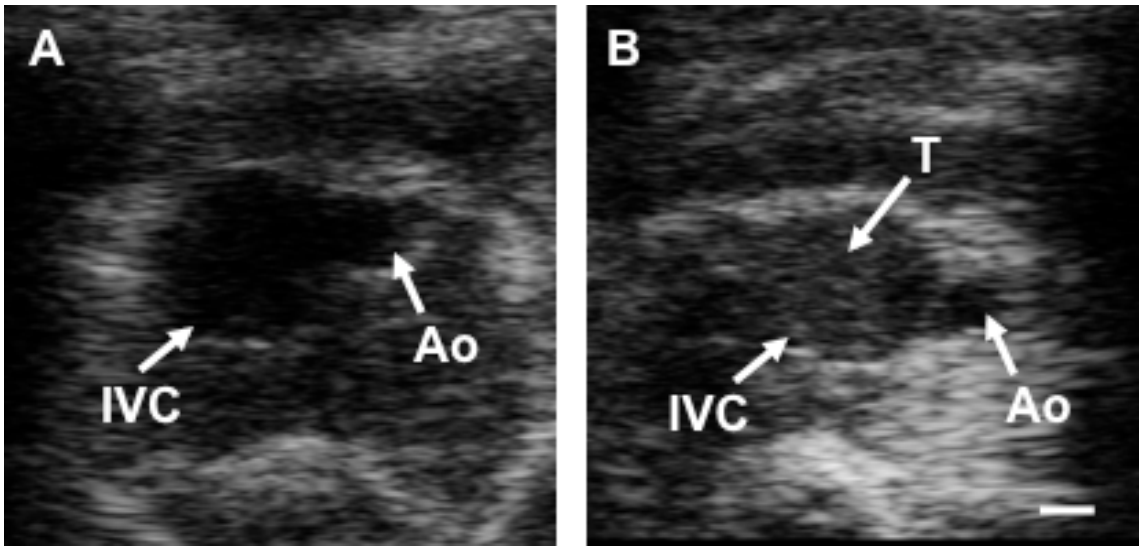

Figure 5.4 HFUS of the thrombosed IVC

Transverse HFUS sections of the IVC in (A) sham-operated and (B) operated mice in which a hyperechoic thrombus (T) is present, scale bar represents 500μm. Identification of the thrombosed IVC can be aided by proximity of the aorta (Ao).

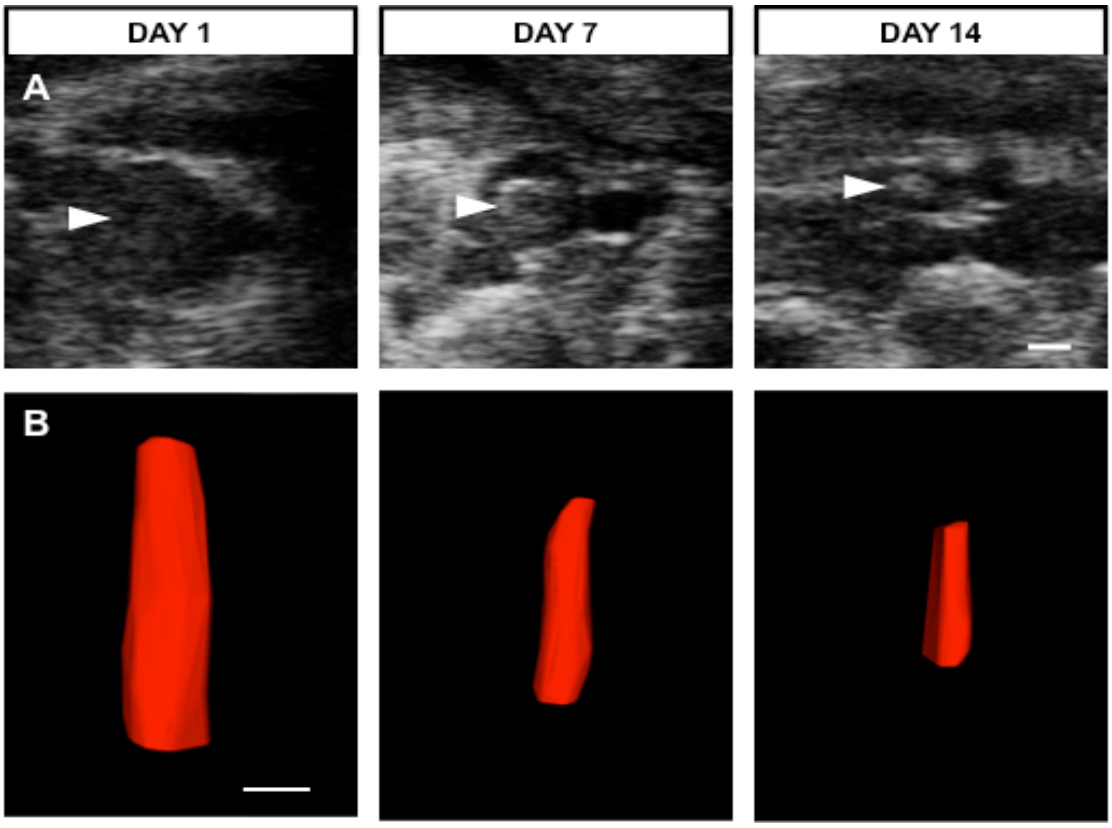

Figure 5.5 3D HFUS and volumetric reconstruction of venous thrombi

(A) Representative transverse HFUS slices of the intraluminal thrombus (white arrowhead) at days 1, 7 and 14 days post-induction, scale bar represents 500μm. (B) Representative 3D volume renders of thrombus at 1, 7 and 14 days post-induction, scale bar represents 200μm.

5.4.2 Demographics

Mass or age of wild-type, heterozygous and homozygous inducible all-cell PHD2 knockout mice was not significantly different between groups (P>0.05, 1-way ANOVA, Table 5.3, Fig 5.6).

Table 5.3 Demographics of inducible *Phd2* knockout mice

Genotype	+/+ (n=7)	+/- (n=5)	-/- (n=6)
Mass (g)	22.3 ± 0.6	23.3 ± 1.1	25.4 ± 1.5
Age (weeks)	10.9 ± 1.7	10.8 ± 1.8	13.1 ± 1.7

Data represented as mean ± SE

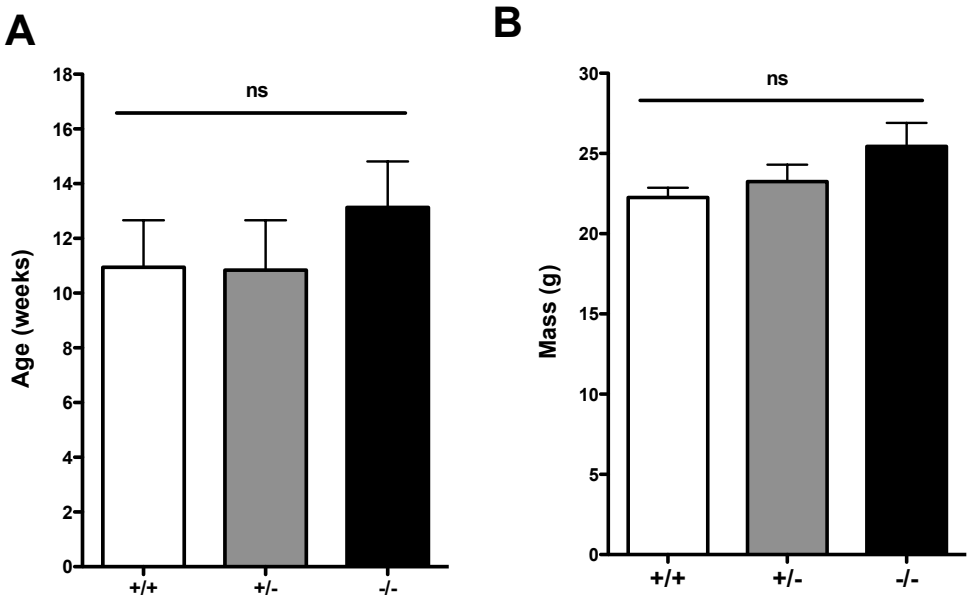

Figure 5.6 Demographics of inducible *Phd2* knockout mice

Measurements of mouse (A) mass and (B) age in inducible *Phd2* knockouts at the time of thrombus induction (n=5-7 per group). No significant difference was observed in baseline characteristics (ns= P>0.05, 1-way ANOVA), data represented as mean ± SE.

5.4.3 Thrombus resolution in *Phd2* inducible knockout measured by 3D HFUS

No significant difference between genotypes was observed in either thrombus volume (P>0.05, 2-way ANOVA, Table 5.4, Fig 5.7A/C) or the rate of thrombus resolution expressed as the percentage decrease in volume between days 1 and day 7 or day 7 and day 14 (P>0.05, 2-way ANOVA, Table 5.5, Fig 5.7B). Data of individual replicates is provided in Appendix C3.

Table 5.4 The effect of inducible *Phd2* gene deletion on thrombus volume

Day	*Phd2* genotype	Volume (mm^3)
1	+/+	13.4 ± 0.8
	+/-	13.3 ± 0.6
	-/-	11.5 ± 1.0
7	+/+	6.50 ± 0.5
	+/-	6.25 ± 0.5
	-/-	6.23 ± 0.7
14	+/+	3.35 ± 0.5
	+/-	3.47 ± 0.3
	-/-	3.29 ± 0.2

Data represented as mean ± SE

Table 5.5 The effect of inducible *Phd2* gene deletion on the rate of thrombus resolution

Time Period	*Phd2* genotype	Percentage change (%)
1-7	+/+	50.1 ± 4.9
	+/-	52.9 ± 3.5
	-/-	45.7 ± 4.1
7-14	+/+	49.4 ± 5.2
	+/-	43.6 ± 5.5
	-/-	45.5 ± 3.5

Data represented as mean ± SE

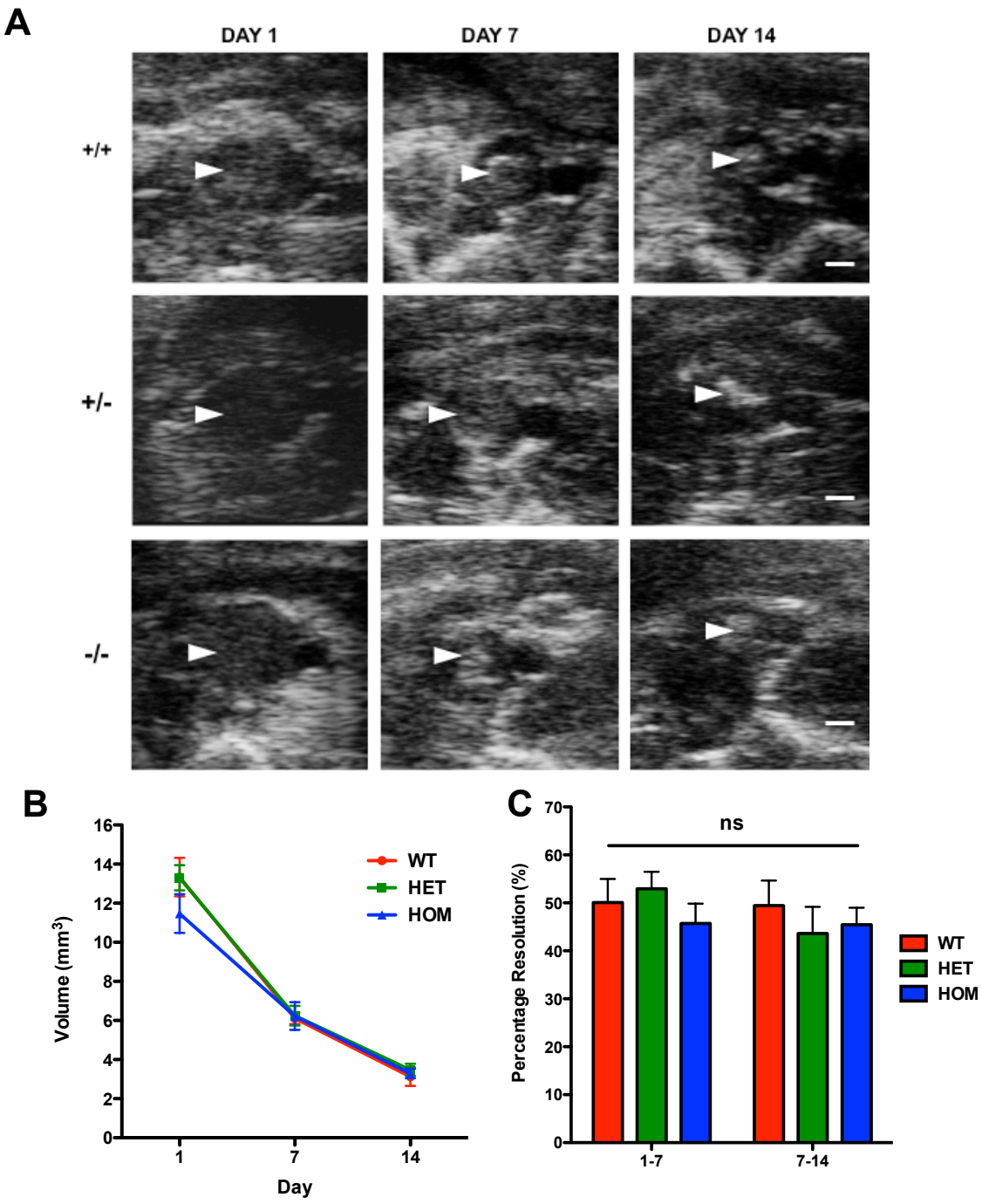

Figure 5.7 Thrombus resolution in inducible *Phd2* knockouts

(A) Representative transverse HFUS sections of thrombus at days 1, 7 and 14 post-induction in wild-type (+/+), heterozygous (+/-) and homozygous (-/-) inducible *Phd2* knockouts, white arrow indicates position of the thrombus and scale bars represent 500μm. Corresponding (B) longitudinal 3D-HFUS derived measurements of thrombus volume and (C) rate of thrombus resolution (n=5-7 per group) were not significantly different between groups (ns= 2-way ANOVA, P>0.05). Data represented as mean ± SE.

5.4.4 Thrombus resolution in *Phd2* inducible knockout measured by histology

Endpoint analysis of thrombus resolution was also investigated by histology at day 14 post-induction. No significant difference in thrombus volume, vein lumen recanalization neovascular channel formation, macrophage recruitment, or collagen deposition was observed between genotypes (P>0.05, 1-way ANOVA, Table 5.6, Fig 5.8-5.11). Data of individual replicates is provided in Appendix C3.

Table 5.6 Measurements of thrombus resolution after inducible *Phd2* gene deletion

Measure	Genotype	Result (mean ± SE)
Volume (mm^3)	+/+	0.67 ± 0.3
	+/-	1.11 ± 0.4
	-/-	0.71 ± 0.3
Recanalisation (%)	+/+	40.3 ± 7.3
	+/-	23.5 ± 2.8
	-/-	33.2 ± 3.0
Neovascularisation (channels/level)	+/+	8.36 ± 2.9
	+/-	12.9 ± 2.1
	-/-	9.48 ± 1.3
Macrophage content (%)	+/+	6.84 ± 1.4
	+/-	6.69 ± 1.1
	-/-	6.10 ± 1.6
Collagen content (%)	+/+	21.4 ± 3.6
	+/-	17.1 ± 1.7
	-/-	20.4 ± 4.0

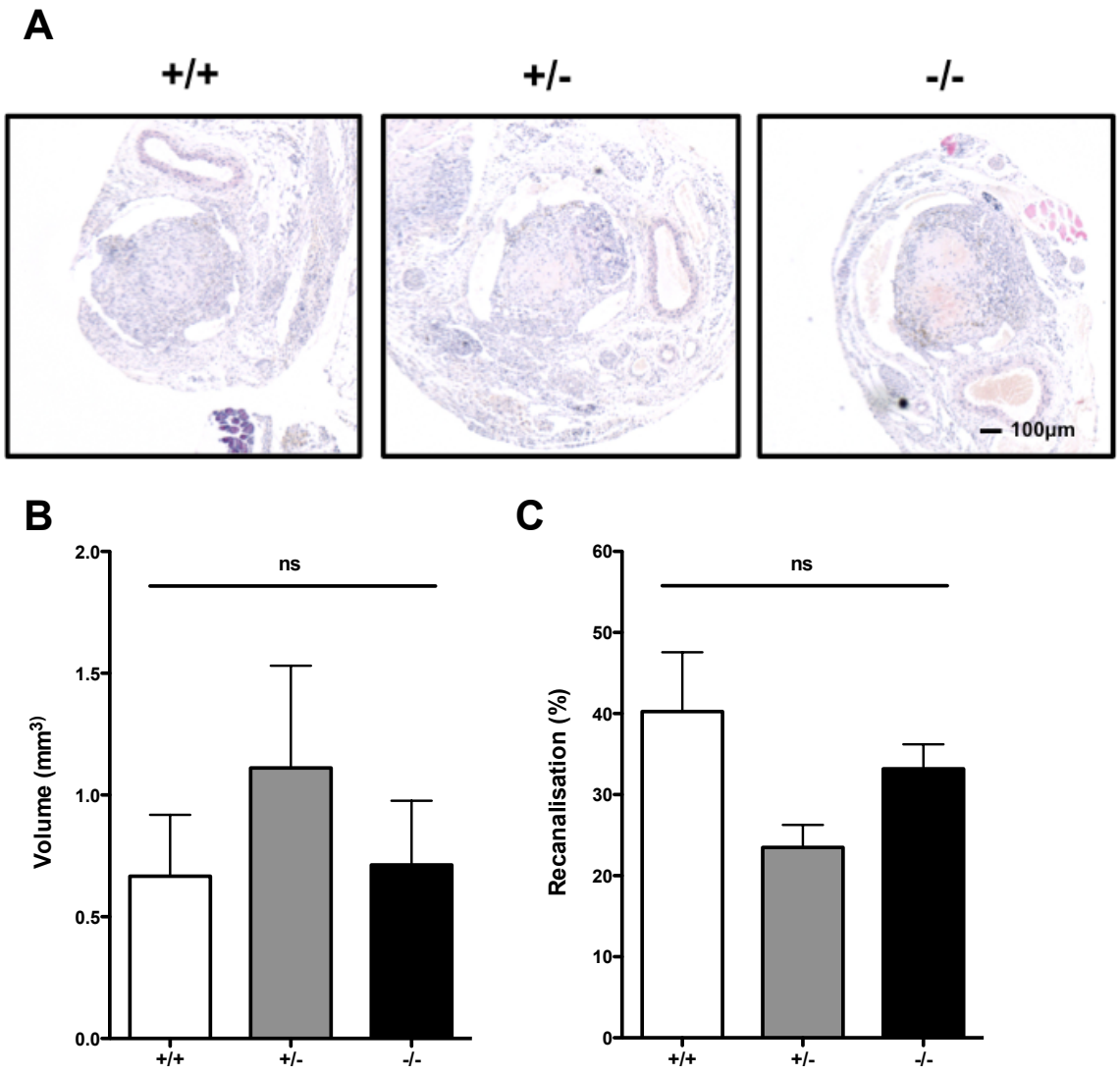

Figure 5.8 Histological analysis of the effect of inducible *Phd2* gene deletion on thrombus volume and vein lumen recanalisation

(A) Representative haematoxylin and eosin stained micrographs of thrombi from inducible *Phd2* knockout mice with effective wild-type (+/+), heterozygous (+/-) and homozygous (-/-) genotypes, images taken at an original magnification of 50x. Quantification of (B) thrombus volume and (C) vein lumen recanalisation (n=5-7 per group) demonstrating no significant difference between genotypes (ns= P>0.05, 1-way ANOVA). Data represented as mean ± SE.

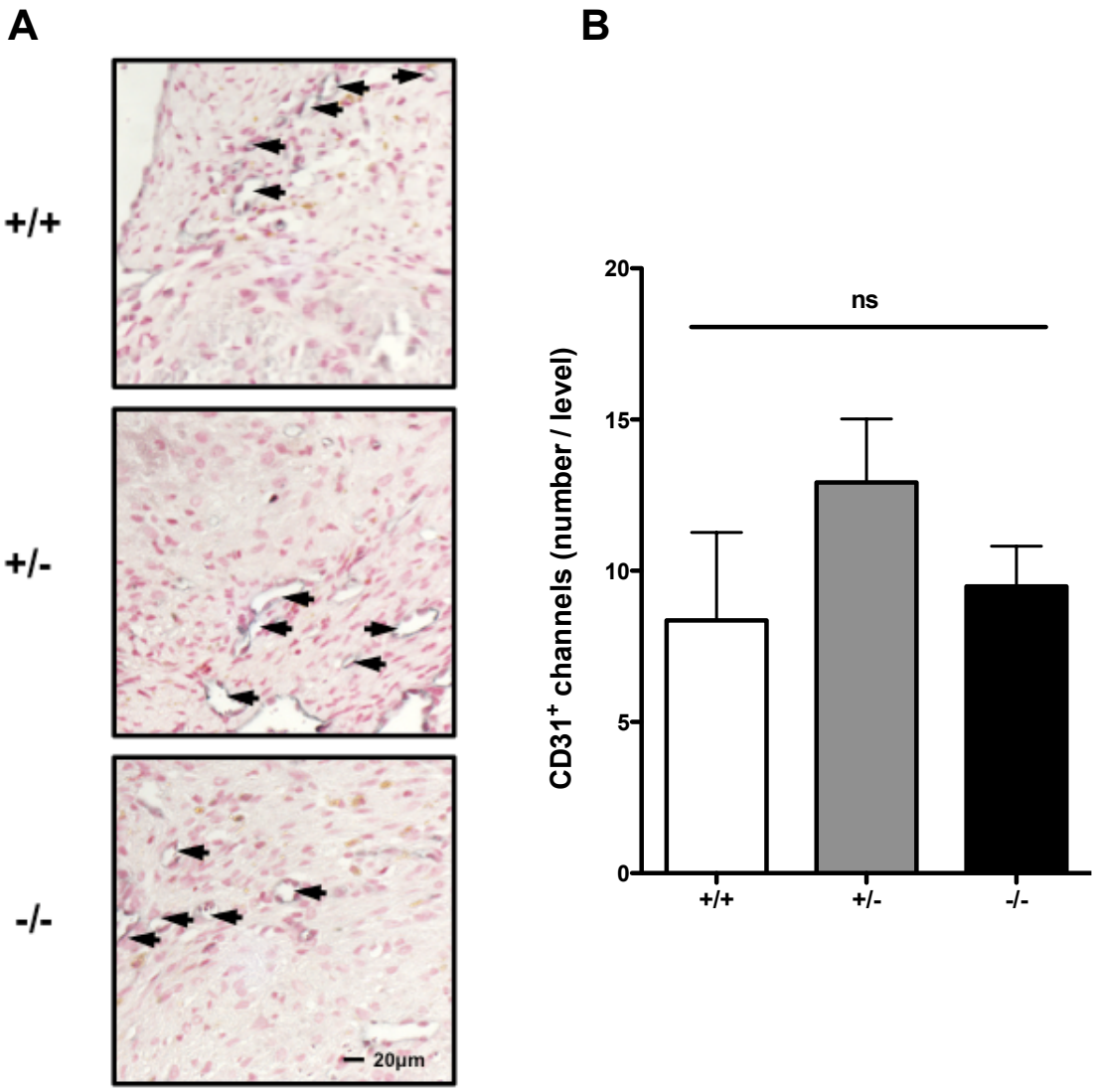

Figure 5.9 Histological analysis of the effect of inducible *Phd2* gene deletion on endpoint thrombus neovascularisation

(A) Representative CD31 stained micrographs of thrombi from inducible *Phd2* knockout mice with effective wild-type (+/+), heterozygous(+/-) and homozygous (-/-) genotypes (n=5-7 per group), images taken at an original magnification of 400x. (B) Quantification of neovascular channels in which no significant difference between genotypes was observed (ns= P>0.05, 1-way ANOVA). Data represented as mean ± SE.

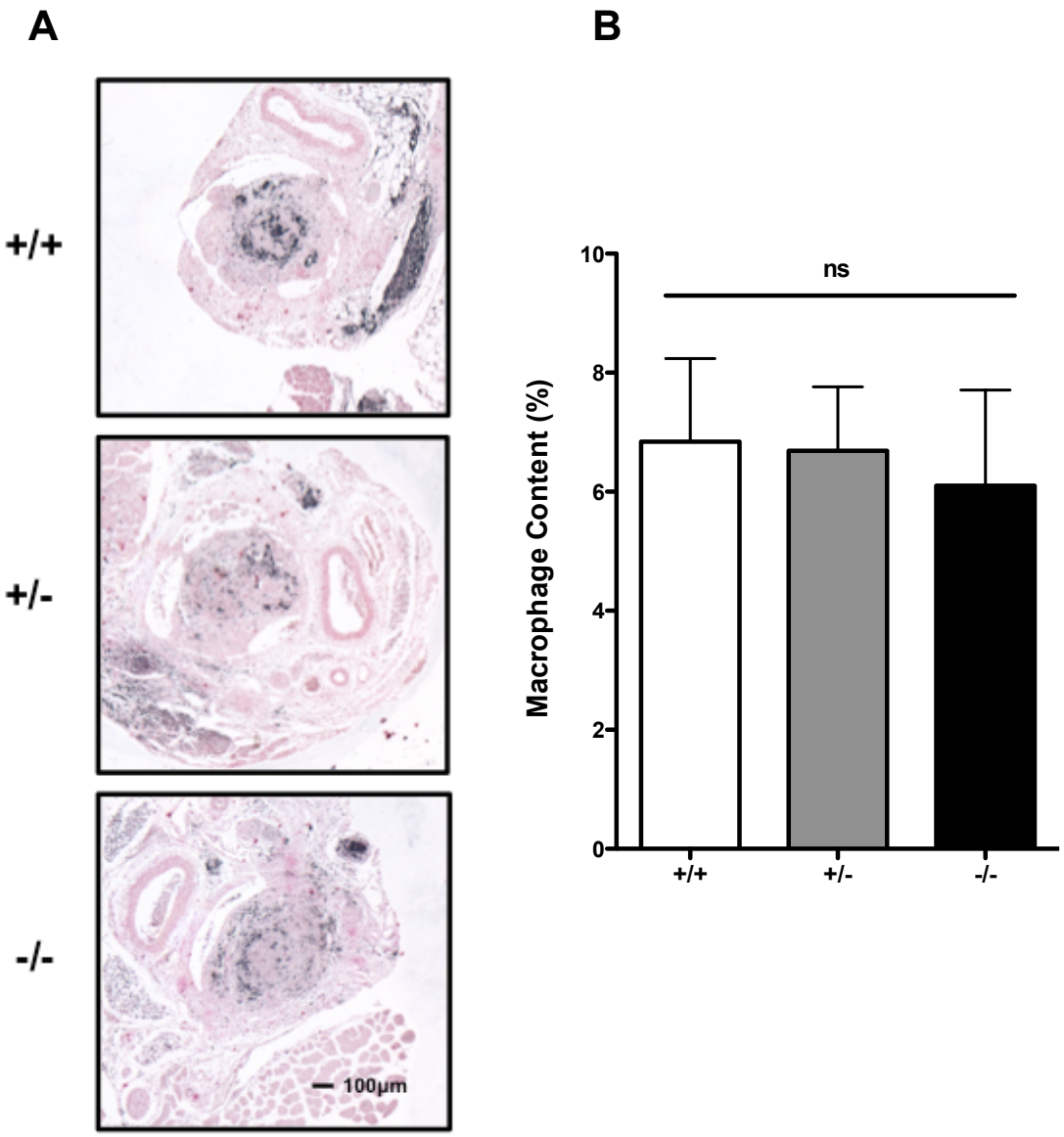

Figure 5.10 Histological analysis of the effect of inducible *Phd2* gene deletion on endpoint thrombus macrophage content

(A) Representative Mac-2 stained micrographs of thrombi from inducible *Phd2* knockout mice with effective wild-type (+/+), heterozygous(+/-) and homozygous (-/-) genotypes (n=5-7 per group), images taken at an original magnification of 50x. (B) Quantification of thrombus macrophage content in which no significant difference between genotypes was observed (ns= P>0.05, 1-way ANOVA,). Data represented as mean ± SE.

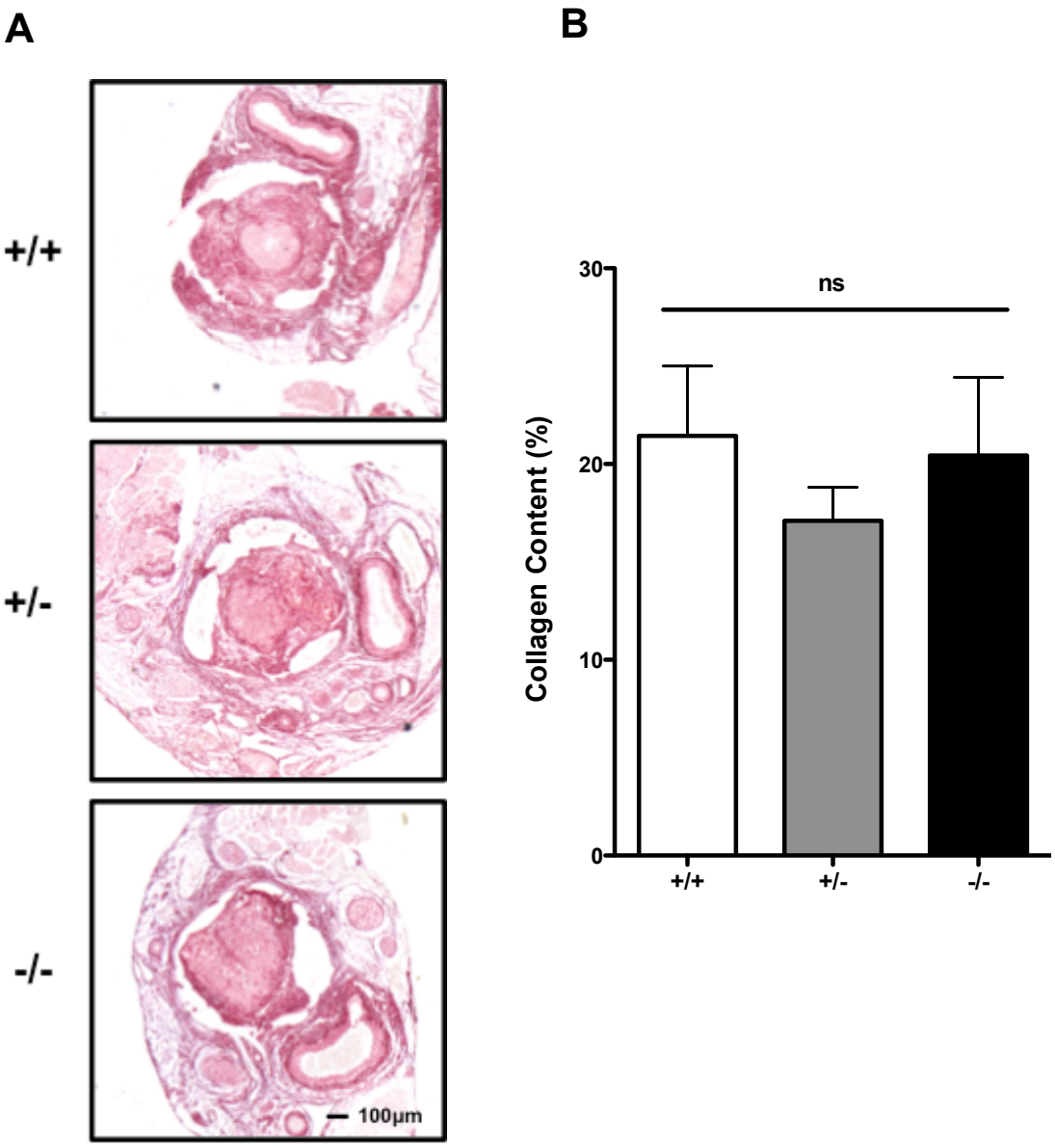

Figure 5.11 Histological analysis of the effect of inducible *Phd2* gene deletion on endpoint thrombus collagen content

(A) Representative picrosirius red stained micrographs of thrombi from inducible *Phd2* knockout mice with effective wild-type (+/+), heterozygous(+/-) and homozygous (-/-) genotypes (n=5-7 per group), images taken at an original magnification of 50x. (B) Quantification of thrombus collagen content in which no significant difference between genotypes was observed (ns= P>0.05, 1-way ANOVA). Data represented as mean ± SE.

5.4.5 Functional assessment of inducible PHD2 deletion

Kidney samples were taken from all thrombosed mice for analysis of PHD2, PHD3 and HIF1α protein expression in wild-type, heterozygous and homozygous inducible *Phd2* gene knockouts (Fig 5.12-5.13). Protein expression of PHD2 was significantly altered by inducible deletion of PHD2 ($P<0.05$, Kruskal-Wallis,). Homozygous *Phd2* gene deletion significantly lowered expression of PHD2 protein compared to littermate controls ($P<0.05$, Dunn's post-hoc) but not in heterozygous knockouts. PHD3 protein expression was not significantly altered after inducible deletion of *Phd2* ($P>0.05$, Kruskal-Wallis). Nuclear accumulation of HIF1α was significantly altered after inducible *Phd2* gene deletion ($P<0.05$, Kruskal-Wallis). Nuclear HIF1α was significantly increased in *Phd2* homozygous knockouts compared to both wild-type and heterozygous knockouts ($P<0.05$, Dunn's post-hoc).

The effect of *Phd2* gene deletion on haematocrit was also investigated. Blood haematocrit was significantly altered by inducible *Phd2* gene deletion ($P<0.001$, Kruskal-Wallis, Fig 5.14). Haematocrit was significantly higher in homozygous PHD2 gene knockouts than wild-type or heterozygous *Phd2* gene knockouts ($P<0.05$, Dunn's post-hoc). The concentration of VEGF in plasma was not significantly altered in inducible homozygous *Phd2* gene knockouts (63.1 ± 4.8pg/ml) compared to vehicle control (61.4 ± 1.9pg/ml, $P>0.05$, student's t-test, Fig 5.15).

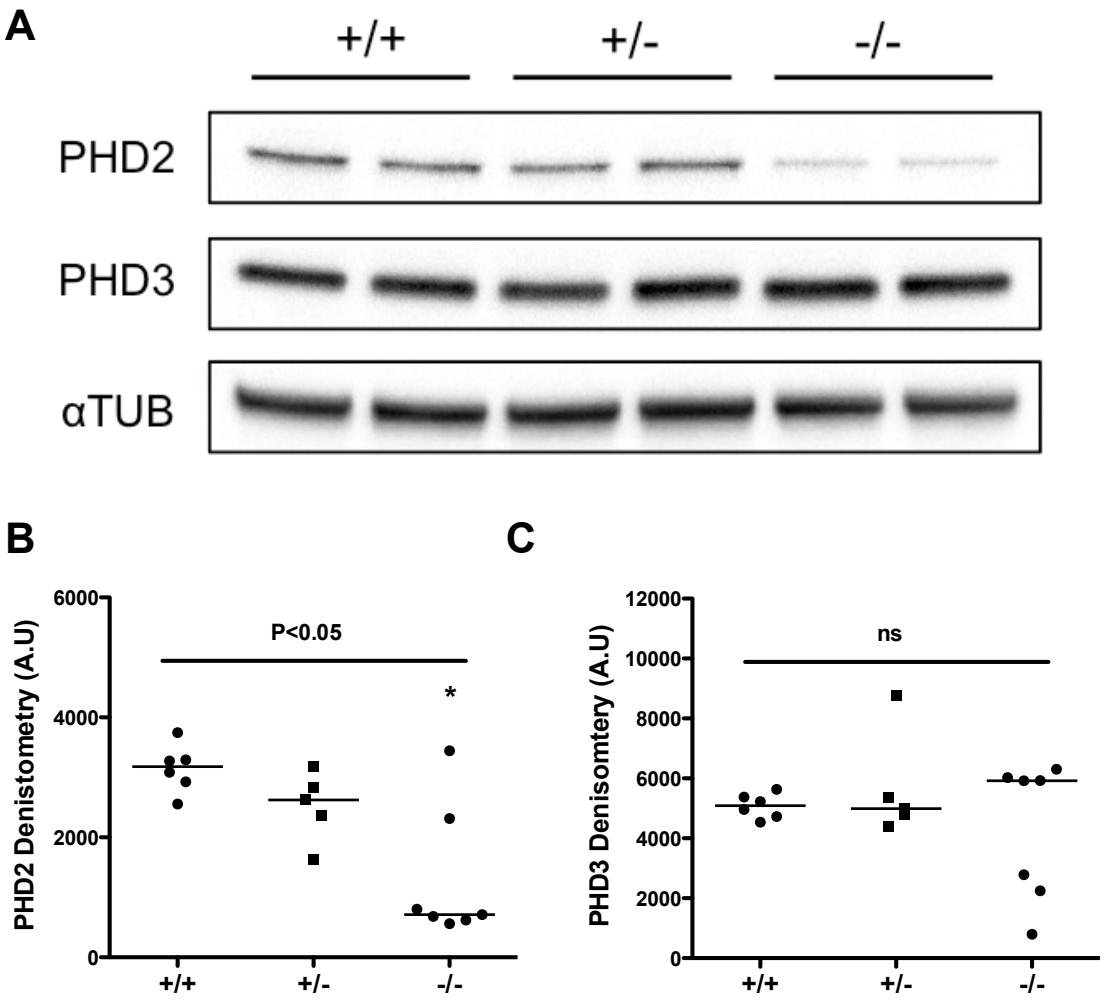

Figure 5.12 Immunoblot of kidney cytoplasmic PHD2 and PHD3 in inducible *Phd2* gene knockout mice

(A) Representative immunoblots of PHD2 and PHD3 protein expression in kidney cytoplasmic extracts from wild-type (+/+), heterozygous (+/-) and homozygous (-/-) inducible *Phd2* gene knockouts. Densitometric analysis of (B) PHD2 and (C) PHD3 expression normalised to αTubulin (Kruskal-Wallis with Dunn's post-hoc, *P<0.05 +/+ vs -/-), data represented as individual points with median.

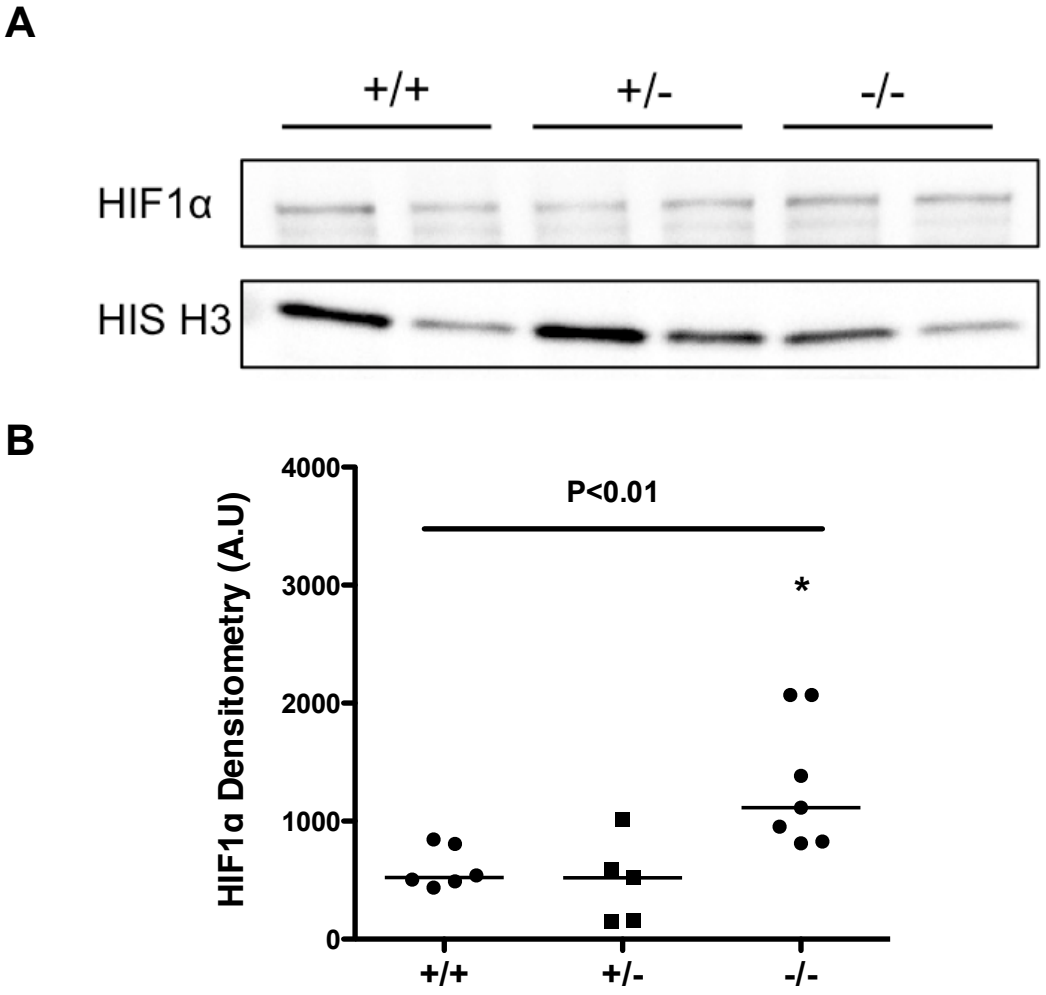

Figure 5.13 Immunoblot of kidney nuclear HIF1α in inducible *Phd2* gene knockout mice

(A) Representative immunoblot of HIF1α protein expression in kidney nuclear extracts from wild-type (+/+), heterozygous (+/-) and homozygous (-/-) inducible *Phd2* gene knockouts. (B) Densitometric analysis of HIF1α expression normalised to Histone H3 (Kruskal-Wallis with Dunn's post-hoc, *P<0.05 -/- vs +/+ and +/-), data represented as individual points with median.

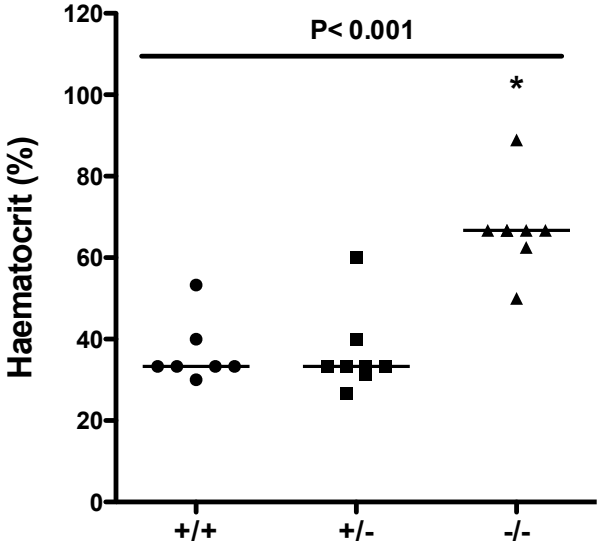

Figure 5.14 The effect of inducible *Phd2* gene deletion on haematocrit

Haematocrit was significantly altered by inducible deletion of *Phd2* (Kruskal-Wallis, P<0.001). Haematocrit was significantly increased in homozygous *Phd2* knockouts (-/-) compared to wild-type (+/+) and heterozygous (+/-) *Phd2* knockouts (Dunn's post-hoc, *P<0.05 -/- vs +/+ and +/-). Data represented as individual points with median.

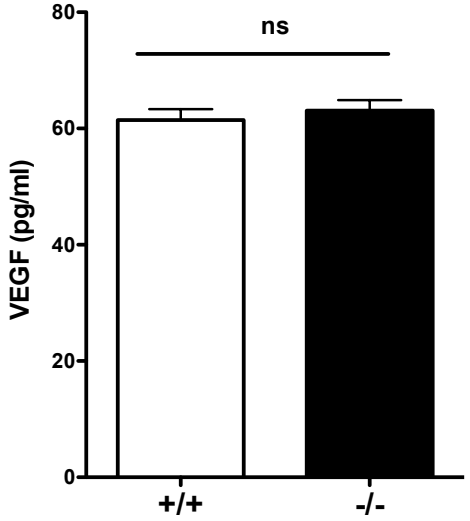

Figure 5.15 Effect of inducible *Phd2* gene deletion on plasma VEGF

Plasma VEGF levels were not significantly different in homozygous *Phd2* gene knockouts (-/-, n=7) compared to wild-type (+/+, n=6) littermate controls (ns= P>0.05, student's t-test). Data represented as mean ± SE.

5.5 Discussion

Homozygous inducible *Phd2* deletion was effective in reducing expression of this isoform at the protein level compared to wild-type littermate controls. This was accompanied by a significant increase in the nuclear accumulation of HIF1α. A comparable study has also observed increases in HIF1α nuclear accumulation in inducible homozygous *Phd2* knockouts; however, this effect was not quantified[169]. As with the constitutive *Phd2* heterozygous knockouts no significant differences in PHD2 expression or HIF1α stabilisation were observed in respective inducible heterozygous *Phd2* knockouts.

Assessment of the efficacy of *Phd2* gene deletion did not rely solely on western blot measurements of nuclear HIF1α accumulation. Previous observations have demonstrated a sustained increase in haematocrit after inducible homozygous deletion of *Phd2*[169, 170]. In the present study, complementary increases in haematocrit were observed in inducible homozygous *Phd2* knockouts. This increase, measured 14 days after completion of tamoxifen treatment, is slightly greater in magnitude than previous reports[169, 170].

Inducible *Phd2* gene deletion did not significantly alter thrombus resolution as determined by either 3D-HFUS or histology. Measurements of thrombus neovascularisation, macrophage content and collagen content were similarly unaffected. The lack of phenotype in inducible homozygous *Phd2* knockouts indicates that PHD2 activity may be dispensable for venous thrombus resolution. This is in stark contrast to the regulation of erythropoiesis that appears to be strongly dependent on PHD2 activity.

Homozygous deletion of *Phd2*, but not *Phd1* or *Phd3*, has previously been found to enhance vessel density in a number of tissues at baseline, accompanied by markedly increased HIF1α stabilisation and VEGFA production[145]. Conversely, selective deletion of endothelial *Hif1a* in a murine model of cancer impaired pathological angiogenesis and reduced tumour growth[279]. Taken together these findings would suggest that PHD2 mediated HIF1α degradation serves as a critical negative regulator of angiogenesis. However, this is not uniformly supported by the literature as others have found

that deletion of *Phd2*, in a range of cell types including those of the endothelial and myeloid lineage, did not significantly alter the absolute quantity of vascular channels during tumour growth but instead selectively improved vessel normalisation[160, 269]. This later finding is consistent with a more limited contribution of PHD2 to angiogenesis in hypoxic tissues and might explain the lack of significant difference in neovascularisation in *Phd2* deficient thrombi.

Phd2 knockdown, specifically in tumours, has been shown to significantly increase infiltration of leukocytes, however, the exact cellular composition of this infiltrate has yet to be determined[158]. Consistent with involvement of the PHD-HIF axis deletion of *Hif1a* and *Hif2a* resulted in corresponding reductions in leukocyte accumulation in inflamed tissues[74, 262]. In contrast, macrophages deficient in *Phd2* after gene deletion, that stabilise significantly increased levels of HIF1α and HIF2α, demonstrate moderate reductions in their migratory capacity towards the chemokine MCP1[278]. These potentially opposing observations would appear to largely nullify one another in global *Phd2* knockouts where heterozygous deletion resulted in similar levels of macrophages in the ischaemic hindlimb[164]. Instead loss of *Phd2* expression was associated with increased skewing of tissue resident macrophages towards an alternately activated (M2) phenotype[164]. The phenotypic shift of PHD2 deficient macrophages is complicated by observed increased expression of the M2 marker CD206 in HIF1α deficient macrophages[280]. Further studies are required to determine the effect of *Phd2* gene deletion on thrombus macrophage skewing.

Thrombus resolution was quantified in a longitudinal manner using HFUS in the range of 40-60MHz, which facilitates high-resolution imaging of the mouse abdomen whilst maintaining adequate tissue penetration. HFUS has previously been used to image acute IVC thrombi *in vivo* with transverse and sagittal planes providing measures of thrombus cross-sectional area and length, however, this did not extend beyond the first few hours post-induction[281]. In the present study, the thrombosed IVC could readily be identified at acute time-points as it was hyperechoic compared with the non-thrombosed vessel. Hyperechoicity of the thrombus appeared to increase with time, consistent with organisation of the thrombus. Integration of a motorised stage with HFUS

facilitates the generation of 3D volume renders of the thrombus[282]. This 3D-HFUS protocol allowed for longitudinal assessment of thrombus volume that may provide a more representative measure of overall thrombus burden. One limitation of non-contrast HFUS is the relatively low levels of tissue contrast particularly at early time-points. This could be overcome by the use of transpulmonary microbubble contrast agents such as Sonovue[283]. In some instances segmentation of the thrombus was hampered by scar tissue at the site of the laparotomy that casts a shadow over regions of the IVC. This problem was largely negated by rotation of the probe (5-15%).

It may be useful to consider instances in other pathologies where deletion of *Phd2* was not associated with an altered phenotype. In a study of tumour biology global *Phd2* deletion or cell-specific *Phd2* deletion in macrophages, fibroblasts and endothelium did not significantly effect tumour development, despite significantly increasing nuclear stabilisation of both HIF1α and HIF2α[269]. This comparison is relevant as angiogenesis and macrophage recruitment are common processes shared by both tumour development and venous thrombus resolution.

An important technical consideration in the design of the current study was the timing of gene deletion. Gene recombination was initiated prior to induction of thrombus by administration of tamoxifen (1mg/mouse/day) for 5 consecutive days, previously reported to be sufficient for excision of the *Phd2* locus[269]. The deletion of *Phd2* immediately prior to thrombus induction was aimed at limiting any potential effects of longer-term *Phd2* gene deletion on thrombus formation. Long term deletion of *Vegfr2* in the endothelium initiated 3 weeks prior to thrombus induction significantly affected acute measurements of thrombus volume that were likely to have confounded subsequent analysis of thrombus resolution[54]. A drawback to this approach is that residual PHD2 protein present in cells that constitute the thrombus may have persisted after thrombus induction.

The initiation of *Phd2* gene deletion prior to induction of thrombosis may have affected the efficiency of thrombus formation. As such measurements of thrombus formation efficiency were made. No significant differences between

wild-type (7/8, 88%), heterozygous (5/9, 56%) and homozygous (6/9, 67%) inducible *Phd2* knockout mice were observed (chi-square test, $P>0.05$). However, a trend towards reduced thrombus formation efficiency was evident and the contribution of PHD2 towards thrombus initiation cannot be discounted. Measurements of thrombus volume at day 1 post-induction were comparable suggesting that any contribution of PHD2 affects thrombus formation in a binary fashion. This study was originally designed with group sizes of between eight and nine but due to the reduced efficiency of thrombus induction, group sizes fell to between five and seven. The power of this study was, therefore, markedly reduced meaning greater differences were required to attain the required level of significance.

Chapter 6 The effect of pharmacological inhibition of PHD enzymes on venous thrombus resolution

6.1 Introduction

Neither constitutive heterozygous *Phd2* knockouts (Chapter 4) nor inducible *Phd2* homozygous knockouts (Chapter 5) significantly altered venous thrombus resolution. The lack of a phenotype suggests that thrombus resolution may occur in a PHD2 independent manner. Alternatively, it is possible that residual PHD2 protein in heterozygous knockouts or PHD3 expression in homozygous knockouts may compensate for loss of PHD2. A broader approach using inhibitors of PHD enzyme activity as considered suitable for investigating the contribution of these enzymes as a whole and largely negate compensatory mechanisms.

PHD inhibition using the iron-chelating agent l-mimosine results in accelerated venous thrombus resolution, as assessed by reduced thrombus weight and volume[57]. L-mimosine was also found to enhance thrombus neovascualarisation and macrophage recruitment. These effects were accompanied by increased thrombus nuclear HIF1α accumulation and corresponding increases in protein expression of HIF1α target genes including *Vegfa* and its receptor *Vegfr1*[57]. However, given the mode of action of l-mimosine as an iron chelator, a number of PHD-HIF1α independent effects may also have contributed to the observed phenotype, for example l-mimosine reduces the secretion of mature collagen through inhibition of a number of iron dependent prolyl 4-hydroxylases[230]. L-mimosine has also be found to inhibit a number of other enzymes by chelation of zinc and copper[284, 285].

A number of novel small molecule PHD inhibitors with increased specificity have recently been developed. One such inhibitor, AKB-4924, is a potent inhibitor of PHD enzyme activity with an inhibitory concentration (IC_{50}) of 14μM for

PHD2[231]. AKB-4924 is a four-substituted 3-hydroxy-2-oxo-1, 2-dihydropyridine derivative, with an iron-binding α-hydroxycarbonyl group similar to that present in l-mimosine. *In vitro* characterization has demonstrated the capacity of AKB-4924 to stabilize HIF1α and induce expression of the HIF1α transcriptional target *Vegfa*[286]. Treatment of neutrophils and macrophages with AKB-4924 significantly increases phagocytosis[233]. This may be of particular interest in the context of venous thrombus resolution given the prevalence of these cell types.

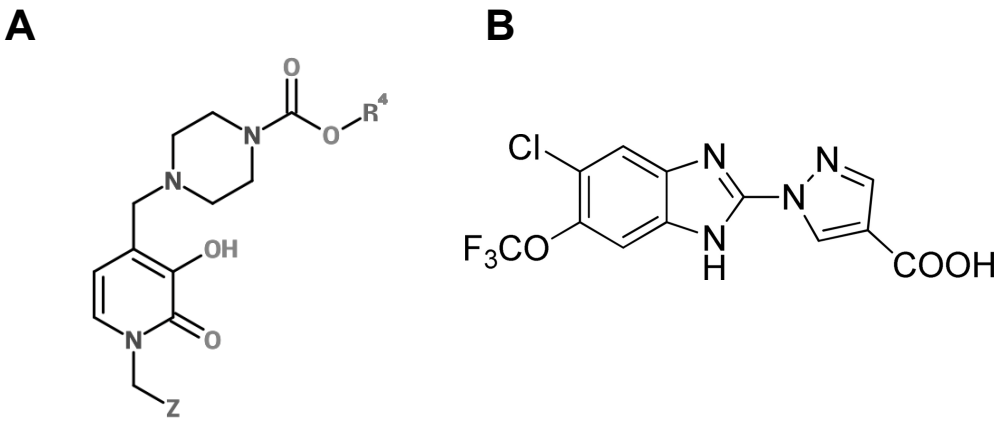

Figure 6.1 Structure of AKB-4924 and JNJ-42041935

The structure of (A) AKB-4924 a four-substituted 3-hydroxy-2-oxo-1,2-dihydropyridine derivative (Z = halogen substituted phenyl, R^4 = linear alkyl salt) and (B) JNJ-42040935 with the chemical formula 1-(5-chloro-6-(trifluoromethoxy)-1H-benzoimidazol-2-yl)-1H-pyrazole-4-carboxylic acid.

An alternative small molecule, JNJ-42041935, has also been developed and unlike either AKB-4924 or l-mimosine inhibits PHD enzyme activity through displacement of the rate-limiting co-substrate 2-oxoglutarate[227]. JNJ-42041935 is a highly selective PHD inhibitor with a low IC_{50} of 0.1μM for PHD2 compared to FIH (IC_{50} 100μM)[227]. JNJ-42041935 is a potent inducer of HIF transcriptional activity as assessed by HIF-luciferase reporter mice[227]. Mice treated with 100μmol/kg JNJ-42041935 demonstrated significantly increased circulating protein levels of the HIF target gene *epo* and an increased haematocrit[227]. Both of these agents have been described as pan-PHD inhibitors through their capacity to increase stabilisation of both HIF1α and HIF2α. However, AKB-4924 may demonstrate a degree of selectivity towards PHD2 as it preferentially stabilises HIF1α[231]. Direct data of isoform specificity of AKB-4924 is not currently available, with analysis to date focussing on HIFα subunit stabilisation. To confirm whether AKB-4924 selectively inhibits a single isoform IC_{50} measurements for PHD1-3 would be required.

6.2 Aim

To investigate the effect of small molecule PHD inhibitors on venous thrombus resolution.

6.3 Methods

6.3.1 Contrast enhanced micro-computed tomography

To visualise thrombus resolution in a longitudinal manner a contrast enhanced microCT imaging protocol was developed. Mice were anaesthetised under 3% isoflurane at an oxygen flow rate of 0.5l/min. The tail was warmed under an infra-red lamp to facilitate contrast injection. Aurovist 15nm nanogold (nAu) contrast agent (Nanoprobes, USA, 200mg/ml nAu) was diluted with sterile PBS, pH7.4 to a concentration of 50mg/ml nAu. A 200µl bolus (10mg nAu) of contrast agent was administered by intravenous injection into the tail vein. Contrast was allowed to circulate for 5mins prior to scanning.

A fusion PET/CT scanner (Mediso, Hungary and Bioscan, USA) was used for contrast-enhanced microCT. The mouse was first placed on the scanner bed in the prone position. A pressure transducer was secured to the animals back for intra-scan monitoring of respiration allowing for adjustment of anaesthesia. An initial scout view was generated from which an area of interest was marked extending from the diaphragm to the lower abdomen. The following scan parameters were used for this study. I would like to acknowledge Dr Kavitha Sunassee and Mr Sobath Premeratne for assistance in developing the microCT imaging protocol.

Table 6.1 MicroCT scanner settings

Parameter	Value
Zoom	Maximum
Projections	360
Pitch	1
Tube Voltage	45kVP
Exposure Time	1000ms
Binning	4 to 1
Scan Length	~20mins

6.3.2 Drug treatment

Experimental venous thrombi were induced in the inferior vena cava (IVC) of 8-10 week old male BALB/C mice as described in Chapter 2.3.1. AKB-4924 (Akebia Therapeutics, USA) was prepared at a concentration of 2mg/ml in 40% (v/v) aqueous 2-hydroxypropyl-beta cyclodextrin (Sigma, UK), 60% (v/v) 50mM citrate buffer pH5. Mice were randomised to receive either AKB-4924 at a dose of 5mg/kg or 10mg/kg, or vehicle control by daily subcutaneous injection starting 24hrs after thrombus induction (Fig 6.3).

Thrombus was induced in a second cohort of mice to investigate a second inhibitor, JNJ-42041935 (Johnson and Johnson, USA). JNJ-42041935 was prepared in 20% (w/v) 2-hydroxypropyl-beta cyclodextrin at a concentration of 3mg/ml. Mice were randomised to receive either JNJ-42041935 at a dose of 100umol/kg or vehicle control by daily intraperitoneal injection starting 24hrs after induction.

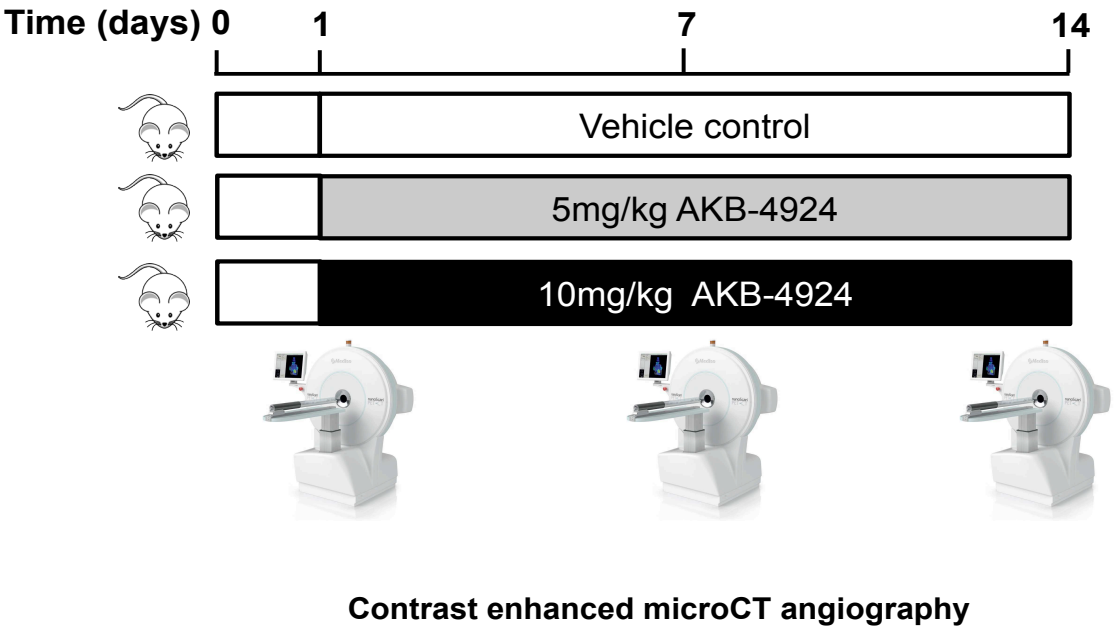

Figure 6.2 AKB-4924 study design

Schematic representation of the experiment time-course and treatment groups

6.3.3 Image reconstruction and analysis

Scans were reconstructed using VivoQuant software (v1.22 Invicro, USA) giving a voxel size of 65μm and exported as a metaimage file. Reconstructed scans were segmented and analysed using ITKsnap software (v2.4, Open Source) in an observer-blinded manner[287]. Image contrast was adjusted linearly to provide optimal parameters for subsequent analysis. Thrombi were reconstructed in 3D using a semi-automatic volumetric bubble propagation system. Using the snake ROI tool a region of interest, containing the thrombus, was marked. Pre-processing of the image was used to delineate thrombosed tissue inside the IVC restricting sphere-based propagation to the thrombus. A series of spheres were then placed along the length of the thrombus. Spheres were propagated with a balloon expansion force of 1.00 and a curvature term of 0.20. The propagated region was extended until the majority of the thrombus was included. Corrections to the segmentation were made using the free-hand tool. When the segmentation was complete a 3D rendered mesh of the thrombus was generated and data on thrombus volume recorded, representative images of the segmentation process are provided in Appendix D1. The microCT bed was removed manually for representative images using Image J software (NIH, USA).

6.3.4 Reproducibility of contrast-enhanced microCT segmentation

To assess the reproducibility of thrombus volume measurements made by segmentation of contrast-enhanced microCT scans measures of both intra and inter observer variability were made. A single observer segmented the same set of scans (n=18) separated by a 2-week interval and two independent observers segmented the same set of scans (n=18) in order to assess intra and inter observer variability.

6.3.5 Tissue processing

Tissues were harvested and processed as described in Chapter 4.3.4.

6.3.6 Histology and immunohistochemistry

Thrombus sections were stained with H&E, CD31, Mac-2 and picrosirius red at described in Chapter 4.3.5-4.3.9. For quantification of Mac-2 Nova Red chromogenic substrate (Vector Laboratories, UK) was used according to the manufacturers instructions.

6.3.7 Western blotting

Kidney samples were blotted for PHD2, PHD3, αTubulin, HIF1α and Histone H3 at detailed in Chapter 4.3.10.

6.3.8 Haematocrit measurements

Measurements of blood haematocrit were determined as described in Chapter 5.3.8.

6.3.9 VEGF ELISA

Plasma VEGF concentration was determined using a murine VEGF ELISA as described in Chapter 5.3.9.

6.3.10 Statistical analysis

Normality of data was assessed by Kolmogrov-Smirnov tests with parametric or non-parametric tests used as appropriate. Reproducibility of contrast-enhanced microCT based measurements of thrombus volume were assessed by Bland-Altman and intra-class correlation (ICC). Differences in thrombus volume and rate of resolution as determined by contrast-enhanced microCT were interrogated by repeated-measure 2-way ANOVA with post-hoc Bonferroni. Histological measurements of thrombus volume after treatment with AKB-4924 and JNJ-42041935 were assessed by 1-way ANOVA with post-hoc Bonferroni and student's t-test respectively. Measurements of protein expression (PHD and HIF1 α) and blood haematocrit were interrogated by Kruskal-Wallis with Dunn's post-hoc and Mann-Whitney U respectively. Measurements of plasma VEGF were analysed using student's t-tests. In all cases $P<0.05$ was considered statistically significant. Statistical analyses were conducted using Prism Software (v5, Graphpad, USA) or for ICC analyses SPSS statistics (v22, IBM, USA). Parametric data represented as mean ± SE and non-parametric data presented by individual data points with median.

6.4 Results

6.4.1 Imaging of venous thrombus by contrast-enhanced microCT

Using this protocol thrombus can effectively be discriminated from surrounding tissue as a result of a filling defect in the IVC lumen that can be observed in sagittal, coronal and transverse planes (Fig 6.3). A 3D image stack of a representative day 1 thrombus visualised by 3D-HFUS is provided in Appendix D2.

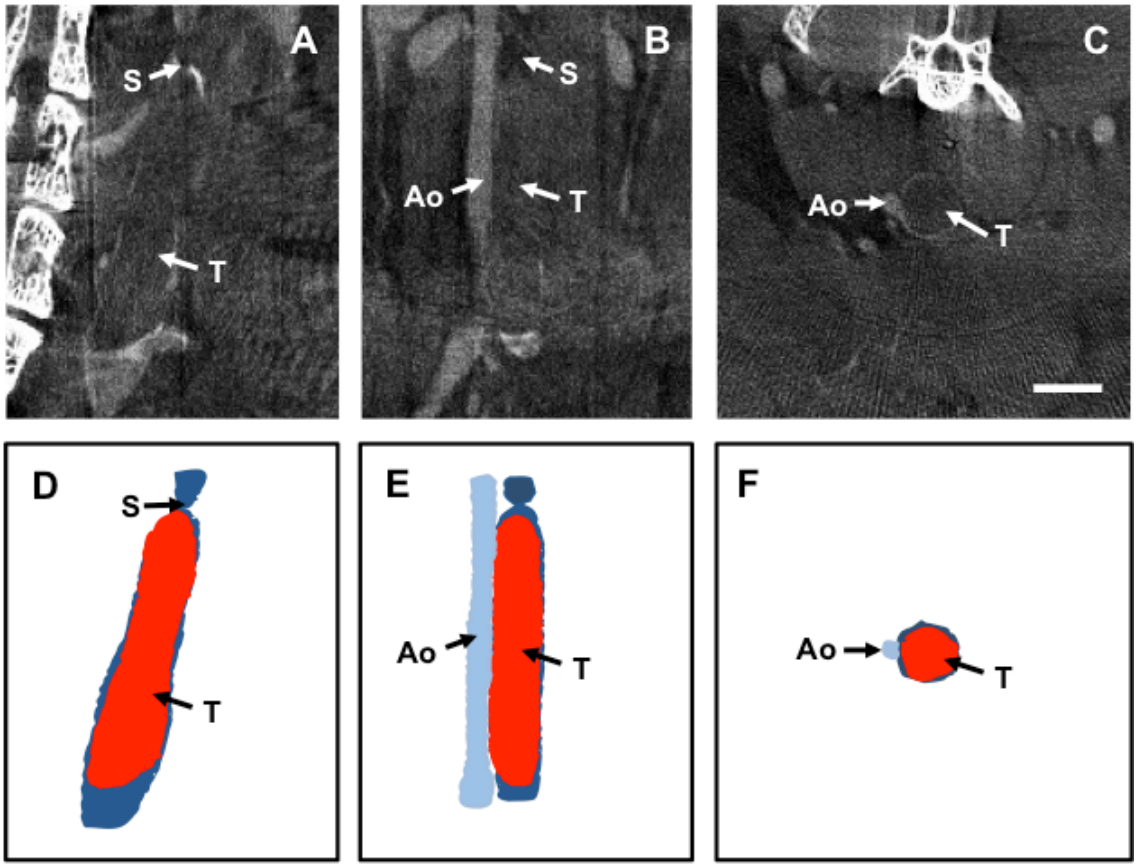

Figure 6.3 Contrast enhanced microCT of venous thrombus 1 day post-induction

Representative contrast enhanced microCT slices and corresponding schematic images of a day 1 thrombus in (A/D) sagittal, (B/E) coronal and (C/F) transverse planes. Images annotated with the location of the site of stenosis (S), the aorta (Ao) and the thrombus (T). Scale bar represents 2mm.

Contrast enhanced microCT scan at days 1, 7 and 14 (Fig 6.4A) post-induction were reconstructed and 3D volume renders generated to provide measurements of thrombus volume and a visual representation of thrombus burden (Fig 6.4B). Volume renders revealed considerable heterogeneity in thrombus cross-sectional area at day 14 post-induction and to a lesser extent at day 7.

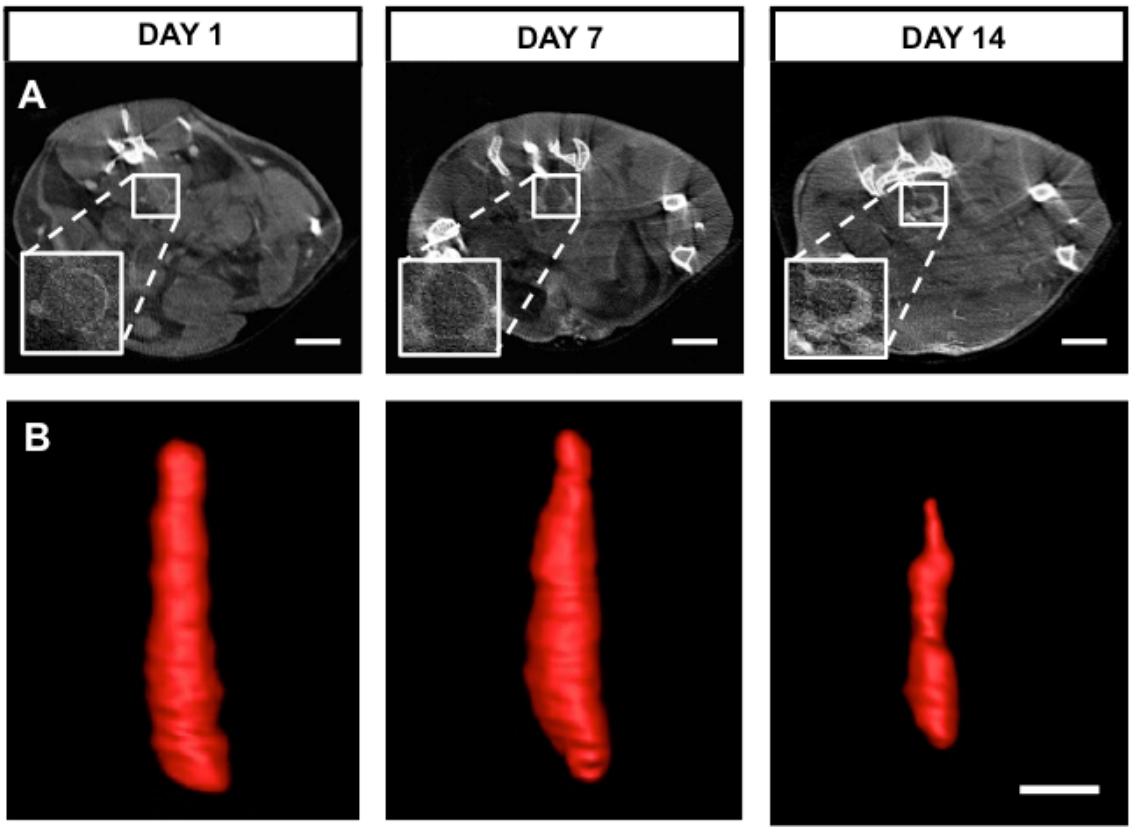

Figure 6.4 Contrast enhanced microCT and 3D volumetric reconstruction
(A) Representative transverse slices of thrombus at days 1, 7 and 14 post-induction, scale bars represent 4mm. (B) Representative 3D volumetric reconstructions of thrombus at days 1, 7 and 14 post-induction, scale bar represents 2mm.

6.4.2 MicroCT variabilty

Regression analyses comparing measurements of thrombus volume between observations (intra-observer) and between observers (inter-observer) suggested that measurements of thrombus volume by contrast-enhanced microCT were reliable and reproducible (Fig 6.5). The strength of the relationship of both comparisons was quantified by ICC. Intra-observer (ICC=0.99, P<0.001) and inter-observer (ICC=0.91, P<0.001) measurements of thrombus volume by contrast enhanced microCT demonstrated strong positive correlations.

Bland-Altman plots were used to visually assess agreement in intra-observer and inter-observer measurements of thrombus volume (Fig 6.6). For measurement of intra-observer variability the limits of agreement were narrow and the mean difference was low suggesting that these measurements were close to equivalence. For measurements of inter-observer variability as thrombus volume increased the difference between measurements also found increased. When combined with a relatively large mean difference of $2mm^3$ this suggests that one observer may over estimate volumes of larger thrombi compared to another.

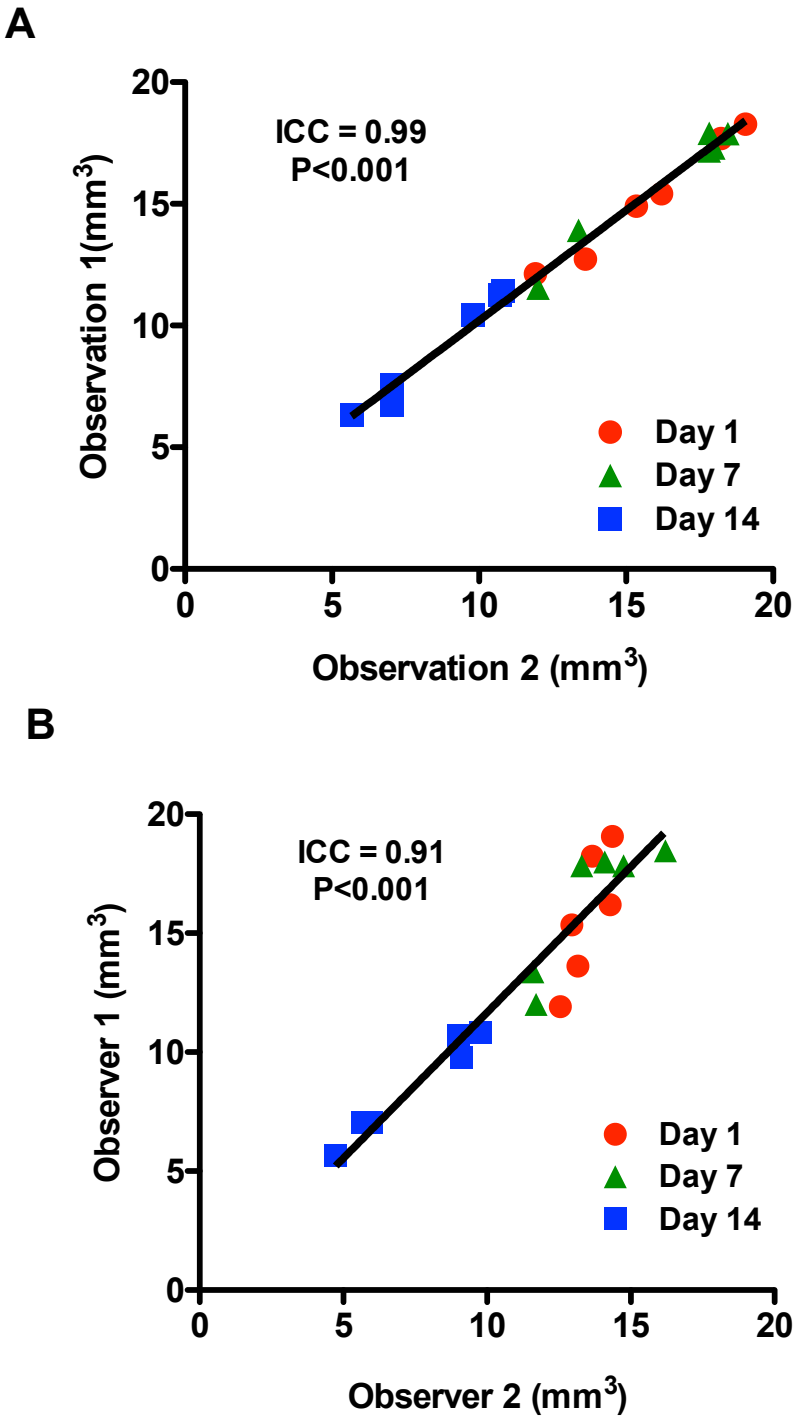

Figure 6.5 Comparison of contrast enhanced microCT measurements of thrombus volume by regression analysis

Regression analysis of (A) intra-observer and (B) inter-observer comparisons of thrombus volume determined by contrast enhanced microCT at days 1, 7 and 14 post-induction (n=6 per time-point).

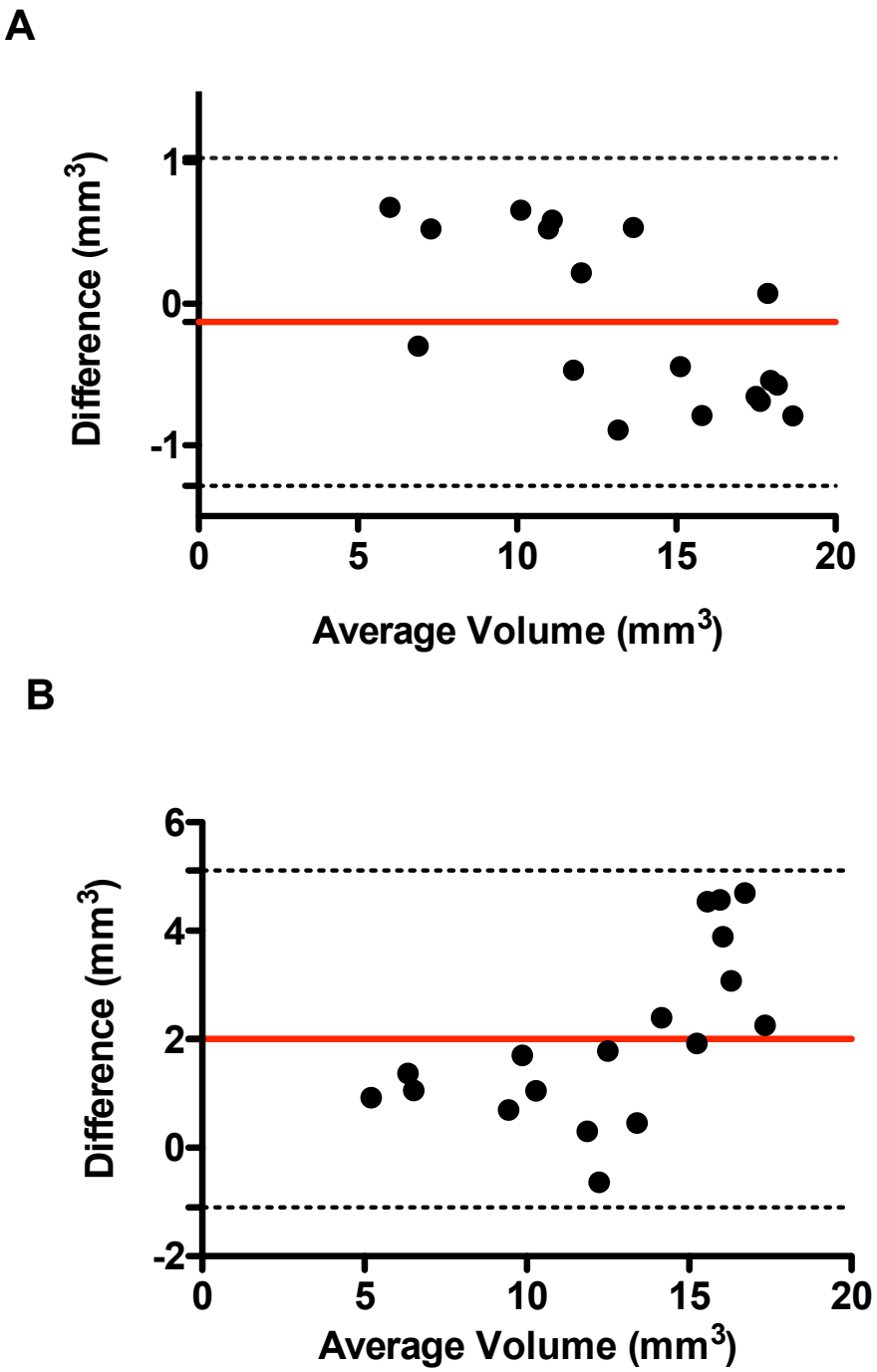

Figure 6.6 Comparison of contrast enhanced microCT measurements of thrombus volume by Bland-Altman

(A) Intra-observer and (B) inter-observer Bland-Altman plots to compare measurements of thrombus volume determined by contrast-enhanced microCT at days 1, 7 and 14 post-induction (n=18). Red lines represent the mean difference and dotted lines represent 1.96 standard deviations from the mean.

6.4.3 Effect of AKB-4924 treatment on venous thrombus resolution

Thrombus volume as measured by contrast enhanced microCT was not significantly different in mice treated with the PHD inhibitor AKB-4924 at either 5mg/kg or 10mg/kg when compared with vehicle treated control (P>0.05, 2-way ANOVA, Fig 6.7A/B and Table 6.2). When thrombus resolution was represented as the percentage change from thrombus volume measured at day 1 post-induction, again no significant difference between treatments was observed (P>0.05, 2-way ANOVA, Fig 6.7C and Table 6.3). Data of individual replicates is provided in Appendix D3.

Table 6.2 The effect of AKB-4924 treatment on thrombus volume

Day	AKB-4924 (mg/kg)	Volume (mm^3)
1	0	13.7 ± 0.3
	5	12.2 ± 1.2
	10	13.9 ± 0.9
7	0	13.4 ± 0.7
	5	11.3 ± 0.6
	10	12.7 ± 0.6
14	0	7.38 ± 0.9
	5	5.59 ± 0.7
	10	5.67 ± 0.8

Data represented as mean ± SE

Table 6.3 The effect of AKB-4924 on the rate of thrombus resolution

Time Period	AKB-4924 (mg/kg)	Percentage Change (%)
1-7	0	0.89 ± 7.2
	5	4.83 ± 7.2
	10	8.24 ± 3.4
7-14	0	45.9 ± 6.4
	5	53.2 ± 5.3
	10	59.3 ± 4.8

Data represented as mean ± SE

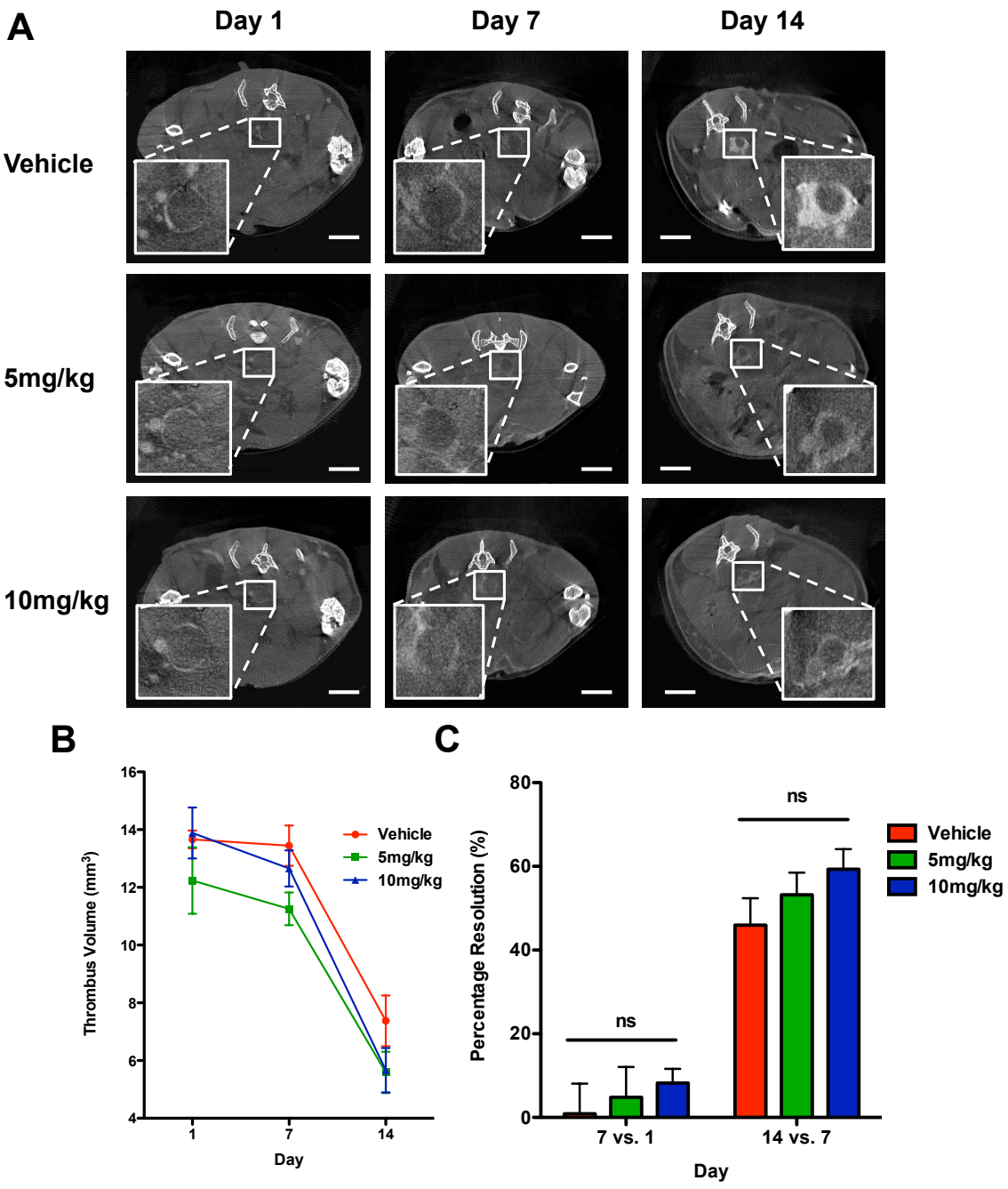

Figure 6.7 Measurement of thrombus volume by microCT after treatment with AKB-4924

Thrombosed mice (n=6 per group) were treated with the PHD inhibitor AKB-4924 at either 5mg/kg or 10mg/kg and compared to vehicle control. (A) Representative transverse slices of IVC thrombi imaged by microCT, scale bars represent 4mm (B) Thrombus volume as measured by segmentation of contrast-enhanced microCT. (C) The rate of thrombus resolution measured as the percentage reduction in thrombus volume over the preceding 7 days. Data represented as mean ± SE.

Complementary thrombus volume measurements were obtained when measured histologically at 14 days post-induction. Treatment with AKB-4924 (5 or 10mg/kg) had no significant effect on thrombus resolution determined by either thrombus volume ($P>0.05$, 1-way ANOVA) or vein recanalisation ($P>0.05$, 1-way ANOVA, Table 6.4, Fig 6.8A-C). Only one marker of thrombus organisation, thrombus neovascularisation, was significantly enhanced after treatment with AKB-4924 ($P<0.001$, 1-way ANOVA, Table 6.4, Fig 6.9). Post-hoc tests revealed that neovascularisation was significantly increased only after treatment with 10mg/kg AKB-4924 ($P>0.05$, post-hoc Bonferroni). Thrombus macrophage and collagen content were not significantly altered by AKB-4924 ($P>0.05$, 1-way ANOVA, Table 6.4, Fig 6.10 and 6.11). Data of individual replicates is provided in Appendix D3.

Table 6.4 Histological measurements of thrombus resolution after treatment with AKB-4924

Measure	AKB-4924 (mg/kg)	Result (mean ± SE)
Volume (mm^3)	0	2.58 ± 0.3
	5	1.93 ± 0.3
	10	1.82 ± 0.4
Recanalisation (%)	0	11.0 ± 1.5
	5	13.8 ± 1.6
	10	10.8 ± 1.9
Neovascularisation (channels/level)	0	4.84 ± 0.3
	5	5.85 ± 0.6
	10	9.16 ± 0.9
Macrophage content (%)	0	10.7 ± 1.1
	5	13.3 ± 1.2
	10	15.7 ± 2.1
Collagen content (%)	0	10.1 ± 1.0
	5	12.7 ± 2.4
	10	14.1 ± 1.5

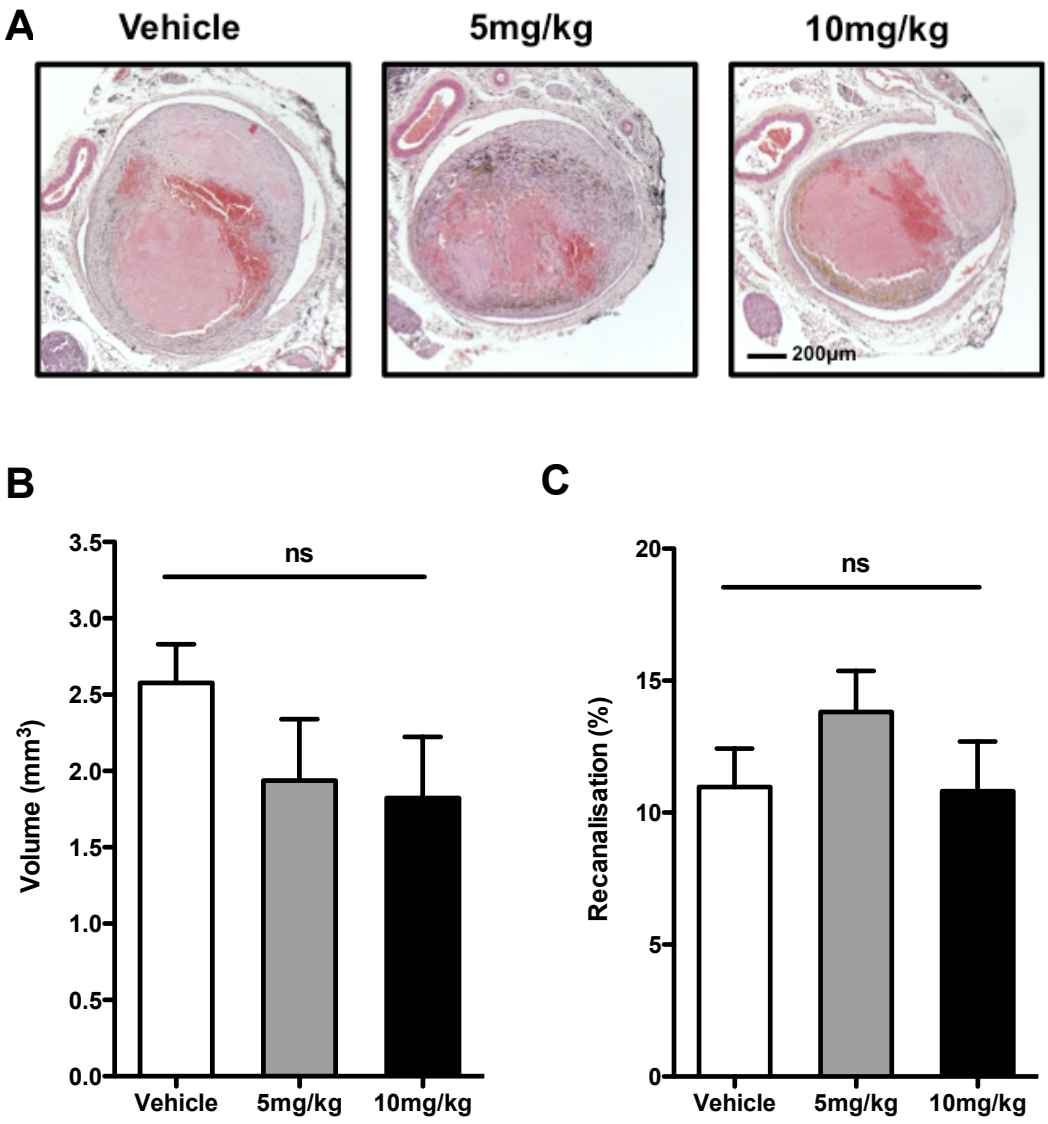

Figure 6.8 The effect of AKB-4924 on thrombus resolution

(A) Representative H&E stained sections of thrombi after treatment with either 5mg/kg or 10mg/kg AKB-4924 compared with vehicle control at day 14 post-induction (n=6 per group). (B) There were no significant differences in either thrombus volume (P>0.05,1-way ANOVA,). or vein lumen recanalisation (P>0.05,1-way ANOVA), across groups. Data represented as mean ± SE.

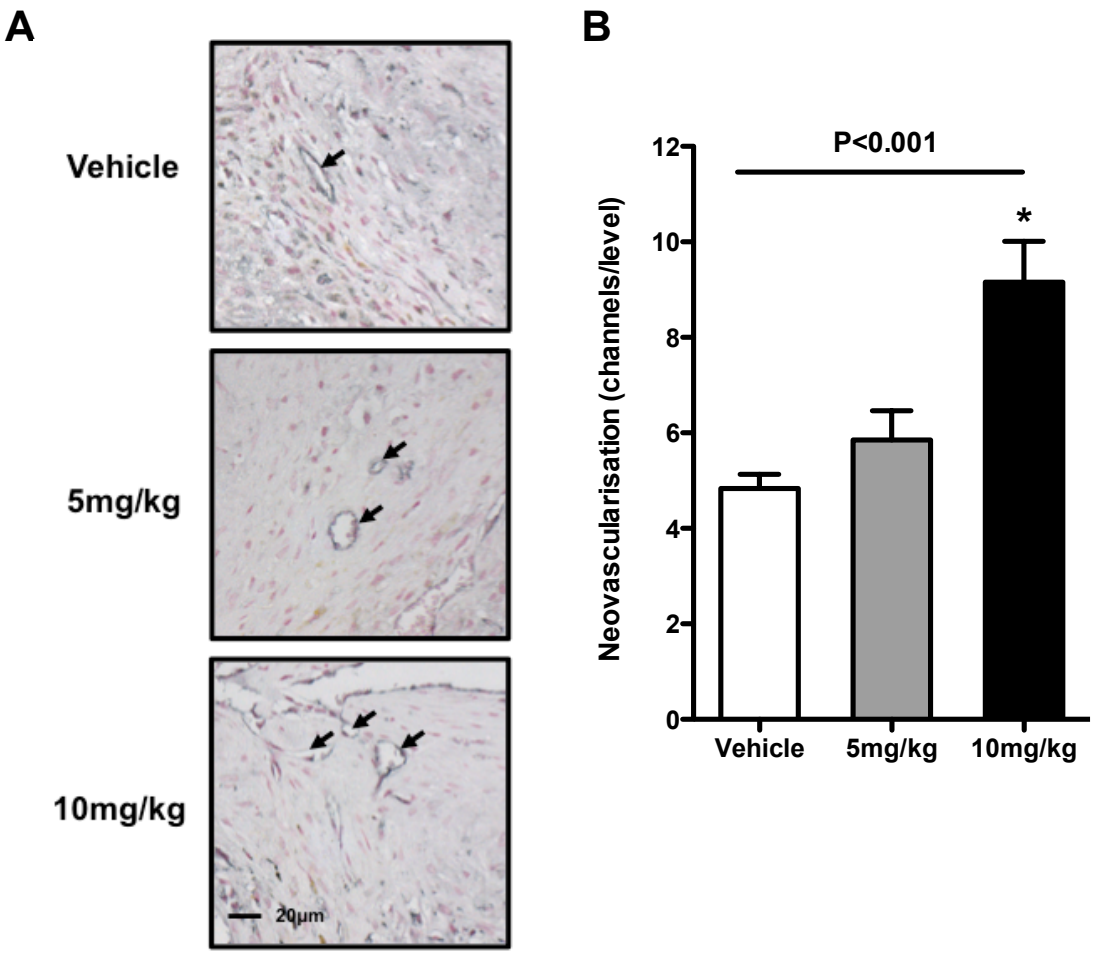

Figure 6.9 The effect of AKB-4924 on thrombus neovascularisation

(A) Representative CD31 stained sections of thrombi after treatment with the PHD inhibitor AKB-4924 at either 5mg/kg or 10mg/kg compared with vehicle treated control at 14 days post-induction (n=6 per group). Neovascular channels are stained black and denoted with black arrows, images taken at an original magnification of 400x. (B) Thrombus neovascularization was found to differ significantly between groups ($P<0.05$, 1-way ANOVA) specifically in mice treated with 10mg/kg AKB-4924 compared to venicle control (*$P<0.05$ post-hoc Bonferroni), data represented as mean ± SE.

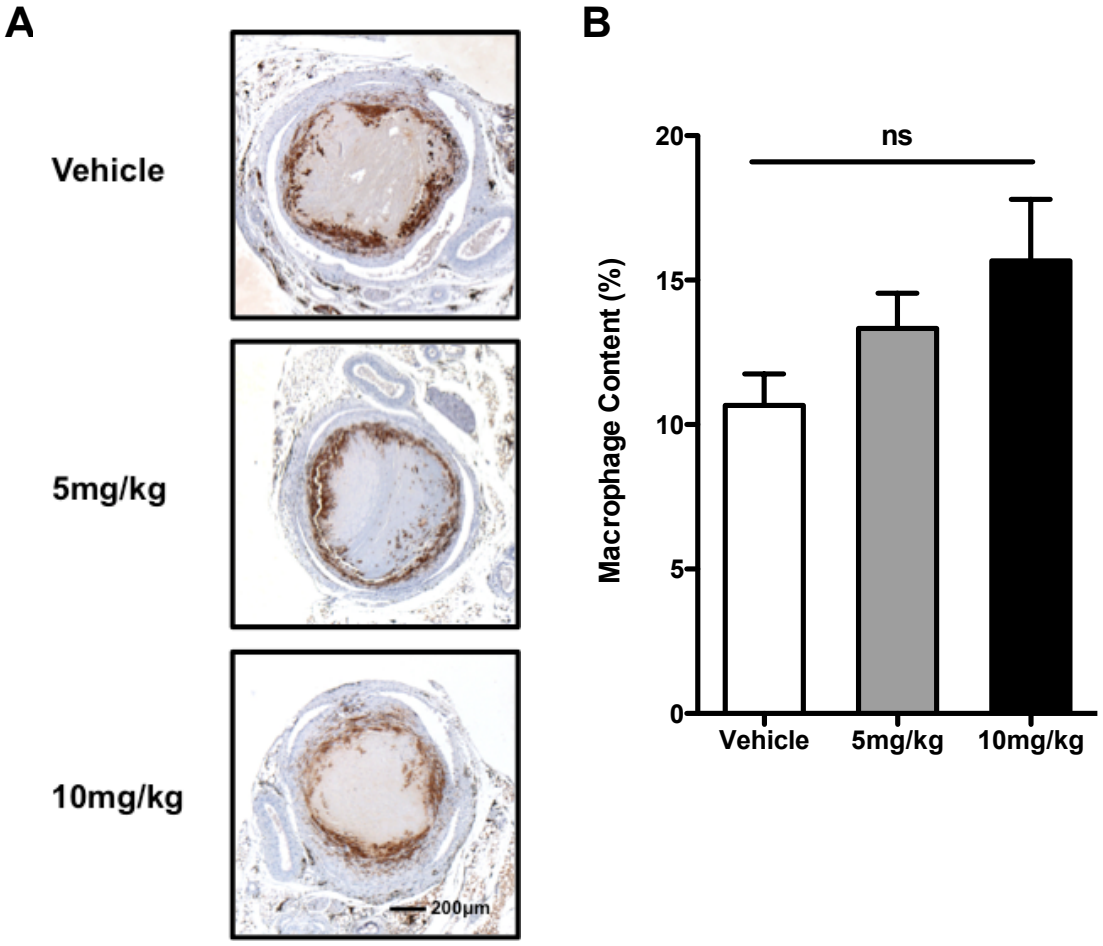

Figure 6.10 The effect of AKB-4924 on thrombus macrophage content

(A) Representative Mac-2 stained sections of thrombi after treatment with the PHD inhibitor AKB-4924 at either 5mg/kg or 10mg/kg compared to vehicle treated control at day 14 post-induction (n=6 per group). Macrophages are stained brown, images taken at an original magnification of 50x. (B) There was no significant effect of treatment on macrophage content ($P>0.05$ 1-way ANOVA), data represented as mean ± SE.

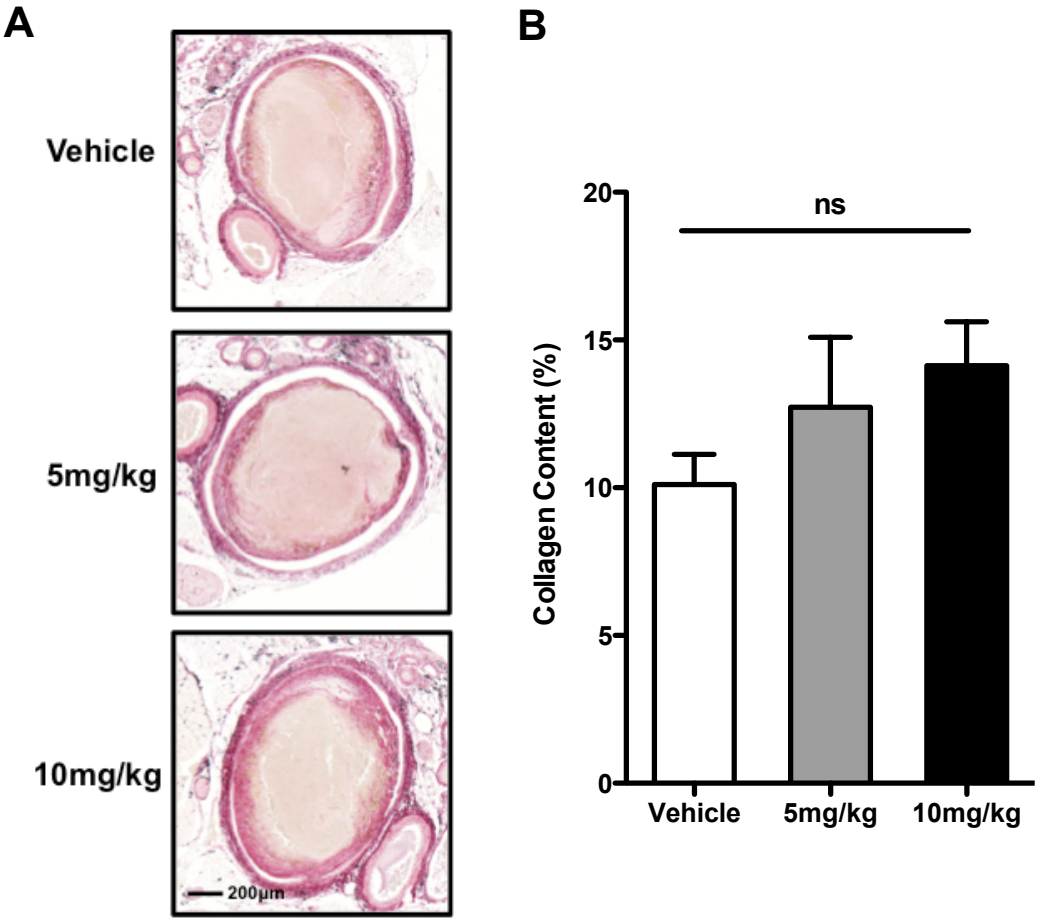

Figure 6.11 Thrombus collagen content after treatment with AKB-4924

(A) Representative picrosirius red stained sections of thrombi after treatment with the PHD inhibitor AKB-4924 at either 5mg/kg or 10mg/kg compared with vehicle treated control at day 14 post-induction (n=6 per group). Collagen is stained red, images taken at an original magnification of 50x. (B) There was no significant difference in collagen content across treatment groups (P>0.05, 1-way ANOVA), data represented as mean ± SE.

To directly compare measurements of thrombus obtained by microCT and histology paired data samples from thrombi at 14 days post induction were analysed. Regression analysis of thrombus volume determined by both techniques suggested that these measurements might agree (Fig 6.12A). Analysis by intra-class correlation revealed a moderately strong correlation between the two measures (ICC=0.75, P<0.01). A Bland-Altman plot revealed that as volume increased the difference between the two measurements also increased (Fig 6.12B). The mean difference between measurements was also high (4.2mm^3) suggesting that the absolute values were markedly different. Comparing both measures, histological thrombus volume (1.99 ± 0.22mm^3) was found to be significantly lower than respective contrast-enhanced microCT values (6.2 ± 0.5mm^3, P<0.0001, paired t-test).

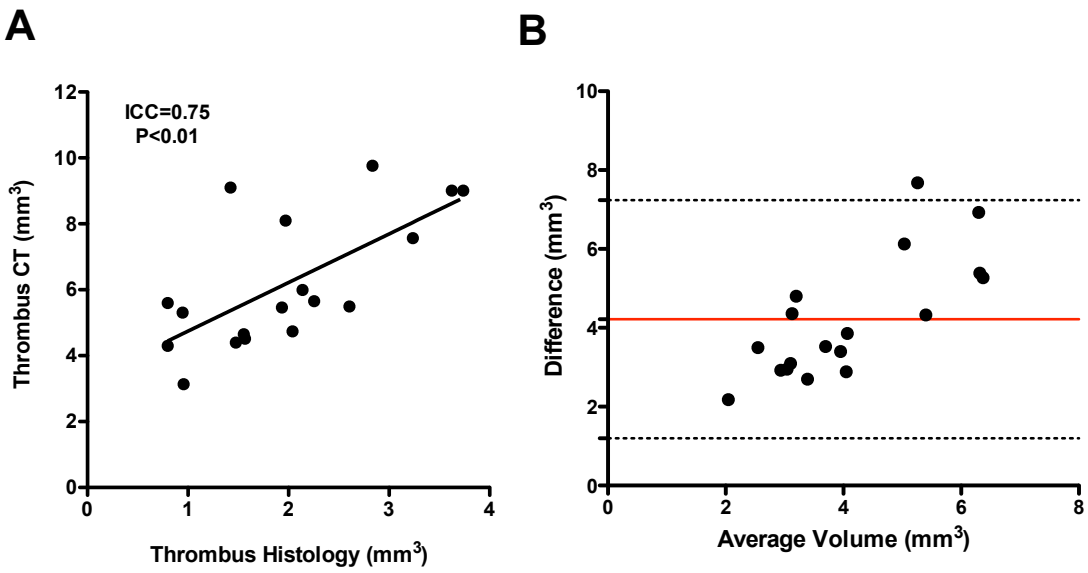

Figure 6.12 Comparison of paired measurements of thrombus volume

Paired measurements of thrombus volume by contrast-enhanced microCT and histology were compared in thrombi at day 14 post-induction (n=18) by (A) linear regression and (B) Bland-Altman where the red lines represents the mean difference and dotted line represent 1.96 standard deviations from the mean.

6.4.4 Efficacy of PHD inhibition by AKB-4924

The effect of PHD inhibition on PHD2 and PHD3 protein expression was assessed by western blotting of kidney cytoplasmic extracts obtained from animals treated with AKB-4924 (Fig 6.13A). Densitometric quantification revealed a slight but insignificant increase in PHD2 expression (P>0.05, 1-way ANOVA, Fig 6.13B) with PHD3 expression remaining largely invariant (P>0.05, 1-way ANOVA, Fig 6.13C). Western blotting of kidney nuclear extracts for HIF1α (Fig 6.14A) revealed significant differences after treatment with AKB-4924 (P<0.001, 1-way ANOVA, Fig 6.14B). HIF1α accumulation was significantly increased after treatment with 10mg/kg AKB-4924 compared with either vehicle control or 5mg/kg AKB-4924 (both P<0.05, post-hoc Bonferroni).

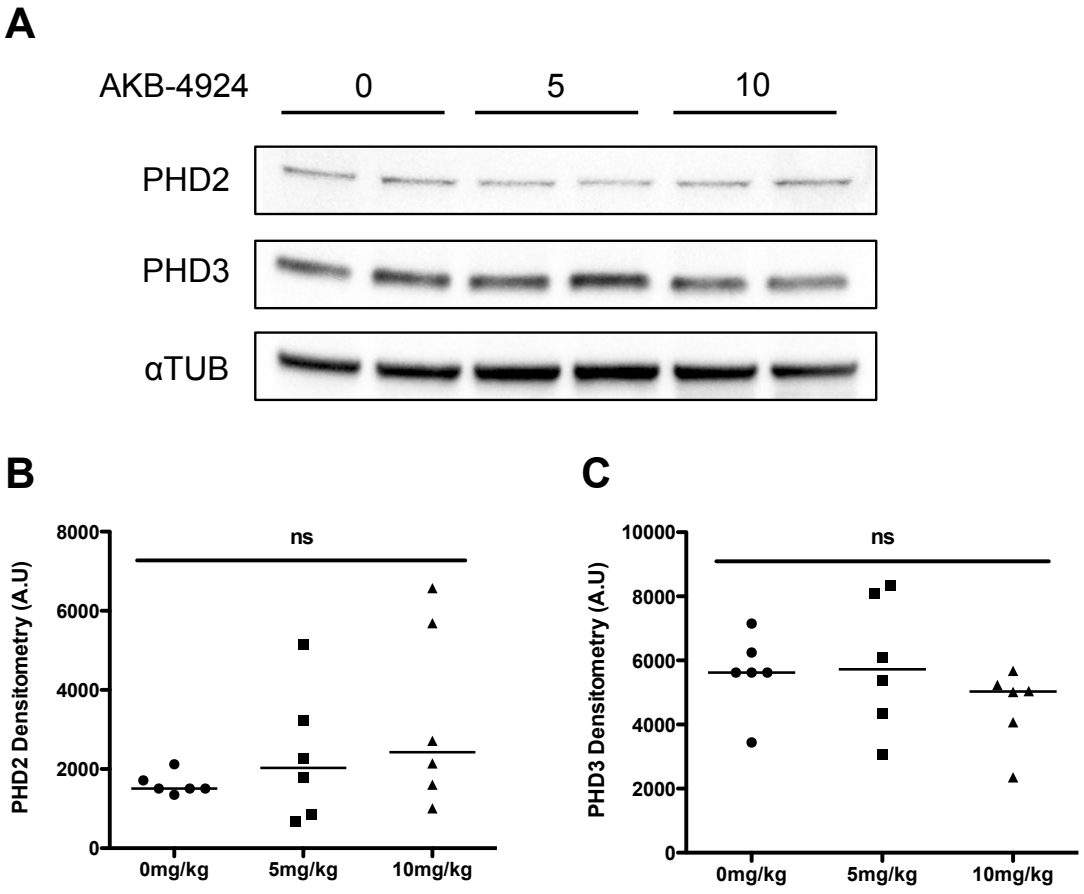

Figure 6.13 PHD protein expression after treatment with AKB-4924

(A) Representative western blots of PHD2, PHD3 and αTubulin expression. Densitometric quantification of (B) PHD2 and (C) PHD3 in kidney cytoplasmic extracts after treatment with AKB-4924 (Kruskal-Wallis, ns P>0.05), data represented as individual pointswith median.

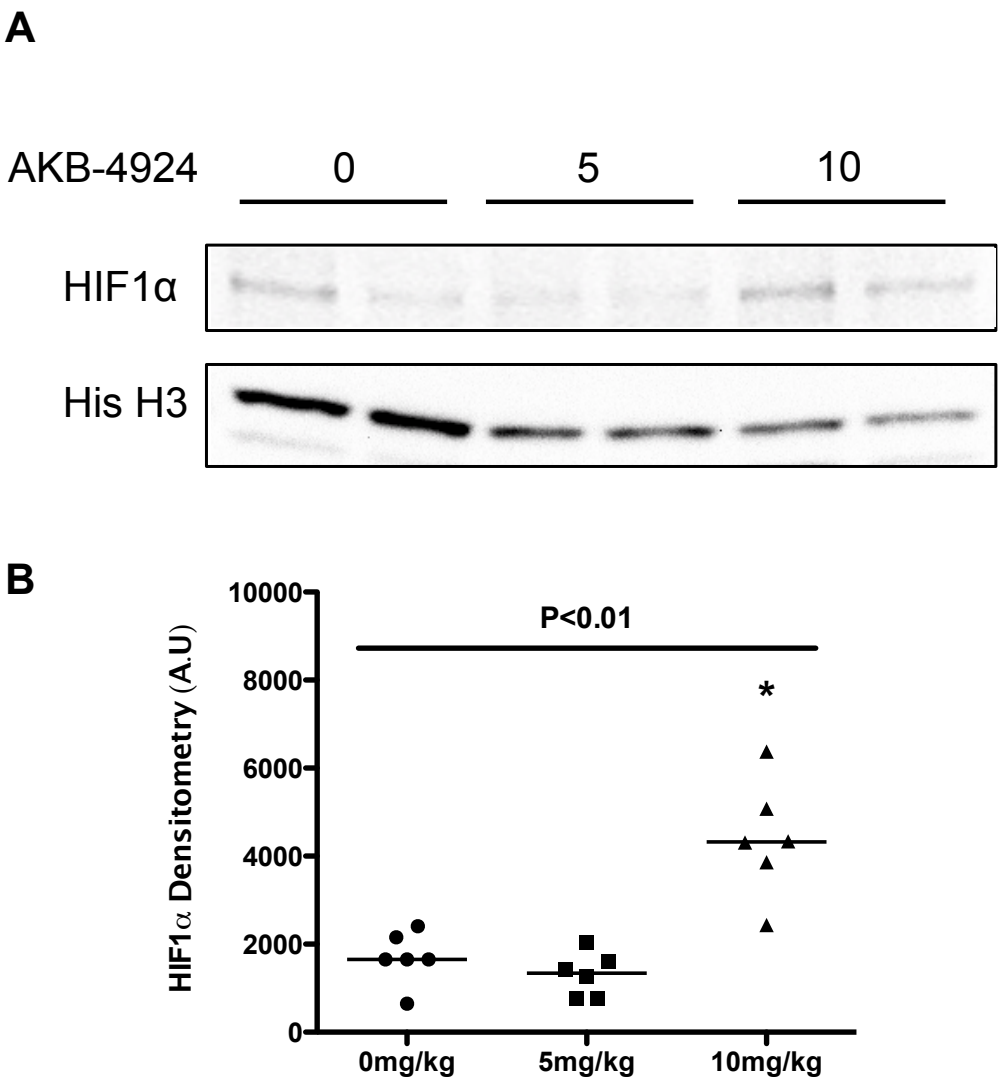

Figure 6.14 HIF1α protein expression after treatment with AKB-4924

(A) Representative western blots of HIF1α and histone H3 protein expression and (B) densitometric quantification of HIF1α in kidney nuclear extracts after treatment with AKB-4924 (Kruskal-Wallis with post-hoc Dunn's), data represented as individual points with median. *P<0.05 0mg/kg vs 10mg/kg and 5mg/kg vs 10mg/kg.

6.4.5 Effect of JNJ-42041935 treatment on venous thrombus resolution

The effect of a second PHD inhibitor, JNJ-42041935, on thrombus resolution was investigated. Histological assessment of thrombus volume and vein lumen recanalisation at day 14 post-induction revealed no significant affect of JNJ-42041935 on thrombus resolution as compared to vehicle control ($P>0.05$, student's t-test, Fig 6.15 and Table 6.5). Thrombus neovascularization was significantly upregulated after treatment with JNJ-42041935 as compared to vehicle control ($P<0.01$, student's t-test, Fig 6.16). Thrombus collagen and macrophage content remained unchanged after treatment with JNJ-42041935 as compared to vehicle control ($P>0.05$, student's t-test, Fig 6.17 and 6.18). Data of individual replicates is provided in Appendix D3.

Table 6.5 Histological measurements of thrombus resolution after treatment with JNJ-42041935

Measure	Vehicle (n=9)	JNJ-42041935 (n=9)
Volume (mm^3)	2.79 ± 0.2	2.57 ± 0.1
Recanalisation (%)	13.7 ± 1.1	14.3 ± 1.2
Neovascularisation (channels/level)	7.32 ± 0.8	11.0 ± 0.5
Macrophage content (%)	7.86 ± 0.4	9.03 ± 0.6
Collagen content (%)	15.7 ± 0.9	15.7 ± 1.2

Data represented as mean ± SE

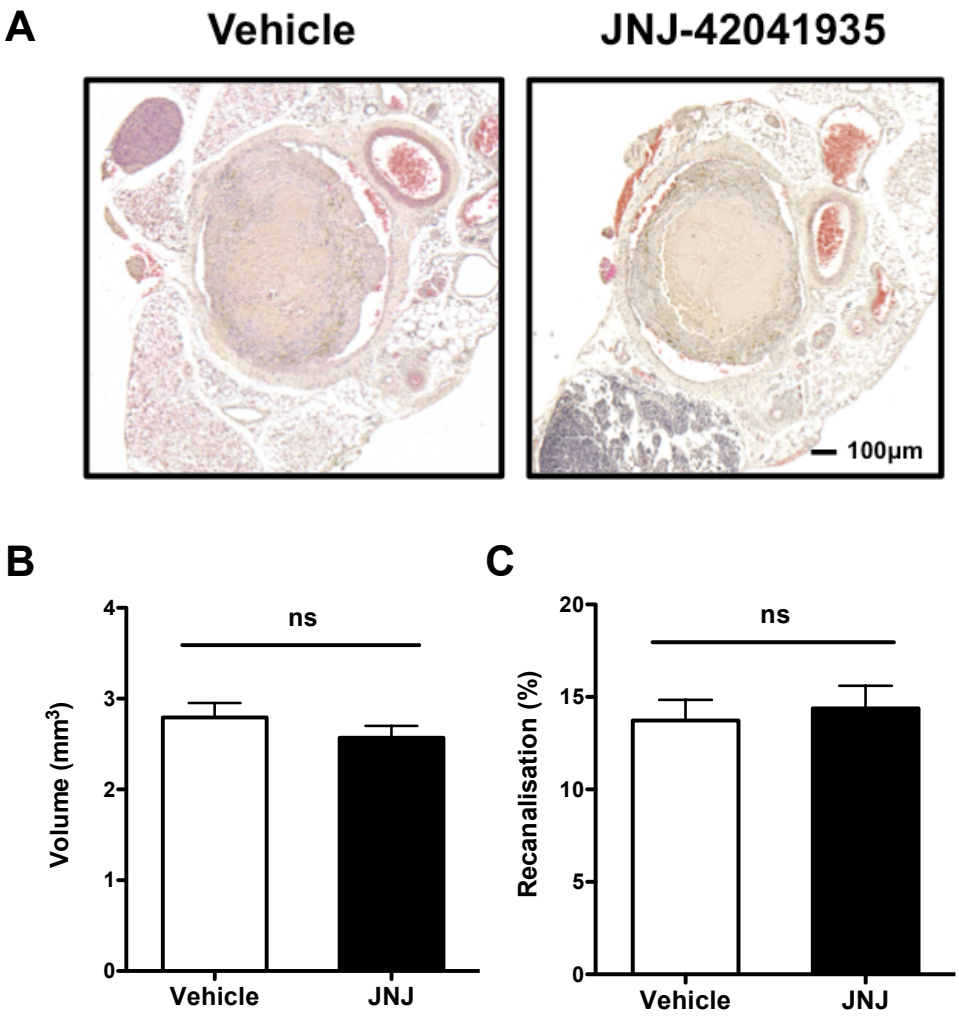

Figure 6.15 The effect of JNJ-42041935 on venous thrombus resolution

(A) Representative H&E stained sections of thrombi after treatment with JNJ-42041935 compared with vehicle control at day 14 post-induction (n=9 per group). (B) No significant difference in thrombus volume was observed (P>0.05, student's t-test). (C) Vein lumen recanalisation was not significantly altered (P>0.05, student's t-test). Data represented as mean ± SE.

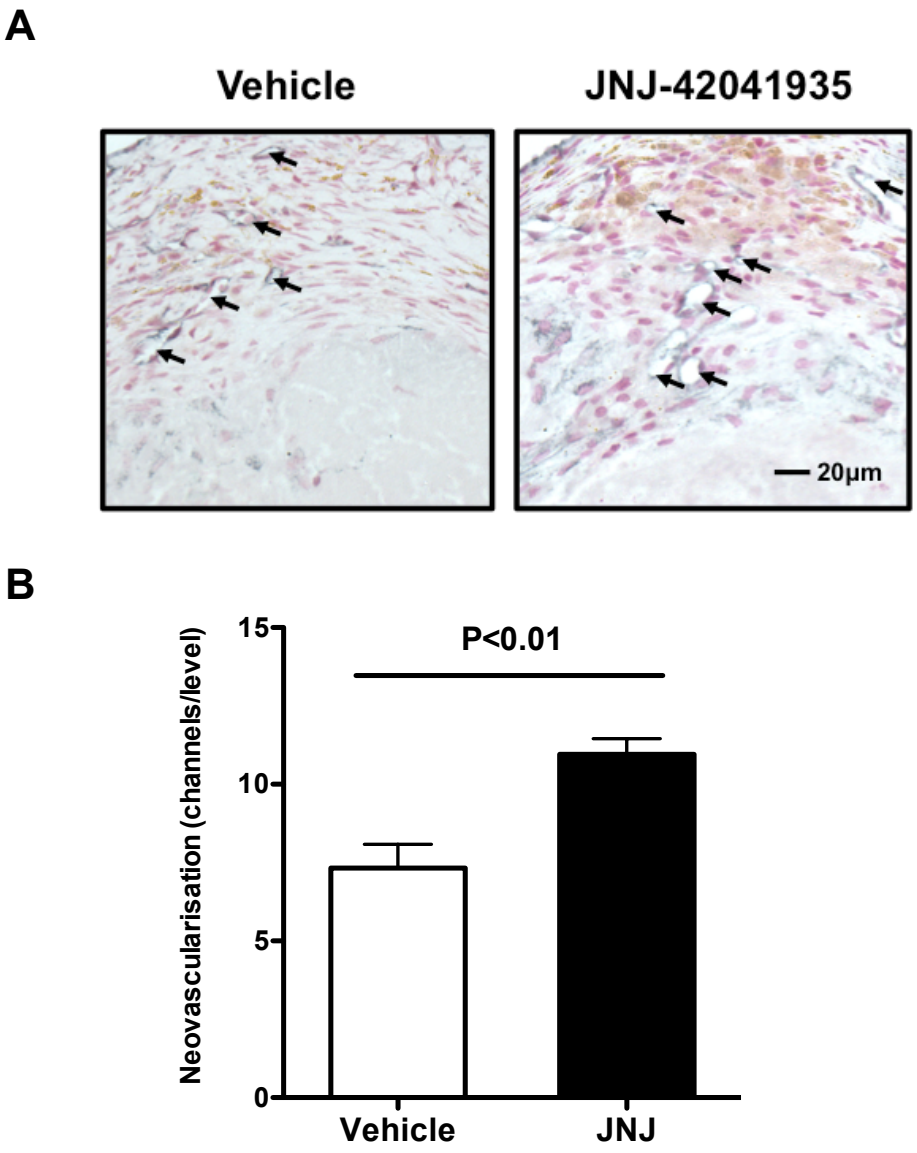

Figure 6.16 The effect of JNJ-42041935 on thrombus neovascularisation

(A) Representative CD31 stained sections of thrombi after treatment with JNJ-42041935 compared with vehicle control at day 14 post-induction (n=9 per group). (B) Neovascularization was significantly increased in JNJ-42041935 treated thrombi when compared to vehicle control (P<0.01, student's t-test), data represented as mean ± SE.

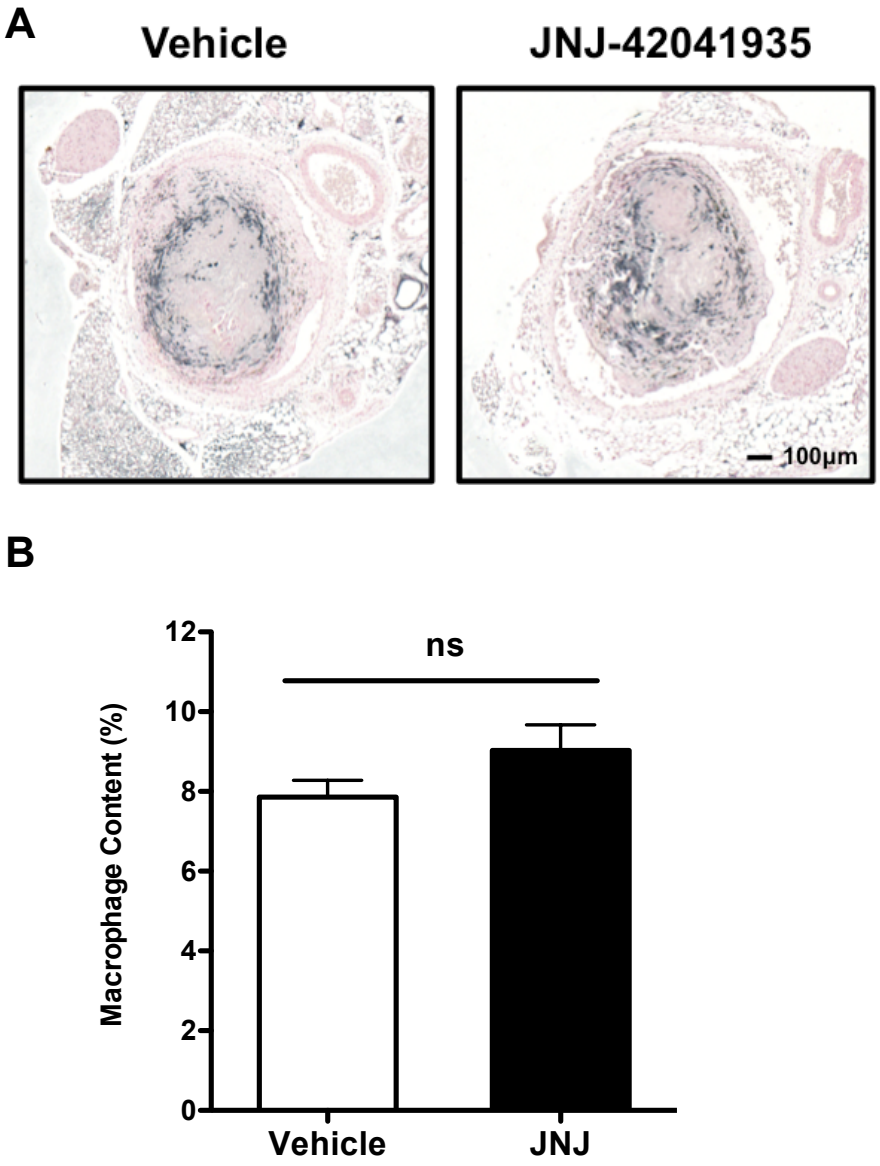

Figure 6.17 The effect of JNJ-42041935 on thrombus macrophage content
(A) Representative Mac-2 stained sections of thrombi after treatment with JNJ-42041935 compared with vehicle control at day 14 post-induction (n=9 per group). (B) No significant difference in thrombus macrophage content was observed (P>0.05, student's t-test), data represented as mean ± SE.

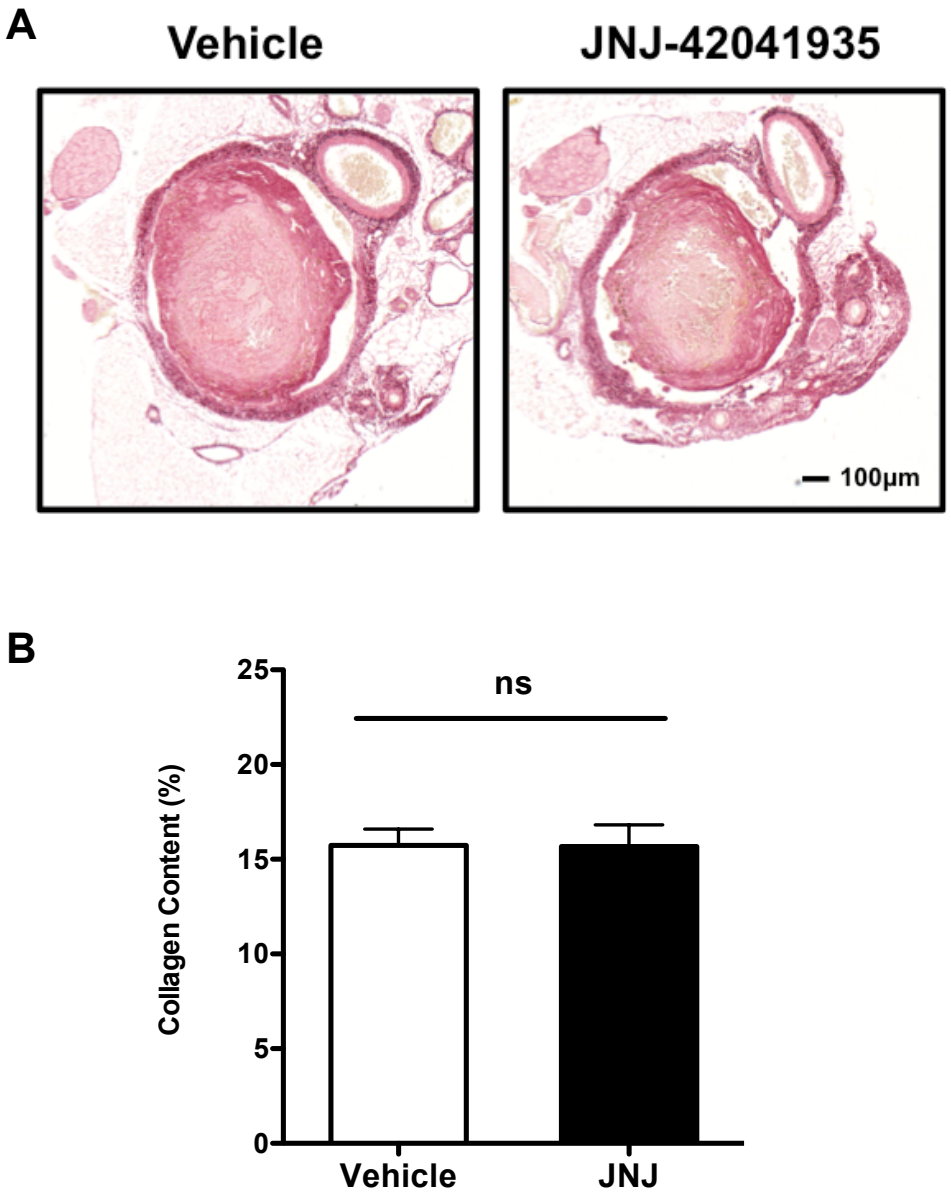

Figure 6.18 The effect of JNJ-42041935 on thrombus collagen content

(A) Representative picrosirius red stained sections of thrombi after treatment with JNJ-42041935 compared with vehicle control at day 14 post-induction (n=9 per group). (B) No significant difference in thrombus collagen content was observed (P>0.05, student's t-test), data represented as mean ± SE.

6.4.6 Efficacy of PHD inhibition by JNJ-42041935

Haematocrit was significantly increased by treatment with JNJ-42041935 as compared to vehicle control (Mann-Whitney, P<0.01, Fig 6.19).

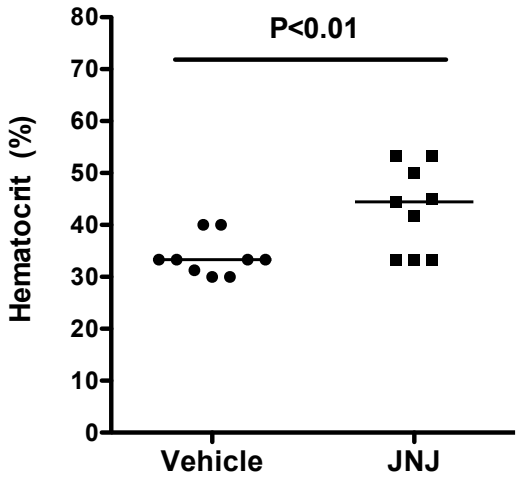

Figure 6.19 Effect of JNJ-42041935 on haematocrit

Haematocrit was significantly increased after treatment with JNJ-42041935 compared to vehicle control (P<0.01, Mann-Whitney), data represented as individual data points with median (n=9 per group).

6.4.7 Effect of PHD inhibition on circulating levels of VEGF

The plasma concentration of VEGF was not significantly altered by 10mg/kg AKB-4924 (72.3 ± 6.5pg/ml) when compared to vehicle control (75.0 ± 4.0pg/ml, P>0.05, student's t-test, Fig 6.20A). Similarly plasma VEGF concentrations were not significantly different in JNJ-42041935 treated mice (69.0 ± 3.1pg/ml) compared to vehicle treated controls (71.4 ± 3.4pg/ml, P>0.05, student's t-test, Fig 6.20B).

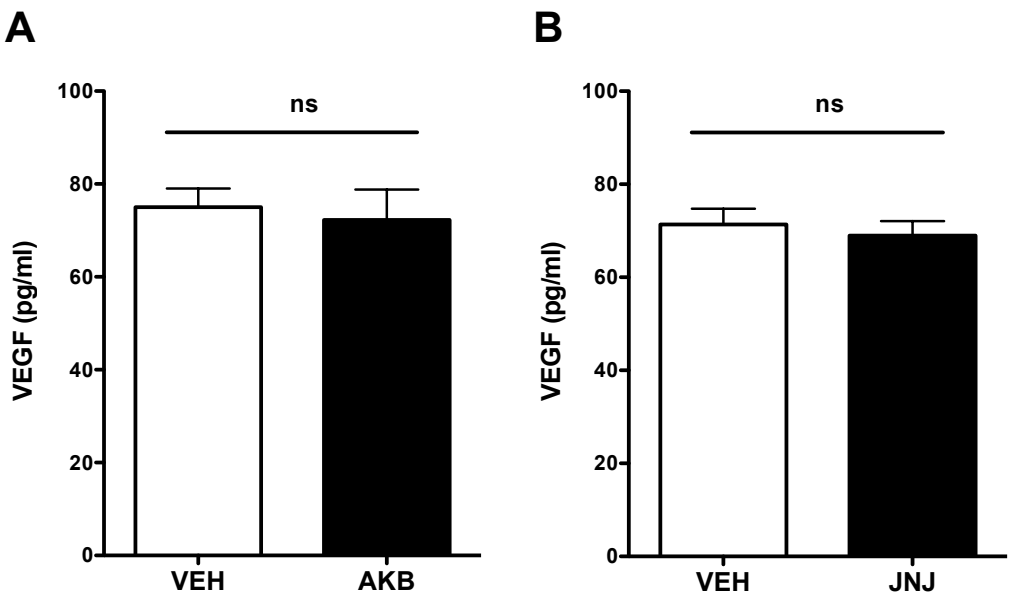

Figure 6.20 The effect of AKB-4924 and JNJ-42041935 on plasma VEGF

Plasma VEGF levels were determined by ELISA after treatment with (A) 10mg/kg AKB-4924 or (B) JNJ-42041935 and compared to respective vehicle controls. No significant difference in plasma VEGF was observed after treatment with either drug (P>0.05, student's t-test), data represented as mean ± SE.

6.5 Discussion

AKB-4924

A pharmacological approach was used to assess the contribution of PHD enzymatic activity towards venous thrombus resolution. The PHD inhibitor, AKB-4924 was administered at a dose of 5mg/kg and 10mg/kg, corresponding respectively to the recommended and maximal tolerated dose in mice. Thrombus resolution was quantified by a novel application of contrast-enhanced microCT and confirmed by end-point histological analysis.

There was a dose dependent trend towards increased thrombus resolution in mice treated with AKB-4924, although this did not reach statistical significance. The failure of this trend to reach the significance is probably the result of the relatively small differences between treatment groups (<25%). This experiment was powered to observe drug effects of greater than 30%, and therefore, in order for significance to be attained, group sizes would need to be increased. End-point measures of thrombus volume obtained by histological analysis were well matched with the microCT analyses.

Histological analysis revealed the novel finding that stabilisation of HIF1α using AKB-4924 was associated with increased thrombus neovascularisation. This finding complements previous studies of increased thrombus neovascularisation after treatment with the PHD inhibitor L-mimosine[57]. The lack of an effect by AKB-4924 on thrombus resolution (in contrast to L-mimosine), in the face of increased nuclear HIF stabilisation, suggests that HIF driven neovascularisation alone is not a major driver of thrombus resolution. This is consistent with work in which treatment of experimental venous thrombi with basic fibroblast growth factor, a downstream target for HIF1α, increased neovascularisation without increasing thrombus resolution [58].

Other measures of thrombus organisation including collagen deposition and macrophage accumulation again showed trends towards enhanced organisation, but did not reach statistical significance. This is surprising given that HIF1α plays an important role in collagen deposition during embryological development[288], and a number of collagen modifying genes including *P4ha1*,

P4ha2 and *Plod2* are HIF1α transcriptional targets[289]. It was hypothesised that PHD inhibition would promote recruitment of macrophages to the resolving venous thrombus given that both HIF1α and HIF2α are critical for migration[74, 262]. It is possible instead that PHD inhibition fine-tunes macrophage activation and skewing as has been previously reported[164].

Direct measurements of HIF1α nuclear accumulation were made in order to assess the efficacy of AKB-4924. This is in contrast to the majority of other studies using AKB-4924 that have relied on *in vitro* measurements of HIF1α or *in vivo* measurements of downstream HIF1α target genes[231, 233, 234, 290]. Mice treated with 10mg/kg of AKB-4924 showed significantly increased nuclear accumulation of HIF1α in kidney tissue. This demonstrates that AKB-4924 is an effective PHD inhibitor *in vivo*. It was also interesting to note the variable protein expression of histone H3 in western blots of kidney nuclear extracts, observed in previous experiments (Chapter 4 and Chapter 5). Studies of HIF1α target genes have not identified histone H3 nor was it possible to find any evidence in the literature to suggests that hypoxia induced expression of histone H3. It would appear more likely that variation in histone H3 protein expression occurs as a result of the tissue extraction protocol, although further experiments would be required to confirm this. Given the need for significant normalisation of these samples this precluded the use of potentially more sensitive HIF1α ELISA.

JNJ-42041935

A potential limitation of the experiments conducted with AKB-4924 was the relative small group sizes used. The study was initially powered to observe a 30% change in thrombus volume by histology with an alpha of 0.05 which required a samples size of six per group. Changes in thrombus volume after treatment with AKB-4924 were less than 30% meaning that this study was not sufficiently powered for the scale of change observed. It was not possible to increase group sizes with AKB-4924 because of the limited supply of this drug. To address this limitation thrombus resolution was studied after treatment with a second PHD inhibitor JNJ-42041935 with a group size of nine per treatment.

Treatment with JNJ-42041935 resulted in an increase in HIF1α transcriptional activity, as determined by significant increases in haematocrit similar in scale to

those previously described for this compound[227]. As with the other HIF stabilising agent, AKB-4924, thrombus resolution was not significantly altered after treatment with JNJ-42041935. Measures of thrombus collagen and macrophage content were similarly unchanged after treatment with this agent. However, treatment with JNJ-42041935 significantly enhanced thrombus neovascularisation (~50% increase), which is a novel finding with this agent that has been characterised with respect to its proerythropoietic activity[227], but not angiogenic potential.

The two PHD inhibitors, AKB-4924 and JNJ-42041935, demonstrate strong phenotypic agreement in terms of their effect on thrombus, resolution and organisation, suggesting that the major contribution of PHD enzyme inhibition to thrombus resolution is the formation of neovascular channels. The use of two inhibitors with differing modes of action and therefore non-overlapping off-target effects, AKB-4924 an iron chelator and JNJ-42041935 a 2-OG mimetic, further strengthens this finding[227, 231].

Contrast-enhanced microCT

Advances in CT imaging technologies have enabled the development of high-resolution microCT imaging platforms suitable for pre-clinical use[291]. MicroCT was selected as it provides improved spatial resolution (22-65μm) compared to 3D-HFUS. It also benefits from greater technical simplicity, only requiring the relevant region of interest to be selected. Imaging of the vasculature by contrast enhanced microCT requires administration of blood-pool contrast agents[292]. Contrast-enhanced microCT has been used extensively in murine models of cardiovascular disease such as critical limb ischaemia, abdominal aortic aneurysms and myocardial infarction[164, 293, 294].Contrast-enhanced microCT of experimental venous thrombi has been reported in the literature, but this has been limited to demonstrating the presence of thrombus or for co-registration with other imaging modalities[254, 295].

In the current study Aurovist, a nanogold based contrast agent, was selected as this offered superior x-ray attenuation, good retention in the vascular compartment and low toxicity compared with other ionidated or microparticle based agents[296]. Previous studies using Aurovist have provided excellent

vascular contrast when administered at a dose of 20mg nAu per mouse. Given the high cost of this agent a lower dose of Aurovist, that still provided sufficient contrast to allow for segmentation of the thrombus, was desirable. Aurovist administered at a dose of 10mg of Au, half that of previous studies, was sufficient to visualise thrombus present in the IVC.

Contrast-enhanced microCT of thrombosed mice at 1, 7 and 14 days post-induction was well tolerated with no adverse events observed. Sufficient vascular contrast was obtained to allow for segmentation of the thrombus at every time-point studied. Others have reported difficulties in repeated administration of Aurovist as a result of tissue leakage at the site of injection[297]. This was avoided in our study by utilisation of distal segments of the caudal vein, allowing subsequent injections to be located in increasingly proximal segments. Injection may have also been aided by the use of a smaller dose of contrast agent.

To quantify thrombus volume, a method of image segmentation and 3D volume reconstruction was required. Using semi-automated propagation-based segmentation software it was possible to generate detailed 3D volume renders of the thrombus from which measurements of volume could be obtained. As the majority of scan segmentations required a degree of manual refinement, it was important to ensure that this component of the analysis was both reliable and reproducible. Encouragingly measures of both inter- and intra observer variability showed strong positive correlations.

Paired analysis of thrombus volume determined by contrast-enhanced microCT and histology revealed a relatively strong correlation. This correlation could be further strengthened by the addition of further time-matched samples as the range of volume measured was relatively narrow. It was also interesting to note the large degree of bias (~4mm^3) between measurements, suggesting that volumes determined by histology were markedly lower than those by contrast-enhanced microCT. This can be explained by the effects of shrinkage observed during processing of tissues for paraffin embedding[298].

Chapter 7 The effect of inhibition of vascular endothelial growth factor receptors (VEGFRs) on venous thrombus resolution

7.1 Introduction

Tissue hypoxia, like that present in the early venous thrombus[57], is considered a key regulator of angiogenesis in a range of human pathologies including myocardial infarction and cancer[299, 300]. Hypoxia-induced angiogenesis is mediated by the expression of a number of HIF1α target genes including *Vegfa*, *Plgf* and *Vegfr1*[301-303]. VEGFA treated endothelial cells demonstrate enhanced migration and proliferation *in vitro* [304, 305]. *In vivo* vessel formation appears to be highly sensitive to gradients of VEGFA that coordinate the migration of specialised tip cells and proliferation of stalk cells[306].

Angiogenesis and the development of neovascular channels during thrombus organisation is thought to be an important process in the resolution of venous thrombi. There is a distinct, temporal pattern of VEGFA expression within the thrombus[48]. Increasing the levels of VEGFA in the resolving thrombus, either through direct injection of recombinant protein, or gene-mediated (plasmid or adenoviral) overexpression, significantly enhances resolution. This is associated with increased lumen recanalisation and macrophage recruitment[49-51].

VEGFA must bind to and activate cognate VEGF receptors (VEGFRs) present on the surface of a wide range of cell types, in order to promote angiogenesis[307]. The VEGFR family consists of three members (VEGFR1, VEGFR2 and VEGFR3) that bind to a variety of ligands (Fig 7.1). On ligand binding VEGFRs undergo auto-phosphorylation of tyrosine residues mediated by receptor tyrosine kinase domains present in cytoplasmic tail[307]. VEGFR auto-phosphorylation triggers downstream signal transduction through activation of kinases in a ligand and receptor specific manner.

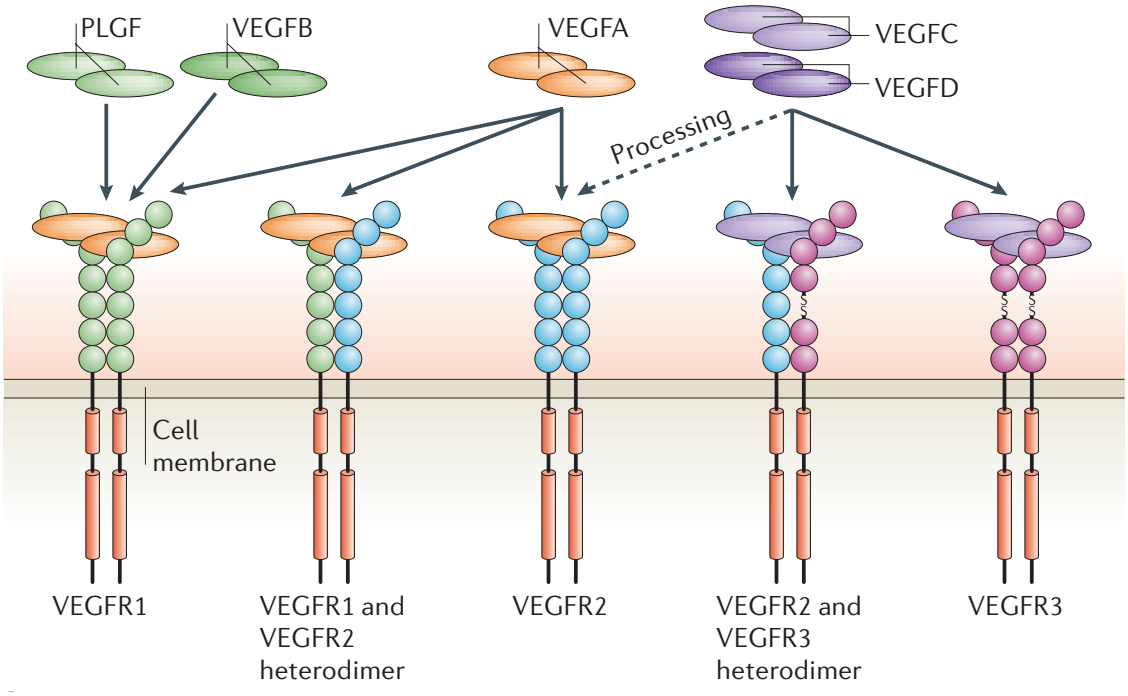

Figure 7.1 VEGFR signalling

VEGFR ligands including VEGFA, VEGFB, VEGFC, VEGFD and PLGF bind to a series of VEGFR present as either hetero- or homo- dimers at the cell surface. Adapted from[307].

The VEGF family of heparin binding glycoproteins also includes a number of related factors produced by separate genes that include VEGFB, VEGFC, VEGFD and PlGF. Whereas VEGFA, VEGFB and PlGF are important promoters of angiogenesis[308-310], VEGFC and VEGFD serve as critical regulators of lymphatic development[311, 312]. A large number of VEGFA splice variants have been identified; VEGFA 165, 189, 121, 206, 183, 145 and 111 (in reference to amino acid length)[313]. These splice variants vary in their capacity to bind to heparin and the extracellular matrix. Similar variants have also been described for VEGFB and PlGF[314, 315]. Comparatively recently an additional cohort of VEGFA splice variants has been identified (VEGFA 165b, 189b, 121b) with greatly reduced angiogenic activity[313].

Targeting of VEGF signalling through cognate VEGFRs has proven an effective strategy for the treatment of a range of cancers[316]. Drugs have been developed that target either the VEGF ligand, such as the monoclonal blocking antibody bevacizumab, or VEGFRs such as the small molecule inhibitors sorafenib and

sunitinib[140, 186]. Axitinib is a novel small molecule VEGFR inhibitor currently in phase I to III trials for multiple tumour types and approved for the treatment of metastatic renal cell carcinoma (Fig 7.2)[317, 318].

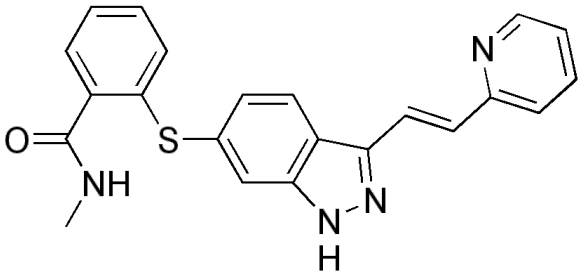

Figure 7.2 Axitinib structure
The molecular structure of the small molecule VEGFR inhibitor axitinib

Axitinib inhibits angiogenesis by blocking ligand-induced VEGFR phosphorylation, significantly reducing tumour vascularisation in a number of murine disease models[319-321]. The anti-angiogenic effects of axitinib are likely to the result of dysregulation of numerous VEGF mediated pathways within the endothelium as treatment results in increased vascular permeability[319], decreased tubule formation and decreased endothelial cell survival[322]. Pharmacokinetic studies show that axitinib is a pan-VEGFR inhibitor with IC_{50} values in the range of 0.1-0.3 nmol/L and active against both human and murine VEGFR protein[322].

Given that a number of VEGF-VEGFR proteins are HIF1α transcriptional targets it is important to understand to what extent signalling through this pathway contributes to venous thrombus neovascularisation and resolution. Unlike previous studies upregulating VEGF[49-51] the use of a VEGFR antagonist allows for the opposite effect of the contribution of endogenous signalling to be investigated.

7.2 Aim

To investigate the effect of VEGFR inhibition on venous thrombus resolution using the anti-angiogenic agent axitinib.

7.3 Methods

7.3.1 Thrombus induction and axitinib treatment

Thrombi were induced in the inferior vena cava of 8-10 week old male BALB/c mice as described in Chapter 2.3.1. Axitinib (25mg/kg) or vehicle control was administered by intra-peritoneal injection twice daily (B.I.D). This dose and treatment schedule is commonly used in the literature and effective in inhibiting VEGFR activation[319-321]. Axitinib was prepared in 30% (v/v) polyethelene glycol 400 (Sigma, UK) 70% (v/v) acidified water. Thrombi were harvested at days 3, 10 and 17days post-induction for analysis by immunohistochemistry (Fig 7.3).

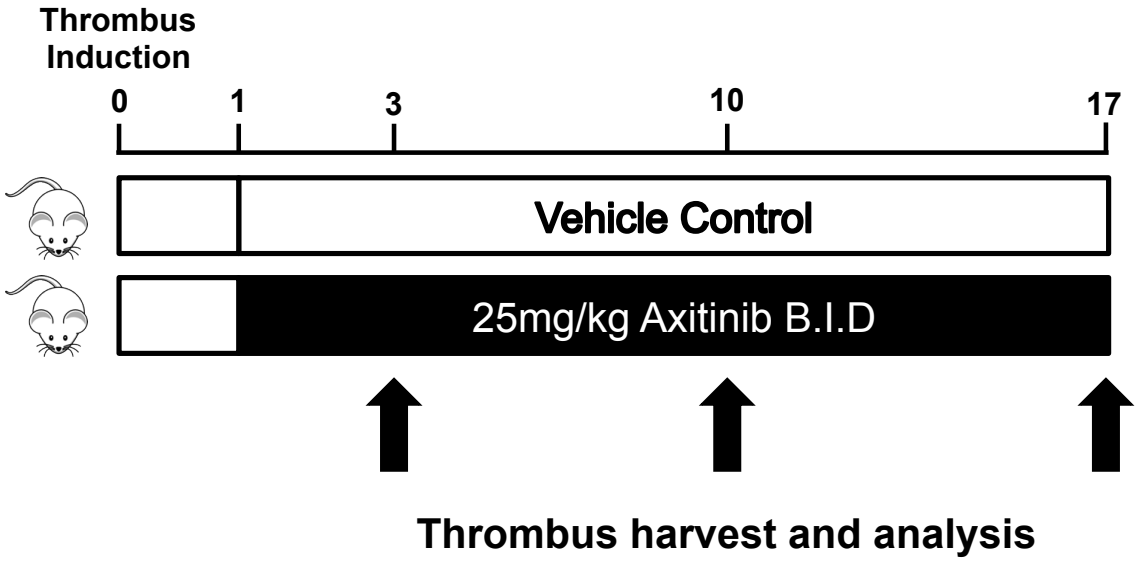

Figure 7.3 Study Design

Thrombus was induced in 8-10 week old male Balb/c mice. Mice were administered 25mg/kg axitinib or vehicle control twice daily by intraperitoneal injection started 24hrs post-induction. Thrombi were harvested at days 2, 10 and 17days post-induction for analysis.

7.3.2 Thrombus processing

Thrombus tissue samples were processed as described in Chapter 4.3.5

7.3.3 Thrombus immunohistochemistry

Thrombus sections were stained with H&E, CD31, Mac-2 and picrosirius red and analysed as described in Chapter 4.3.6-4.3.9

7.3.4 Statistical analysis

Kolmogorov-Smirnov tests were used to assess normality of data and parametric or non-parametric tests were used as appropriate. The effect of axitinib treatment on thrombus resolution was assessed by 2-way ANOVA with post-hoc Bonferroni. In all cases $P<0.05$ was considered statistically significant. Statistical analyses were conducted using Prism Software (v5, Graphpad, USA). Parametric data represented as mean ± SE.

7.4 Results

Axitinib treatment resulted in impaired thrombus resolution shown by a greater thrombus size and reduced vein recanalisation compared with vehicle treated control ($P<0.002$, and $P<0.001$ respectively, 2-way ANOVA, Fig 7.4 and Table 7.1). Thrombus volume was temporally increased at day 10 after treatment with axitinib while recanalization was increased at day 17 ($P<0.01$, post-hoc Bonferroni). Thrombus organisation was also significantly impaired after treatment as shown by reduced thrombus neovascularisation ($P<0.0001$, 2-way ANOVA, Fig 7.5), macrophage content ($P<0.0001$, 2-way ANOVA, Fig 7.6) and reduced fibrillar collagen content ($P<0.0001$, 2-way ANOVA, Fig 7.7) compared with vehicle control. These markers were impaired at both days 10 and 17 after axitinib treatment ($P<0.05$, post-hoc Bonferroni). Data of individual replicates is provided in Appendix E1.

Table 7.1 Thrombus volume, recanalisation and neovascularisation

Measure	Day	Vehicle	Axitinib
Volume (mm^3)	3	5.81 ± 0.3	6.38 ± 0.4
	10	2.40 ± 0.2	4.10 ± 0.5
	17	1.71 ± 0.3	2.47 ± 0.3
Recanalisation (%)	3	6.59 ± 1.2	5.46 ± 1.3
	10	10.2 ± 1.5	4.87 ± 1.2
	17	19.0 ± 1.6	11.5 ± 2.0

Data represented as mean ± SE

Table 7.2 Thrombus macrophage and collagen content

Measure	Day	Vehicle	Axitinib
Neovascularisation (channels/level)	3	0.33 ± 0.0	0.17 ± 0.0
	10	2.86 ± 0.3	2.00 ± 0.3
	17	5.29 ± 0.3	2.29 ± 0.3
Collagen content (%)	3	1.41 ± 0.1	1.30 ± 0.1
	10	4.46 ± 0.4	1.09 ± 0.1
	17	19.5 ± 1.6	11.6 ± 1.3
Macrophage content (%)	3	0.06 ± 0.0	0.05 ± 0.0
	10	6.89 ± 0.3	2.91 ± 0.4
	17	8.51 ± 0.7	5.23 ± 0.4

Data represented as mean ± SE

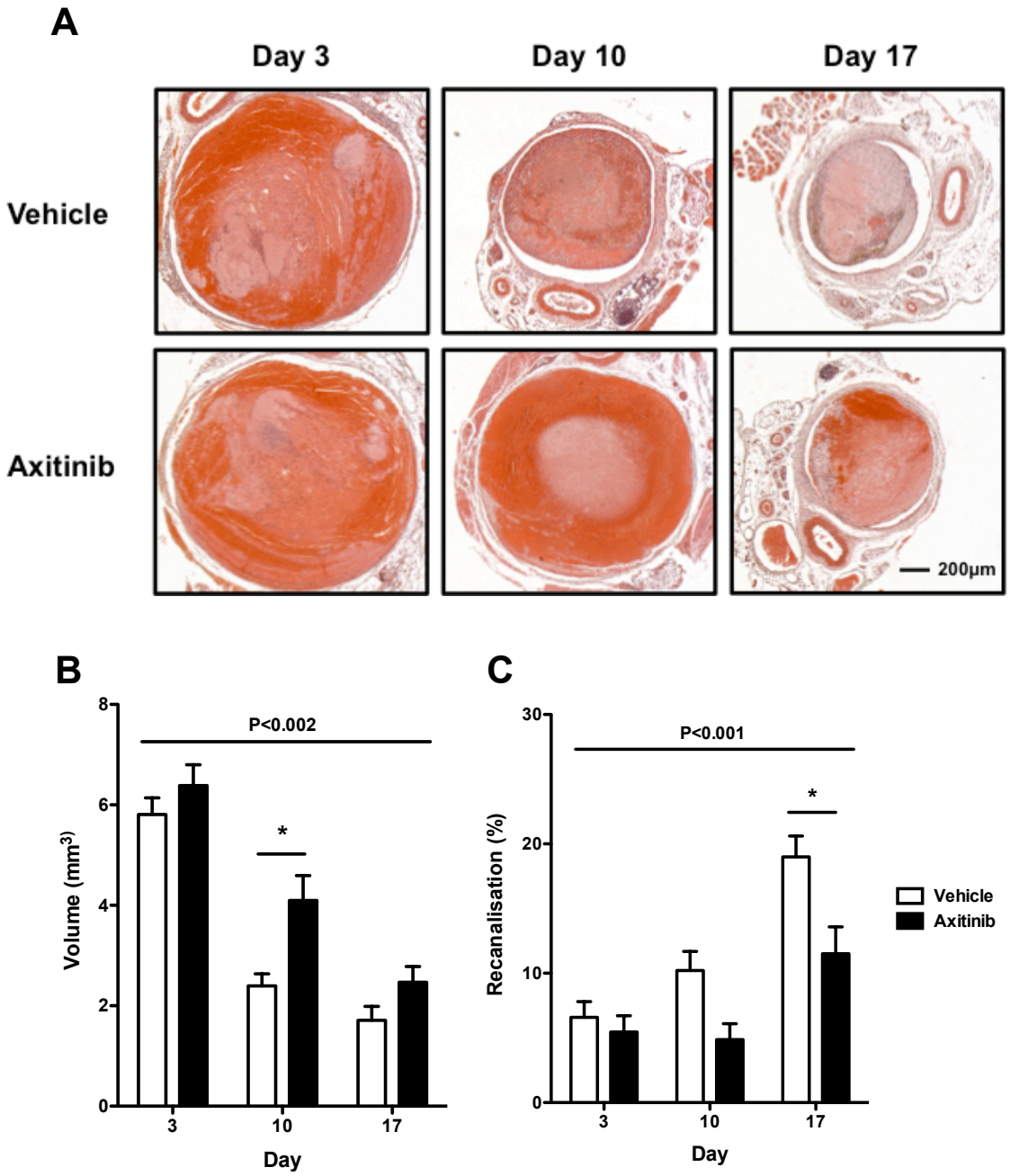

Figure 7.4 Thrombus volume and vein lumen recanalisation after axitinib treatment

(A) Representative H&E sections of thrombi at days 3, 10 and 17 post-induction treated with either axitinib or vehicle control (n=6-8 per group), images taken at an original magnification of x50. (B) Thrombus volume was significantly greater by axitinib treatment (2-way ANOVA). (C) Vein recanalisation expressed as a percentage of lumen area was significantly reduced (2-way ANOVA). Data represents mean ± SE. *P<0.01 Bonferroni post-hoc test. Adapted from[82].

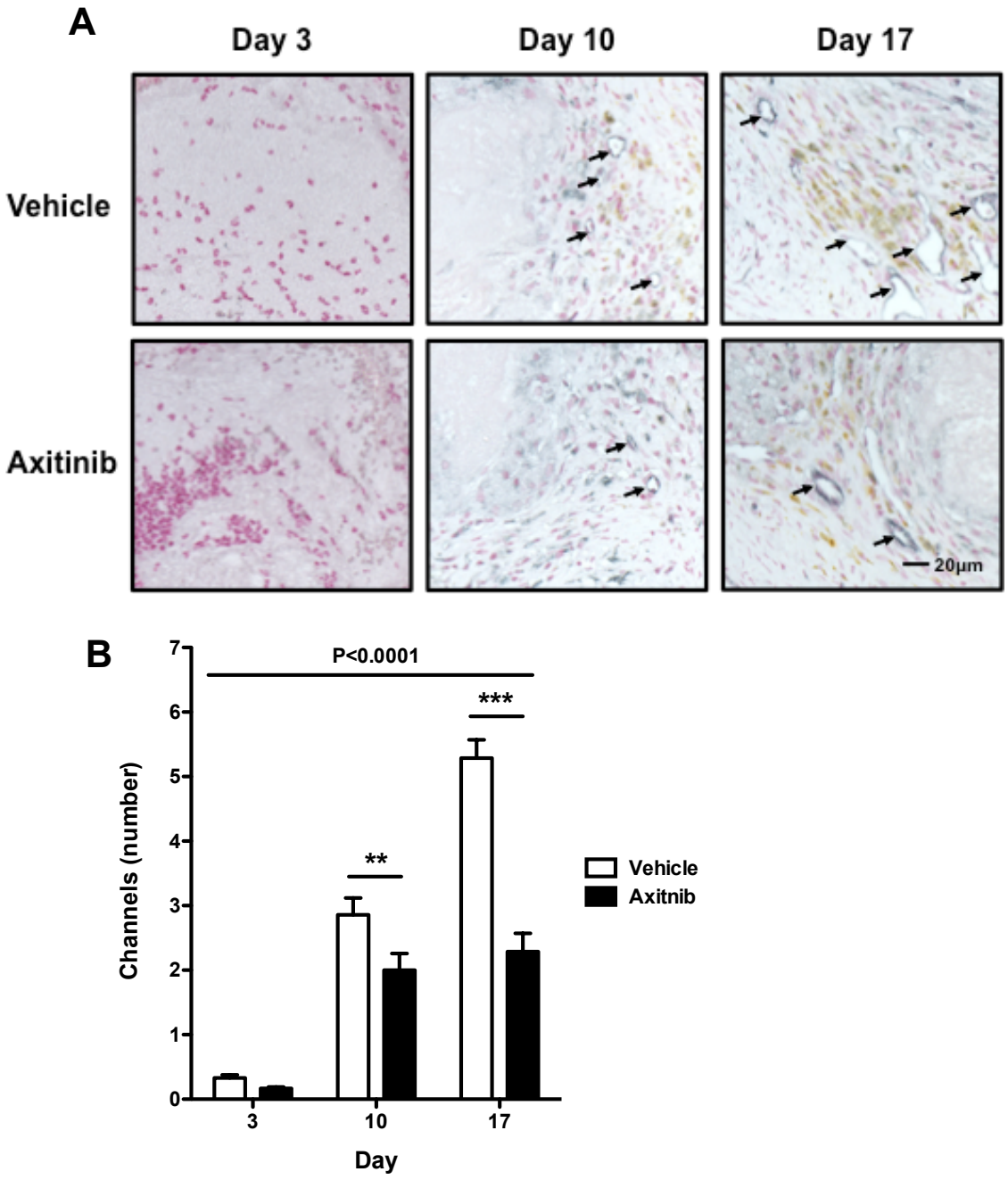

Figure 7.5 Thrombus neovascularisation after axitinib treatment

(A) Representative micrographs of CD31 positive channels at days 3, 10 and 17 post-induction treated with axitinib or vehicle control, images taken at an original magnification of x400. (B) The mean number of CD31 positive channels per level was significantly reduced after axitinib treatment (2-way ANOVA). Data represents mean ± SE, n=6-8 per group. **P<0.05, ***P<0.001 Bonferroni post-hoc test. Adapted from[82].

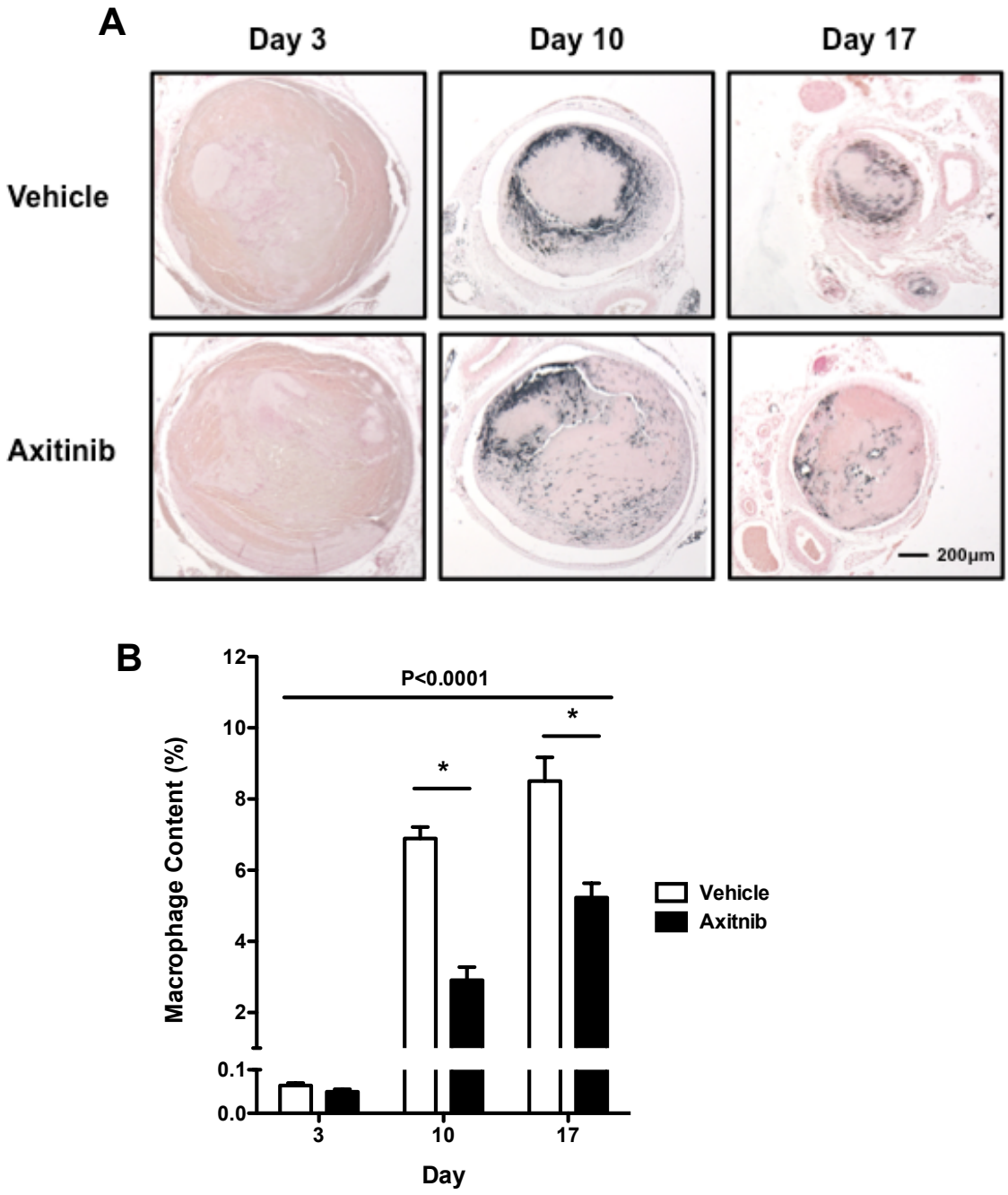

Figure 7.6 Quantification of thrombus macrophage content after axitinib treatment

(A) Representative Mac-2 stained micrographs of thrombi at days 3, 10 and 17 post-induction treated with axitinib or vehicle control. (B) Macrophage content was significantly reduced in the thrombus of mice treated with axitinib compared with control (2-way ANOVA). Data represents mean ± SE, n=6-8 per group. *P<0.001 vs. control (Bonferroni post-hoc test). Adapted from[82].

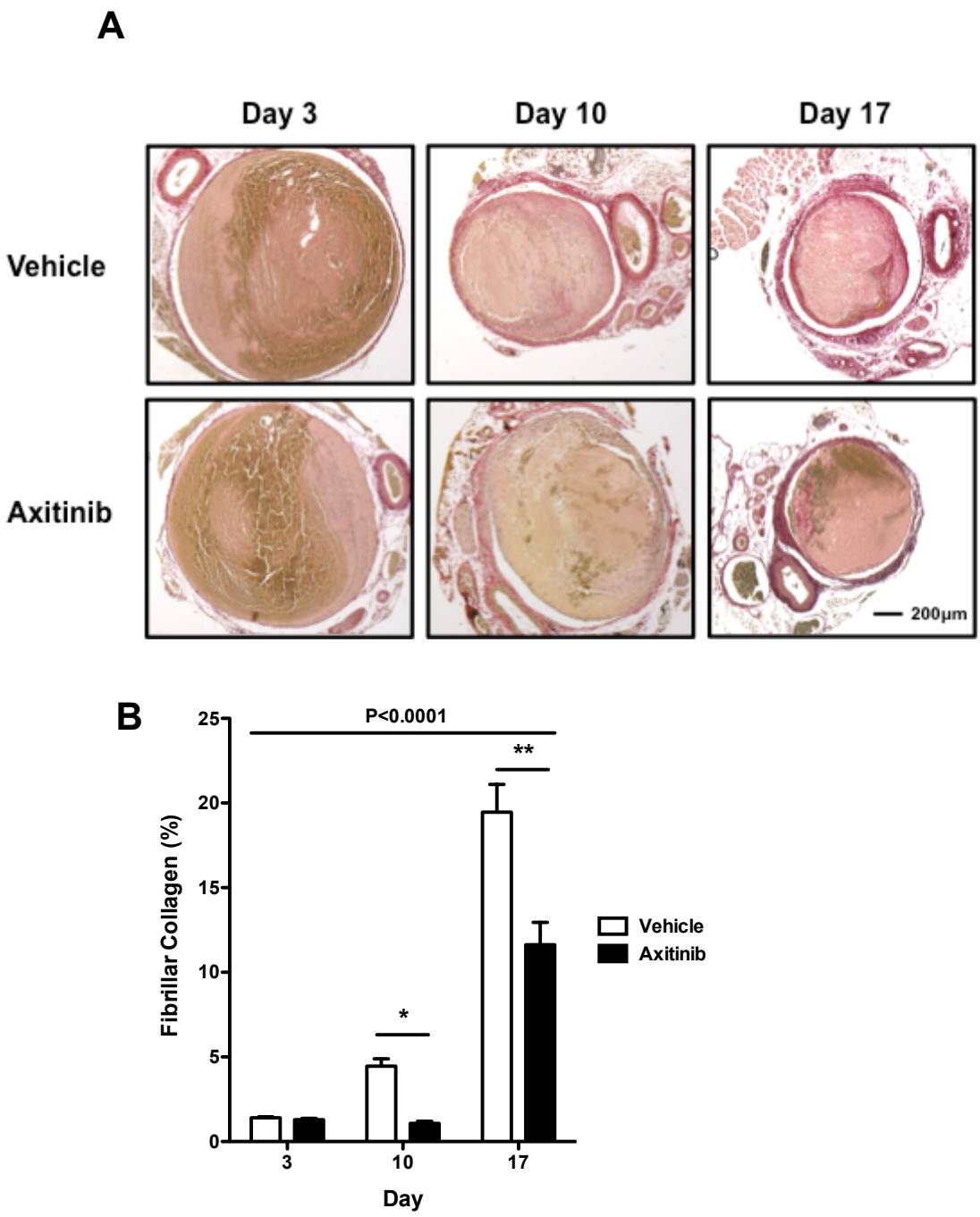

Figure 7.7 Quantification of thrombus collagen content after axitinib treatment

(A) Representative picrosirius red stained micrographs of thrombi at days 3, 10 and 17 post-induction treated with axitinib or vehicle control, images taken at an original magnification of x50. (B) Collagen content was significantly reduced in the thrombus of mice treated with axitinib compared with control (2-way ANOVA). Data represents mean ± SE, n=6-8 per group. *P<0.05 vs. control. **P<0.001 vs. control (Bonferroni post-hoc test). Adapted from[82].

7.5 Discussion

In this study, axitinib treatment significantly impaired thrombus resolution as assessed by measurements of thrombus volume and vein lumen recanalisation[82]. In axitinib treated mice thrombus burden remained high for an extended period of time. Thrombi were significantly (~60%) larger at day 10 in the axitinib treatment group when compared to vehicle control. However, at day 17 no significant difference was observed despite axitinib treated thrombi remaining ~40% larger than respective controls. The increased proportional variability at the later time-point may have contributed to the lack of significance. It is also likely that venous thrombus resolution is mediated, in parallel, by a series of VEGFR independent mechanisms such as endogenous uPA mediated thrombolysis that enables a degree of phenotypic catch up[32]. Alternatively, mice treated with axitinib for a prolonged period may have acquired a degree of drug resistance. Acquired drug resistance has been observed in cancer cell lines treated with either axitinib or sunitinib, however, this phenomenon has not been described in non-cancer derived cell lines[323].

The impairment of vein recanalisation observed after axitinib treatment is most likely a result of the increased thrombus volume in this group. Alternatively, it is possible that axitinib acts on the thrombosed vessel affecting either tone or pathological vein wall remodelling. Anti-angiogenic agents such as axitinib are thought to be vaso-active because of the high incidence of hypertension in patients treated with these drugs[324]. This is further supported by evidence that bevacizumab, targeting the same VEGF-VEGFR signalling pathway, significantly reduces endothelial-dependent vasodilatation in man[325].

To investigate whether axitinib treatment affected thrombus organisation, neovascularisation, collagen content and macrophage content were quantified. Axitinib treatment resulted in a sustained impairment in thrombus neovascularisation consistent with the role of axitinib as a potent inhibitor of tumour microvasculature development[319-321]. Sensing of VEGFA gradients by primarily VEGFR2 present on the surface of endothelial cells is critical to the formation of neovessels[306]. VEGFC is also an important promoter of angiogenesis, stimulating endothelial cell migration and proliferation in a

VEGFR2 and VEGFR3 dependent manner[326]. Inhibition of VEGFR2 and VEGFR3 signalling using monoclonal antibodies has been shown to reduce vascular network development and endothelial sprouting during embryogenesis[306, 327].

Axitinib also significantly reduce thrombus macrophage content. Macrophage accumulation is a hallmark of venous thrombus resolution[25, 328]. Inhibition of macrophage accumulation within the thrombus through deletion of the gene encoding CC chemokine receptor 2 (CCR2), or through inhibition of the CC chemokine system as a whole results in impaired thrombus resolution[43, 329]. Conversely, directly increasing macrophage numbers has been found to enhance thrombus resolution[25]. VEGFR1, present on the surface of primary human monocytes, stimulates their migration into tissues[330, 331]. Inhibition of VEGFR1 activity on macrophages by axitinib may therefore account for the reduced number of these cells accumulating in the thrombus.

The very low levels of fibrillar collagen deposition observed in untreated thrombus at day 3 post induction are consistent with previous observations which show that fibrin predominates in the early thrombus[257]. Treatment with axitinib resulted in a ~75% reduction in thrombus collagen deposition by day 10 and 50% at day 17 post-induction. There is conflicting evidence on the role of VEGF-VEGFR signalling in collagen-mediated fibrosis. Loss of VEGFA expression in myeloid cells enhances pulmonary fibrosis, suggesting that production of VEGFA in this cell type has important anti-fibrotic activity[332]. Blockade of VEGFR signalling by either sVEGFR1 transduction or pharmacological inhibition significantly reduces collagen deposition in a murine model of pulmonary fibrosis[333, 334]. In the present study the antifibrotic effects of VEGFR disruption may be secondary to impaired recruitment of collagen producing macrophages[335]. Fibroblasts are the major cellular producers of collagen, but their role in the pathogenesis of venous thrombus resolution is currently not known and is worthy of investigation.

Given that axitinib acts as a pan-VEGFR inhibitor it has not been possible to investigate the contribution of individual VEGFR isoforms to thrombus resolution. In a recent study endothelial specific deletion of VEGFR2 was found

to significantly impair thrombus resolution[54]. Measurements of thrombus volume and weight at day 1 post-induction reveal that the thrombus in VEGFR2 deficient mice was, however, more than double the size of respective littermate controls. This initial difference in thrombus size is likely to confound subsequent studies of resolution.

The observed impairment in venous thrombus resolution attributed to axitinib treatment may also have important implications for patients receiving this drug. Patients with cancer already possess an elevated risk of venous thrombosis than found in the general population[336]. There is evidence to suggest that treatment with anti-tumourigenic agents may increase the incidence of venous thrombosis further, possibly by reducing endothelial anti-thrombotic activity and increasing platelet pro-thrombotic activity[337, 338]. A meta-analysis of bevacizumab trials suggests that patients receiving this agent are at a higher risk of developing VTE[339]. However, the findings of this meta-analysis are strongly contested on the basis that the authors failed to correct for the length of time on treatment.

Whilst only a few phase III trials of axitinib have reached completion in a landmark study comparing the effect of axitinib to sorafenib in patients with metastatic renal cell carcinoma (clinicaltrials.gov, NCT00835978) a marked increase in the incidence of venous thromboembolism (VTE) was noted[317]. Even when adjusted for the time on treatment the axitinib treatment arm had a significantly higher incidence of all grade VTE (7/359) than the sorafenib arm (1/359) as assessed by chi squared test ($P<0.05$, relative-risk 1.76, 95% confidence interval 1.34 – 2.30). It is interesting to note that in this trial patients with a recent history of VTE were excluded, but since being licensed axitinib is available to these patients.

Chapter 8 General discussion and future studies

8.1 Discussion

8.1.1 Expression of PHD isoforms in the thrombus

PHD proteins serve as key molecular oxygen sensors regulating the cellular response to tissue hypoxia through the oxygen-dependent hydroxylation and of HIF1α leading to proteasomal degradation. Previous studies have demonstrated that the newly formed venous thrombus was acutely hypoxic, which lead to increased nuclear accumulation of HIF1α and expression of HIF1α target genes including *Vegfa*. During resolution oxygen tension in the thrombus increases, resulting in a loss of HIF1α nuclear accumulation presumably through the restoration of PHD enzymatic activity[57].

In the present study, quantification of PHD expression at the gene and protein levels revealed that all three isoforms (PHD1, PHD2 and PHD3) are expressed in the resolving thrombus. At the gene level different temporal patterns in expression of *Phd1*, *Phd2* and *Phd3* were observed. Expression of *Phd1* remained relatively constant across the time-course of the experiment. Hypoxia has not been found to induce expression of the *Phd1* gene[142] and expression of this gene can be down regulated by hypoxia in certain cell types[340]. The *Phd1* gene promoter lacks an HRE sequence instead possessing a HIFβ/Single Minded binding sequence[340] that represses HIF1α transcriptional activity[341]. The expression of *Phd2* and *Phd3* was found to change significantly over time in the resolving venous thrombus. At early and late time-points phd2 gene expression was elevated compared to that at mid time-points. Expression of *Phd2* has been observed in neutrophils, which predominate in the early thrombus, and macrophages, which accumulate as the thrombus resolves. PHD2 is an important regulator of monocyte/ macrophage cell function, regulating phenotypic skewing and angiogenic potential[165]. The expression of the *Phd3* gene was greatest in the acute thrombus before falling. *Phd3* gene expression is likely maximal at this time-point as hypoxia potently upregulates expression of this isoform in neutrophils[175]. Expression of *Phd3* has also been observed in a

pro-inflammatory subset of macrophages[173].

At the protein level PHD1, PHD2 and PHD3 expression was localised to the cellular component of the thrombus by immunohistochemistry. Based on morphological appearance, PHD expression was distributed amongst neutrophils and macrophages. It was interesting to note that not all cells present in thrombus at later time-points stained positively for PHDs. Differential expression of PHD3 protein has been observed in macrophages; with classically-activated macrophages expressing significantly higher levels than alternately activated cells[173]. It is unclear whether expression of PHD2 is regulated in a similar manner in macrophages. The differential expression of PHD isoforms in the thrombus could also be attributed to the presence of other cell types, such as fibroblasts.

In order to determine the cellular origin of PHD expression in the resolving venous thrombus it would be necessary to carry out further flow cytometric analyses. Flow cytometry based cell sorting is a powerful technique that allows for more detailed phenotypic analysis and isolation of specific cell populations by examining the expression of multiple cell surface markers. Cells known to be present in the resolving venous thrombus including; neutrophils, monocytes, macrophages, and endothelial cells could be isolated using appropriate panels of antibodies (Table 8.1). Once isolated RT-PCR and western blotting of individual cell populations could be used to quantify PHD, HIFα and HIFα transcriptional targets expression at the gene and protein level. This approach would provide powerful cellular data, as opposed to whole tissue, and may overcome some of the challenges, such as protein dilution, highlighted during the present study.

Table 8.1 Cell surface markers for flow cytometry

Cell type	Surface markers
Neutrophil	Ter199- NK1.1- CD3- CD9- Ly6C- CD45+ Ly6G+
Monocyte	Ter199- NK1.1- CD3- CD9- Ly6G- F480- CD45+ Ly6C+
Macrophage	Ter199- NK1.1- CD3- CD9- Ly6G- CD45+ Ly6C+ F480+
Endothelial cell	Ter199- NK1.1- CD3- CD9- Ly6G- CD45- VEGFR2+ CD31+

8.1.2 The effect of *Phd2* gene deletion on thrombus resolution

It was unclear, whether a single, specific PHD isoform was responsible for regulation of HIF1α during thrombus resolution, as all isoforms have demonstrated the capacity to hydroxylate HIF1α[272]. However, gene knockdown studies suggested that under normoxic conditions PHD2 activity, but not PHD1 or PHD3, was required for efficient degradation of HIF1α[241]. Combined with expression studies in the thrombus this highlighted PHD2 as an isoform of particular interest, leading to the investigation of thrombus resolution in *Phd2* gene specific knockouts. Somewhat surprisingly neither constitutive nor inducible all-cell *Phd2* knockouts had any detectable effect on venous thrombus resolution or organisation. In *Phd2* constitutive heterozygous knockouts this could be accounted for by the lack of significant up-regulation in HIF1α nuclear accumulation. However, in homozygous inducible *Phd2* knockouts, in which HIF1α nuclear accumulation and transcriptional activity was significantly increased, no difference in thrombus resolution or organisation was observed. The confirmation of previously reported elevations in haematocrit makes it unlikely that loss of PHD2 is compensated for by other isoforms[169]. However, from the present study of *Phd2* gene knockouts it is not possible to discount the contribution of other PHD isoforms or PHD enzyme activity as a whole.

Non-overlapping functions for individual PHD isoforms have been described and may be attributed to: the HIFα subunit selectivity, the kinetics of HIFα hydroxylation or differential expression of PHD isoforms[138, 272]. Gene specific deletion of *Phd3* results in impaired neutrophil cell survival and increased macrophage migration[41, 172], cell types important to thrombus resolution. Relatively little is known about the specific contribution of PHD1 to the cellular response to hypoxia. Initial studies have shown this enzyme, but not PHD2 or PHD3, regulates changes in cellular metabolism in response to hypoxia[144]. Although the levels of *Phd1* gene expression were invariant during thrombus resolution, this does not mean that this enzyme is redundant. Studying venous thrombus resolution in available *Phd1* and *Phd3* gene knockouts may improve understanding of the role that these specific isozymes play[144, 176]. Cooperation of PHD isoforms could similarly be investigated using a double knockout strategy as previously reported[143].

8.1.3 The effect of PHD inhibition on thrombus resolution

PHD inhibition using the iron chelating agent l-mimosine significantly increased venous thrombus resolution[57]. It is possible, however, that because of the broad activity of l-mimosine, other enzymes including the collagen-modifying prolyl-4-hydroxylases may also have been inhibited[230, 342]. After studies on the effects of l-mimosine on thrombus resolution were completed, a new class of PHD inhibitors, with improved selectivity and specificity, were developed. It was possible to secure access to two of these PHD inhibitors, AKB-4924 (Akebia Therapeutics, USA) and JNJ-42041935 (Johnson and Johnson, USA)[227, 231]. This provided the opportunity to reassess the effect of pan-PHD inhibition on venous thrombus resolution. Importantly, AKB-4924 and JNJ-420241935 have distinct modes of action with the former inhibiting PHD activity through chelation of iron at the active site [231]and the later competing with the co-factor 2-OG[227]. Use of these agents in the thrombosis model was aimed at identifying processes affected specifically by PHD inhibition.

Treatment with either AKB-4924 or JNJ-42041935 did not alter thrombus resolution, despite significantly increasing HIF1α nuclear accumulation and haematocrit respectively. Both AKB-4924 and JNJ-42041935 had similar effects on thrombus organisation, with significantly increased thrombus neovascularisation, but no effect on macrophage and collagen content. This would suggest that pan-PHD inhibition selectively affects the formation of neovascular channels, a process that is akin to angiogenesis and occurs during natural resolution[52]. A number of studies have demonstrated that inhibition of PHD enzymes strongly upregulates angiogenesis *in vivo*[194, 196, 197]. PHD2 and PHD3 have also been found to cooperate in the induction of angiogenesis[343]. Cooperation of multiple PHD enzymes could explain why neovascularisation was increased in mice treated with PHD inhibitors but not in *Phd2* gene knockouts.

Having demonstrated that PHD inhibition resulted in a significant upregulation in neovascular channel formation further investigation of this pro-angiogenic effect would be advantageous. *In vitro* tubule formation assay could demonstrate whether PHD inhibition in endothelial cells directly affects angiogenesis. Alternatively, tubule formation could be observed in co-cultures of endothelial

cells and macrophages pretreated with PHD inhibitors as this cell type is known to aid co-ordination of neovessel formation[344]. The effect of PHD inhibition on endothelial proliferation could also be investigated using a bromodeoxyuridine-based assay given that HIF1α is known to regulate apoptosis and proliferation of this cell type[345].

It is possible that deletion of *Phd2* and PHD inhibition may affect skewing of macrophage populations present in the resolving venous thrombus[164]. Recent flow cytometric analysis of macrophage populations in the resolving venous thrombus has revealed accumulation of distinct subsets of macrophages, based on expression of MHC class II[346]. The effect of PHD inhibition on skewing of thrombus resident macrophages could be investigated using a similar flow cytometric technique. Alternatively in vitro analysis of monocyte skewing in response to macrophage colony-stimulating factor (MCSF) and granulocyte macrophage colony stimulating factor (GMCSF) could be studied in conjunction with PHD inhibition or *Phd2* gene deletion.

Increased haematocrit has been implicated as a causative factor in the formation of venous thrombi[347]. In the present study both PHD inhibition with JNJ-42041935 and inducible homozygous *Phd2* gene deletion resulted in increase haematocrit levels measured at 14 days post thrombus induction that were consistent with previous reports[143, 169, 227]. It is possible that elevated haematocrit could affect thrombus propagation after initial induction. Thrombus volumes in inducible *Phd2* knockouts were not significantly different from that of littermate controls when measured at days 1 and 7 post-induction suggesting that propagation was unaffected by increased haematocrit. It is unclear whether increased haematocrit affected thrombus resolution after treatment with JNJ-42041935. It is also possible that haematocrit was not induced until thrombus resolution was well under way; further intermediate measurements of haematocrit would be needed to measure the rapidity of onset.

Both *Phd2* gene deletion and PHD inhibition have been associated with increasing circulating levels of VEGF[145, 196], although others have failed to reconfirm these initial findings[269]. In the present study VEGF plasma concentrations determined by ELISA remained unchanged after inducible *phd2*

homozygous deletion and inhibition of PHD with either AKB-4924 or JNJ-42041935. It is possible that PHD mediated changes in VEGF levels were masked by surgical injury and the presence of a thrombotic insult both of which contribute to elevated levels of circulating VEGF [48].

8.1.4 Contribution of VEGFR signalling to thrombus resolution

Previous studies have demonstrated the potential benefit of enhanced VEGFA expression, and presumably downstream VEGFR signalling activity, in accelerating venous thrombus resolution. The requirement of endogenous VEGFR signalling for venous thrombus resolution was much less clear. Gradients of VEGFA are required for organised migration of endothelial cells[348] whereas absolute levels of VEGFA regulate proliferation and the propensity to form tubules[349, 350]. VEGFA is also an important regulator of monocyte chemotaxis and transmigration[330, 351]. Given that numerous cell types present in the thrombus are regulated by VEGFR signalling activity, it was reasonable to suggest that this pathway might be required for venous thrombus resolution. To investigate the requirement of endogenous VEGFR signalling thrombus resolution was studied in mice treated with the small molecule pan-VEGFR inhibitor axitinib.

Treatment with axitinib significantly delayed venous thrombus resolution, with thrombus volume approximately 60% greater than respective vehicle control at 10 days post induction. Thrombus resolution at day 17 whilst still impaired by axitinib treatment (~40%) was not significantly different. The temporal impairment in venous thrombus resolution suggests that VEGFR signalling is required for the early phases of thrombus resolution (day 3-10) but is perhaps dispensable at later time-points (day 10-17). Reduced thrombus recanalisation after axitinib treatment may occur primarily as a consequence of reduced thrombus resolution. However, vessel tone may also be affected by axitinib treatment as VEGFA induced activation of eNOS results in generation of the potent vasoldilator NO[352]. The reduction in neovascular channel formation is most likely dependent on endothelial VEGFR2 activation[306] as endothelial specific deletion of *Vegfr2* has been found to impair neovascular channel formation in the resolving venous thrombus[54]. Loss of VEGFR1 activity could

account for the impaired recruitment of monocytes/macrophages to the thrombus after axitinib treatment as this receptor is the major VEGFR expressed on monocytes and is required for VEGFA and PlGF mediated monocyte migration[330, 331]. However, a subpopulation of monocytes, present in the thrombus, also express VEGFR2, and the contribution of this receptor to cellular function cannot be discounted[56].

Loss of HIF1α stabilisation and hence activity has also been studied in venous thrombus resolution. Treatment of thrombosed animals with 2-methoxy estradiol (2ME) a microtubule depolimerising agent that prevents the accumulation of HIF1α in the cell nucleus, was found to significantly impair thrombus resolution. It is interesting to note that the scale of impairment in thrombus resolution after 2ME treatment was similar to that found with axitinib. The similarity between the phenotypes following treatment with axitinib or 2ME suggests that endogenous VEGFR activity could account for the majority of HIF1α biological activity in venous thrombus resolution. Consistent with this concept endothelium-specific *hif1a* gene deletion strongly inhibits angiogenesis in a VEGFA-VEGFR2 dependent manner[279]. However, VEGFA independent processes have been attributed to HIF1α, specifically recruitment of myeloid cells to an inflammatory nidus[74].

8.1.5 Imaging of thrombus resolution

The cost and availability of imaging techniques currently used to assess thrombus resolution represents a significant barrier to researchers. Application of new quantitative imaging modalities that enable longitudinal analysis of thrombi could be of considerable benefit. These techniques would not only provide powerful, paired data but also reduce the number of animals required for experimentation.

High frequency ultrasonography (HFUS) is one such technique that is both affordable and readily available for imaging of small animals. Its applicability in imaging of IVC thrombi has already been demonstrated[281], however, the two-dimensional data so far reported using HFUS provides only qualitative, rather than quantitative, measures of thrombus burden. In the present study, use of a 3D-HFUS imaging platform allowed quantitative measurements of thrombus

volume to be made. 3D-HFUS also allowed for segmentation of thrombus from surrounding tissue, however, the relatively low contrast of the early thrombus presented a technical challenge. The lack of contrast could be overcome by the use of a highly echogenic blood pool contrast agent[283]. Targeted contrast agents for both fibrin and platelets have been developed and these would enable imaging at the molecular and cellular level[353, 354]. Another limitation of 3D-HFUS was the low resolution achieved in the z-axis (110μm); this was necessitated by the relatively small memory buffer of the ultrasound machine combined with a need to scan the entire thrombosed segment of the IVC.

Contrast-enhanced microCT has been reported as an effective method of delineating the thrombus from surrounding tissue[254]. In the present study a method of contrast-enhanced microCT was developed using a low volume bolus injection of the blood pool contrast agent, Aurovist, which facilitated longitudinal imaging of thrombus resolution. Computational image segmentation and volumetric rendering allowed measurement of thrombus volume. Inter- and intra-observer analysis showed this technique to be robust and reliable. Thrombus volumes derived from microCT compared favourably to histological measurements which is the most common method of assessing thrombus size. A notable bias was, however, apparent when comparing the two measures, with histological measurements consistently smaller than those by microCT. This could be explained by shrinkage of histological samples during post-fixation processing and tissue sectioning[298].

In the present study contrast enhanced microCT scans were reconstructed at a resolution of 65μm, however, with the microCT datasets obtained it would have been possible to reconstruct images with a voxel size of 22μm, almost tripling the resolution. Initial attempts at analysis of high-resolution reconstructions proved challenging as files sizes were too large to be handled by the analysis software based on current computing capacity. Improved computing power or more restricted ROI placement would likely overcome this technical limitation and may improve fidelity of thrombus segmentation. It is also possible that high-resolution reconstructions could be used to identify neovascular channels in the organised thrombus and this would merit further investigation.

Comparing these two modalities for imaging of the venous thrombus contrast-enhanced microCT was considered technically superior to 3D-HFUS. Contrast-enhanced microCT provided higher spatial resolution compared to 3D-HFUS, with potential for further such increases. Contrast between thrombus and surrounding tissue was not only greater by contrast-enhanced microCT than 3D-HFUS but also more consistent across the thrombus aiding segmentation. Whereas a single scan was sufficient to image the thrombus by microCT, 3D-HFUS often required multiple scans with adjustments to the positioning of the probe so as to capture the entire length of the thrombosed IVC while avoiding wound tissue that impaired ultrasound conductance.

8.2 Limitations of the study

8.2.1 PHD quantification

It was not possible to measure the expression of PHD proteins in the resolving thrombus in a quantitative manner. Attempts to quantify PHD protein expression in the thrombus by western blotting proved unsuccessful as expression was below the detectable limits of this methodology. It may be possible to improve the sensitivity of the western blot technique using substrates with increased sensitivity or signal amplification techniques such as those afforded by biotinyl tyramide conjugates. However, at best, densitometric analysis of western blots can only be considered semi-quantitative. ELISA would provide the most sensitive and quantitative measure of thrombus PHD protein expression, but there are presently no robust commercially available kits for these proteins. Although IHC analysis of protein expression in the thrombus provides a highly amplified signal and hence very high sensitivity, this technique is not quantitative in its current state. Recent developments in this area, suggest that it may be possible to use IHC to quantify proteins in situ[355]. The main drawback to this procedure is the amount of time involved and the accuracy/reproducibility of the addition of the assay components.

8.2.2 HIF1α quantification

Another potential limitation of the western blot technique used in the present study was observed when quantifying HIF1α in the nuclear extracts of kidney samples, where there was marked variability in expression of the nuclear loading control Histone H3. The use of frozen tissue samples could have reduced the reproducibility of nuclear protein extraction, in the future it would be advantageous to extract protein from fresh tissue samples. Extensive normalisation of samples was required to reveal significant differences in nuclear HIF1α accumulation. Had a commercially available HIF1α ELISA been used these differences would not have been detected and may have skewed quantification.

Alternatively, it is possible that the lysis protocol used in the present study may have resulted in inefficient recovery of HIF1α protein. Considerable success has been achieved using stronger solubilising agents, in particular 8M urea, to generate total cell lysates. This method, whilst quantifying total HIF1α levels, is sensitive to changes in HIF1α stability as a result of gene knockdown of *Phd2*[356]. To further strengthen the observed phenotype of increased HIF1α stabilisation after both *Phd2* gene deletion and pan-PHD inhibition it would be useful to quantify downstream transcriptional targets of HIF1α in kidney tissue lysates. Quantification of targets such as Glut1, VEGFA and carbonic anhydrase IX (CAIX) by western blotting would provide a measurement of HIF1α transcriptional activity[357].

8.2.3 PHD IHC specificity

In this study, the specificity of IHC antibodies to the target PHD isoforms was assessed by comparison of patterns of staining in the kidney to those previously reported. It may have been possible to validate IHC staining of PHD2 in sections of thrombus from inducible homozygous phd2 knockouts. These knockout mice should have no PHD2 and therefore no staining. Any staining seen would therefore be non-specific. This would be expanded to both PHD1 and PHD3 immunohistochemistry. However, it is important to note that conditional knockout may not result in complete loss of protein as some protein may be retained in the cell following deletion of the gene.

8.2.4 Factor inhibiting HIF

When investigating the regulation of HIF1α stabilisation by PHD deletion and inhibition, the expression of a related enzyme factor inhibiting HIF (FIH) was not investigated. FIH has been proposed to regulate HIF transcriptional activity through hydroxylation of an asparagine residue present in the C-terminal activation domain of HIFα subunits[181]. The activity of FIH is of particular relevance to studies of PHD inhibition as it is also a 2-OG dependent dioxygenase that requires iron as a co-factor[181]. The increased haematocrit observed in homozygous inducible *phd2* knockouts would suggest that FIH activity does not prevent transcription of HIF target genes. Commonly used PHD inhibitors such as DMOG and DFO are therefore effective antagonists of FIH enzyme activity[181, 358]. However, while JNJ-420241935 is a potent inhibitor of PHD2 activity, it is a much weaker inhibitor of FIH[227]. Little is known with regards to the selectivity of the agent AKB-4924 in the inhibition of FIH.

8.2.5 VEGFR inhibition

In mice treated with the VEGFR antagonist, axitinib, measurements of drug efficacy were not made. While widely reported as a potent and selective inhibitor of VEGFR the finding of this study would be further strengthened by direct measurements of VEGFR inhibition in the thrombus. VEGFR activation results in downstream phosphorylation of multiple kinases, in particular Akt and ERK, and this could also be quantified by conventional western blotting techniques or more sensitively by PhosFlow cytometry[359].

8.2.6 Imaging

All imaging technologies involve a degree of subjective interpretation and therefore must be validated not only against a standard technique (e.g. histology) but also by a number of assessors. In this study this was carried out for the microCT analysis, but not for HFUS measurements. The lack of contrast, made HFUS analysis more subjective compared with contrast-enhanced MicroCT and potentially less reliable. More detailed validation of this technique for assessment of venous thrombus resolution is therefore required.

8.3 Future work

An important finding of this study was the requirement of endogenous VEGFR signalling as a significant stimulus for venous thrombus resolution. While a detailed phenotypic characterisation of thrombus resolution after axitinib treatment was completed, further investigation into the cellular effects of VEGFR inhibition are warranted. Axitinib treatment may prevent monocyte/macrophage chemotaxis along VEGF gradients and thus explain reduced accumulation of macrophages into the thrombus. A Boyden chamber based assay could be used to determine the effect of axitinib treatment on monocyte and macrophage migration towards VEGF and PlGF[330, 331]. Short interfering RNA mediated gene knockdown of VEGFR1 and VEGFR2 in monocytes and macrophages could be used to determine whether an individual receptor drives VEGFR dependent cell migration.

Axitinib is a broad acting VEGFR inhibitor preventing activation of all three receptors and did, therefore, not allow the contribution of individual VEGFRs to be assessed. The importance of VEGFR family members could be further investigated using conditional gene specific *Vegfr1*, *Vegfr2* and *Vegfr3* knockouts[360-362]. Given the observed reductions in neovascular channel formation and macrophage recruitment after axitinib treatment it would be of particular interest to study specific gene deletion in these cell types. Studies of endothelial-specific *Vegfr2* gene deletion have highlighted difficulties using this approach as deletion prior to induction of thrombosis can affect formation[54]. Alternatively, selective small molecule inhibitors of *Vegfr2*, such as vandetanib or apatanib, could be investigated in the context of venous thrombus resolution[363, 364]. The major benefit of pharmacological inhibition when studying thrombus resolution is that treatment can be initiated after induction, preventing confounding effects on thrombus formation.

Increased HIF1α stability, as a result of either PHD inhibition of *Phd2* gene deletion was not sufficient to accelerate thrombus resolution. This does not, however, discount the requirement of endogenous HIF1α transcriptional activity for natural thrombus resolution. Endogenous thrombus HIF1α transcriptional activity could be studied using ODD-luciferase reporter mice[225]. Whilst ODD-

luciferase is most commonly used to determine the efficacy of HIF1α stabilising interventions it has also been used to study physiological HIF1α transcriptional activity in small subcutaneous tumours and may therefore be sufficiently sensitive to detect activity in the thrombus[365]. The contribution of endogenous HIF1α to thrombus resolution could be studied using tissue-specific gene knockouts[366]. Loss of HIF1α transcriptional activity is likely to lead to impaired myeloid cell recruitment and angiogenesis as has been previously reported[74]. Recently, expression of HIF2α has been localised to the venous thrombus, accumulating as resolution progresses[261]. Thrombus resolution in tissue-specific *Hif2a* gene knockouts may also be worthy of investigation[111].

8.4 Conclusion

The data from this study shows that PHD isoforms are expressed in the resolving venous thrombus at both the gene and protein level. Specific loss of *Phd2* expression, whether by constitutive heterozygous or inducible homozygous deletion, was not found to affect any measure of venous thrombus resolution. Pharmacological inhibition of PHD enzyme activity selectively enhanced the formation of neovascular channels in the thrombus, without affecting thrombus resolution or other markers of organisation. This finding challenges the notion that the formation of neovascular channels in the thrombus contributes significantly to resolution. Pharmacological blockade of VEGFR signalling, in which a number of HIF1α transcriptional targets are involved, significantly impaired thrombus resolution and organisation. It is not clear whether inflammatory cell accumulation or angiogenesis drives VEGFR mediated resolution.

Appendix A

A1. Murine thrombus qPCR

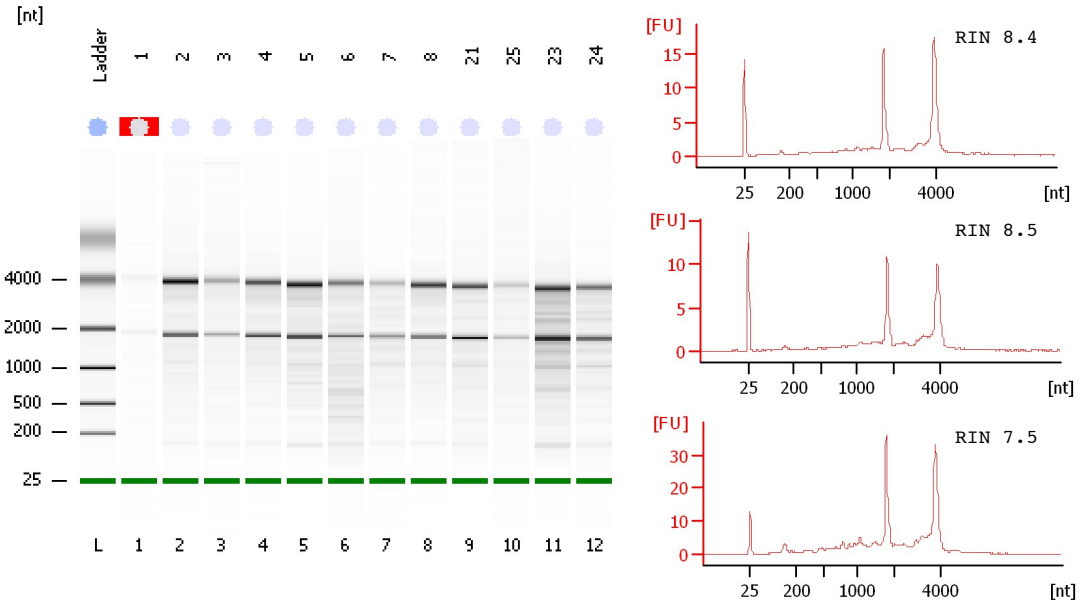

Figure A1 Analysis of RNA integrity

RNA integrity was assessed using a Nano 6100 microfluidic chip. (A) Representative electrophoretic traces of RNA samples. (B) Graphical representation of traces from which algorithm based RNA integrity values (RIN) values were calculated.

A2. Murine thrombus micro-array method

i) Target Preparation

Total RNA (400ng) was concentrated to 3µl using a Gyrovap vacuum (Howe and co, UK)system at 2,800g (20ºC). RNA obtained from HeLa cells (1mg/ml) was used as a positive control. Samples were spiked with synthetic polyadenylated RNA (Poly A RNA) transcripts of *B. subtilis* genes to monitor amplification and labeling.

ii) cDNA Synthesis

First strand master mix (FSM, 4µl 1st strand buffer, 1µl transcriptase) was added to each RNA sample containing T7-Oligo(dT) primer mix and incubated for 1hr at 25ºC, 1hr at 42ºC and 2mins at 4ºC. Second strand master mix (SSM, 12.5µl 2nd strand buffer, 32.5µl RNase-free water, 5µl polymerase) was added to each sample and incubated for 1hr at 16ºC, 10mins at 65ºC and 2mins at 4ºC. IVT master mix, 24µl IVT buffer, 6µl IVT enzyme) was added to each sample followed by incubation for 16hr at 40ºC. cRNA was purified using nucleic acid binding beads (10µl beads, 50µl buffer, Applied Biosystems, USA) and 60µl of isopropanol were added to each sample followed by a 2min incubation. Nucleic acid binding beads were isolated using a magnetic stand, washed twice using 100µl of nucleic acid wash solution and cRNA eluted with 40µl of preheated elution buffer (55ºC). cRNA was quantified by nanodrop as described in Chapter 3.3.3 and 455ng/µl of template added to 2µl of random primers and incubated for 5mins at 70ºC, 5mins at 25ºC and 2mins at 4ºC. Second-cycle master mix (8µl 2nd-cycle buffer, 8µl 2nd-cycle enzyme) was added to each sample and incubated for 10mins at 25ºC, 90mins at 42ºC, 10mins at 70ºC and 2mins at 4ºC.

iii) Purification of Second-cycle cDNA

Samples were treated with RNase H (2µl) and incubated for 45min at 37ºC, 5min at 95ºC and 2min at 4ºC to hydrolyse cRNA template. cDNA binding mix Nucleic acid binding beads were prepared as previously described, diluted with 18µl of nuclease-free water and 120µl ethanol and incubated with samples for 2mins on a plate shaker. Nucleic acid binding beads were isolated using a magnetic stand, washed twice using 100µl of nucleic acid wash solution and

cDNA eluted with 40µl of preheated elution buffer (55ºC). Quantification of cRNA and cDNA was conducted as described in Chapter 3.3.3.

iv) GeneChip Array Hybridisation

cDNA was fragmented by the addition of 8µl of 5x fragmentation buffer, diluted to a total of 40µl with RNase-free water and incubated for 1hr at 37ºC, 2mins at 93ºC and 2mins at 4ºC. Fragmented cDNA (45µl) was added to 12µl 5x TdT buffer, 2µl TdT and 1µl DNA labelling reagent (5mM) and incubated for 1hr at 37ºC, 10mins at 70ºC and 2mins at 4ºC for labelling of samples. A hybridisation cocktail was prepared using the following reagents; 5µl control oligonucleotide B2 (3nM), 3µl herring sperm DNA (10mg/ml), 3µl bovine serum albumin (50mg/ml), 150µl 2x hybridisation buffer, 30µl DMSO, RNase-free water up to 300µl and 15µl 20x eukaryotic hybridisation controls (bioB, bioC, bioD, Cre). Hybridisation cocktail was added to each cDNA sample (15µg) and heated for 5mins at 99ºC. Probe arrays were equilibrated to room temperatre and filled with 80µl hybridisation cocktail and hybridised for 16h at 45ºC with rotation (60rpm). Probe arrays were washed using an automated washing and staining protocol on a fluidics work-station. Arrays were scanned on an Affymetrix 3000 GeneChip scanner (Affymetrix, USA).

v) Probe Array Analysis

The scanned probe array image for each sample was inspected for artifacts and a grid placed over the image to demarcate each probe cell. Hybridisation of an oligonucleotide B2 control was used for correct alignment of the grid. Spot signal intensity was analysed using Expression Console software (Affymetrix, USA). The robust multi-array analysis (RMA) algorithm was used to normalise data, correct for background fluorescence, perform probe summarisation and scale the intensity values obtained (Tukey's Bioweight average).

A3. qPCR Amplification efficiency

Gene	Slope	Efficiency (%)
Actb	-3.49	93
Gak	-3.28	102
Phd1	-3.30	101
Phd2	-3.34	99
Phd3	-3.18	106
Hif2a	-3.43	96
Hif3a	-3.57	91

A4. Representative amplification curves

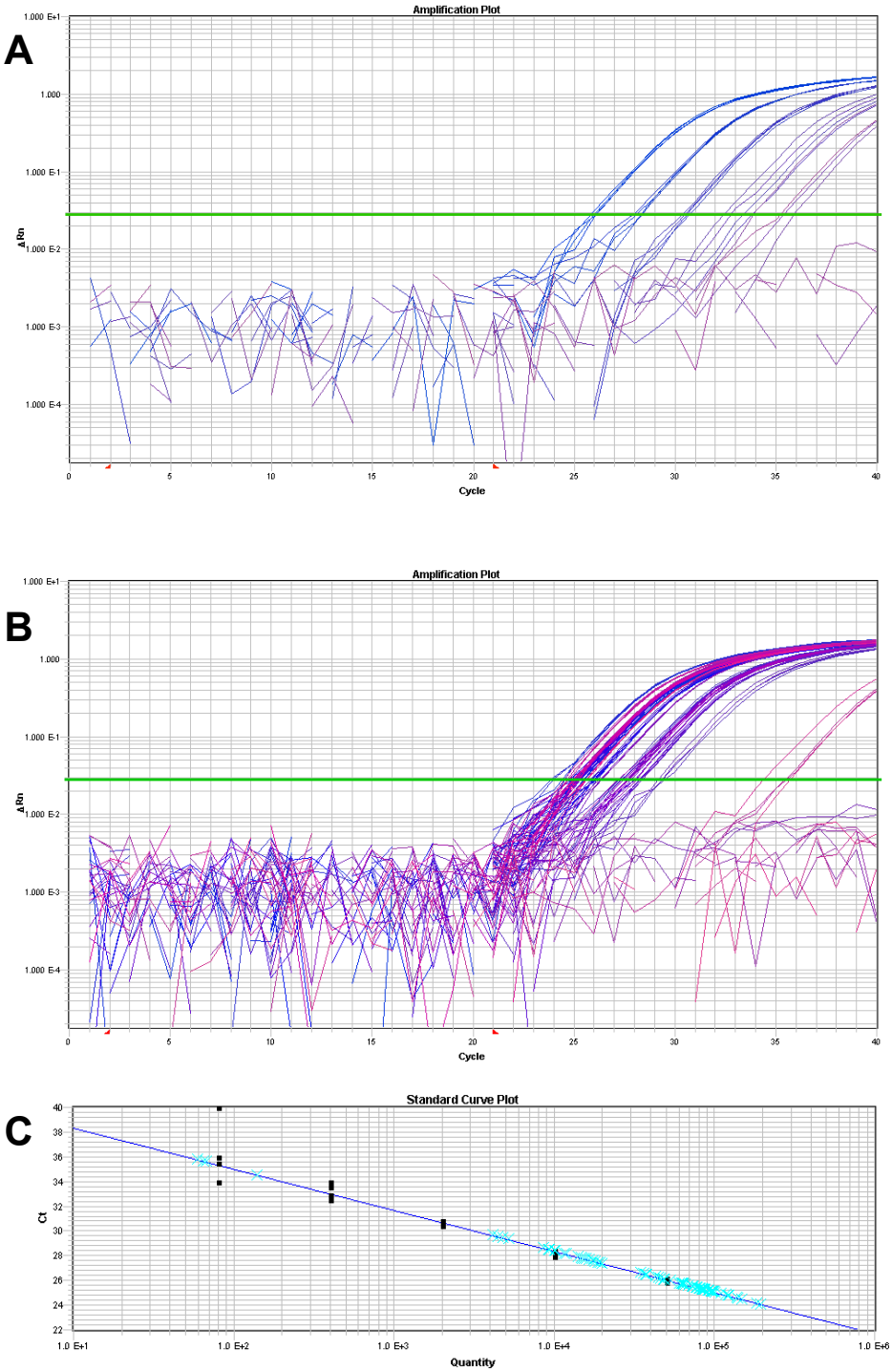

Figure A2 Representative qPCR amplification curves

Amplification curves of (A) *Phd2* standard serial dilutions and (B) unknowns with fluorescence plotted as $\log_{10}$ against cycle number, sample amplification is recorded when the plot passes through the threshold (green line). (C) *Phd2* serial dilutions are used to plot a standard curve of amplification cycle number against standard concentration (■) plotted as $\log_{10}$ from which unknowns can be interpolated (x).

A5. Representative whole-membrane western blots

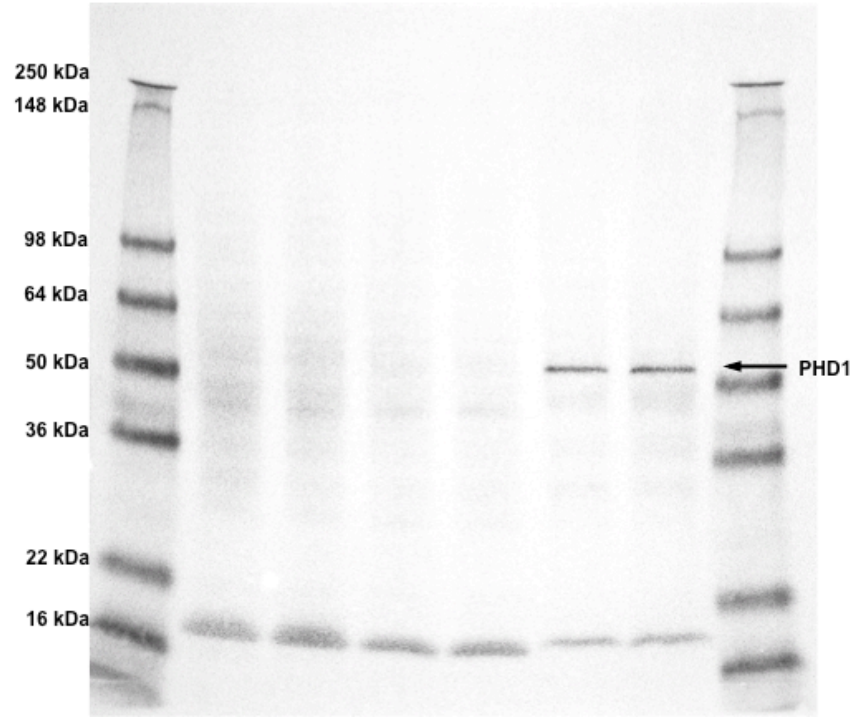

Figure A3 Representative PHD1 western blot

A single discrete band for PHD1 with a molecular weight of 51kDa (predicted 44kDa) was observed. An additional band with a molecular weight of 18kDa was also observed mainly in the cytoplasm.

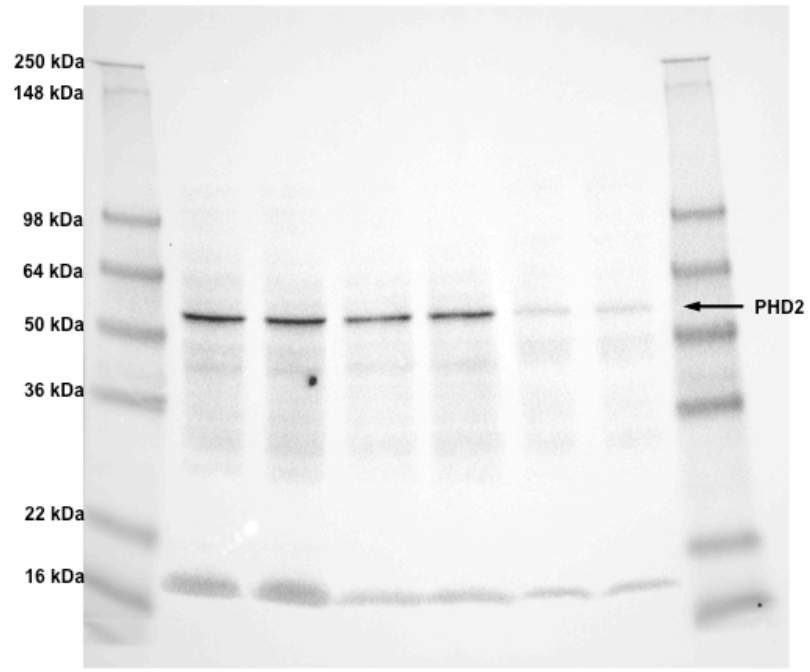

Figure A4 Representative PHD2 western blot

A single discrete band for PHD2 with a molecular weight of 53kDa (predicted 46kDa) was observed. Some diffuse background staining was also apparent.

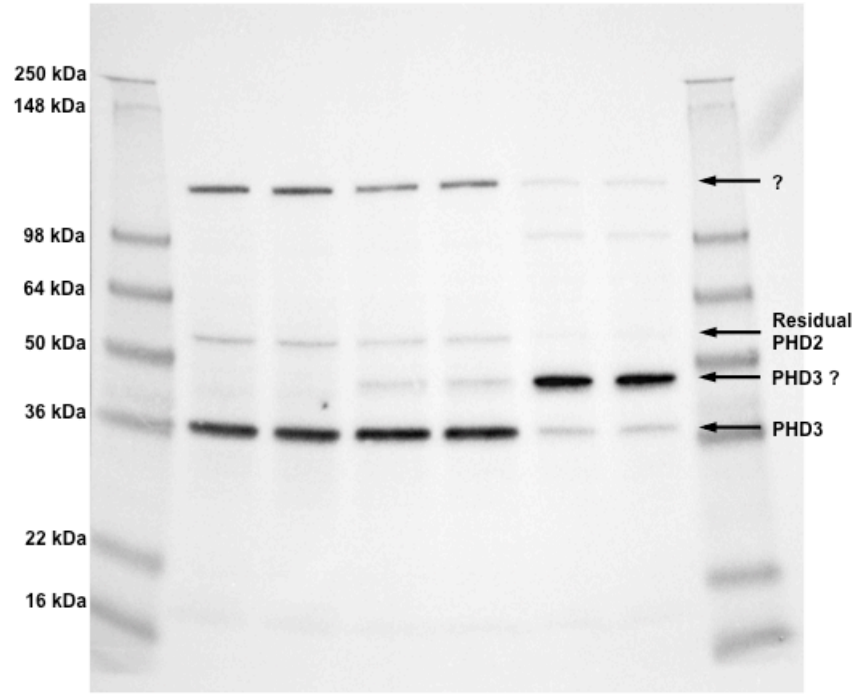

Figure A5 Representative PHD3 western blot

Multiple bands were present in PHD3 immunoblots possibly resulting from the polyclonal antibody used. The PHD3 band was selected on the basis of the observed molecular weight of 36kDa (predicted 27kDa). Of interest a band of equal intensity was present in nuclear extracts (lane 6 and 7) with an observed molecular weight of 47kDa.

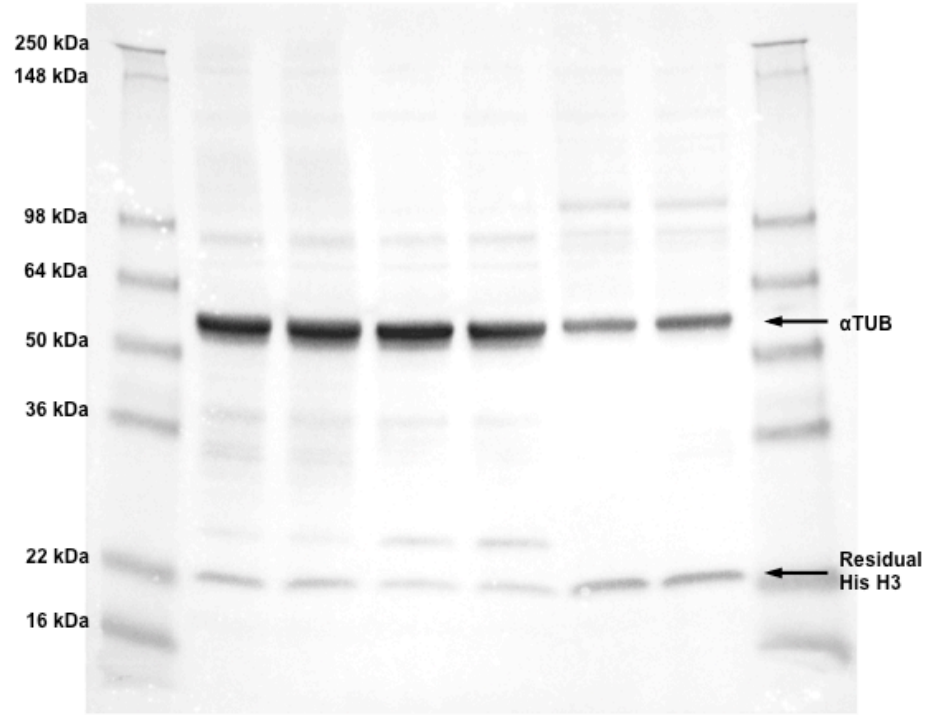

Figure A6 Representative αTubulin western blot

An intense αTubulin (αTUB) band with a molecular weight of 55kDa (predicted 50kDa) was observed. Residual Histone H3 (His H3) staining was apparent.

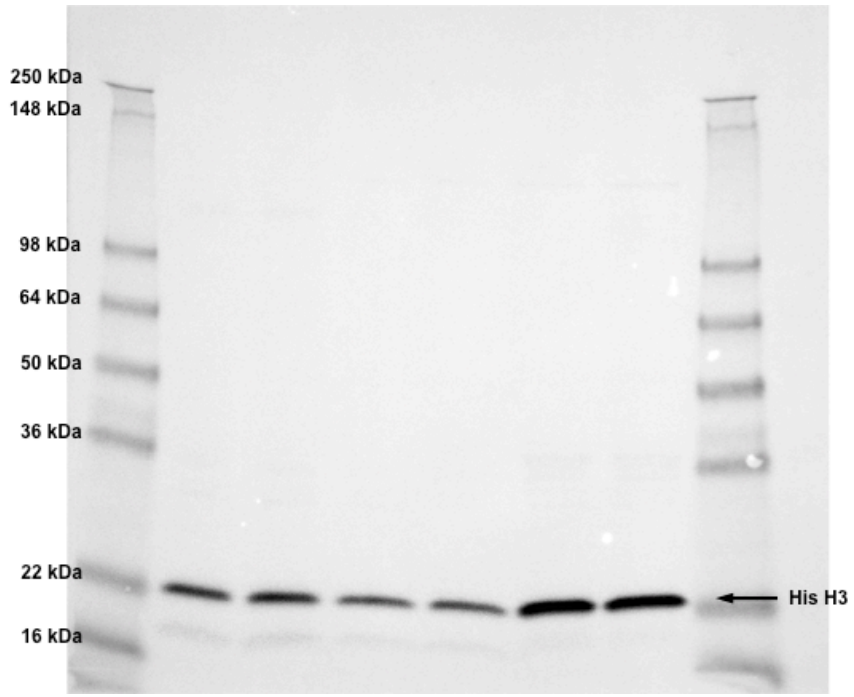

Figure A7 Representative Histone H3 western blot

A discrete Histone H3 (His H3) band with a molecular weight of 22kDa (predicted 17kDa) was observed.

A6. Nuclear extraction in fresh or snap-frozen tissue samples

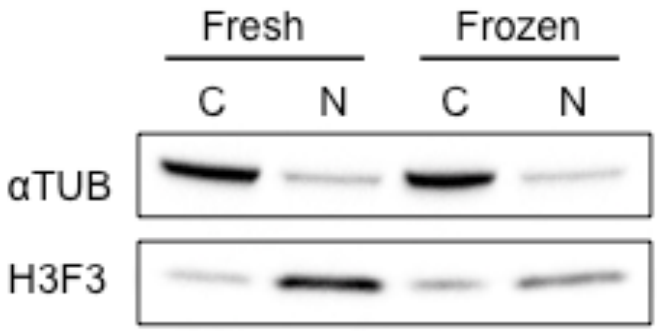

Figure A8 Cellular fractionation of fresh and snap frozen murine kidney
Kidney samples will be used to assess the effects of *Phd2* gene deletion and pharmacological PHD2 inhibition. Do to the constraints of harvesting a large number of samples tissue must be snap frozen. The effect of snap freezing of tissues on cellular fractionation is unclear. To assess this freshly isolated and snap frozen kidney samples were subject to nuclear cytoplasmic extraction. Fractionation was assessed by immunoblotting for the cytoplasmic (C) marker αtubulin and the nuclear (N) marker Histone H3. αTubulin was well segregated to the cytoplasm in both fresh and frozen kidney samples while Histone H3 was enriched in the nuclear fraction of both samples, although to a greater extent in fresh kidney samples.

A7 Thrombus PHD2 immunohistochemistry

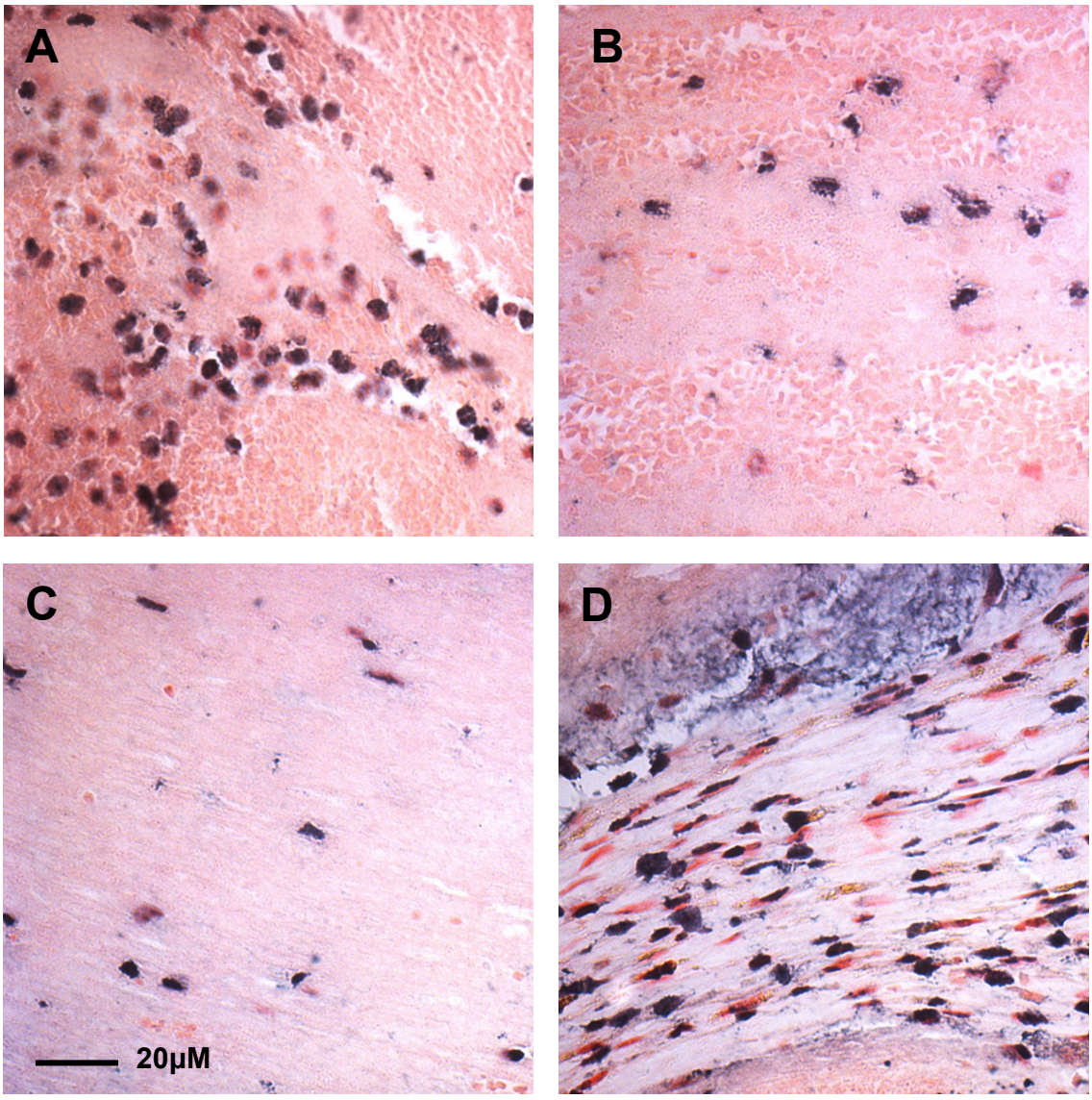

Figure A9 Representative PHD2 immunohistochemistry in the resolving venous thrombus

Localisation of PHD2 in the resolving venous thrombus at (A) Day 1 (B) Day 3 (C) Day 7 and (D) Day 14 post-induction.

Appendix B

B1. Thrombus resolution in constitutive *Phd2* gene knockouts

Supplementary Data File

The accompanying Excel spreadsheet provides data at the level of individual replicates for histological measurements of thrombus volume, vein lumen recanalisation, thrombus neovascularisation, thrombus macrophage content and thrombus collagen content.

Filename:

Grover_PHD2_cKO_dataset.xlsx

Appendix C

C1. Segmentation of 3D HFUS

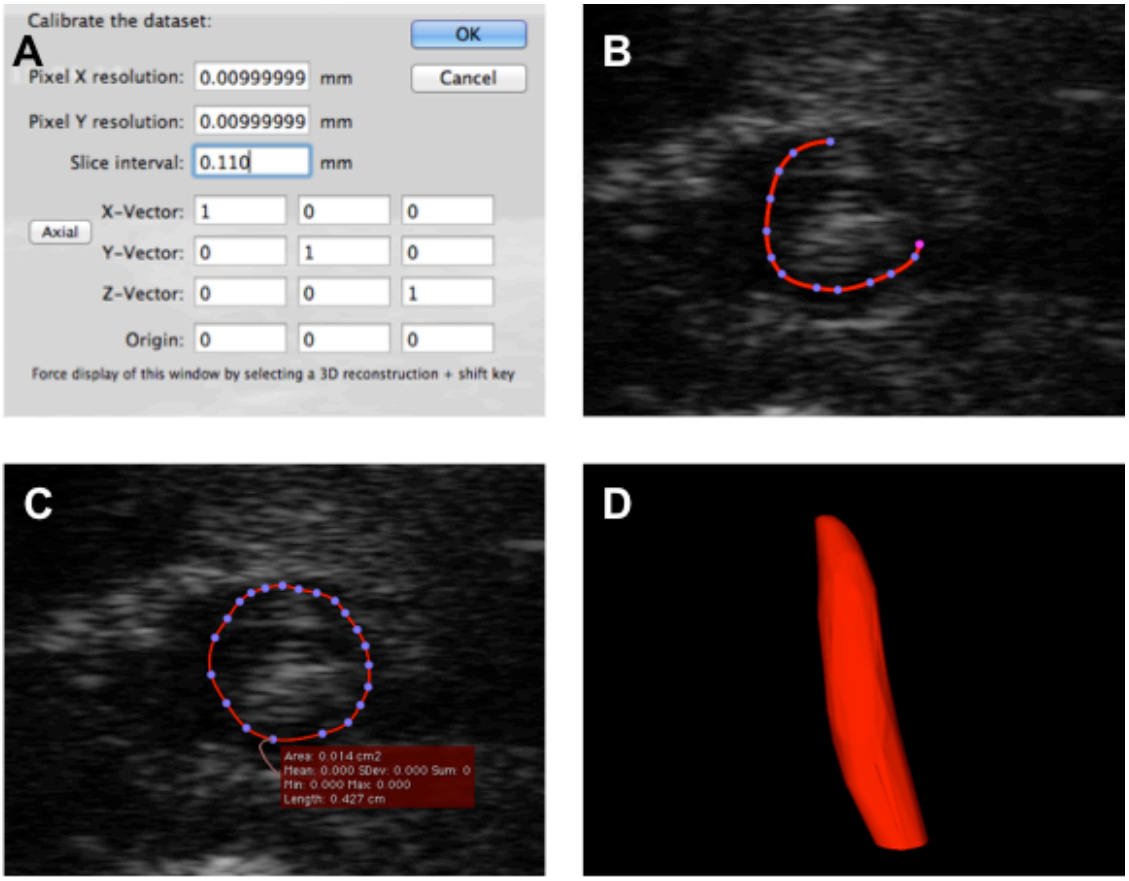

Figure A9 Segmentation of 3D-HFUS scans

(A) Scans analysed in Osirix software are first calibrated in the z axis so that slices are spaced 110μm apart. (B) Using a closed polygon tool the thrombosed segment of the vein is demarked. (C) This segmentation is repeated across the length of the thrombus providing individual measurements of thrombus cross sectional area. (D) This data was used to generated 3D volume renders of the thrombus from which measurements of thrombus volume can be made.

C2. Visualisation of the thrombus by 3D-HFUS

Supplementary Video File:

The accompanying video file is of a day 1 thrombus imaged by 3D-HFUS. The video starts at the iliac confluence moving proximally along the IVC towards the renal veins and the site of stenosis. The thrombus presents as a hyperechoic structure in the IVC lumen the identification of which is aided using the aorta.

Filename:

3DHFUS_Thrombus_Day1.mp4

C3. Thrombus resolution in inducible *Phd2* gene knockouts

Supplementary Data File:

The accompanying Excel spreadsheet provides data at the level of individual replicates for 3D-HFUS measurements of thrombus volume and rate of thrombus resolution. Histological measurements of thrombus volume, vein lumen recanalisation, thrombus neovascularisation, thrombus macrophage content and thrombus collagen content are also provided.

Filename:

Grover_PHD2_iKO_dataset.xlsx

Appendix D

D1. Segmentation of contrast-enhanced microCT scans

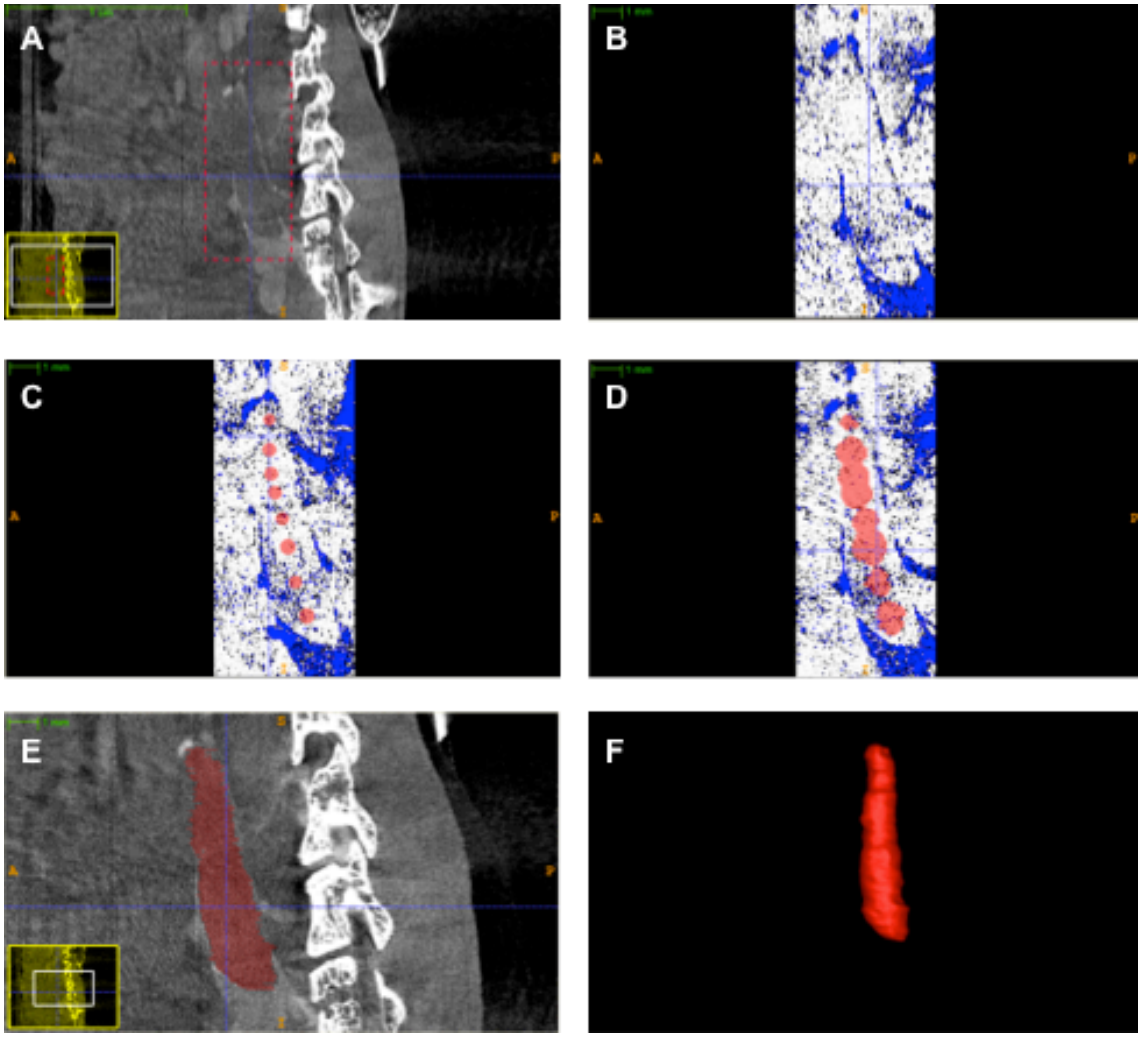

Figure A10 Segmentation of a day 1 thrombus imaged by contrast enhanced microCT

Using ITK-SNAP software (A) a small region of interest was selected (red box). (B) The scan was processed to restrict “bubble propagation” to regions of hypo-intensity (white area). (C) Small “bubbles” were placed along the length of the thrombus and (D) propagated until the thrombosed region was filled. (E) The segmentation was manually refined until all of the thrombus was selected before (F) a 3D volume render was generated from which a measurement of thrombus volume was taken.

D2. Visualisation of thrombus by contrast-enhanced microCT

Supplementary Video File:

The accompanying video file is of a day 1 thrombus imaged by contrast-enhanced microCT. The video starts at the level of the renal veins moving distally towards the iliac confluence. The thrombus presents as a hypoperfused structure in the IVC lumen intermittently generating a “halo” with surrounding contrast agent.

Filename:

MicroCT_Thrombus_Day1.mp4

D3. Thrombus resolution after PHD inhibitor treatment

Supplementary Data File:

The accompanying Excel spreadsheet provides data at the level of individual replicates for contrast enhanced microCT measurements of thrombus volume and rate of thrombus resolution after treatment with AKB-4924. Histological measurements of thrombus volume, vein lumen recanalisation, thrombus neovascularisation, thrombus macrophage content and thrombus collagen content are also provided for AKB-4924 and JNJ-42041935 treatment.

Filename:

Grover_PHD_inhibitor_dataset.xlsx

Appendix E

E1. Thrombus resolution after treatment with the VEGFR inhibitor axitnib

Supplementary Data File

The accompanying Excel spreadsheet provides data at the level of individual replicates for histological measurements of thrombus volume, vein lumen recanalisation, thrombus neovascularisation, thrombus macrophage content and thrombus collagen content.

Filename:

Grover_axitinib_dataset.xlsx

References

1. Fowkes FJ, Price JF, Fowkes FG. Incidence of diagnosed deep vein thrombosis in the general population: Systematic review. *Eur J Vasc Endovasc Surg*. 2003;25:1-5
2. Heit JA. The epidemiology of venous thromboembolism in the community. *Arterioscler Thromb Vasc Biol*. 2008;28:370-372
3. Hunt BJ. Awareness and politics of venous thromboembolism in the united kingdom. *Arterioscler Thromb Vasc Biol*. 2008;28:398-399
4. Anderson FA, Jr., Wheeler HB, Goldberg RJ, Hosmer DW, Patwardhan NA, Jovanovic B, Forcier A, Dalen JE. A population-based perspective of the hospital incidence and case-fatality rates of deep vein thrombosis and pulmonary embolism. The worcester dvt study. *Arch Intern Med*. 1991;151:933-938
5. Silverstein MD, Heit JA, Mohr DN, Petterson TM, O'Fallon WM, Melton LJ, 3rd. Trends in the incidence of deep vein thrombosis and pulmonary embolism: A 25-year population-based study. *Arch Intern Med*. 1998;158:585-593
6. Kearon C. Natural history of venous thromboembolism. *Circulation*. 2003;107:I22-I30
7. Prandoni P, Lensing AW, Cogo A, Cuppini S, Villalta S, Carta M, Cattelan AM, Polistena P, Bernardi E, Prins MH. The long-term clinical course of acute deep venous thrombosis. *Ann Intern Med*. 1996;125:1-7
8. Franzeck UK, Schalch I, Bollinger A. On the relationship between changes in the deep veins evaluated by duplex sonography and the postthrombotic syndrome 12 years after deep vein thrombosis. *Thromb Haemost*. 1997;77:1109-1112
9. Kahn SR, Ginsberg JS. The post-thrombotic syndrome: Current knowledge, controversies, and directions for future research. *Blood Rev*. 2002;16:155-165
10. Committee TH. The prevention of venous thromboembolism in hospitalised patients. *House of Commons Health Committee*. 2005;2:11-12
11. Hirsh J, Fuster V, Ansell J, Halperin JL. American heart association/american college of cardiology foundation guide to warfarin therapy. *Circulation*. 2003;107:1692-1711
12. Sevitt S. Natural history of postoperative deep-vein thrombosis. *Lancet*. 1969;2:378-379
13. Virchow RR. *Cellular pathology*. London: Churchill; 1856.
14. McLachlin AD, McLachlin JA, Jory TA, Rawling EG. Venous stasis in the lower extremities. *Ann Surg*. 1960;152:678-685
15. Spyropoulos AC, Anderson FA, Jr., Fitzgerald G, Decousus H, Pini M, Chong BH, Zotz RB, Bergmann JF, Tapson V, Froehlich JB, Monreal M, Merli GJ, Pavanello R, Turpie AG, Nakamura M, Piovella F, Kakkar AK, Spencer FA. Predictive and associative models to identify hospitalized medical patients at risk for venous thromboembolism. *Chest*. 2011
16. Hamer JD, Malone PC, Silver IA. The po2 in venous valve pockets: Its possible bearing on thrombogenesis. *Br J Surg*. 1981;68:166-170
17. Ogawa S, Gerlach H, Esposito C, Pasagian-Macaulay A, Brett J, Stern D. Hypoxia modulates the barrier and coagulant function of cultured bovine endothelium. Increased monolayer permeability and induction of procoagulant properties. *J Clin Invest*. 1990;85:1090-1098

18. Radomski MW, Palmer RM, Moncada S. Endogenous nitric oxide inhibits human platelet adhesion to vascular endothelium. *Lancet*. 1987;2:1057-1058
19. Esmon CT. Thrombomodulin as a model of molecular mechanisms that modulate protease specificity and function at the vessel surface. *Faseb J*. 1995;9:946-955
20. Dahlback B, Carlsson M, Svensson PJ. Familial thrombophilia due to a previously unrecognized mechanism characterized by poor anticoagulant response to activated protein c: Prediction of a cofactor to activated protein c. *P Natl Acad Sci USA*. 1993;90:1004-1008
21. Zoller B, Svensson PJ, He X, Dahlback B. Identification of the same factor v gene mutation in 47 out of 50 thrombosis-prone families with inherited resistance to activated protein c. *J Clin Invest*. 1994;94:2521-2524
22. Schwarz HP, Fischer M, Hopmeier P, Batard MA, Griffin JH. Plasma protein s deficiency in familial thrombotic disease. *Blood*. 1984;64:1297-1300
23. Koster T, Rosendaal FR, de Ronde H, Briet E, Vandenbroucke JP, Bertina RM. Venous thrombosis due to poor anticoagulant response to activated protein c: Leiden thrombophilia study. *Lancet*. 1993;342:1503-1506
24. Anderson FA, Jr., Spencer FA. Risk factors for venous thromboembolism. *Circulation*. 2003;107:I9-16
25. Saha P, Humphries J, Modarai B, Mattock K, Waltham M, Evans CE, Ahmad A, Patel AS, Premaratne S, Lyons OT, Smith A. Leukocytes and the natural history of deep vein thrombosis: Current concepts and future directions. *Arterioscler Thromb Vasc Biol*. 2011;31:506-512
26. Meissner MH, Manzo RA, Bergelin RO, Markel A, Strandness DE, Jr. Deep venous insufficiency: The relationship between lysis and subsequent reflux. *J Vasc Surg*. 1993;18:596-605; discussion 606-598
27. Meissner MH, Caps MT, Zierler BK, Polissar N, Bergelin RO, Manzo RA, Strandness DE, Jr. Determinants of chronic venous disease after acute deep venous thrombosis. *J Vasc Surg*. 1998;28:826-833
28. Undas A, Ariens RA. Fibrin clot structure and function: A role in the pathophysiology of arterial and venous thromboembolic diseases. *Arterioscler Thromb Vasc Biol*. 2011;31:e88-99
29. Wiman B, Collen D. Molecular mechanism of physiological fibrinolysis. *Nature*. 1978;272:549-550
30. Hoylaerts M, Rijken DC, Lijnen HR, Collen D. Kinetics of the activation of plasminogen by human tissue plasminogen activator. Role of fibrin. *J Biol Chem*. 1982;257:2912-2919
31. Bugge TH, Flick MJ, Danton MJ, Daugherty CC, Romer J, Dano K, Carmeliet P, Collen D, Degen JL. Urokinase-type plasminogen activator is effective in fibrin clearance in the absence of its receptor or tissue-type plasminogen activator. *P Natl Acad Sci USA*. 1996;93:5899-5904
32. Singh I, Burnand KG, Collins M, Luttun A, Collen D, Boelhouwer B, Smith A. Failure of thrombus to resolve in urokinase-type plasminogen activator gene-knockout mice: Rescue by normal bone marrow-derived cells. *Circulation*. 2003;107:869-875
33. Siefert SA, Chabasse C, Mukhopadhyay S, Hoofnagle MH, Strickland DK, Sarkar R, Antalis TM. Enhanced venous thrombus resolution in plasminogen activator inhibitor type-2 deficient mice. *J Thromb Haemost*.

2014
34. Visse R, Nagase H. Matrix metalloproteinases and tissue inhibitors of metalloproteinases: Structure, function, and biochemistry. *Circ Res*. 2003;92:827-839
35. Nosaka M, Ishida Y, Kimura A, Kondo T. Immunohistochemical detection of mmp-2 and mmp-9 in a stasis-induced deep vein thrombosis model and its application to thrombus age estimation. *Int J Legal Med*. 2010;124:439-444
36. Deatrick KB, Eliason JL, Lynch EM, Moore AJ, Dewyer NA, Varma MR, Pearce CG, Upchurch GR, Wakefield TW, Henke PK. Vein wall remodeling after deep vein thrombosis involves matrix metalloproteinases and late fibrosis in a mouse model. *J Vasc Surg*. 2005;42:140-148
37. Sood V, Luke CE, Deatrick KB, Baldwin J, Miller EM, Elfline M, Upchurch GR, Jr., Wakefield TW, Henke PK. Urokinase plasminogen activator independent early experimental thrombus resolution: Mmp2 as an alternative mechanism. *Thromb Haemost*. 2010;104:1174-1183
38. Deatrick KB, Luke CE, Elfline MA, Sood V, Baldwin J, Upchurch GR, Jr., Jaffer FA, Wakefield TW, Henke PK. The effect of matrix metalloproteinase 2 and matrix metalloproteinase 2/9 deletion in experimental post-thrombotic vein wall remodeling. *J Vasc Surg*. 2013;58:1375-1384 e1372
39. Varma MR, Varga AJ, Knipp BS, Sukheepod P, Upchurch GR, Kunkel SL, Wakefield TW, Henke PK. Neutropenia impairs venous thrombosis resolution in the rat. *J Vasc Surg*. 2003;38:1090-1098
40. Plesner T, Ploug M, Ellis V, Ronne E, Hoyer-Hansen G, Wittrup M, Pedersen TL, Tscherning T, Dano K, Hansen NE. The receptor for urokinase-type plasminogen activator and urokinase is translocated from two distinct intracellular compartments to the plasma membrane on stimulation of human neutrophils. *Blood*. 1994;83:808-815
41. Moir E, Booth NA, Bennett B, Robbie LA. Polymorphonuclear leucocytes mediate endogenous thrombus lysis via a u-pa-dependent mechanism. *Br J Haematol*. 2001;113:72-80
42. Henke PK, Varga A, De S, Deatrick CB, Eliason J, Arenberg DA, Sukheepod P, Thanaporn P, Kunkel SL, Upchurch GR, Wakefield TW. Deep vein thrombosis resolution is modulated by monocyte cxcr2-mediated activity in a mouse model. *Arterioscler Thromb Vasc Biol*. 2004;24:1130-1137
43. Henke PK, Pearce CG, Moaveni DM, Moore AJ, Lynch EM, Longo C, Varma M, Dewyer NA, Deatrick KB, Upchurch GR, Wakefield TW, Hogaboam C, Kunkel SL. Targeted deletion of ccr2 impairs deep vein thombosis resolution in a mouse model. *J Immunol*. 2006;177:3388-3397
44. Humphries J, McGuinness CL, Smith A, Waltham M, Poston R, Burnand KG. Monocyte chemotactic protein-1 (mcp-1) accelerates the organization and resolution of venous thrombi. *J Vasc Surg*. 1999;30:894-899
45. Tsou CL, Peters W, Si Y, Slaymaker S, Aslanian AM, Weisberg SP, Mack M, Charo IF. Critical roles for ccr2 and mcp-3 in monocyte mobilization from bone marrow and recruitment to inflammatory sites. *J Clin Invest*. 2007;117:902-909
46. Han KH, Tangirala RK, Green SR, Quehenberger O. Chemokine receptor ccr2 expression and monocyte chemoattractant protein-1-

mediated chemotaxis in human monocytes. A regulatory role for plasma ldl. *Arterioscler Thromb Vasc Biol*. 1998;18:1983-1991
47. Gerszten RE, Garcia-Zepeda EA, Lim YC, Yoshida M, Ding HA, Gimbrone MA, Jr., Luster AD, Luscinskas FW, Rosenzweig A. Mcp-1 and il-8 trigger firm adhesion of monocytes to vascular endothelium under flow conditions. *Nature*. 1999;398:718-723
48. Waltham M, Burnand KG, Collins M, Smith A. Vascular endothelial growth factor and basic fibroblast growth factor are found in resolving venous thrombi. *J Vasc Surg*. 2000;32:988-996
49. Waltham M, Burnand KG, Collins M, McGuinness CL, Singh I, Smith A. Vascular endothelial growth factor enhances venous thrombus recanalisation and organisation. *Thromb Haemost*. 2003;89:169-176
50. Waltham M, Burnand K, Fenske C, Modarai B, Humphries J, Smith A. Vascular endothelial growth factor naked DNA gene transfer enhances thrombus recanalization and resolution. *J Vasc Surg*. 2005;42:1183-1189
51. Modarai B, Humphries J, Burnand KG, Gossage JA, Waltham M, Wadoodi A, Kanaganayagam GS, Afuwape A, Paleolog E, Smith A. Adenovirus-mediated vegf gene therapy enhances venous thrombus recanalization and resolution. *Arterioscler Thromb Vasc Biol*. 2008;28:1753-1759
52. Modarai B, Burnand KG, Humphries J, Waltham M, Smith A. The role of neovascularisation in the resolution of venous thrombus. *Thromb Haemost*. 2005;93:801-809
53. Hoeben A, Landuyt B, Highley MS, Wildiers H, Van Oosterom AT, De Bruijn EA. Vascular endothelial growth factor and angiogenesis. *Pharmacol Rev*. 2004;56:549-580
54. Alias S, Redwan B, Panzenbock A, Winter MP, Schubert U, Voswinckel R, Frey MK, Jakowitsch J, Alimohammadi A, Hobohm L, Mangold A, Bergmeister H, Sibilia M, Wagner EF, Mayer E, Klepetko W, Holzenbein TJ, Preissner KT, Lang IM. Defective angiogenesis delays thrombus resolution: A potential pathogenetic mechanism underlying chronic thromboembolic pulmonary hypertension. *Arterioscler Thromb Vasc Biol*. 2014;34:810-819
55. Lewis CE, De Palma M, Naldini L. Tie2-expressing monocytes and tumor angiogenesis: Regulation by hypoxia and angiopoietin-2. *Cancer Res*. 2007;67:8429-8432
56. Modarai B, Burnand KG, Sawyer B, Smith A. Endothelial progenitor cells are recruited into resolving venous thrombi. *Circulation*. 2005;111:2645-2653
57. Evans CE, Humphries J, Mattock K, Waltham M, Wadoodi A, Saha P, Modarai B, Maxwell PH, Smith A. Hypoxia and upregulation of hypoxia-inducible factor 1{alpha} stimulate venous thrombus recanalization. *Arterioscler Thromb Vasc Biol*. 2010;30:2443-2451
58. Varma MR, Moaveni DM, Dewyer NA, Varga AJ, Deatrick KB, Kunkel SL, Upchurch GR, Jr., Wakefield TW, Henke PK. Deep vein thrombosis resolution is not accelerated with increased neovascularization. *J Vasc Surg*. 2004;40:536-542
59. Wilson WR, Hay MP. Targeting hypoxia in cancer therapy. *Nat Rev Cancer*. 2011;11:393-410
60. Whelan RS, Kaplinskiy V, Kitsis RN. Cell death in the pathogenesis of heart disease: Mechanisms and significance. *Annu Rev Physiol*. 2010;72:19-44

61. Bovill EG, van der Vliet A. Venous valvular stasis-associated hypoxia and thrombosis: What is the link? *Annu Rev Physiol*. 2011;73:527-545
62. Semenza GL. Hif-1 mediates metabolic responses to intratumoral hypoxia and oncogenic mutations. *J Clin Invest*. 2013;123:3664-3671
63. Loor G, Schumacker PT. Role of hypoxia-inducible factor in cell survival during myocardial ischemia-reperfusion. *Cell Death Diff*. 2008;15:686-690
64. Pugh CW, Ratcliffe PJ. Regulation of angiogenesis by hypoxia: Role of the hif system. *Nat Med*. 2003;9:677-684
65. Murdoch C, Giannoudis A, Lewis CE. Mechanisms regulating the recruitment of macrophages into hypoxic areas of tumors and other ischemic tissues. *Blood*. 2004;104:2224-2234
66. Majmundar AJ, Wong WJ, Simon MC. Hypoxia-inducible factors and the response to hypoxic stress. *Molecular cell*. 2010;40:294-309
67. Huang LE, Gu J, Schau M, Bunn HF. Regulation of hypoxia-inducible factor 1alpha is mediated by an o2-dependent degradation domain via the ubiquitin-proteasome pathway. *Proc Natl Acad Sci U S A*. 1998;95:7987-7992
68. Masson N, Willam C, Maxwell PH, Pugh CW, Ratcliffe PJ. Independent function of two destruction domains in hypoxia-inducible factor-alpha chains activated by prolyl hydroxylation. *EMBO J*. 2001;20:5197-5206
69. Wang GL, Jiang BH, Rue EA, Semenza GL. Hypoxia-inducible factor 1 is a basic-helix-loop-helix-pas heterodimer regulated by cellular o2 tension. *P Natl Acad Sci USA*. 1995;92:5510-5514
70. Huang LE, Gu J, Schau M, Bunn HF. Regulation of hypoxia-inducible factor 1alpha is mediated by an o2-dependent degradation domain via the ubiquitin-proteasome pathway. *P Natl Acad Sci USA*. 1998;95:7987-7992
71. Stroka DM, Burkhardt T, Desbaillets I, Wenger RH, Neil DA, Bauer C, Gassmann M, Candinas D. Hif-1 is expressed in normoxic tissue and displays an organ-specific regulation under systemic hypoxia. *Faseb J*. 2001;15:2445-2453
72. Walczak-Drzewiecka A, Ratajewski M, Wagner W, Dastych J. Hif-1alpha is up-regulated in activated mast cells by a process that involves calcineurin and nfat. *J Immunol*. 2008;181:1665-1672
73. Kotch LE, Iyer NV, Laughner E, Semenza GL. Defective vascularization of hif-1alpha-null embryos is not associated with vegf deficiency but with mesenchymal cell death. *Dev Biol*. 1999;209:254-267
74. Cramer T, Yamanishi Y, Clausen BE, Forster I, Pawlinski R, Mackman N, Haase VH, Jaenisch R, Corr M, Nizet V, Firestein GS, Gerber HP, Ferrara N, Johnson RS. Hif-1alpha is essential for myeloid cell-mediated inflammation. *Cell*. 2003;112:645-657
75. Peyssonnaux C, Datta V, Cramer T, Doedens A, Theodorakis EA, Gallo RL, Hurtado-Ziola N, Nizet V, Johnson RS. Hif-1alpha expression regulates the bactericidal capacity of phagocytes. *J Clin Invest*. 2005;115:1806-1815
76. Imanirad P, Solaimani Kartalaei P, Crisan M, Vink C, Yamada-Inagawa T, de Pater E, Kurek D, Kaimakis P, van der Linden R, Speck N, Dzierzak E. Hif1alpha is a regulator of hematopoietic progenitor and stem cell development in hypoxic sites of the mouse embryo. *Stem Cell Res*. 2014;12:24-35
77. Takubo K, Goda N, Yamada W, Iriuchishima H, Ikeda E, Kubota Y,

Shima H, Johnson RS, Hirao A, Suematsu M, Suda T. Regulation of the hif-1alpha level is essential for hematopoietic stem cells. *Cell Stem Cell*. 2010;7:391-402
78. Sarkar K, Rey S, Zhang X, Sebastian R, Marti GP, Fox-Talbot K, Cardona AV, Du J, Tan YS, Liu L, Lay F, Gonzalez FJ, Harmon JW, Semenza GL. Tie2-dependent knockout of hif-1 impairs burn wound vascularization and homing of bone marrow-derived angiogenic cells. *Cardiovasc Res*. 2012;93:162-169
79. Evans CE. A role for hypoxia in venous thrombus resolution. *King's College London*. 2010;PhD
80. D'Amato RJ, Lin CM, Flynn E, Folkman J, Hamel E. 2-methoxyestradiol, an endogenous mammalian metabolite, inhibits tubulin polymerization by interacting at the colchicine site. *Proc Natl Acad Sci U S A*. 1994;91:3964-3968
81. Ricker JL, Chen Z, Yang XP, Pribluda VS, Swartz GM, Van Waes C. 2-methoxyestradiol inhibits hypoxia-inducible factor 1alpha, tumor growth, and angiogenesis and augments paclitaxel efficacy in head and neck squamous cell carcinoma. *Clin Cancer Res*. 2004;10:8665-8673
82. Evans CE, Grover SP, Humphries J, Saha P, Patel AP, Patel AS, Lyons OT, Modarai B, Smith A. Antiangiogenic therapy inhibits venous thrombus resolution. *Arterioscler Thromb Vasc Biol*. 2014;34:565-570
83. Staller P, Sulitkova J, Lisztwan J, Moch H, Oakeley EJ, Krek W. Chemokine receptor cxcr4 downregulated by von hippel-lindau tumour suppressor pvhl. *Nature*. 2003;425:307-311
84. Sanchez-Elsner T, Botella LM, Velasco B, Langa C, Bernabeu C. Endoglin expression is regulated by transcriptional cooperation between the hypoxia and transforming growth factor-beta pathways. *J Biol Chem*. 2002;277:43799-43808
85. Schito L, Rey S, Tafani M, Zhang H, Wong CC, Russo A, Russo MA, Semenza GL. Hypoxia-inducible factor 1-dependent expression of platelet-derived growth factor b promotes lymphatic metastasis of hypoxic breast cancer cells. *P Natl Acad Sci USA*. 2012;109:E2707-2716
86. Feldser D, Agani F, Iyer NV, Pak B, Ferreira G, Semenza GL. Reciprocal positive regulation of hypoxia-inducible factor 1alpha and insulin-like growth factor 2. *Cancer Res*. 1999;59:3915-3918
87. Liu Y, Cox SR, Morita T, Kourembanas S. Hypoxia regulates vascular endothelial growth factor gene expression in endothelial cells. Identification of a 5' enhancer. *Circ Res*. 1995;77:638-643
88. Gerber HP, Condorelli F, Park J, Ferrara N. Differential transcriptional regulation of the two vascular endothelial growth factor receptor genes. Flt-1, but not flk-1/kdr, is up-regulated by hypoxia. *J Biol Chem*. 1997;272:23659-23667
89. Takahashi Y, Takahashi S, Shiga Y, Yoshimi T, Miura T. Hypoxic induction of prolyl 4-hydroxylase alpha (i) in cultured cells. *J Biol Chem*. 2000;275:14139-14146
90. Erler JT, Bennewith KL, Nicolau M, Dornhofer N, Kong C, Le QT, Chi JT, Jeffrey SS, Giaccia AJ. Lysyl oxidase is essential for hypoxia-induced metastasis. *Nature*. 2006;440:1222-1226
91. Ben-Yosef Y, Lahat N, Shapiro S, Bitterman H, Miller A. Regulation of endothelial matrix metalloproteinase-2 by hypoxia/reoxygenation. *Circ Res*. 2002;90:784-791
92. Kietzmann T, Roth U, Jungermann K. Induction of the plasminogen

activator inhibitor-1 gene expression by mild hypoxia via a hypoxia response element binding the hypoxia-inducible factor-1 in rat hepatocytes. *Blood*. 1999;94:4177-4185
93. Semenza GL, Jiang BH, Leung SW, Passantino R, Concordet JP, Maire P, Giallongo A. Hypoxia response elements in the aldolase a, enolase 1, and lactate dehydrogenase a gene promoters contain essential binding sites for hypoxia-inducible factor 1. *J Biol Chem*. 1996;271:32529-32537
94. Lu S, Gu X, Hoestje S, Epner DE. Identification of an additional hypoxia responsive element in the glyceraldehyde-3-phosphate dehydrogenase gene promoter. *Biochim Biophys Acta*. 2002;1574:152-156
95. Semenza GL, Roth PH, Fang HM, Wang GL. Transcriptional regulation of genes encoding glycolytic enzymes by hypoxia-inducible factor 1. *J Biol Chem*. 1994;269:23757-23763
96. Minchenko A, Leshchinsky I, Opentanova I, Sang N, Srinivas V, Armstead V, Caro J. Hypoxia-inducible factor-1-mediated expression of the 6-phosphofructo-2-kinase/fructose-2,6-bisphosphatase-3 (pfkfb3) gene. Its possible role in the warburg effect. *J Biol Chem*. 2002;277:6183-6187
97. Metzen E, Stiehl DP, Doege K, Marxsen JH, Hellwig-Burgel T, Jelkmann W. Regulation of the prolyl hydroxylase domain protein 2 (phd2/egln-1) gene: Identification of a functional hypoxia-responsive element. *Biochem J*. 2005;387:711-717
98. Pescador N, Cuevas Y, Naranjo S, Alcaide M, Villar D, Landazuri MO, Del Peso L. Identification of a functional hypoxia-responsive element that regulates the expression of the egl nine homologue 3 (egln3/phd3) gene. *Biochem J*. 2005;390:189-197
99. Bhattacharya S, Michels CL, Leung MK, Arany ZP, Kung AL, Livingston DM. Functional role of p35srj, a novel p300/cbp binding protein, during transactivation by hif-1. *Genes Dev*. 1999;13:64-75
100. Hu J, Discher DJ, Bishopric NH, Webster KA. Hypoxia regulates expression of the endothelin-1 gene through a proximal hypoxia-inducible factor-1 binding site on the antisense strand. *Biochem Bioph Res Co*. 1998;245:894-899
101. Melillo G, Musso T, Sica A, Taylor LS, Cox GW, Varesio L. A hypoxia-responsive element mediates a novel pathway of activation of the inducible nitric oxide synthase promoter. *J Exp Med*. 1995;182:1683-1693
102. Coulet F, Nadaud S, Agrapart M, Soubrier F. Identification of hypoxia-response element in the human endothelial nitric-oxide synthase gene promoter. *J Biol Chem*. 2003;278:46230-46240
103. Lee PJ, Jiang BH, Chin BY, Iyer NV, Alam J, Semenza GL, Choi AM. Hypoxia-inducible factor-1 mediates transcriptional activation of the heme oxygenase-1 gene in response to hypoxia. *J Biol Chem*. 1997;272:5375-5381
104. Semenza GL, Nejfelt MK, Chi SM, Antonarakis SE. Hypoxia-inducible nuclear factors bind to an enhancer element located 3' to the human erythropoietin gene. *P Natl Acad Sci USA*. 1991;88:5680-5684
105. Percy MJ, Furlow PW, Beer PA, Lappin TR, McMullin MF, Lee FS. A novel erythrocytosis-associated phd2 mutation suggests the location of a hif binding groove. *Blood*. 2007;110:2193-2196
106. Peng J, Zhang L, Drysdale L, Fong GH. The transcription factor epas-1/hypoxia-inducible factor 2alpha plays an important role in vascular

remodeling. *Proc Natl Acad Sci U S A*. 2000;97:8386-8391
107. Tian H, Hammer RE, Matsumoto AM, Russell DW, McKnight SL. The hypoxia-responsive transcription factor epas1 is essential for catecholamine homeostasis and protection against heart failure during embryonic development. *Genes Dev*. 1998;12:3320-3324
108. Rankin EB, Biju MP, Liu Q, Unger TL, Rha J, Johnson RS, Simon MC, Keith B, Haase VH. Hypoxia-inducible factor-2 (hif-2) regulates hepatic erythropoietin in vivo. *J Clin Invest*. 2007;117:1068-1077
109. Skuli N, Majmundar AJ, Krock BL, Mesquita RC, Mathew LK, Quinn ZL, Runge A, Liu L, Kim MN, Liang J, Schenkel S, Yodh AG, Keith B, Simon MC. Endothelial hif-2alpha regulates murine pathological angiogenesis and revascularization processes. *J Clin Invest*. 2012;122:1427-1443
110. Mastrogiannaki M, Matak P, Keith B, Simon MC, Vaulont S, Peyssonnaux C. Hif-2alpha, but not hif-1alpha, promotes iron absorption in mice. *J Clin Invest*. 2009;119:1159-1166
111. Thompson AA, Elks PM, Marriott HM, Eamsamarng S, Higgins KR, Lewis A, Williams L, Parmar S, Shaw G, McGrath EE, Formenti F, Van Eeden FJ, Kinnula VL, Pugh CW, Sabroe I, Dockrell DH, Chilvers ER, Robbins PA, Percy MJ, Simon MC, Johnson RS, Renshaw SA, Whyte MK, Walmsley SR. Hypoxia-inducible factor 2alpha regulates key neutrophil functions in humans, mice, and zebrafish. *Blood*. 2014;123:366-376
112. Manalo DJ, Rowan A, Lavoie T, Natarajan L, Kelly BD, Ye SQ, Garcia JG, Semenza GL. Transcriptional regulation of vascular endothelial cell responses to hypoxia by hif-1. *Blood*. 2005;105:659-669
113. Takeda N, Maemura K, Imai Y, Harada T, Kawanami D, Nojiri T, Manabe I, Nagai R. Endothelial pas domain protein 1 gene promotes angiogenesis through the transactivation of both vascular endothelial growth factor and its receptor, flt-1. *Circ Res*. 2004;95:146-153
114. Maynard MA, Qi H, Chung J, Lee EH, Kondo Y, Hara S, Conaway RC, Conaway JW, Ohh M. Multiple splice variants of the human hif-3 alpha locus are targets of the von hippel-lindau e3 ubiquitin ligase complex. *J Biol Chem*. 2003;278:11032-11040
115. Makino Y, Kanopka A, Wilson WJ, Tanaka H, Poellinger L. Inhibitory pas domain protein (ipas) is a hypoxia-inducible splicing variant of the hypoxia-inducible factor-3alpha locus. *J Biol Chem*. 2002;277:32405-32408
116. Hara S, Hamada J, Kobayashi C, Kondo Y, Imura N. Expression and characterization of hypoxia-inducible factor (hif)-3alpha in human kidney: Suppression of hif-mediated gene expression by hif-3alpha. *Biochem Biophys Res Commun*. 2001;287:808-813
117. Makino Y, Cao R, Svensson K, Bertilsson G, Asman M, Tanaka H, Cao Y, Berkenstam A, Poellinger L. Inhibitory pas domain protein is a negative regulator of hypoxia-inducible gene expression. *Nature*. 2001;414:550-554
118. Yamashita T, Ohneda O, Nagano M, Iemitsu M, Makino Y, Tanaka H, Miyauchi T, Goto K, Ohneda K, Fujii-Kuriyama Y, Poellinger L, Yamamoto M. Abnormal heart development and lung remodeling in mice lacking the hypoxia-inducible factor-related basic helix-loop-helix pas protein nepas. *Mol Cell Biol*. 2008;28:1285-1297
119. Huang Y, Kapere Ochieng J, Kempen MB, Munck AB, Swagemakers S, van Ijcken W, Grosveld F, Tibboel D, Rottier RJ. Hypoxia inducible factor

3alpha plays a critical role in alveolarization and distal epithelial cell differentiation during mouse lung development. *Plos One*. 2013;8:e57695
120. Jaakkola P, Mole DR, Tian YM, Wilson MI, Gielbert J, Gaskell SJ, Kriegsheim A, Hebestreit HF, Mukherji M, Schofield CJ, Maxwell PH, Pugh CW, Ratcliffe PJ. Targeting of hif-alpha to the von hippel-lindau ubiquitylation complex by o2-regulated prolyl hydroxylation. *Science*. 2001;292:468-472
121. Kibel A, Iliopoulos O, DeCaprio JA, Kaelin WG, Jr. Binding of the von hippel-lindau tumor suppressor protein to elongin b and c. *Science*. 1995;269:1444-1446
122. Baek JH, Liu YV, McDonald KR, Wesley JB, Hubbi ME, Byun H, Semenza GL. Spermidine/spermine-n1-acetyltransferase 2 is an essential component of the ubiquitin ligase complex that regulates hypoxia-inducible factor 1alpha. *J Biol Chem*. 2007;282:23572-23580
123. Iwai K, Yamanaka K, Kamura T, Minato N, Conaway RC, Conaway JW, Klausner RD, Pause A. Identification of the von hippel-lindau tumor-suppressor protein as part of an active e3 ubiquitin ligase complex. *Proc Natl Acad Sci U S A*. 1999;96:12436-12441
124. Kallio PJ, Wilson WJ, O'Brien S, Makino Y, Poellinger L. Regulation of the hypoxia-inducible transcription factor 1alpha by the ubiquitin-proteasome pathway. *J Biol Chem*. 1999;274:6519-6525
125. Chilov D, Camenisch G, Kvietikova I, Ziegler U, Gassmann M, Wenger RH. Induction and nuclear translocation of hypoxia-inducible factor-1 (hif-1): Heterodimerization with arnt is not necessary for nuclear accumulation of hif-1alpha. *J Cell Sci*. 1999;112 (Pt 8):1203-1212
126. Erbel PJ, Card PB, Karakuzu O, Bruick RK, Gardner KH. Structural basis for pas domain heterodimerization in the basic helix--loop--helix-pas transcription factor hypoxia-inducible factor. *Proc Natl Acad Sci U S A*. 2003;100:15504-15509
127. Ema M, Taya S, Yokotani N, Sogawa K, Matsuda Y, Fujii-Kuriyama Y. A novel bhlh-pas factor with close sequence similarity to hypoxia-inducible factor 1alpha regulates the vegf expression and is potentially involved in lung and vascular development. *P Natl Acad Sci USA*. 1997;94:4273-4278
128. Chapman-Smith A, Whitelaw ML. Novel DNA binding by a basic helix-loop-helix protein. The role of the dioxin receptor pas domain. *J Biol Chem*. 2006;281:12535-12545
129. Semenza GL, Wang GL. A nuclear factor induced by hypoxia via de novo protein synthesis binds to the human erythropoietin gene enhancer at a site required for transcriptional activation. *Mol Cell Biol*. 1992;12:5447-5454
130. Kimura H, Weisz A, Ogura T, Hitomi Y, Kurashima Y, Hashimoto K, D'Acquisto F, Makuuchi M, Esumi H. Identification of hypoxia-inducible factor 1 ancillary sequence and its function in vascular endothelial growth factor gene induction by hypoxia and nitric oxide. *J Biol Chem*. 2001;276:2292-2298
131. Lee FS, Percy MJ. The hif pathway and erythrocytosis. *Annu Rev Pathol*. 2011;6:165-192
132. Epstein AC, Gleadle JM, McNeill LA, Hewitson KS, O'Rourke J, Mole DR, Mukherji M, Metzen E, Wilson MI, Dhanda A, Tian YM, Masson N, Hamilton DL, Jaakkola P, Barstead R, Hodgkin J, Maxwell PH, Pugh

CW, Schofield CJ, Ratcliffe PJ. C. Elegans egl-9 and mammalian homologs define a family of dioxygenases that regulate hif by prolyl hydroxylation. *Cell*. 2001;107:43-54
133. Duran RV, MacKenzie ED, Boulahbel H, Frezza C, Heiserich L, Tardito S, Bussolati O, Rocha S, Hall MN, Gottlieb E. Hif-independent role of prolyl hydroxylases in the cellular response to amino acids. *Oncogene*. 2013;32:4549-4556
134. Flashman E, Davies SL, Yeoh KK, Schofield CJ. Investigating the dependence of the hypoxia-inducible factor hydroxylases (factor inhibiting hif and prolyl hydroxylase domain 2) on ascorbate and other reducing agents. *Biochem J*. 2010;427:135-142
135. Fong GH, Takeda K. Role and regulation of prolyl hydroxylase domain proteins. *Cell Death Differ*. 2008;15:635-641
136. McDonough MA, Li V, Flashman E, Chowdhury R, Mohr C, Lienard BM, Zondlo J, Oldham NJ, Clifton IJ, Lewis J, McNeill LA, Kurzeja RJ, Hewitson KS, Yang E, Jordan S, Syed RS, Schofield CJ. Cellular oxygen sensing: Crystal structure of hypoxia-inducible factor prolyl hydroxylase (phd2). *Proc Natl Acad Sci U S A*. 2006;103:9814-9819
137. Chowdhury R, McDonough MA, Mecinovic J, Loenarz C, Flashman E, Hewitson KS, Domene C, Schofield CJ. Structural basis for binding of hypoxia-inducible factor to the oxygen-sensing prolyl hydroxylases. *Structure*. 2009;17:981-989
138. Hirsila M, Koivunen P, Gunzler V, Kivirikko KI, Myllyharju J. Characterization of the human prolyl 4-hydroxylases that modify the hypoxia-inducible factor. *J Biol Chem*. 2003;278:30772-30780
139. Ivan M, Kondo K, Yang H, Kim W, Valiando J, Ohh M, Salic A, Asara JM, Lane WS, Kaelin WG, Jr. Hifalpha targeted for vhl-mediated destruction by proline hydroxylation: Implications for o2 sensing. *Science*. 2001;292:464-468
140. Koivunen P, Tiainen P, Hyvarinen J, Williams KE, Sormunen R, Klaus SJ, Kivirikko KI, Myllyharju J. An endoplasmic reticulum transmembrane prolyl 4-hydroxylase is induced by hypoxia and acts on hypoxia-inducible factor alpha. *J Biol Chem*. 2007;282:30544-30552
141. Tian YM, Yeoh KK, Lee MK, Eriksson T, Kessler BM, Kramer HB, Edelmann MJ, Willam C, Pugh CW, Schofield CJ, Ratcliffe PJ. Differential sensitivity of hypoxia inducible factor hydroxylation sites to hypoxia and hydroxylase inhibitors. *J Biol Chem*. 2011;286:13041-13051
142. Willam C, Maxwell PH, Nichols L, Lygate C, Tian YM, Bernhardt W, Wiesener M, Ratcliffe PJ, Eckardt KU, Pugh CW. Hif prolyl hydroxylases in the rat; organ distribution and changes in expression following hypoxia and coronary artery ligation. *J Mol Cell Cardiol*. 2006;41:68-77
143. Takeda K, Aguila HL, Parikh NS, Li X, Lamothe K, Duan LJ, Takeda H, Lee FS, Fong GH. Regulation of adult erythropoiesis by prolyl hydroxylase domain proteins. *Blood*. 2008;111:3229-3235
144. Aragones J, Schneider M, Van Geyte K, Fraisl P, Dresselaers T, Mazzone M, Dirkx R, Zacchigna S, Lemieux H, Jeoung NH, Lambrechts D, Bishop T, Lafuste P, Diez-Juan A, Harten SK, Van Noten P, De Bock K, Willam C, Tjwa M, Grosfeld A, Navet R, Moons L, Vandendriessche T, Deroose C, Wijeyekoon B, Nuyts J, Jordan B, Silasi-Mansat R, Lupu F, Dewerchin M, Pugh C, Salmon P, Mortelmans L, Gallez B, Gorus F, Buyse J, Sluse F, Harris RA, Gnaiger E, Hespel P, Van Hecke P, Schuit F, Van Veldhoven P, Ratcliffe P, Baes M, Maxwell P, Carmeliet P.

Deficiency or inhibition of oxygen sensor phd1 induces hypoxia tolerance by reprogramming basal metabolism. *Nat Genet*. 2008;40:170-180
145. Takeda K, Cowan A, Fong GH. Essential role for prolyl hydroxylase domain protein 2 in oxygen homeostasis of the adult vascular system. *Circulation*. 2007;116:774-781
146. Metzen E, Berchner-Pfannschmidt U, Stengel P, Marxsen JH, Stolze I, Klinger M, Huang WQ, Wotzlaw C, Hellwig-Burgel T, Jelkmann W, Acker H, Fandrey J. Intracellular localisation of human hif-1 alpha hydroxylases: Implications for oxygen sensing. *J Cell Sci*. 2003;116:1319-1326
147. Huang J, Zhao Q, Mooney SM, Lee FS. Sequence determinants in hypoxia-inducible factor-1alpha for hydroxylation by the prolyl hydroxylases phd1, phd2, and phd3. *J Biol Chem*. 2002;277:39792-39800
148. Pientka FK, Hu J, Schindler SG, Brix B, Thiel A, Johren O, Fandrey J, Berchner-Pfannschmidt U, Depping R. Oxygen sensing by the prolyl-4-hydroxylase phd2 within the nuclear compartment and the influence of compartmentalisation on hif-1 signalling. *J Cell Sci*. 2012;125:5168-5176
149. Mak P, Chang C, Pursell B, Mercurio AM. Estrogen receptor beta sustains epithelial differentiation by regulating prolyl hydroxylase 2 transcription. *P Natl Acad Sci USA*. 2013;110:4708-4713
150. Souvenir R, Flores JJ, Ostrowski RP, Manaenko A, Duris K, Tang J. Erythropoietin inhibits hif-1alpha expression via upregulation of phd-2 transcription and translation in an in vitro model of hypoxia-ischemia. *Transl Stroke Res*. 2014;5:118-127
151. Nakayama K, Frew IJ, Hagensen M, Skals M, Habelhah H, Bhoumik A, Kadoya T, Erdjument-Bromage H, Tempst P, Frappell PB, Bowtell DD, Ronai Z. Siah2 regulates stability of prolyl-hydroxylases, controls hif1alpha abundance, and modulates physiological responses to hypoxia. *Cell*. 2004;117:941-952
152. Fraisl P, Aragones J, Carmeliet P. Inhibition of oxygen sensors as a therapeutic strategy for ischaemic and inflammatory disease. *Nat Rev Drug Discov*. 2009;8:139-152
153. Cummins EP, Berra E, Comerford KM, Ginouves A, Fitzgerald KT, Seeballuck F, Godson C, Nielsen JE, Moynagh P, Pouyssegur J, Taylor CT. Prolyl hydroxylase-1 negatively regulates ikappab kinase-beta, giving insight into hypoxia-induced nfkappab activity. *Proc Natl Acad Sci U S A*. 2006;103:18154-18159
154. Tak PP, Firestein GS. Nf-kappab: A key role in inflammatory diseases. *J Clin Invest*. 2001;107:7-11
155. Takeda K, Ho VC, Takeda H, Duan LJ, Nagy A, Fong GH. Placental but not heart defects are associated with elevated hypoxia-inducible factor alpha levels in mice lacking prolyl hydroxylase domain protein 2. *Mol Cell Biol*. 2006;26:8336-8346
156. Moser SC, Bensaddek D, Ortmann B, Maure JF, Mudie S, Blow JJ, Lamond AI, Swedlow JR, Rocha S. Phd1 links cell-cycle progression to oxygen sensing through hydroxylation of the centrosomal protein cep192. *Dev Cell*. 2013;26:381-392
157. Siddiq A, Aminova LR, Troy CM, Suh K, Messer Z, Semenza GL, Ratan RR. Selective inhibition of hypoxia-inducible factor (hif) prolyl-hydroxylase 1 mediates neuroprotection against normoxic oxidative death via hif- and creb-independent pathways. *J Neurosci*.

2009;29:8828-8838
158. Chan DA, Kawahara TL, Sutphin PD, Chang HY, Chi JT, Giaccia AJ. Tumor vasculature is regulated by phd2-mediated angiogenesis and bone marrow-derived cell recruitment. *Cancer Cell*. 2009;15:527-538
159. Wu S, Nishiyama N, Kano MR, Morishita Y, Miyazono K, Itaka K, Chung UI, Kataoka K. Enhancement of angiogenesis through stabilization of hypoxia-inducible factor-1 by silencing prolyl hydroxylase domain-2 gene. *Mol Ther*. 2008;16:1227-1234
160. Mazzone M, Dettori D, Leite de Oliveira R, Loges S, Schmidt T, Jonckx B, Tian YM, Lanahan AA, Pollard P, Ruiz de Almodovar C, De Smet F, Vinckier S, Aragones J, Debackere K, Luttun A, Wyns S, Jordan B, Pisacane A, Gallez B, Lampugnani MG, Dejana E, Simons M, Ratcliffe P, Maxwell P, Carmeliet P. Heterozygous deficiency of phd2 restores tumor oxygenation and inhibits metastasis via endothelial normalization. *Cell*. 2009;136:839-851
161. Chen RL, Nagel S, Papadakis M, Bishop T, Pollard P, Ratcliffe PJ, Pugh CW, Buchan AM. Roles of individual prolyl-4-hydroxylase isoforms in the first 24 hours following transient focal cerebral ischaemia: Insights from genetically modified mice. *J Physiol*. 2012;590:4079-4091
162. Kunze R, Zhou W, Veltkamp R, Wielockx B, Breier G, Marti HH. Neuron-specific prolyl-4-hydroxylase domain 2 knockout reduces brain injury after transient cerebral ischemia. *Stroke*. 2012;43:2748-2756
163. Duan LJ, Takeda K, Fong GH. Prolyl hydroxylase domain protein 2 (phd2) mediates oxygen-induced retinopathy in neonatal mice. *Am J Pathol*. 2011;178:1881-1890
164. Takeda Y, Costa S, Delamarre E, Roncal C, Leite de Oliveira R, Squadrito ML, Finisguerra V, Deschoemaeker S, Bruyere F, Wenes M, Hamm A, Serneels J, Magat J, Bhattacharyya T, Anisimov A, Jordan BF, Alitalo K, Maxwell P, Gallez B, Zhuang ZW, Saito Y, Simons M, De Palma M, Mazzone M. Macrophage skewing by phd2 haplodeficiency prevents ischaemia by inducing arteriogenesis. *Nature*. 2011;479:122-126
165. Hamm A, Veschini L, Takeda Y, Costa S, Delamarre E, Squadrito ML, Henze AT, Wenes M, Serneels J, Pucci F, Roncal C, Anisimov A, Alitalo K, De Palma M, Mazzone M. Phd2 regulates arteriogenic macrophages through tie2 signalling. *EMBO Mol Med*. 2013;5:843-857
166. Laoui D, Van Overmeire E, Di Conza G, Aldeni C, Keirsse J, Morias Y, Movahedi K, Houbracken I, Schouppe E, Elkrim Y, Karroum O, Jordan B, Carmeliet P, Gysemans C, De Baetselier P, Mazzone M, Van Ginderachter JA. Tumor hypoxia does not drive differentiation of tumor-associated macrophages but rather fine-tunes the m2-like macrophage population. *Cancer research*. 2014;74:24-30
167. Percy MJ, Zhao Q, Flores A, Harrison C, Lappin TR, Maxwell PH, McMullin MF, Lee FS. A family with erythrocytosis establishes a role for prolyl hydroxylase domain protein 2 in oxygen homeostasis. *P Natl Acad Sci USA*. 2006;103:654-659
168. Ladroue C, Carcenac R, Leporrier M, Gad S, Le Hello C, Galateau-Salle F, Feunteun J, Pouyssegur J, Richard S, Gardie B. Phd2 mutation and congenital erythrocytosis with paraganglioma. *NEJM*. 2008;359:2685-2692
169. Minamishima YA, Moslehi J, Bardeesy N, Cullen D, Bronson RT, Kaelin WG, Jr. Somatic inactivation of the phd2 prolyl hydroxylase causes

polycythemia and congestive heart failure. *Blood*. 2008;111:3236-3244
170. Franke K, Kalucka J, Mamlouk S, Singh RP, Muschter A, Weidemann A, Iyengar V, Jahn S, Wieczorek K, Geiger K, Muders M, Sykes AM, Poitz DM, Ripich T, Otto T, Bergmann S, Breier G, Baretton G, Fong GH, Greaves DR, Bornstein S, Chavakis T, Fandrey J, Gassmann M, Wielockx B. Hif-1alpha is a protective factor in conditional phd2-deficient mice suffering from severe hif-2alpha-induced excessive erythropoiesis. *Blood*. 2013;121:1436-1445
171. Cervera AM, Apostolova N, Luna-Crespo F, Sanjuan-Pla A, Garcia-Bou R, McCreath KJ. An alternatively spliced transcript of the phd3 gene retains prolyl hydroxylase activity. *Cancer Lett*. 2006;233:131-138
172. Kiss J, Mollenhauer M, Walmsley SR, Kirchberg J, Radhakrishnan P, Niemietz T, Dudda J, Steinert G, Whyte MK, Carmeliet P, Mazzone M, Weitz J, Schneider M. Loss of the oxygen sensor phd3 enhances the innate immune response to abdominal sepsis. *J Immunol*. 2012;189:1955-1965
173. Escribese MM, Sierra-Filardi E, Nieto C, Samaniego R, Sanchez-Torres C, Matsuyama T, Calderon-Gomez E, Vega MA, Salas A, Sanchez-Mateos P, Corbi AL. The prolyl hydroxylase phd3 identifies proinflammatory macrophages and its expression is regulated by activin a. *J Immunol*. 2012;189:1946-1954
174. Swain L, Wottawa M, Hillemann A, Beneke A, Odagiri H, Terada K, Endo M, Oike Y, Farhat K, Katschinski DM. Prolyl-4-hydroxylase domain 3 (phd3) is a critical terminator for cell survival of macrophages under stress conditions. *J Leukoc Biol*. 2014;96:365-375
175. Walmsley SR, Chilvers ER, Thompson AA, Vaughan K, Marriott HM, Parker LC, Shaw G, Parmar S, Schneider M, Sabroe I, Dockrell DH, Milo M, Taylor CT, Johnson RS, Pugh CW, Ratcliffe PJ, Maxwell PH, Carmeliet P, Whyte MK. Prolyl hydroxylase 3 (phd3) is essential for hypoxic regulation of neutrophilic inflammation in humans and mice. *J Clin Invest*. 2011;121:1053-1063
176. Walmsley SR, Print C, Farahi N, Peyssonnaux C, Johnson RS, Cramer T, Sobolewski A, Condliffe AM, Cowburn AS, Johnson N, Chilvers ER. Hypoxia-induced neutrophil survival is mediated by hif-1alpha-dependent nf-kappab activity. *J Exp Med*. 2005;201:105-115
177. Taniguchi CM, Finger EC, Krieg AJ, Wu C, Diep AN, LaGory EL, Wei K, McGinnis LM, Yuan J, Kuo CJ, Giaccia AJ. Cross-talk between hypoxia and insulin signaling through phd3 regulates hepatic glucose and lipid metabolism and ameliorates diabetes. *Nat Med*. 2013;19:1325-1330
178. McNeill LA, Hewitson KS, Claridge TD, Seibel JF, Horsfall LE, Schofield CJ. Hypoxia-inducible factor asparaginyl hydroxylase (fih-1) catalyses hydroxylation at the beta-carbon of asparagine-803. *Biochem J*. 2002;367:571-575
179. Elkins JM, Hewitson KS, McNeill LA, Seibel JF, Schlemminger I, Pugh CW, Ratcliffe PJ, Schofield CJ. Structure of factor-inhibiting hypoxia-inducible factor (hif) reveals mechanism of oxidative modification of hif-1 alpha. *J Biol Chem*. 2003;278:1802-1806
180. Mahon PC, Hirota K, Semenza GL. Fih-1: A novel protein that interacts with hif-1alpha and vhl to mediate repression of hif-1 transcriptional activity. *Genes Dev*. 2001;15:2675-2686
181. Lando D, Peet DJ, Gorman JJ, Whelan DA, Whitelaw ML, Bruick RK. Fih-1 is an asparaginyl hydroxylase enzyme that regulates the

transcriptional activity of hypoxia-inducible factor. *Genes Dev*. 2002;16:1466-1471
182. Zhang N, Fu Z, Linke S, Chicher J, Gorman JJ, Visk D, Haddad GG, Poellinger L, Peet DJ, Powell F, Johnson RS. The asparaginyl hydroxylase factor inhibiting hif-1alpha is an essential regulator of metabolism. *Cell Metab*. 2010;11:364-378
183. Cockman ME, Lancaster DE, Stolze IP, Hewitson KS, McDonough MA, Coleman ML, Coles CH, Yu X, Hay RT, Ley SC, Pugh CW, Oldham NJ, Masson N, Schofield CJ, Ratcliffe PJ. Posttranslational hydroxylation of ankyrin repeats in ikappab proteins by the hypoxia-inducible factor (hif) asparaginyl hydroxylase, factor inhibiting hif (fih). *P Natl Acad Sci USA*. 2006;103:14767-14772
184. Coleman ML, McDonough MA, Hewitson KS, Coles C, Mecinovic J, Edelmann M, Cook KM, Cockman ME, Lancaster DE, Kessler BM, Oldham NJ, Ratcliffe PJ, Schofield CJ. Asparaginyl hydroxylation of the notch ankyrin repeat domain by factor inhibiting hypoxia-inducible factor. *J Biol Chem*. 2007;282:24027-24038
185. Zheng X, Linke S, Dias JM, Gradin K, Wallis TP, Hamilton BR, Gustafsson M, Ruas JL, Wilkins S, Bilton RL, Brismar K, Whitelaw ML, Pereira T, Gorman JJ, Ericson J, Peet DJ, Lendahl U, Poellinger L. Interaction with factor inhibiting hif-1 defines an additional mode of cross-coupling between the notch and hypoxia signaling pathways. *P Natl Acad Sci USA*. 2008;105:3368-3373
186. Ferguson JE, 3rd, Wu Y, Smith K, Charles P, Powers K, Wang H, Patterson C. Asb4 is a hydroxylation substrate of fih and promotes vascular differentiation via an oxygen-dependent mechanism. *Mol Cell Biol*. 2007;27:6407-6419
187. Kelly BD, Hackett SF, Hirota K, Oshima Y, Cai Z, Berg-Dixon S, Rowan A, Yan Z, Campochiaro PA, Semenza GL. Cell type-specific regulation of angiogenic growth factor gene expression and induction of angiogenesis in nonischemic tissue by a constitutively active form of hypoxia-inducible factor 1. *Circ Res*. 2003;93:1074-1081
188. Patel TH, Kimura H, Weiss CR, Semenza GL, Hofmann LV. Constitutively active hif-1alpha improves perfusion and arterial remodeling in an endovascular model of limb ischemia. *Cardiovasc Res*. 2005;68:144-154
189. Bosch-Marce M, Okuyama H, Wesley JB, Sarkar K, Kimura H, Liu YV, Zhang H, Strazza M, Rey S, Savino L, Zhou YF, McDonald KR, Na Y, Vandiver S, Rabi A, Shaked Y, Kerbel R, Lavallee T, Semenza GL. Effects of aging and hypoxia-inducible factor-1 activity on angiogenic cell mobilization and recovery of perfusion after limb ischemia. *Circ Res*. 2007;101:1310-1318
190. Sarkar K, Fox-Talbot K, Steenbergen C, Bosch-Marce M, Semenza GL. Adenoviral transfer of hif-1alpha enhances vascular responses to critical limb ischemia in diabetic mice. *P Natl Acad Sci USA*. 2009;106:18769-18774
191. Pajusola K, Kunnapuu J, Vuorikoski S, Soronen J, Andre H, Pereira T, Korpisalo P, Yla-Herttuala S, Poellinger L, Alitalo K. Stabilized hif-1alpha is superior to vegf for angiogenesis in skeletal muscle via adeno-associated virus gene transfer. *Faseb J*. 2005;19:1365-1367
192. Rajagopalan S, Olin J, Deitcher S, Pieczek A, Laird J, Grossman PM, Goldman CK, McEllin K, Kelly R, Chronos N. Use of a constitutively

active hypoxia-inducible factor-1alpha transgene as a therapeutic strategy in no-option critical limb ischemia patients: Phase i dose-escalation experience. *Circulation*. 2007;115:1234-1243
193. Soda Y, Marumoto T, Friedmann-Morvinski D, Soda M, Liu F, Michiue H, Pastorino S, Yang M, Hoffman RM, Kesari S, Verma IM. Transdifferentiation of glioblastoma cells into vascular endothelial cells. *P Natl Acad Sci USA*. 2011;108:4274-4280
194. Nangaku M, Izuhara Y, Takizawa S, Yamashita T, Fujii-Kuriyama Y, Ohneda O, Yamamoto M, van Ypersele de Strihou C, Hirayama N, Miyata T. A novel class of prolyl hydroxylase inhibitors induces angiogenesis and exerts organ protection against ischemia. *Arterioscler Thromb Vasc Biol*. 2007;27:2548-2554
195. Ikeda Y, Tajima S, Yoshida S, Yamano N, Kihira Y, Ishizawa K, Aihara K, Tomita S, Tsuchiya K, Tamaki T. Deferoxamine promotes angiogenesis via the activation of vascular endothelial cell function. *Atherosclerosis*. 2011;215:339-347
196. Knowles HJ, Tian YM, Mole DR, Harris AL. Novel mechanism of action for hydralazine: Induction of hypoxia-inducible factor-1alpha, vascular endothelial growth factor, and angiogenesis by inhibition of prolyl hydroxylases. *Circ Res*. 2004;95:162-169
197. Milkiewicz M, Pugh CW, Egginton S. Inhibition of endogenous hif inactivation induces angiogenesis in ischaemic skeletal muscles of mice. *J Physiol*. 2004;560:21-26
198. Rey S, Lee K, Wang CJ, Gupta K, Chen S, McMillan A, Bhise N, Levchenko A, Semenza GL. Synergistic effect of hif-1alpha gene therapy and hif-1-activated bone marrow-derived angiogenic cells in a mouse model of limb ischemia. *Proc Natl Acad Sci U S A*. 2009;106:20399-20404
199. Rey S, Luo W, Shimoda LA, Semenza GL. Metabolic reprogramming by hif-1 promotes the survival of bone marrow-derived angiogenic cells in ischemic tissue. *Blood*. 2011;117:4988-4998
200. Ockaili R, Natarajan R, Salloum F, Fisher BJ, Jones D, Fowler AA, 3rd, Kukreja RC. Hif-1 activation attenuates postischemic myocardial injury: Role for heme oxygenase-1 in modulating microvascular chemokine generation. *Am J Physiol Heart Circ Physiol*. 2005;289:H542-548
201. Hams E, Saunders SP, Cummins EP, O'Connor A, Tambuwala MT, Gallagher WM, Byrne A, Campos-Torres A, Moynagh PM, Jobin C, Taylor CT, Fallon PG. The hydroxylase inhibitor dimethyloxallyl glycine attenuates endotoxic shock via alternative activation of macrophages and il-10 production by b1 cells. *Shock*. 2011;36:295-302
202. Eckle T, Kohler D, Lehmann R, El Kasmi K, Eltzschig HK. Hypoxia-inducible factor-1 is central to cardioprotection: A new paradigm for ischemic preconditioning. *Circulation*. 2008;118:166-175
203. Dendorfer A, Heidbreder M, Hellwig-Burgel T, Johren O, Qadri F, Dominiak P. Deferoxamine induces prolonged cardiac preconditioning via accumulation of oxygen radicals. *Free Radic Biol Med*. 2005;38:117-124
204. Bao W, Qin P, Needle S, Erickson-Miller CL, Duffy KJ, Ariazi JL, Zhao S, Olzinski AR, Behm DJ, Pipes GC, Jucker BM, Hu E, Lepore JJ, Willette RN. Chronic inhibition of hypoxia-inducible factor prolyl 4-hydroxylase improves ventricular performance, remodeling, and vascularity after myocardial infarction in the rat. *J Cardiovasc Pharmacol*. 2010;56:147-

155
205. Ong SG, Lee WH, Theodorou L, Kodo K, Lim SY, Shukla DH, Briston T, Kiriakidis S, Ashcroft M, Davidson SM, Maxwell PH, Yellon DM, Hausenloy DJ. Hif-1 reduces ischaemia-reperfusion injury in the heart by targeting the mitochondrial permeability transition pore. *Cardiovasc Res*. 2014;104:24-36
206. Bernhardt WM, Campean V, Kany S, Jurgensen JS, Weidemann A, Warnecke C, Arend M, Klaus S, Gunzler V, Amann K, Willam C, Wiesener MS, Eckardt KU. Preconditional activation of hypoxia-inducible factors ameliorates ischemic acute renal failure. *J Am Soc Nephrol*. 2006;17:1970-1978
207. Hill P, Shukla D, Tran MG, Aragones J, Cook HT, Carmeliet P, Maxwell PH. Inhibition of hypoxia inducible factor hydroxylases protects against renal ischemia-reperfusion injury. *J Am Soc Nephrol*. 2008;19:39-46
208. Zhang XL, Yan ZW, Sheng WW, Xiao J, Zhang ZX, Ye ZB. Activation of hypoxia-inducible factor-1 ameliorates postischemic renal injury via inducible nitric oxide synthase. *Mol Cell Biochem*. 2011
209. Prass K, Ruscher K, Karsch M, Isaev N, Megow D, Priller J, Scharff A, Dirnagl U, Meisel A. Desferrioxamine induces delayed tolerance against cerebral ischemia in vivo and in vitro. *J Cereb Blood Flow Metab*. 2002;22:520-525
210. Siddiq A, Ayoub IA, Chavez JC, Aminova L, Shah S, LaManna JC, Patton SM, Connor JR, Cherny RA, Volitakis I, Bush AI, Langsetmo I, Seeley T, Gunzler V, Ratan RR. Hypoxia-inducible factor prolyl 4-hydroxylase inhibition. A target for neuroprotection in the central nervous system. *J Biol Chem*. 2005;280:41732-41743
211. Freret T, Valable S, Chazalviel L, Saulnier R, Mackenzie ET, Petit E, Bernaudin M, Boulouard M, Schumann-Bard P. Delayed administration of deferoxamine reduces brain damage and promotes functional recovery after transient focal cerebral ischemia in the rat. *Eur J Neurosci*. 2006;23:1757-1765
212. Nagel S, Papadakis M, Chen R, Hoyte LC, Brooks KJ, Gallichan D, Sibson NR, Pugh C, Buchan AM. Neuroprotection by dimethyloxalylglycine following permanent and transient focal cerebral ischemia in rats. *J Cereb Blood Flow Metab*. 2011;31:132-143
213. Floyd ZE, Kilroy G, Wu X, Gimble JM. Effects of prolyl hydroxylase inhibitors on adipogenesis and hypoxia inducible factor 1 alpha levels under normoxic conditions. *J Cell Biochem*. 2007;101:1545-1557
214. Sridharan V, Guichard J, Bailey RM, Kasiganesan H, Beeson C, Wright GL. The prolyl hydroxylase oxygen-sensing pathway is cytoprotective and allows maintenance of mitochondrial membrane potential during metabolic inhibition. *Am J Physiol Cell Physiol*. 2007;292:C719-728
215. Cummins EP, Seeballuck F, Keely SJ, Mangan NE, Callanan JJ, Fallon PG, Taylor CT. The hydroxylase inhibitor dimethyloxalylglycine is protective in a murine model of colitis. *Gastroenterology*. 2008;134:156-165
216. Philipp S, Cui L, Ludolph B, Kelm M, Schulz R, Cohen MV, Downey JM. Desferoxamine and ethyl-3,4-dihydroxybenzoate protect myocardium by activating nos and generating mitochondrial ros. *Am J Physiol Heart Circ Physiol*. 2006;290:H450-457
217. Bergeron M, Gidday JM, Yu AY, Semenza GL, Ferriero DM, Sharp FR. Role of hypoxia-inducible factor-1 in hypoxia-induced ischemic tolerance

in neonatal rat brain. *Ann Neurol*. 2000;48:285-296
218. Sarco DP, Becker J, Palmer C, Sheldon RA, Ferriero DM. The neuroprotective effect of deferoxamine in the hypoxic-ischemic immature mouse brain. *Neurosci Lett*. 2000;282:113-116
219. Hamrick SE, McQuillen PS, Jiang X, Mu D, Madan A, Ferriero DM. A role for hypoxia-inducible factor-1alpha in desferoxamine neuroprotection. *Neurosci Lett*. 2005;379:96-100
220. Warnecke C, Griethe W, Weidemann A, Jurgensen JS, Willam C, Bachmann S, Ivashchenko Y, Wagner I, Frei U, Wiesener M, Eckardt KU. Activation of the hypoxia-inducible factor-pathway and stimulation of angiogenesis by application of prolyl hydroxylase inhibitors. *Faseb J*. 2003;17:1186-1188
221. Nwogu JI, Geenen D, Bean M, Brenner MC, Huang X, Buttrick PM. Inhibition of collagen synthesis with prolyl 4-hydroxylase inhibitor improves left ventricular function and alters the pattern of left ventricular dilatation after myocardial infarction. *Circulation*. 2001;104:2216-2221
222. Bernhardt WM, Wiesener MS, Scigalla P, Chou J, Schmieder RE, Gunzler V, Eckardt KU. Inhibition of prolyl hydroxylases increases erythropoietin production in esrd. *J Am Soc Nephrol*. 2010;21:2151-2156
223. Hsieh MM, Linde NS, Wynter A, Metzger M, Wong C, Langsetmo I, Lin A, Smith R, Rodgers GP, Donahue RE, Klaus SJ, Tisdale JF. Hif prolyl hydroxylase inhibition results in endogenous erythropoietin induction, erythrocytosis, and modest fetal hemoglobin expression in rhesus macaques. *Blood*. 2007;110:2140-2147
224. Linden T, Katschinski DM, Eckhardt K, Scheid A, Pagel H, Wenger RH. The antimycotic ciclopiroxolamine induces hif-1alpha stability, vegf expression, and angiogenesis. *Faseb J*. 2003;17:761-763
225. Safran M, Kim WY, O'Connell F, Flippin L, Gunzler V, Horner JW, Depinho RA, Kaelin WG, Jr. Mouse model for noninvasive imaging of hif prolyl hydroxylase activity: Assessment of an oral agent that stimulates erythropoietin production. *P Natl Acad Sci USA*. 2006;103:105-110
226. Rosenberger C, Rosen S, Shina A, Frei U, Eckardt KU, Flippin LA, Arend M, Klaus SJ, Heyman SN. Activation of hypoxia-inducible factors ameliorates hypoxic distal tubular injury in the isolated perfused rat kidney. *Nephrol Dial Transplant*. 2008;23:3472-3478
227. Barrett TD, Palomino HL, Brondstetter TI, Kanelakis KC, Wu X, Haug PV, Yan W, Young A, Hua H, Hart JC, Tran DT, Venkatesan H, Rosen MD, Peltier HM, Sepassi K, Rizzolio MC, Bembenek SD, Mirzadegan T, Rabinowitz MH, Shankley NP. Pharmacological characterization of 1-(5-chloro-6-(trifluoromethoxy)-1h-benzoimidazol-2-yl)-1h-pyrazole-4-carb oxylic acid (jnj-42041935), a potent and selective hypoxia-inducible factor prolyl hydroxylase inhibitor. *Mol Pharmacol*. 2011;79:910-920
228. Thirstrup K, Christensen S, Moller HA, Ritzen A, Bergstrom AL, Sager TN, Jensen HS. Endogenous 2-oxoglutarate levels impact potencies of competitive hif prolyl hydroxylase inhibitors. *Pharmacol Res*. 2011;64:268-273
229. McDonough MA, McNeill LA, Tilliet M, Papamicael CA, Chen QY, Banerji B, Hewitson KS, Schofield CJ. Selective inhibition of factor inhibiting hypoxia-inducible factor. *J Am Chem Soc*. 2005;127:7680-7681
230. Ju H, Hao J, Zhao S, Dixon IM. Antiproliferative and antifibrotic effects of mimosine on adult cardiac fibroblasts. *Biochim Biophys Acta*. 1998;1448:51-60

231. Okumura CY, Hollands A, Tran DN, Olson J, Dahesh S, von Kockritz-Blickwede M, Thienphrapa W, Corle C, Jeung SN, Kotsakis A, Shalwitz RA, Johnson RS, Nizet V. A new pharmacological agent (akb-4924) stabilizes hypoxia inducible factor-1 (hif-1) and increases skin innate defenses against bacterial infection. *J Mol Med*. 2012;90:1079-1089
232. Leire E, Olson J, Isaacs H, Nizet V, Hollands A. Role of hypoxia inducible factor-1 in keratinocyte inflammatory response and neutrophil recruitment. *J Inflamm*. 2013;10:28
233. Keely S, Campbell EL, Baird AW, Hansbro PM, Shalwitz RA, Kotsakis A, McNamee EN, Eltzschig HK, Kominsky DJ, Colgan SP. Contribution of epithelial innate immunity to systemic protection afforded by prolyl hydroxylase inhibition in murine colitis. *Mucosal Immunol*. 2014;7:114-123
234. Campbell EL, Bruyninckx WJ, Kelly CJ, Glover LE, McNamee EN, Bowers BE, Bayless AJ, Scully M, Saeedi BJ, Golden-Mason L, Ehrentraut SF, Curtis VF, Burgess A, Garvey JF, Sorensen A, Nemenoff R, Jedlicka P, Taylor CT, Kominsky DJ, Colgan SP. Transmigrating neutrophils shape the mucosal microenvironment through localized oxygen depletion to influence resolution of inflammation. *Immunity*. 2014;40:66-77
235. Robinson A, Keely S, Karhausen J, Gerich ME, Furuta GT, Colgan SP. Mucosal protection by hypoxia-inducible factor prolyl hydroxylase inhibition. *Gastroenterology*. 2008;134:145-155
236. Hindryckx P, De Vos M, Jacques P, Ferdinande L, Peeters H, Olievier K, Bogaert S, Brinkman B, Vandenabeele P, Elewaut D, Laukens D. Hydroxylase inhibition abrogates tnf-alpha-induced intestinal epithelial damage by hypoxia-inducible factor-1-dependent repression of fadd. *J Immunol*. 2010;185:6306-6316
237. Hong YR, Kim HT, Lee SC, Ro S, Cho JM, Kim IS, Jung YH. [(4-hydroxyl-benzo[4,5]thieno[3,2-c]pyridine-3-carbonyl)-amino]-acetic acid derivatives; hif prolyl 4-hydroxylase inhibitors as oral erythropoietin secretagogues. *Bioorg Med Chem Lett*. 2013;23:5953-5957
238. Adamcio B, Sperling S, Hagemeyer N, Walkinshaw G, Ehrenreich H. Hypoxia inducible factor stabilization leads to lasting improvement of hippocampal memory in healthy mice. *Behav Brain Res*. 2010;208:80-84
239. Salvarani C, Baricchi R, Lasagni D, Boiardi L, Piccinini R, Brunati C, Macchioni P, Portioli I. Effects of desferrioxamine therapy on chronic disease anemia associated with rheumatoid arthritis. *Rheum Int*. 1996;16:45-48
240. Lee CT, Liao SC, Hsu KT, Lam KK, Chen JB. Low dose desferrioxamine can improve erythropoiesis in iron-overload hemodialysis patients without side effects. *Ren Fail*. 1999;21:665-673
241. Berra E, Benizri E, Ginouves A, Volmat V, Roux D, Pouyssegur J. Hif prolyl-hydroxylase 2 is the key oxygen sensor setting low steady-state levels of hif-1alpha in normoxia. *EMBO J*. 2003;22:4082-4090
242. Diaz JA, Obi AT, Myers DD, Jr., Wrobleski SK, Henke PK, Mackman N, Wakefield TW. Critical review of mouse models of venous thrombosis. *Arterioscler Thromb Vasc Biol*. 2012;32:556-562
243. Wang X, Smith PL, Hsu MY, Ogletree ML, Schumacher WA. Murine model of ferric chloride-induced vena cava thrombosis: Evidence for effect of potato carboxypeptidase inhibitor. *J Thromb Haemost*. 2006;4:403-410

244. Chauhan AK, Kisucka J, Lamb CB, Bergmeier W, Wagner DD. Von willebrand factor and factor viii are independently required to form stable occlusive thrombi in injured veins. *Blood*. 2007;109:2424-2429
245. Buyue Y, Whinna HC, Sheehan JP. The heparin-binding exosite of factor ixa is a critical regulator of plasma thrombin generation and venous thrombosis. *Blood*. 2008;112:3234-3241
246. Wang X, Xu L. An optimized murine model of ferric chloride-induced arterial thrombosis for thrombosis research. *Thromb Res*. 2005;115:95-100
247. Barr JD, Chauhan AK, Schaeffer GV, Hansen JK, Motto DG. Red blood cells mediate the onset of thrombosis in the ferric chloride murine model. *Blood*. 2013;121:3733-3741
248. Diaz JA, Hawley AE, Alvarado CM, Berguer AM, Baker NK, Wrobleski SK, Wakefield TW, Lucchesi BR, Myers DD, Jr. Thrombogenesis with continuous blood flow in the inferior vena cava. A novel mouse model. *Thromb Haemost*. 2010;104:366-375
249. Diaz JA, Alvarado CM, Wrobleski SK, Slack DW, Hawley AE, Farris DM, Henke PK, Wakefield TW, Myers DD, Jr. The electrolytic inferior vena cava model (eim) to study thrombogenesis and thrombus resolution with continuous blood flow in the mouse. *Thromb Haemost*. 2013;109:1158-1169
250. Brill A, Fuchs TA, Chauhan AK, Yang JJ, De Meyer SF, Kollnberger M, Wakefield TW, Lammle B, Massberg S, Wagner DD. Von willebrand factor-mediated platelet adhesion is critical for deep vein thrombosis in mouse models. *Blood*. 2011;117:1400-1407
251. Nosaka M, Ishida Y, Kimura A, Kuninaka Y, Inui M, Mukaida N, Kondo T. Absence of ifn-gamma accelerates thrombus resolution through enhanced mmp-9 and vegf expression in mice. *J Clin Invest*. 2011;121:2911-2920
252. Brill A, Fuchs TA, Savchenko AS, Thomas GM, Martinod K, De Meyer SF, Bhandari AA, Wagner DD. Neutrophil extracellular traps promote deep vein thrombosis in mice. *J Thromb Haemost*. 2012;10:136-144
253. Martinod K, Demers M, Fuchs TA, Wong SL, Brill A, Gallant M, Hu J, Wang Y, Wagner DD. Neutrophil histone modification by peptidylarginine deiminase 4 is critical for deep vein thrombosis in mice. *P Natl Acad Sci USA*. 2013;110:8674-8679
254. von Bruhl ML, Stark K, Steinhart A, Chandraratne S, Konrad I, Lorenz M, Khandoga A, Tirniceriu A, Coletti R, Kollnberger M, Byrne RA, Laitinen I, Walch A, Brill A, Pfeiler S, Manukyan D, Braun S, Lange P, Riegger J, Ware J, Eckart A, Haidari S, Rudelius M, Schulz C, Echtler K, Brinkmann V, Schwaiger M, Preissner KT, Wagner DD, Mackman N, Engelmann B, Massberg S. Monocytes, neutrophils, and platelets cooperate to initiate and propagate venous thrombosis in mice in vivo. *J Exp Med*. 2012;209:819-835
255. Geddings J, Aleman MM, Wolberg A, von Bruhl ML, Massberg S, Mackman N. Strengths and weaknesses of a new mouse model of thrombosis induced by inferior vena cava stenosis: Communication from the ssc of the isth. *J Thromb Haemost*. 2014;12:571-573
256. Sevitt S. The structure and growth of valve-pocket thrombi in femoral veins. *J Clin Pathol*. 1974;27:517-528
257. Saha P, Andia ME, Modarai B, Blume U, Humphries J, Patel AS, Phinikaridou A, Evans CE, Mattock K, Grover SP, Ahmad A, Lyons OT,

Attia RQ, Renne T, Premaratne S, Wiethoff AJ, Botnar RM, Schaeffter T, Waltham M, Smith A. Magnetic resonance t1 relaxation time of venous thrombus is determined by iron processing and predicts susceptibility to lysis. *Circulation*. 2013;128:729-736
258. Henke PK, Wakefield TW, Kadell AM, Linn MJ, Varma MR, Sarkar M, Hawley A, Fowlkes JB, Strieter RM. Interleukin-8 administration enhances venous thrombosis resolution in a rat model. *J Surg Res*. 2001;99:84-91
259. Rozen S, Skaletsky H. Primer3 on the www for general users and for biologist programmers. *Methods Mol Biol*. 2000;132:365-386
260. D'Angelo G, Duplan E, Boyer N, Vigne P, Frelin C. Hypoxia up-regulates prolyl hydroxylase activity: A feedback mechanism that limits hif-1 responses during reoxygenation. *J Biol Chem*. 2003;278:38183-38187
261. Evans CE, Wadoodi A, Humphries J, Lu X, Grover SP, Saha P, Smith A. Local accumulation of hypoxia-inducible factor 2 alpha during venous thrombus resolution. *Thromb Res*. 2014;134:757-760
262. Imtiyaz HZ, Williams EP, Hickey MM, Patel SA, Durham AC, Yuan LJ, Hammond R, Gimotty PA, Keith B, Simon MC. Hypoxia-inducible factor 2alpha regulates macrophage function in mouse models of acute and tumor inflammation. *J Clin Invest*. 2010;120:2699-2714
263. Negus RP, Turner L, Burke F, Balkwill FR. Hypoxia down-regulates mcp-1 expression: Implications for macrophage distribution in tumors. *J Leukoc Biol*. 1998;63:758-765
264. Graven KK, McDonald RJ, Farber HW. Hypoxic regulation of endothelial glyceraldehyde-3-phosphate dehydrogenase. *Am J Physiol*. 1998;274:C347-355
265. Schodel J, Klanke B, Weidemann A, Buchholz B, Bernhardt W, Bertog M, Amann K, Korbmacher C, Wiesener M, Warnecke C, Kurtz A, Eckardt KU, Willam C. Hif-prolyl hydroxylases in the rat kidney: Physiologic expression patterns and regulation in acute kidney injury. *Am J Pathol*. 2009;174:1663-1674
266. Li N, Yi F, Sundy CM, Chen L, Hilliker ML, Donley DK, Muldoon DB, Li PL. Expression and actions of hif prolyl-4-hydroxylase in the rat kidneys. *Am J Physiol Renal Physiol*. 2007;292:F207-216
267. Soilleux EJ, Turley H, Tian YM, Pugh CW, Gatter KC, Harris AL. Use of novel monoclonal antibodies to determine the expression and distribution of the hypoxia regulatory factors phd-1, phd-2, phd-3 and fih in normal and neoplastic human tissues. *Histopathology*. 2005;47:602-610
268. Toda Y, Kono K, Abiru H, Kokuryo K, Endo M, Yaegashi H, Fukumoto M. Application of tyramide signal amplification system to immunohistochemistry: A potent method to localize antigens that are not detectable by ordinary method. *Pathol Int*. 1999;49:479-483
269. Leite de Oliveira R, Deschoemaeker S, Henze AT, Debackere K, Finisguerra V, Takeda Y, Roncal C, Dettori D, Tack E, Jonsson Y, Veschini L, Peeters A, Anisimov A, Hofmann M, Alitalo K, Baes M, D'Hooge J, Carmeliet P, Mazzone M. Gene-targeting of phd2 improves tumor response to chemotherapy and prevents side-toxicity. *Cancer Cell*. 2012;22:263-277
270. Fujita N, Markova D, Anderson DG, Chiba K, Toyama Y, Shapiro IM, Risbud MV. Expression of prolyl hydroxylases (phds) is selectively controlled by hif-1 and hif-2 proteins in nucleus pulposus cells of the intervertebral disc: Distinct roles of phd2 and phd3 proteins in controlling

hif-1alpha activity in hypoxia. *J Biol Chem*. 2012;287:16975-16986
271. Takahashi N, Brooks HL, Wade JB, Liu W, Kondo Y, Ito S, Knepper MA, Smithies O. Posttranscriptional compensation for heterozygous disruption of the kidney-specific nak2cl cotransporter gene. *J Am Soc Nephrol*. 2002;13:604-610
272. Appelhoff RJ, Tian YM, Raval RR, Turley H, Harris AL, Pugh CW, Ratcliffe PJ, Gleadle JM. Differential function of the prolyl hydroxylases phd1, phd2, and phd3 in the regulation of hypoxia-inducible factor. *J Biol Chem*. 2004;279:38458-38465
273. McDonald AP, Meier TR, Hawley AE, Thibert JN, Farris DM, Wrobleski SK, Henke PK, Wakefield TW, Myers DD, Jr. Aging is associated with impaired thrombus resolution in a mouse model of stasis induced thrombosis. *Thromb Res*. 2010;125:72-78
274. Hemmeryckx B, Van Hove CE, Fransen P, Emmerechts J, Kauskot A, Bult H, Lijnen HR, Hoylaerts MF. Progression of the prothrombotic state in aging bmal1-deficient mice. *Arterioscler Thromb Vasc Biol*. 2011;31:2552-2559
275. Sternberg N, Hamilton D, Hoess R. Bacteriophage p1 site-specific recombination. Ii. Recombination between loxp and the bacterial chromosome. *J Mol Biol*. 1981;150:487-507
276. Sauer B, Henderson N. Site-specific DNA recombination in mammalian cells by the cre recombinase of bacteriophage p1. *P Natl Acad Sci USA*. 1988;85:5166-5170
277. Indra AK, Warot X, Brocard J, Bornert JM, Xiao JH, Chambon P, Metzger D. Temporally-controlled site-specific mutagenesis in the basal layer of the epidermis: Comparison of the recombinase activity of the tamoxifen-inducible cre-er(t) and cre-er(t2) recombinases. *Nucleic Acids Res*. 1999;27:4324-4327
278. Ikeda J, Ichiki T, Matsuura H, Inoue E, Kishimoto J, Watanabe A, Sankoda C, Kitamoto S, Tokunou T, Takeda K, Fong GH, Sunagawa K. Deletion of phd2 in myeloid lineage attenuates hypertensive cardiovascular remodeling. *J Am Heart Assoc*. 2013;2:e000178
279. Tang N, Wang L, Esko J, Giordano FJ, Huang Y, Gerber HP, Ferrara N, Johnson RS. Loss of hif-1alpha in endothelial cells disrupts a hypoxia-driven vegf autocrine loop necessary for tumorigenesis. *Cancer Cell*. 2004;6:485-495
280. Werno C, Menrad H, Weigert A, Dehne N, Goerdt S, Schledzewski K, Kzhyshkowska J, Brune B. Knockout of hif-1alpha in tumor-associated macrophages enhances m2 polarization and attenuates their pro-angiogenic responses. *Carcinogenesis*. 2010;31:1863-1872
281. Aghourian MN, Lemarie CA, Blostein MD. In vivo monitoring of venous thrombosis in mice. *J Thromb Haemost*. 2012;10:447-452
282. Goldberg A, Pakkiri P, Dai E, Lucas A, Fenster A. Measurements of aneurysm morphology determined by 3-d micro-ultrasound imaging as potential quantitative biomarkers in a mouse aneurysm model. *Ultrasound Med Biol*. 2007;33:1552-1560
283. Guenther F, Herr N, Mauler M, Witsch T, Roming F, Hein L, Boeynaems JM, Robaye B, Idzko M, Bode C, Von Zur Muhlen C, Duerschmied D. Contrast ultrasound for the quantification of deep vein thrombosis in living mice: Effects of enoxaparin and p2y12 receptor inhibition. *J Thromb Haemost*. 2013;11:1154-1162
284. Hashiguchi H, Takahashi H. Inhibition of two copper-containing enzymes,

tyrosinase and dopamine beta-hydroxylase, by l-mimosine. *Mol Pharmacol*. 1977;13:362-367
285. Perry C, Sastry R, Nasrallah IM, Stover PJ. Mimosine attenuates serine hydroxymethyltransferase transcription by chelating zinc. Implications for inhibition of DNA replication. *J Biol Chem*. 2005;280:396-400
286. Branitzki-Heinemann K, Okumura CY, Vollger L, Kawakami Y, Kawakami T, Naim HY, Nizet V, Von Kockritz-Blickwede M. A novel role for the transcription factor hif-1alpha in the formation of mast cell extracellular traps. *Biochem J*. 2012;446:159-163
287. Yushkevich PA, Piven J, Hazlett HC, Smith RG, Ho S, Gee JC, Gerig G. User-guided 3d active contour segmentation of anatomical structures: Significantly improved efficiency and reliability. *Neuroimage*. 2006;31:1116-1128
288. Bentovim L, Amarilio R, Zelzer E. Hif1alpha is a central regulator of collagen hydroxylation and secretion under hypoxia during bone development. *Development*. 2012;139:4473-4483
289. Gilkes DM, Bajpai S, Chaturvedi P, Wirtz D, Semenza GL. Hypoxia-inducible factor 1 (hif-1) promotes extracellular matrix remodeling under hypoxic conditions by inducing p4ha1, p4ha2, and plod2 expression in fibroblasts. *J Biol Chem*. 2013;288:10819-10829
290. Leire E, Olson J, Isaacs H, Nizet V, Hollands A. Role of hypoxia inducible factor-1 in keratinocyte inflammatory response and neutrophil recruitment. *Journal of inflammation*. 2013;10:28
291. Ritman EL. Current status of developments and applications of micro-ct. *Annu Rev Biomed Eng*. 2011;13:531-552
292. Zagorchev L, Oses P, Zhuang ZW, Moodie K, Mulligan-Kehoe MJ, Simons M, Couffinhal T. Micro computed tomography for vascular exploration. *J Angiogenes Res*. 2010;2:7
293. Kaijzel EL, van Heijningen PM, Wielopolski PA, Vermeij M, Koning GA, van Cappellen WA, Que I, Chan A, Dijkstra J, Ramnath NW, Hawinkels LJ, Bernsen MR, Lowik CW, Essers J. Multimodality imaging reveals a gradual increase in matrix metalloproteinase activity at aneurysmal lesions in live fibulin-4 mice. *Circ Cardiovasc Imaging*. 2010;3:567-577
294. Nahrendorf M, Badea C, Hedlund LW, Figueiredo JL, Sosnovik DE, Johnson GA, Weissleder R. High-resolution imaging of murine myocardial infarction with delayed-enhancement cine micro-ct. *Am J Physiol Heart Circ Physiol*. 2007;292:H3172-3178
295. Hara T, Truelove J, Tawakol A, Wojtkiewicz GR, Hucker WJ, MacNabb MH, Brownell AL, Jokivarsi K, Kessinger CW, Jaff MR, Henke PK, Weissleder R, Jaffer FA. 18f-fluorodeoxyglucose positron emission tomography/computed tomography enables the detection of recurrent same-site deep vein thrombosis by illuminating recently formed, neutrophil-rich thrombus. *Circulation*. 2014;130:1044-1052
296. Nebuloni L, Kuhn GA, Muller R. A comparative analysis of water-soluble and blood-pool contrast agents for in vivo vascular imaging with micro-ct. *Acad Radiol*. 2013;20:1247-1255
297. Lieb ME, Menzies K, Moschella MC, Ni R, Taubman MB. Mammalian egln genes have distinct patterns of mrna expression and regulation. *Biochem Cell Biol*. 2002;80:421-426
298. Fox CH, Johnson FB, Whiting J, Roller PP. Formaldehyde fixation. *J Histochem Cytochem*. 1985;33:845-853
299. Kido M, Du L, Sullivan CC, Li X, Deutsch R, Jamieson SW,

Thistlethwaite PA. Hypoxia-inducible factor 1-alpha reduces infarction and attenuates progression of cardiac dysfunction after myocardial infarction in the mouse. *J Am Coll Cardiol*. 2005;46:2116-2124
300. Du R, Lu KV, Petritsch C, Liu P, Ganss R, Passegue E, Song H, Vandenberg S, Johnson RS, Werb Z, Bergers G. Hif1alpha induces the recruitment of bone marrow-derived vascular modulatory cells to regulate tumor angiogenesis and invasion. *Cancer Cell*. 2008;13:206-220
301. Carmeliet P, Ferreira V, Breier G, Pollefeyt S, Kieckens L, Gertsenstein M, Fahrig M, Vandenhoeck A, Harpal K, Eberhardt C, Declercq C, Pawling J, Moons L, Collen D, Risau W, Nagy A. Abnormal blood vessel development and lethality in embryos lacking a single vegf allele. *Nature*. 1996;380:435-439
302. Carmeliet P, Moons L, Luttun A, Vincenti V, Compernolle V, De Mol M, Wu Y, Bono F, Devy L, Beck H, Scholz D, Acker T, DiPalma T, Dewerchin M, Noel A, Stalmans I, Barra A, Blacher S, VandenDriessche T, Ponten A, Eriksson U, Plate KH, Foidart JM, Schaper W, Charnock-Jones DS, Hicklin DJ, Herbert JM, Collen D, Persico MG. Synergism between vascular endothelial growth factor and placental growth factor contributes to angiogenesis and plasma extravasation in pathological conditions. *Nat Med*. 2001;7:575-583
303. Cao Y. Positive and negative modulation of angiogenesis by vegfr1 ligands. *Sci Signal*. 2009;2:re1
304. Morales-Ruiz M, Fulton D, Sowa G, Languino LR, Fujio Y, Walsh K, Sessa WC. Vascular endothelial growth factor-stimulated actin reorganization and migration of endothelial cells is regulated via the serine/threonine kinase akt. *Circ Res*. 2000;86:892-896
305. Bernatchez PN, Soker S, Sirois MG. Vascular endothelial growth factor effect on endothelial cell proliferation, migration, and platelet-activating factor synthesis is flk-1-dependent. *J Biol Chem*. 1999;274:31047-31054
306. Gerhardt H, Golding M, Fruttiger M, Ruhrberg C, Lundkvist A, Abramsson A, Jeltsch M, Mitchell C, Alitalo K, Shima D, Betsholtz C. Vegf guides angiogenic sprouting utilizing endothelial tip cell filopodia. *J Cell Biol*. 2003;161:1163-1177
307. Olsson AK, Dimberg A, Kreuger J, Claesson-Welsh L. Vegf receptor signalling - in control of vascular function. *Nat Rev Mol Cell Biol*. 2006;7:359-371
308. Ferrara N, Houck KA, Jakeman LB, Winer J, Leung DW. The vascular endothelial growth factor family of polypeptides. *J Cell Biochem*. 1991;47:211-218
309. Silvestre JS, Tamarat R, Ebrahimian TG, Le-Roux A, Clergue M, Emmanuel F, Duriez M, Schwartz B, Branellec D, Levy BI. Vascular endothelial growth factor-b promotes in vivo angiogenesis. *Circ Res*. 2003;93:114-123
310. Autiero M, Waltenberger J, Communi D, Kranz A, Moons L, Lambrechts D, Kroll J, Plaisance S, De Mol M, Bono F, Kliche S, Fellbrich G, Ballmer-Hofer K, Maglione D, Mayr-Beyrle U, Dewerchin M, Dombrowski S, Stanimirovic D, Van Hummelen P, Dehio C, Hicklin DJ, Persico G, Herbert JM, Shibuya M, Collen D, Conway EM, Carmeliet P. Role of plgf in the intra- and intermolecular cross talk between the vegf receptors flt1 and flk1. *Nat Med*. 2003;9:936-943
311. Karkkainen MJ, Haiko P, Sainio K, Partanen J, Taipale J, Petrova TV, Jeltsch M, Jackson DG, Talikka M, Rauvala H, Betsholtz C, Alitalo K.

Vascular endothelial growth factor c is required for sprouting of the first lymphatic vessels from embryonic veins. *Nat Immunol*. 2004;5:74-80
312. Astin JW, Haggerty MJ, Okuda KS, Le Guen L, Misa JP, Tromp A, Hogan BM, Crosier KE, Crosier PS. Vegfd can compensate for loss of vegfc in zebrafish facial lymphatic sprouting. *Development*. 2014;141:2680-2690
313. Harper SJ, Bates DO. Vegf-a splicing: The key to anti-angiogenic therapeutics? *Nat Rev Cancer*. 2008;8:880-887
314. Olofsson B, Korpelainen E, Pepper MS, Mandriota SJ, Aase K, Kumar V, Gunji Y, Jeltsch MM, Shibuya M, Alitalo K, Eriksson U. Vascular endothelial growth factor b (vegf-b) binds to vegf receptor-1 and regulates plasminogen activator activity in endothelial cells. *P Natl Acad Sci USA*. 1998;95:11709-11714
315. Mattei MG, Borg JP, Rosnet O, Marme D, Birnbaum D. Assignment of vascular endothelial growth factor (vegf) and placenta growth factor (plgf) genes to human chromosome 6p12-p21 and 14q24-q31 regions, respectively. *Genomics*. 1996;32:168-169
316. Ebos JM, Kerbel RS. Antiangiogenic therapy: Impact on invasion, disease progression, and metastasis. *Nat Rev Clin Oncol*. 2011;8:210-221
317. Rini BI, Escudier B, Tomczak P, Kaprin A, Szczylik C, Hutson TE, Michaelson MD, Gorbunova VA, Gore ME, Rusakov IG, Negrier S, Ou YC, Castellano D, Lim HY, Uemura H, Tarazi J, Cella D, Chen C, Rosbrook B, Kim S, Motzer RJ. Comparative effectiveness of axitinib versus sorafenib in advanced renal cell carcinoma (axis): A randomised phase 3 trial. *Lancet*. 2011;378:1931-1939
318. Motzer RJ, Escudier B, Tomczak P, Hutson TE, Michaelson MD, Negrier S, Oudard S, Gore ME, Tarazi J, Hariharan S, Chen C, Rosbrook B, Kim S, Rini BI. Axitinib versus sorafenib as second-line treatment for advanced renal cell carcinoma: Overall survival analysis and updated results from a randomised phase 3 trial. *Lancet Oncol*. 2013;14:552-562
319. Nakahara T, Norberg SM, Shalinsky DR, Hu-Lowe DD, McDonald DM. Effect of inhibition of vascular endothelial growth factor signaling on distribution of extravasated antibodies in tumors. *Cancer Res*. 2006;66:1434-1445
320. Sennino B, Kuhnert F, Tabruyn SP, Mancuso MR, Hu-Lowe DD, Kuo CJ, McDonald DM. Cellular source and amount of vascular endothelial growth factor and platelet-derived growth factor in tumors determine response to angiogenesis inhibitors. *Cancer Res*. 2009;69:4527-4536
321. Rossler J, Monnet Y, Farace F, Opolon P, Daudigeos-Dubus E, Bourredjem A, Vassal G, Geoerger B. The selective vegfr1-3 inhibitor axitinib (ag-013736) shows antitumor activity in human neuroblastoma xenografts. *Int J Cancer*. 2011;128:2748-2758
322. Hu-Lowe DD, Zou HY, Grazzini ML, Hallin ME, Wickman GR, Amundson K, Chen JH, Rewolinski DA, Yamazaki S, Wu EY, McTigue MA, Murray BW, Kania RS, O'Connor P, Shalinsky DR, Bender SL. Nonclinical antiangiogenesis and antitumor activities of axitinib (ag-013736), an oral, potent, and selective inhibitor of vascular endothelial growth factor receptor tyrosine kinases 1, 2, 3. *Clin Cancer Res*. 2008;14:7272-7283
323. Hudson CD, Hagemann T, Mather SJ, Avril N. Resistance to the tyrosine kinase inhibitor axitinib is associated with increased glucose metabolism in pancreatic adenocarcinoma. *Cell Death Dis*. 2014;5:e1160

324. Qi WX, He AN, Shen Z, Yao Y. Incidence and risk of hypertension with a novel multi-targeted kinase inhibitor axitinib in cancer patients: A systematic review and meta-analysis. *Br J Clin Pharmacol*. 2013;76:348-357
325. Thijs AM, van Herpen CM, Sweep FC, Geurts-Moespot A, Smits P, van der Graaf WT, Rongen GA. Role of endogenous vascular endothelial growth factor in endothelium-dependent vasodilation in humans. *Hypertension*. 2013;61:1060-1065
326. Cao Y, Linden P, Farnebo J, Cao R, Eriksson A, Kumar V, Qi JH, Claesson-Welsh L, Alitalo K. Vascular endothelial growth factor c induces angiogenesis in vivo. *Proc Natl Acad Sci U S A*. 1998;95:14389-14394
327. Tammela T, Zarkada G, Wallgard E, Murtomaki A, Suchting S, Wirzenius M, Waltari M, Hellstrom M, Schomber T, Peltonen R, Freitas C, Duarte A, Isoniemi H, Laakkonen P, Christofori G, Yla-Herttuala S, Shibuya M, Pytowski B, Eichmann A, Betsholtz C, Alitalo K. Blocking vegfr-3 suppresses angiogenic sprouting and vascular network formation. *Nature*. 2008;454:656-660
328. Wakefield TW, Myers DD, Henke PK. Mechanisms of venous thrombosis and resolution. *Arterioscler Thromb Vasc Biol*. 2008;28:387-391
329. Ali T, Humphries J, Burnand K, Sawyer B, Bursill C, Channon K, Greaves D, Rollins B, Charo IF, Smith A. Monocyte recruitment in venous thrombus resolution. *J Vasc Surg*. 2006;43:601-608
330. Clauss M, Weich H, Breier G, Knies U, Rockl W, Waltenberger J, Risau W. The vascular endothelial growth factor receptor flt-1 mediates biological activities. Implications for a functional role of placenta growth factor in monocyte activation and chemotaxis. *J Biol Chem*. 1996;271:17629-17634
331. Tchaikovski V, Fellbrich G, Waltenberger J. The molecular basis of vegfr-1 signal transduction pathways in primary human monocytes. *Arterioscler Thromb Vasc Biol*. 2008;28:322-328
332. Stockmann C, Kerdiles Y, Nomaksteinsky M, Weidemann A, Takeda N, Doedens A, Torres-Collado AX, Iruela-Arispe L, Nizet V, Johnson RS. Loss of myeloid cell-derived vascular endothelial growth factor accelerates fibrosis. *Proc Natl Acad Sci U S A*. 2010;107:4329-4334
333. Hamada N, Kuwano K, Yamada M, Hagimoto N, Hiasa K, Egashira K, Nakashima N, Maeyama T, Yoshimi M, Nakanishi Y. Anti-vascular endothelial growth factor gene therapy attenuates lung injury and fibrosis in mice. *J Immunol*. 2005;175:1224-1231
334. Ou XM, Li WC, Liu DS, Li YP, Wen FQ, Feng YL, Zhang SF, Huang XY, Wang T, Wang K, Wang X, Chen L. Vegfr-2 antagonist su5416 attenuates bleomycin-induced pulmonary fibrosis in mice. *Int Immunopharmacol*. 2009;9:70-79
335. Murakami M, Zheng Y, Hirashima M, Suda T, Morita Y, Ooehara J, Ema H, Fong GH, Shibuya M. Vegfr1 tyrosine kinase signaling promotes lymphangiogenesis as well as angiogenesis indirectly via macrophage recruitment. *Arterioscler Thromb Vasc Biol*. 2008;28:658-664
336. Falanga A, Zacharski L. Deep vein thrombosis in cancer: The scale of the problem and approaches to management. *Ann Oncol*. 2005;16:696-701
337. Zangari M, Fink LM, Elice F, Zhan F, Adcock DM, Tricot GJ. Thrombotic events in patients with cancer receiving antiangiogenesis agents. *J Clin*

Oncol. 2009;27:4865-4873
338. Drouet L. [thromboembolic risk associated with use of angiogenesis inhibitors used for the treatment of cancers]. *Pathol Biol (Paris)*. 2008;56:195-204
339. Nalluri SR, Chu D, Keresztes R, Zhu X, Wu S. Risk of venous thromboembolism with the angiogenesis inhibitor bevacizumab in cancer patients: A meta-analysis. *JAMA*. 2008;300:2277-2285
340. Erez N, Stambolsky P, Shats I, Milyavsky M, Kachko T, Rotter V. Hypoxia-dependent regulation of phd1: Cloning and characterization of the human phd1/egln2 gene promoter. *FEBS letters*. 2004;567:311-315
341. Woods SL, Whitelaw ML. Differential activities of murine single minded 1 (sim1) and sim2 on a hypoxic response element. Cross-talk between basic helix-loop-helix/per-arnt-sim homology transcription factors. *J Biol Chem*. 2002;277:10236-10243
342. McCaffrey TA, Pomerantz KB, Sanborn TA, Spokojny AM, Du B, Park MH, Folk JE, Lamberg A, Kivirikko KI, Falcone DJ, et al. Specific inhibition of eif-5a and collagen hydroxylation by a single agent. Antiproliferative and fibrosuppressive effects on smooth muscle cells from human coronary arteries. *J Clin Invest*. 1995;95:446-455
343. Loinard C, Ginouves A, Vilar J, Cochain C, Zouggari Y, Recalde A, Duriez M, Levy BI, Pouyssegur J, Berra E, Silvestre JS. Inhibition of prolyl hydroxylase domain proteins promotes therapeutic revascularization. *Circulation*. 2009;120:50-59
344. Fantin A, Vieira JM, Gestri G, Denti L, Schwarz Q, Prykhozhij S, Peri F, Wilson SW, Ruhrberg C. Tissue macrophages act as cellular chaperones for vascular anastomosis downstream of vegf-mediated endothelial tip cell induction. *Blood*. 2010;116:829-840
345. Carmeliet P, Dor Y, Herbert JM, Fukumura D, Brusselmans K, Dewerchin M, Neeman M, Bono F, Abramovitch R, Maxwell P, Koch CJ, Ratcliffe P, Moons L, Jain RK, Collen D, Keshert E. Role of hif-1alpha in hypoxia-mediated apoptosis, cell proliferation and tumour angiogenesis. *Nature*. 1998;394:485-490
346. Saha P. Magnetic resonance t1 relaxation during venous thrombus resolution. *King's College London*. 2012;PhD
347. Braekkan SK, Mathiesen EB, Njolstad I, Wilsgaard T, Hansen JB. Hematocrit and risk of venous thromboembolism in a general population. The tromso study. *Haematologica*. 2010;95:270-275
348. Barkefors I, Le Jan S, Jakobsson L, Hejll E, Carlson G, Johansson H, Jarvius J, Park JW, Li Jeon N, Kreuger J. Endothelial cell migration in stable gradients of vascular endothelial growth factor a and fibroblast growth factor 2: Effects on chemotaxis and chemokinesis. *J Biol Chem*. 2008;283:13905-13912
349. Li ZD, Bork JP, Krueger B, Patsenker E, Schulze-Krebs A, Hahn EG, Schuppan D. Vegf induces proliferation, migration, and tgf-beta1 expression in mouse glomerular endothelial cells via mitogen-activated protein kinase and phosphatidylinositol 3-kinase. *Biochem Bioph Res Co*. 2005;334:1049-1060
350. Pepper MS, Ferrara N, Orci L, Montesano R. Potent synergism between vascular endothelial growth factor and basic fibroblast growth factor in the induction of angiogenesis in vitro. *Biochem Bioph Res Co*. 1992;189:824-831
351. Heil M, Clauss M, Suzuki K, Buschmann IR, Willuweit A, Fischer S,

Schaper W. Vascular endothelial growth factor (vegf) stimulates monocyte migration through endothelial monolayers via increased integrin expression. *Eur J Cell Biol*. 2000;79:850-857
352. Hood JD, Meininger CJ, Ziche M, Granger HJ. Vegf upregulates ecnos message, protein, and no production in human endothelial cells. *Am J Physiol*. 1998;274:H1054-1058
353. Guenther F, von zur Muhlen C, Ferrante EA, Grundmann S, Bode C, Klibanov AL. An ultrasound contrast agent targeted to p-selectin detects activated platelets at supra-arterial shear flow conditions. *Invest Radiol*. 2010;45:586-591
354. Lanza GM, Wallace KD, Scott MJ, Cacheris WP, Abendschein DR, Christy DH, Sharkey AM, Miller JG, Gaffney PJ, Wickline SA. A novel site-targeted ultrasonic contrast agent with broad biomedical application. *Circulation*. 1996;94:3334-3340
355. Srivastava S, Alfieri A, Siow RC, Mann GE, Fraser PA. Temporal and spatial distribution of nrf2 in rat brain following stroke: Quantification of nuclear to cytoplasmic nrf2 content using a novel immunohistochemical technique. *J Physiol*. 2013;591:3525-3538
356. Muz B, Larsen H, Madden L, Kiriakidis S, Paleolog EM. Prolyl hydroxylase domain enzyme 2 is the major player in regulating hypoxic responses in rheumatoid arthritis. *Arthritis Rheum*. 2012;64:2856-2867
357. Fu L, Wang G, Shevchuk MM, Nanus DM, Gudas LJ. Generation of a mouse model of von hippel-lindau kidney disease leading to renal cancers by expression of a constitutively active mutant of hif1alpha. *Cancer research*. 2011;71:6848-6856
358. Hirsila M, Koivunen P, Xu L, Seeley T, Kivirikko KI, Myllyharju J. Effect of desferrioxamine and metals on the hydroxylases in the oxygen sensing pathway. *Faseb J*. 2005;19:1308-1310
359. Krutzik PO, Nolan GP. Intracellular phospho-protein staining techniques for flow cytometry: Monitoring single cell signaling events. *Cytometry A*. 2003;55:61-70
360. Ho VC, Duan LJ, Cronin C, Liang BT, Fong GH. Elevated vascular endothelial growth factor receptor-2 abundance contributes to increased angiogenesis in vascular endothelial growth factor receptor-1-deficient mice. *Circulation*. 2012;126:741-752
361. Hooper AT, Butler JM, Nolan DJ, Kranz A, Iida K, Kobayashi M, Kopp HG, Shido K, Petit I, Yanger K, James D, Witte L, Zhu Z, Wu Y, Pytowski B, Rosenwaks Z, Mittal V, Sato TN, Rafii S. Engraftment and reconstitution of hematopoiesis is dependent on vegfr2-mediated regeneration of sinusoidal endothelial cells. *Cell Stem Cell*. 2009;4:263-274
362. Tammela T, Zarkada G, Nurmi H, Jakobsson L, Heinolainen K, Tvorogov D, Zheng W, Franco CA, Murtomaki A, Aranda E, Miura N, Yla-Herttuala S, Fruttiger M, Makinen T, Eichmann A, Pollard JW, Gerhardt H, Alitalo K. Vegfr-3 controls tip to stalk conversion at vessel fusion sites by reinforcing notch signalling. *Nat Cell Biol*. 2011;13:1202-1213
363. Wedge SR, Ogilvie DJ, Dukes M, Kendrew J, Chester R, Jackson JA, Boffey SJ, Valentine PJ, Curwen JO, Musgrove HL, Graham GA, Hughes GD, Thomas AP, Stokes ES, Curry B, Richmond GH, Wadsworth PF, Bigley AL, Hennequin LF. Zd6474 inhibits vascular endothelial growth factor signaling, angiogenesis, and tumor growth following oral administration. *Cancer Res*. 2002;62:4645-4655

364. Tian S, Quan H, Xie C, Guo H, Lu F, Xu Y, Li J, Lou L. Yn968d1 is a novel and selective inhibitor of vascular endothelial growth factor receptor-2 tyrosine kinase with potent activity in vitro and in vivo. *Cancer Sci*. 2011;102:1374-1380
365. Goldman SJ, Chen E, Taylor R, Zhang S, Petrosky W, Reiss M, Jin S. Use of the odd-luciferase transgene for the non-invasive imaging of spontaneous tumors in mice. *Plos One*. 2011;6:e18269
366. Ryan HE, Poloni M, McNulty W, Elson D, Gassmann M, Arbeit JM, Johnson RS. Hypoxia-inducible factor-1alpha is a positive factor in solid tumor growth. *Cancer Res*. 2000;60:4010-4015